INFORMATION TO USERS

This manuscript has been reproduced from the microfilm master. UMI films the text directly from the original or copy submitted. Thus, some thesis and dissertation copies are in typewriter face, while others may be from any type of computer printer.

The quality of this reproduction is dependent upon the quality of the copy submitted. Broken or indistinct print, colored or poor quality illustrations and photographs, print bleedthrough, substandard margins, and improper alignment can adversely affect reproduction.

In the unlikely event that the author did not send UMI a complete manuscript and there are missing pages, these will be noted. Also, if unauthorized copyright material had to be removed, a note will indicate the deletion.

Oversize materials (e.g., maps, drawings, charts) are reproduced by sectioning the original, beginning at the upper left-hand corner and continuing from left to right in equal sections with small overlaps. Each original is also photographed in one exposure and is included in reduced form at the back of the book.

Photographs included in the original manuscript have been reproduced xerographically in this copy. Higher quality 6" x 9" black and white photographic prints are available for any photographs or illustrations appearing in this copy for an additional charge. Contact UMI directly to order.

UMI®

Bell & Howell Information and Learning
300 North Zeeb Road, Ann Arbor, MI 48106-1346 USA
800-521-0600

Stratosphere-Troposphere Exchange and the Impact of Commercial Aviation on the Atmosphere

Andrew Gettelman

A dissertation submitted in partial fulfillment
of the requirements for the degree of

Doctor of Philosophy

University of Washington

1999

Program Authorized to Offer Degree: Atmospheric Sciences

In presenting this dissertation in partial fulfillment of the requirements for the Doctorial degree at the University of Washington, I agree that the Library shall make its copies freely available for inspection. I further agree that extensive copying of this thesis is allowable only for scholary purposes, consistant with "fair use" as prescribed in the U.S. Copyright Law. Requests for copying or reproduction of this dissertation may be referred to University Microfilms, 1490 Eisenhower Place, P.O. Box 975, Ann Arbor, MI 48106, to whom the author has granted "the right to reproduce and sell (a) copies of the manuscript in microform and/or (b) printed copies of the manuscript made from microform."

Signature 

Date April 23 1999

University of Washington

Graduate School

This is to certify that I have examined this copy of a doctoral dissertation by

Andrew Gettelman

and have found that it is complete and satisfactory in all respects,
and that any and all revisions required by the final
examining committee have been made.

Chair of Supervisory Committee:

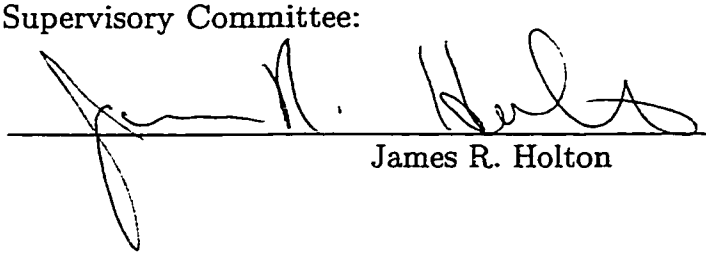

James R. Holton

Reading Committee:

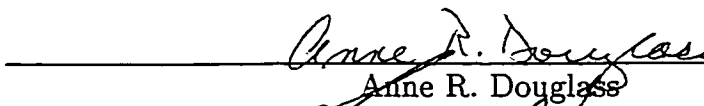

Anne R. Douglass

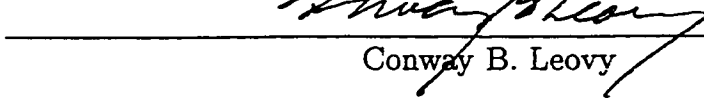

Conway B. Leovy

Date: April 23, 1999

University of Washington

Abstract

Stratosphere-Troposphere Exchange and the Impact of Commercial Aviation on the Atmosphere

by Andrew Gettelman

Chair of Supervisory Committee

Professor James R. Holton
Atmospheric Sciences

The exchange of mass and chemical constituents between the stratosphere and the troposphere is examined on a variety of time scales using various techniques. Estimates are developed of the stratosphere-troposphere exchange of important chemical species, and commercial aircraft emissions. Various methods for stratosphere-troposphere exchange are discussed. The circulation of the stratosphere (expressed using the Transformed Eulerian Mean residual circulation) is used to estimate fluxes of ozone, methane, nitrous oxide and CF_2Cl_2. These fluxes are found to be within the range of previous estimates. Depending upon the tropopause definition, between 18% and 44% of global aircraft emissions are deposited annually into the stratosphere. The distribution of emissions is found to be most sensitive to the tropopause definition, and not sensitive to the data set used or to inter-annual variability of the tropopause. Using a transport model as well as a trajectory model, the residence time of these aircraft emissions in the stratosphere is determined to be about 50 days, shorter in January than July. Simulations of water vapor emissions in the upper troposphere and lower stratosphere are found to qualitatively reproduce the water vapor distribution in

this region. The stratosphere-troposphere exchange of water vapor across the tropical tropopause is examined in detail. Large scale processes dominate the stratosphere-troposphere exchange of water vapor, but small scale processes are important in the upper tropical troposphere. A diagnostic of cross-tropopause transport is calculated at the tropopause and evaluated. Sensitivity tests and theoretical considerations indicate that the two-way cross tropopause flux may be significantly exaggerated by this method. The exaggeration is plausibly related to the type of data used to evaluate the diagnostic. The various methods for examining stratosphere troposphere exchange are summarized, along with illustrative quantitative estimates from the literature. Different methods are found to yield consistently different results. Observed and hypothesized mechanisms for stratosphere-troposphere exchange are discussed along with conclusions about the impact of aircraft emissions on the atmosphere.

TABLE OF CONTENTS

LIST OF FIGURES

LIST OF TABLES

ACKNOWLEDGMENTS

The author wishes to thank Jim Holton and Anne Douglass for their support and advice throughout this work. I can't think of two better mentors for a young scientist. Significant portions of this thesis have been published as work co-authored with a number of individuals who deserve acknowledgment, and from whom I have learned immensely. And as always, no contemporary scientific work, particularly in the atmospheric sciences, occurs in a (sic) vacuum:

The work in Chapter 3 utilizing the residual circulation was co-authored with Jim Holton and Karen H. Rosenlof. Thanks are also due to Eric Ray for interpolation and programming advice and to Christof Appenzeller for comments. I would also like to thank the UARS instrument teams for their input, comments, and background: J. M. Russell III (HALOE), J. W. Waters (MLS), and A. E. Roche (CLAES).

Chapter 5 was co-authored with Steve L. Baughcum of the Boeing company. K. Sage (NASA) and I. Köhler (DLR) provided data for this project. I also thank M. J. Prather, P. A. Newman and three anonymous reviewers for their comments.

The aircraft emissions transport work (Chapter 6) and the water vapor simulations (Chapter 7) would have been impossible without the assistance of C. J. Weaver and M. C. Cerniglia, NASA/GSFC. C. J. Weaver provided some of the simulations from which the burden calculations were drawn.

The simulations of water vapor in Chapter 7 were accomplished with thanks to E.A. Ray and A.E. Dessler for discussions and making available their work in progress for comparison. W.J. Randel provided HALOE data for this project.

The analysis of diagnostics of STE (Chapter 8) was co-authored with A. H. Sobel,

without whose encouragement and enthusiasm the work would not have happened. Thanks are due to V. Wirth and J. Egger for providing us with a pre-print of their paper. J. A. Kettleborough, J. R. Holton, P. C. Siegmund and two anonymous reviewers also provided invaluable comments.

I would also like to thank the 'Goddard Gang' at the Laboratory for Atmospheres for their patience with all my questions and for keeping me in running shape while on center (especially Kawa, Rood, Schoeberl, Coy, Weaver and Cerniglia).

This endeavor would not have been at all fun without the many graduate students who have suffered as my officemates, or without the patience and understanding of Ms. Francesca Gates. "You're the Best Baby"

DEDICATION

This work is dedicated to my parents, Nancy Nathan Gettelman and Alan Gettelman, whose encouragement, support and advice have been invaluable. From them I have learned, directly or by example, the most important words of Mark Twain: "Never let school interfere with your education."

Chapter 1

INTRODUCTION

The importance of the exchange of air between the stratosphere and the troposphere was probably first discussed by Brewer (1949) to explain the distribution of water vapor between the troposphere and the stratosphere. The exchange of air between the stratosphere and troposphere as well as the stratospheric circulation was also used by Dobson (1956) to explain the distribution of ozone in the stratosphere[1] Staley (1962) and Danielsen (1968) noted the reverse, the exchange of air from the stratosphere to the troposphere in tropopause folding events, diagnosed using observations of radioactive isotopes from atomic bomb tests. Danielsen and Mohnen (1977) used further case studies to estimate the annual flux of ozone from the stratosphere into the troposphere for the northern hemisphere. Staley (1982), based on radioactive isotope concentrations noted that midlatitude transport from the stratosphere to the troposphere peaks in spring. In recent years this flux has been quantified on various scales. The hemispheric mass budget analysis of Appenzeller et al. (1996) confirmed the results of Staley (1982) and others. On smaller scales, numerous authors such as Lamarque and Hess (1994) and Wirth and Egger (1999) have studied stratosphere-troposphere exchange in individual storms.

While the general picture of stratosphere-troposphere exchange (STE) is now well understood (Holton et al., 1995), the details of the timing and magnitude of the exchange are still less than certain. These details are important for understanding

[1]The stratospheric circulation was actually first hypothesized by Dobson et al. (1929). It is commonly known as the 'Brewer-Dobson' circulation after Brewer (1949) and Dobson et al. (1929).

the effects of anthropogenic changes on the global atmosphere.

Stratosphere-troposphere exchange regulates the atmospheric lifetime of species whose major sinks are in the stratosphere, such as methane (CH_4), nitrous oxide (N_2O) and the ozone depleting chlorofluorcarbons (CFC's). Exchange between the stratosphere and the troposphere also regulates the residence of aircraft emissions (chiefly carbon dioxide, water vapor and nitrogen oxides) emitted into the upper troposphere and lower stratosphere. The exchange of these species is important for the subsequent determination of their impact on the stratospheric ozone layer (in the case of CFC's) and their radiative forcing of the global climate system (in the case of methane, nitrous oxide and CFC's). Furthermore, the timing and magnitude of the stratospheric exchange of methane and water vapor are important for the chemical balance of the stratosphere, which is expected to change as the budgets of these species change. There may also be important feedbacks on the stratospheric circulation. The exchange of water vapor into the stratosphere from the troposphere may also have important consequences for the radiative balance of the upper troposphere, with subsequent effects on the surface temperature.

This work seeks to investigate the timing and magnitude of STE as it relates to these changing chemical forcings on the atmosphere. First, a detailed geography of the tropopause region and the stratosphere will be presented (Chapter 2), along with some background on STE in the extratropics and tropics. In Chapter 3, the flux of trace species into the middle and upper stratosphere will be examined, with the goal of using the stratosphere-troposphere exchange of mass to estimate the lifetime of long lived trace gases. The work builds especially upon the work of Holton et al. (1995) and Rosenlof (1995).

Constraining estimates of the potential impacts from the present and future commercial aircraft fleet is a particular focus of this study, and requires a detailed picture of stratosphere-troposphere exchange in the extratropics. The assimilation data sets and models used for analyzing processes that occur in the lower stratosphere and

upper troposphere (in Chapters 5 through 8) are described in Chapter 4. These tools are used to estimate the deposition (Chapter 5) and transport (Chapter 6) of aircraft emissions in the upper troposphere and lower stratosphere.

The study will also examine in detail some important aspects of the exchange of air between the stratosphere and troposphere in the tropics, focusing on the distribution of water vapor in the upper troposphere and lower stratosphere. Water vapor differs from aircraft emissions (which are mostly emitted into the stratosphere and upper troposphere in the extratropics as described in Chapter 5) in that the most important processes controlling the exchange between the stratosphere and the troposphere occur in the tropics. Model studies of the distribution and stratosphere-troposphere exchange of water vapor will be presented in Chapter 7.

After looking at both the extratropics and the tropics, we will consider a detailed critique of a common methods for describing the exchange of constituents across the tropopause generally in Chapter 8. Finally, Chapter 9 contains a summary and conclusions with some further scientific questions and avenues for follow up work.

Chapter 2

GEOGRAPHY OF THE LOWER STRATOSPHERE

In order to understand the exchange of mass between the stratosphere and the troposphere (and vice versa) it is instructive to first review the "geography" of the region in which the exchange occurs. Throughout this work, 'Stratosphere-Troposphere Exchange' (STE) will refer to the exchange of mass or constituents across the tropopause surface without a bias as to the direction of the exchange. STE may be bi-directional, and when net or gross exchange is considered these terms will be applied as necessary.

The troposphere and stratosphere are divided by the tropopause or the tropopause region, which will be discussed more fully below. Stratosphere, meaning roughly 'constant sphere' is derived from the Latin *'stratum'* (meaning smooth layer)[1] and the Greek *'sphere'*. Troposphere means roughly 'changing sphere' from the Latin *'tropica'* (changes). Vertical motions in the stratosphere are inhibited by the large temperature inversion caused by absorption of ultraviolet (UV) solar radiation by ozone, while motion in the troposphere is driven by heat input from the surface into a weakly stable vertical profile, and the variability of the input in time and space.

The stratosphere may be usefully divided into two regions when discussing STE. Between the tropopause and about the 380K potential temperature surface, near 100 hPa (Figure 2.1), exchange with the troposphere can occur along a surface of constant potential temperature (an isentrope). This region, shaded in Figure 2.1, has been termed the stratospheric portion of the 'middleworld' (Hoskins, 1991) or 'extrat-

[1]Latin and Greek definitions from the Perseus Project at Tufts University, http://www.perseus.tufts.edu/

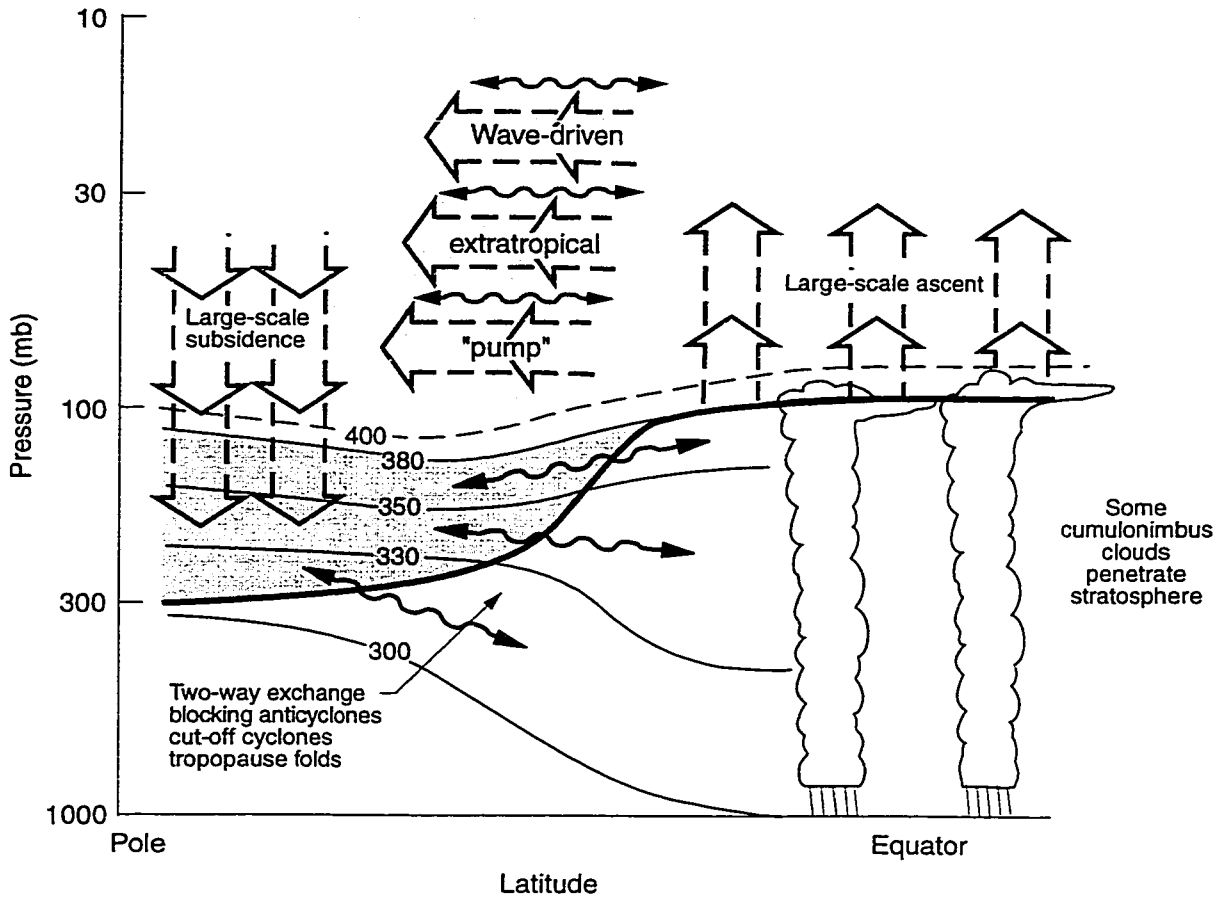

Figure 2.1: Dynamical aspects of stratosphere-troposphere exchange. Figure 3 from Holton et al. (1995). Thick line is the tropopause. Dark shading is the "lowermost stratosphere".

ropical lowermost stratosphere' (Holton et al., 1995) (also called simply the 'lowermost stratosphere'). The stratospheric 'overworld' is the region above this surface, where STE can only occur diabatically. Both these regions and the tropopause are discussed in more detail below, along with an overview of Stratosphere-Troposphere Exchange in the tropics and extratropics. References to further discussion and analysis in subsequent chapters are included throughout.

2.1 The Overworld

The lower boundary of the overworld is the potential temperature surface which just intersects the tropical tropopause, typically 380 K to 400 K. The overworld contains approximately 60% of the mass of the total stratosphere (Appenzeller et al., 1996). Above this surface in the overworld, exchange with the troposphere is possible only by diabatic motion across isentropic surfaces.

The basic character of how trace species are transported in the stratosphere and troposphere is quite different. The troposphere is well mixed by fast vertical motions associated with extratropical cyclones and tropical convection. The stratosphere is not mixed by these motions, but has a large-scale mean circulation that is driven by the deposition of momentum by eddies (waves) from the troposphere. Like a 'fluid-dynamical suction pump' (Holton et al., 1995), these eddies pull air upward and poleward. Continuity requires an upward flux at the tropical tropopause, and a corresponding downward flux near the poles (Figure 2.1). Bi-directional exchange of mass across the 380K surface in and out of the stratospheric overworld is characterized by upward motion in the tropics and downward motion in the extratropics. Plumb and Eluszkiewicz (1999) have recently discussed the details of this circulation and how it is affected by thermal and mechanical forcings.

The circulation in the overworld can be visualized by examining the zonally averaged distribution of methane, illustrated in Figure 2.2 with data from the Halogen Occultation Experiment (HALOE) on the Upper Atmosphere Research Satellite (UARS). The gradients are a consequence of the upward motion of air rich in methane (which has a tropospheric source and is destroyed by oxidation in the upper stratosphere) and the downward advection of air from the upper stratosphere with lower methane concentrations. The region of sharp meridional gradients at about 30 degrees north and south of the equator is a barrier to meridional transport which divides the equatorial region of upward motion from the regions of downward motion in the

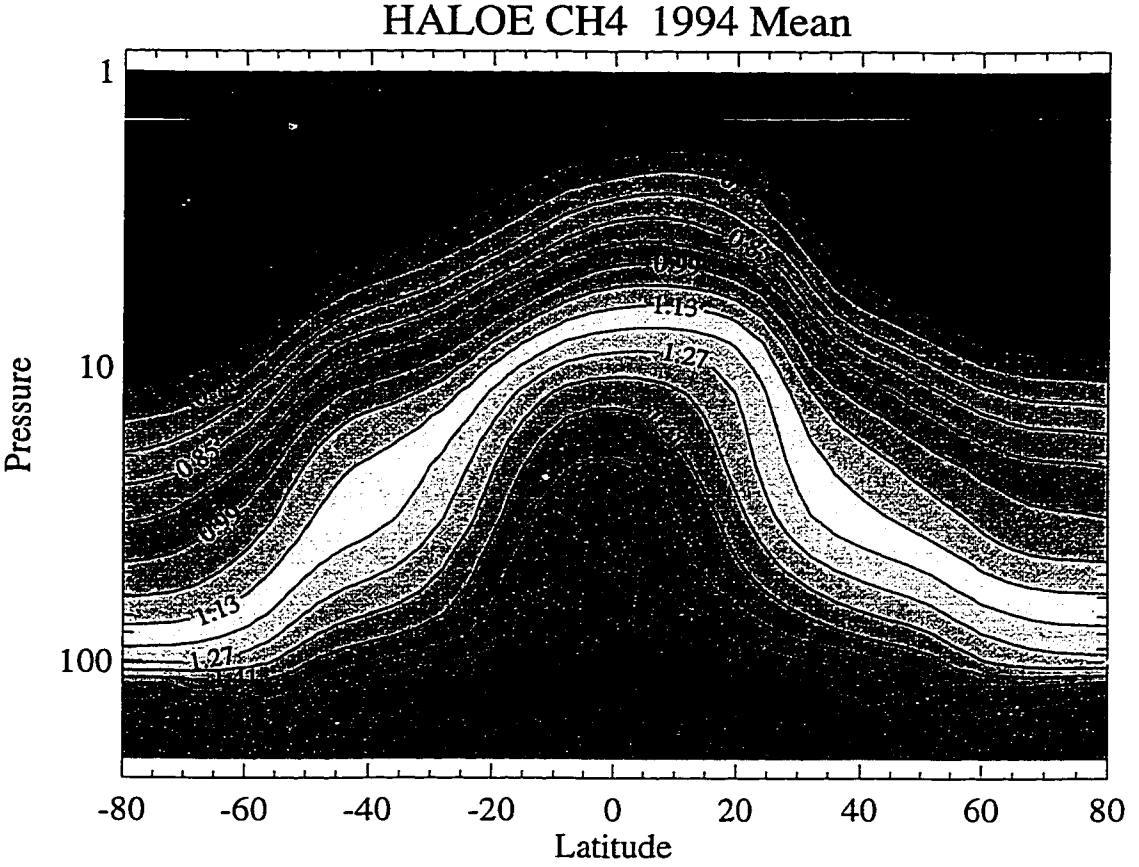

Figure 2.2: 1994 Annual zonal mean methane mixing ratio (ppmv) from HALOE instrument on UARS. Figure courtesy of Eric Ray

extratropics. The barrier between the two is strongest in the lower to middle stratosphere (Plumb, 1996), being weak near the 380K surface and again farther up (Mote et al., 1996).

The diabatic circulation in the overworld, termed the 'residual circulation' (Holton, 1990; Rosenlof, 1995), is described using the Transformed Eulerian Mean (TEM) equations (see Andrews et al., 1987, section 3.5). The TEM equations describe the portion of the eddy heat flux not balanced by mean adiabatic processes (hence it is a residual). Being diabatic and irreversible, it resembles most closely the relevant circulation for tracer transport. The TEM circulation is used in Chapter 3 to describe tracer trans-

port in the overworld. The TEM residual circulation can be calculated in several ways (Rosenlof, 1995): from the vertical velocity and horizontal eddy heat flux convergence (Andrews and McIntyre, 1976), from the temperature tendency and derived heating rates (Dunkerton, 1978; Eluszkiewicz et al., 1996; Yang and Tung, 1996), or based on the eddy forcing at higher altitudes– the 'downward control' principle (Haynes et al., 1991; Rosenlof and Holton, 1993).

Many tracers in the lowermost stratosphere can be considered conservative or semi-conservative (that is—their chemical lifetime is much longer than the transport time through the lowermost stratosphere). Thus the cross-isentropic flux at 380K based on the TEM circulation, termed the Middleworld-Overworld Exchange (MOE) by Chen (1995), can be used to estimate the stratosphere-troposphere exchange of long lived tracers. Fluxes of air mass (Rosenlof and Holton, 1993; Appenzeller et al., 1996) have been examined using this circulation. The estimates for the northern hemisphere winter (DJF) extratropical MOE (across the 380K or 100hPa surface) range from 8-12 x 10^9 kg s^{-1}. Fluxes of trace constituents such as ozone and methane from Gettelman et al. (1997) are presented in Chapter 3 along with spatial and temporal details of this flux.

The lower part of the stratospheric overworld is, however, strongly influenced by the troposphere below it, as well as from the non-local dynamical wave forcing described by the residual circulation. Rosenlof et al. (1997) describe the lower part of the overworld between the bottom boundary (380K) and about the 450K surface as the "tropically controlled transition region". They note that the 'overworld' which is under nonlocal dynamical control from higher altitudes is really only the region above 60–50 hPa, and that below this the influence of tropospheric processes affects transport. Meridional transport at these altitudes is more rapid than in the region above 450K (Plumb, 1996). Rapid meridional transport is illustrated by the relatively flat meridional gradients in the lower stratosphere (100–60 hPa) in long lived species, such as methane in Figure 2.2. Transport in this region and the implications for the

cross-troposphere exchange of water vapor is discussed using a transport simulation in Chapter 7. Rapid meridional transport occurs in the middleworld as well, and is discussed below.

2.2 The Middleworld

The region intersected by isentropes which span the tropopause is unique because STE may occur along surfaces of constant potential temperature (also constant entropy or *isentropic* surfaces). This distinction was noted first by Hoskins (1991). It is an important distinction because air entering this region of the stratosphere does not have to pass through the tropical tropopause, and quasi-isentropic exchange can occur from the tropics to mid-latitudes in a short time. The trace gas concentrations of the lowermost stratosphere are thus different in many ways from those of the overworld. Perhaps the best known difference is the water vapor mixing ratio in the extratropical lowermost stratosphere, which Dessler et al. (1995) have shown to have come not from the stratospheric overworld through the tropical cold trap and subsequently into the middleworld by the residual circulation, but through quasi-isentropic exchange with the tropical tropopause or exchange with the midlatitude tropopause (see Chapter 7 for further discussion). The annual cycle of middleworld mass has been described by Appenzeller et al. (1996) and is discussed further in Section 8.4.1. It varies as the pressure on the upper (380K) and lower (tropopause) surfaces varies over the course of the year, and is not symmetric between the northern and southern hemispheres.

The middleworld is of particular concern because a significant fraction of the emissions of commercial aircraft (18% to 44%, see Chapter 5) are deposited in the lowermost stratosphere. For these often short lived species, knowledge of the residual circulation is insufficient to describe the exchange of these constituents between the stratosphere and the troposphere, and an explicit description of the middleworld is necessary. The middleworld exchanges directly with the troposphere through ex-

change across the tropopause and is strongly affected by tropopause processes, both in the tropics (Dessler et al., 1995) and in midlatitudes (Lelieveld et al., 1997; Hintsa et al., 1998), as discussed further in Section 2.4.

2.3 The Tropopause

The tropopause marks the boundary between the stratosphere and troposphere. The zonal mean tropopause height is high in the tropics (approximately 100 hPa) and below 300 hPa near the poles, as indicated in Figure 2.1. The tropopause has a highly variable structure in three dimensions. While the figures present a zonal mean picture for clarity, most analyses throughout this work are conducted using three dimensional daily tropopause surfaces which are zonally asymmetric. For this analysis, the tropopause is defined in several ways to test the sensitivity of the results to varying tropopause definitions.

The tropopause is conventionally defined as the beginning of the change in vertical stratification that marks the lower limit of the stratosphere using either a 'thermal' or 'dynamic' definition. The thermal definition of the tropopause is based on the vertical lapse rate, and is given as the lowest point above 500 mb where the lapse rate is less than 2° C per km for 2 km (Holton et al., 1995). The dynamic definition is based on a value of potential vorticity (PV) which marks the beginning of the strong vertical PV gradient in the stratosphere where Ertel's PV (EPV or just PV) is defined in the usual way (Holton, 1992) as:

$$PV = -g\left(\frac{\partial\theta}{\partial p}\right)(\zeta + f) \tag{2.1}$$

where g is the gravitational acceleration, θ is potential temperature, p is pressure, ζ is the vertical component of relative vorticity (the curl of velocity) and f is the coriolis parameter (a function of latitude). Note that PV is normally negative in the southern hemisphere. In most of the analyses to be presented, unless noted otherwise, PV refers to the absolute value of the quantity in equation 2.1 in units of

$Kkg^{-1}m^2s^{-1}$. For convenience, a Potential Vorticity Unit (PVU) is defined such that 1 PVU $= 10^{-6}Kkg^{-1}m^2s^{-1}$.

PV has a strong cross-tropopause gradient in mid latitudes but not in the tropics because PV normally goes to zero at the equator. We thus define the tropical 'dynamic' tropopause as the 380K potential temperature surface (located near 100 hPa), in accordance with Holton et al. (1995). The definition of the tropical tropopause is invoked when the pressure on the PV tropopause surface is less than the pressure on 380K. Accepted values for the PV tropopause range from 1.6 PVU (World Meteorological Organization, 1986) to 3.5 PVU (Hoerling et al., 1991).

The tropopause has also been defined indirectly, by characteristic conditions or constituent values in the region of the tropopause. The tropopause in the tropics is often near the cold point, or minimum temperature, which Highwood and Hoskins (1998) have used to define the tropopause. In the extratropics, Bethan et al. (1996) have utilized the ozone gradient to help define the tropopause.

A number of studies have evaluated these different definitions. In particular, Hoerling et al. (1991) have compared the thermal and dynamic definitions using radiosonde and analysis data over North America. Gettelman and Baughcum (1999) have also compared the zonal mean structure of the thermal and dynamic tropopause (see Chapter 5). The variability of the tropopause height throughout the year has been investigated by Appenzeller et al. (1996) in the extratropics, while Highwood and Hoskins (1998) have focused primarily upon the tropics.

The tropopause is in reality not so much a surface, as a region. Different definitions are usually appropriate for different applications. Throughout this work, the sensitivity of STE to the definition of the tropopause is repeatedly tested. The tropopause is defined in multiple ways, typically using the thermal and dynamic definitions. The latter is defined using different isosurfaces of potential vorticity in the extratropics.

2.4 Stratosphere-Troposphere Exchange

The tropopause or tropopause region serves as a barrier to transport whether it is defined as a sudden change in the static stability, or a sharp gradient in potential vorticity. The tropopause is variable in pressure and altitude, being high (16km) in the tropics and low (10km) near the poles as indicated in Figure 2.1. Stratosphere-Troposphere Exchange is also different between the tropics and extratropics. Chapters 5 and 6 focus on aircraft emissions in the extratropical lowermost stratosphere, while Chapter 7 focuses is on transport of water vapor from the tropical upper troposphere. Below we briefly discuss some of the important processes affecting stratosphere-troposphere exchange in the extratropics (Section 2.4.1) and the tropics (Section 2.4.2).

2.4.1 The Extratropics

The global scale circulation pictured in Figure 2.1 (from Holton et al. (1995)) gives the general sense of motion from the stratosphere to the troposphere in the extratropics. The actual exchange of mass across the extratropical tropopause is thought to occur through transient synoptic scale events, such as tropopause folds (Danielsen, 1968), cut off lows (Ebel et al., 1996), and cumulus overshooting (Poulida et al., 1996). Synoptic scale folding events and stratospheric intrusions into the troposphere have been examined in detail from observations (Danielsen, 1968; Shapiro, 1980), models (Lamarque and Hess, 1994; Spaete et al., 1994; Rood et al., 1997; Bithell et al., 1999) and using global budgets of the number of folding events (Ebel et al., 1996; Postel and Hitchman, 1999). Most model studies have noted the dissipation of folds in the troposphere (Lamarque and Hess, 1994) and the subsequent deposition of the the stratospheric air contained within them into the troposphere.

Several different processes are invoked to describe the exchange that occurs. Shapiro (1980) notes the importance of clear air turbulence and mixing in breaking down folds,

resulting in irreversible transport into the troposphere. Stoelinga (1996) noted that the non-conservation of potential vorticity occurs either (1) through surface friction along the gradient of potential temperature or (2) through a vertical gradient of diabatic heating. In this context the general diabatic cooling in the extratropical lowermost stratosphere, with a heat source in the tropopause below (positive vertical gradient with decreasing pressure), creates conditions for the decrease in PV of descending parcels and in the aggregate, exchange into the troposphere. Wirth (1996) studied an idealized upper level anticyclone and found that radiation can also change PV and cause exchange across the tropopause.

These diabatic processes can transport mass in the extratropics from the troposphere to the stratosphere as well as from the stratosphere to the troposphere, though as noted by Danielsen (1968) this is likely to affect only the lowest few kilometers of the lowermost stratosphere, a result confirmed by the diagnostic analysis of Grewe and Dameris (1996). Quasi-adiabatic mixing out of the tropical troposphere along isentropic surfaces in midlatitudes is important for affecting the composition of the extratropical lowermost stratosphere, as described by Dessler et al. (1995). Mixing on isentropic surfaces that span the tropopause is analyzed by Chen (1995) and Postel and Hitchman (1999).

For effectively simulating episodic STE by all of these processes, a realistic depiction of individual events is necessary, but also necessary is some inclusion of the large scale circulation in the stratospheric overworld. Assimilated data sets derived from observations and models driven by them are well suited for this purpose. These data and tools are described in Chapter 4 and used in Chapters 5 and 6 to describe the global evolution of aircraft emissions in the atmosphere. Chapter 8 will use assimilated data to quantitatively describe both troposphere to stratosphere and stratosphere to troposphere exchange at the tropopause. Quantitative estimates of the net mass flux across the extratropical tropopause as high as 90 x 10^9 kg s^{-1} in the northern hemisphere have been derived using ozone fluxes in synoptic events and

statistical extrapolation (Ebel et al., 1996). Eulerian diagnostics of the net cross tropopause flux (Wei, 1987; Hoerling et al., 1993; Grewe and Dameris, 1996; Siegmund et al., 1996) indicate winter (December, January and February) air mass fluxes in the northern hemisphere of 13–21 x 10^9 kg s^{-1}. These and other previous studies are further examined in Chapter 8.

2.4.2 Tropics

As noted in Chapter 1, the extremely low water vapor concentrations in the stratosphere led Brewer (1949) to the conclusion that most air must enter the stratosphere in the tropics at very cold temperatures where the saturation vapor mixing ratio of water is only a few parts per million by volume. These temperatures at tropopause level are found only in the tropics. Any theory which explains the transport of air between the troposphere and the stratosphere in the tropics must be consistent with the distribution, in time and space, of water vapor in the lower stratosphere and upper troposphere. Chapter 7 will attempt to simulate the water vapor distribution in the upper troposphere and lower stratosphere to help understand tropical STE.

Temperature and water vapor analyses indicate that exchange at the tropical tropopause may be driven more by non-local processes than by episodic events in the tropopause region as in the extratropics. The large scale circulation creates an annual cycle in tropical temperatures (Yulaeva, 1994) which affects the entry of water vapor into the stratosphere as discussed by Mote et al. (1996). Furthermore, Reid and Gage (1996) found that temperatures in the upper tropical troposphere down to 125 hPa were correlated with stratospheric temperatures at 80 hPa. These analyses indicate that the general picture of stratosphere-troposphere exchange, as indicated in Figure 2.1, is of large scale ascent forced by the stratospheric wave driven circulation (Holton et al., 1995).

However, vertical motion in the tropical troposphere is dominated by motions associated with convective activity which can penetrate well into the stratosphere

(400K or higher) for the deepest convection, as recorded by Kelly et al. (1993) during the STEP experiment. Danielsen (1993) concludes from aircraft observations near and over convection during the STEP experiment that radiative heating in the anvils formed from convective turrets penetrating the stratosphere is the dominant mechanism for depositing tropospheric air into the stratosphere irreversibly. Newell and Gould-Stewart (1981) hypothesized that most of the air must be entering the stratosphere over the Western Pacific (the region of the convection examined by Danielsen (1993)) for stratospheric mixing ratios to be as low as observed. Dessler (1998) has recently questioned this hypothesis using radiosonde data, arguing that temperatures may be cold enough for air to be entering the stratosphere everywhere in the tropics. Reid and Gage (1996) found that convection and entrainment would modify the tropopause height over the course of the year, affecting the lapse rate and subsequent convective penetration. Such evidence suggests that local convective processes are also important for tropical STE.

There are also explanations for temperature variations at the tropical tropopause which affect stratosphere-troposphere exchange forced by local or non-local wave activity from the troposphere. Tsuda et al. (1994) and Fujiwara et al. (1998) note the importance of equatorial Kelvin wave propagation and breaking on changing the height of the tropopause. Potter and Holton (1995) note that convectively forced buoyancy waves might contribute to the dehydration of the stratosphere by formation of ice crystal clouds above convection. Pfister et al. (1993) note the importance of gravity waves in forcing the diabatic circulation at the tropical tropopause. Sub-visible cirrus clouds may also affect the local diabatic heating as discussed by Rosenfield et al. (1998).

It is fairly clear from available data that below 200 hPa or so the tropical upper troposphere is controlled by convective processes, and above 80 hPa or so the tropical stratosphere is dominated by the residual circulation. In between these regions the relative roles of these thermodynamic (local) and wave driven (non-local) processes

are uncertain. Plumb and Eluszkiewicz (1999) have recently modeled the Brewer-Dobson circulation in the stratosphere and noted that while the driving by wave drag is dominant, in the tropics the residual circulation may be significantly influenced by local processes such as those discussed above. These local processes combine to govern the temperature profile of the coldest region of the lower atmosphere, which is critically important for determining the stratosphere-troposphere exchange of water vapor. Observations can help us to gauge the relative importance of these processes. Unfortunately, observations of the tropical tropopause from satellites and in-situ aircraft are sparse and radiosonde records are often unreliable (Gaffen, 1999), limiting the available data in the tropical tropopause region. To shed light on these mechanisms of tropical STE and interactions of the tropical upper troposphere with the extratropical middleworld and the overworld, the exchange of water vapor is considered in detail in Chapter 7 using a transport model and recent observations.

Chapter 3

MASS FLUXES OF LONG LIVED TRACE SPECIES IN THE LOWER STRATOSPHERE

In the past, studies of stratosphere-troposphere exchange (STE) have generally focused only on the transfer of mass and trace constituents across the tropopause, particularly in the extratropics. In a recent review, Holton et al. (1995) emphasized, however, that it is often more useful to consider the rate at which constituents are transferred to and from the photochemically active region of the stratosphere. For many constituents this region lies above the ~400 K potential temperature surface, a surface that in the tropics lies just above the tropopause but is well above the tropopause in the extratropics. This chapter is concerned with transport across the boundary between the overworld and the lowermost stratosphere.

As discussed in Chapter 2. the upwelling and mass transport into the overworld by the tropical branch of the diabatic (or cross-isentropic) circulation is not caused by radiative heating but rather is a nonlocal dynamical response to wave-induced forcing in the extratropical stratosphere (Haynes et al., 1991; Holton et al., 1995). This forcing exerts a fluid dynamical pumping action that pulls air upward and poleward from the tropical lower stratosphere and pushes it poleward and downward into the extra-tropical troposphere. The resulting global-scale circulation drives the stratosphere away from radiative equilibrium conditions and maintains the temperature below radiative equilibrium in the tropical upwelling region and above radiative equilibrium in the extratropics. Thus there is a characteristic pattern of radiative heating in the tropics and radiative cooling in the extratropics accompanying the global-scale

circulation, and this can be used to quantitatively estimate the cross-isentropic circulation. Combining the cross-isentropic circulation with observed trace gas mixing ratios yields an estimate of the net constituent transport across surfaces in the lower stratosphere.

Both upward and downward transport can be important. Ozone is transported downward from the photochemically active source region in the overworld and ultimately into the troposphere. Downward transport is important for the budget of ozone in the troposphere. Upward transport into the stratosphere affects the atmospheric residence times of those atmospheric trace gases whose major sinks are photochemical destruction in the stratosphere.

Numerous trace constituent observations have confirmed that upward transport in the stratosphere is mostly limited to the tropics, while downward transport occurs in the extratropics, particularly in the winter season (Brasseur and Solomon, 1986). This tropical-up and extratropical-down pattern of meridional overturning tends to produce tracer mixing ratio isopleths that slope relative to the isentropes, so globally integrated cross-isentropic trace constituent fluxes are positive for tracers with tropospheric sources and negative for tracers with stratospheric sources.

Recently available trace gas mixing ratio data from the Upper Atmosphere Research Satellite (UARS) together with estimates of the global-scale atmospheric mass circulation allow a detailed examination of the vertical transport of several of these species across the boundary between the overworld and the lowermost stratosphere. The trace gases examined here include ozone (O_3), nitrous oxide (N_2O), methane (CH_4), and chlorofluorocarbon-12 (CF_2Cl_2) .

3.1 Methodology

The transformed Eulerian mean (TEM) residual circulation (Andrews and McIntyre, 1976) is here used as an approximation for the global-scale cross-isentropic circulation,

what Yang and Tung (1996) call the "diabatic" or "meridional" circulation. The time and zonally averaged TEM circulation approximates the Lagrangian mean motion of air parcels in the meridional plane (Dunkerton, 1978) and hence approximates cross-isentropic tracer transport (e.g., Holton, 1992). Monthly mean TEM streamfunctions were obtained for the period January 1992 to December 1995 using the thermodynamic method described by Rosenlof (1995). Heating rates were computed with the radiative transfer model of Olaguer et al. (1992) using United Kingdom Meteorological Office (UKMO) analyzed temperatures (Swinbank and O'Neill, 1994) and UARS ozone and water vapor data as inputs.

Since the TEM stream function and the UARS trace constituent data are available on isobaric surfaces, we have here computed trace constituent fluxes across several isobaric surfaces in the overworld. Some deviation from the cross-isentropic flux is introduced by this procedure since the mean isentropes move up and down seasonally, particularly in high latitudes (Mahlman, 1985; Appenzeller et al., 1996). However, this should not introduce any errors in estimates of annual fluxes into and out of the overworld. The analysis also presumes that tracers are more or less zonally symmetric. In the overworld at 50 hPa longitudinal gradients in these long-lived species should be small and the errors introduced through this assumption minimal. A more serious problem is the decreased reliability of UARS trace constituent observations at altitudes below about the 50 hPa isobaric surface, since the satellite was designed for measurements between 10 and 1 hPa. The 50 hPa surface is located near 21 km or 500 K in isentropic coordinates. This height is a few kilometers above the nominal boundary of the overworld. However, for most of the species of interest here, photochemical timescales are much longer than dynamical timescales below 50 hPa, and thus little photochemical error should be introduced by using 50 hPa as the primary reference surface for the boundary between the overworld and the lowermost stratosphere.

The vertical mass flux F of a tracer in kilograms per second for the area bounded by two latitude circles can be expressed in a form analogous to the air mass flux given

by Rosenlof (1995) as:

$$F(p, \phi_1, \phi_2, t) = 2\pi a \int_{\phi_1}^{\phi_2} \bar{w}^* \bar{\chi} \rho_0 a \cos\phi \, d\phi \tag{3.1}$$

Here the overbars denote zonal mean quantities; ρ_0 is the basic state air density (a function of pressure only); a is the radius of the Earth; ϕ is latitude; $\bar{\chi}$ is the tracer mass mixing ratio; and $\bar{w}^*$ is the TEM residual vertical velocity, which following Rosenlof and Holton (1993) is related to the TEM stream function (ψ) by:

$$\bar{w}^* = \frac{1}{a\rho_0 \cos\phi} \frac{\partial \Psi}{\partial \phi} \tag{3.2}$$

Substituting from equation 3.2 into equation 3.1 yields the alternate form:

$$F(p, \phi_1, \phi_2, t) = 2\pi a \int_{\phi_1}^{\phi_2} \bar{\chi} \frac{\partial \Psi}{\partial \phi} \, d\phi \tag{3.3}$$

which is the form that we use for computing the tracer mass flux in kg s^{-1} for the area bounded by latitude circles ϕ_1 and ϕ_2.

3.1.1 Residual Circulation

Using the method of Rosenlof (1995), the monthly mean residual stream function was used to compute monthly means of the net upward air mass flux in the tropics and downward air mass flux in the extratropics at 20 hPa, 32 hPa, 50 hPa, and 67 hPa. Figure 3.1 illustrates the "tropical" and "extratropical" mass fluxes at the 50 hPa reference surface. Upward air mass fluxes are indicated by positive values throughout this study. The region of tropical upwelling is defined as the region where the vertical velocity given by equation 3.2 is positive. The meridional extent of this region varies from month to month with the residual circulation. The extratropics are the regions in which the vertical velocity is generally downward. As previously noted by Rosenlof (1995) and Rosenlof and Rosenlof and Holton (1993), there is a strong annual cycle to the residual circulation. Upwelling throughout the tropics

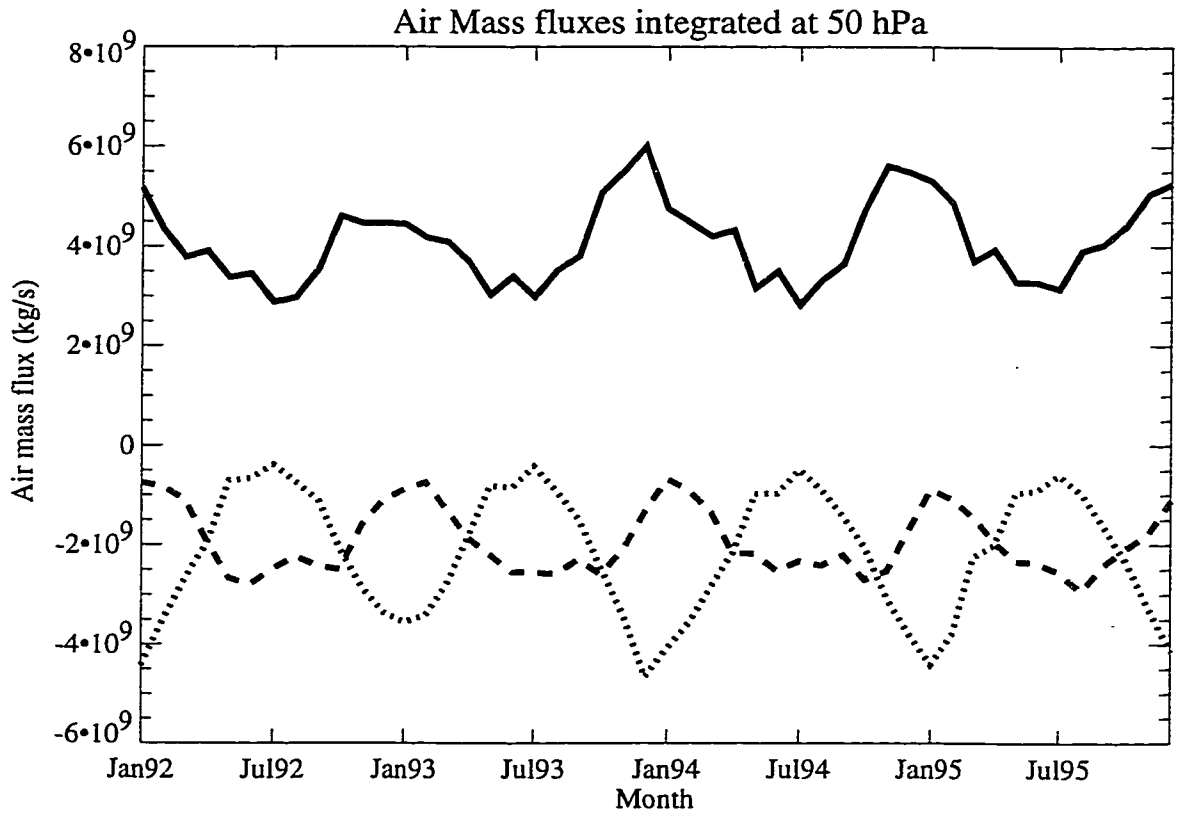

Figure 3.1: Air mass flux calculated from the transformed Eulerian mean (TEM) stream function at 50 hPa. Positive tropical upward component, solid curve. Northern hemisphere downward flux, dotted curve, and southern hemisphere extra-tropical downward flux, dashed curve.

peaks during December, associated with the strong wave-induced pumping during that season in the extratropical winter northern hemisphere. Downward fluxes in the extratropics also have a seasonal cycle shown in Figure 3.1. The peak downward flux occurs during the winter season in each hemisphere, with a stronger annual cycle in the northern hemisphere. The air mass flux integrated over all latitudes (90°S to 90°N) on a pressure surface is identically equal to zero to maintain mass balance.

There are several significant sources of uncertainty in the calculation of the residual circulation. It is difficult to get accurate or precise quantitative estimates of uncertainty due to the combination of steps in the calculation. Errors in calculating the heating rates have been estimated at around 10% by comparing with a line-by-line calculation (Olaguer et al., 1992). If the heating rates are biased high or low, the mass correction, which constrains the integrated flux to zero, may exaggerate or reduce the error. Shine (1989) found that the sign of the computed circulation in the upper stratosphere and mesosphere can change depending on the correction method used. Temperature biases will affect the spatial distribution of errors. Percent uncertainties increase as the heating rates get small lower in the stratosphere. A best guess of uncertainty in the calculated vertical velocity from comparing radiative, dynamical, and model estimates is about 30% at 50 hPa. This rises to near 100% at 100 hPa and hence also argues for a choice of a reference surface at 50 hPa.

3.1.2 Tracer Mixing Ratio Data

Instruments on board UARS allow nearly simultaneous measurement of different chemical species at various vertical resolutions. Measurements in this study are taken from three instruments: the Microwave Limb Sounder (MLS), the Cryogenic Limb Array Etalon Spectrometer (CLAES), and the Halogen Occultation Experiment (HALOE). Data sets used are version 3 for MLS, version 17 for HALOE and version 7 for CLAES. UARS trace gas mixing ratios from these instruments are processed and interpolated as outlined in Table 3.1 for the time periods and UARS standard pres-

Table 3.1: UARS Trace Species Data

Instrument & Species	Pressure (hPa)	Period	Validation Reference	Error Estimate (Type)	Interpolation Method
MLS O_3	46,22	10/91-10/95	Froidevaux et al. (1996)	~10% (total)	90-day running mean
HALOE O_3	68,46,32,22	10/91-10/95	Brühl et al. (1996)	5% (total)	no interpolation
HALOE CH_4	68,46,32,22	10/91-10/95	Park et al. (1996)	15% (total)	yaw period average
CLAES O_3	68,46,32,22	1/92-4/93	Bailey et al. (1996)	13% (systematic)	90-day running mean
CLAES N_2O, CH_4	68,46,32,22	1/92-4/93	Roche et al. (1996)	15% (systematic) 7% (random)	90-day running mean
CLAES CF_2Cl_2	68,46,32,22	1/92-4/93	Nightingale et al. (1996)	17% (total)	90-day running mean

HALOE, Halogen Occultation Experiment; CLAES, Cryogenic Limb Array Etalon Spectrometer; MLS, Microwave Limb Sounder.

sure levels indicated. Vertical resolution is approximately 2 to 3 km for HALOE and CLAES, while MLS resolution is about 1.5km (not all levels are shown). Table 3.1 also includes references to validation papers for each instrument and species. Estimated uncertainties in the UARS data, either total error or systematic error, are also given in Table 3.1 from the references noted. Uncertainties for various instruments are generally reported as less than 15% (Table 3.1). There are two spectrometer channels that register ozone on the CLAES instrument, here designated on the ozone plots as CLAES 1 (780 cm^{-1}) and CLAES 2 (792 cm^{-1}), see Bailey et al. (1996) for further CLAES validation details.

Because of the geometry of the UARS orbit, observations poleward of 30° latitude are only available on alternate months, so considerable interpolation is required to form a complete set of monthly means. Two different interpolation schemes were employed to generate continuous zonally averaged monthly mean mixing ratio fields as indicated in Table 3.1. One scheme used a smoothed 90-day running time mean at each latitude, which was then averaged for each calendar month. The other scheme

averaged available latitude data around the times when the instruments shifted hemispheres and then interpolated these periods to calendar months. The integrated mass flux calculations were found to be insensitive to alternative interpolation methods of generating continuous fields from the complex UARS orbital geometry. Interpolated fields agree qualitatively with results published in validation papers and with species climatologies. Because of missing data points and large gaps due to limited sampling, HALOE ozone data was not interpolated in the extratropics due to insufficient coverage during parts of this period. HALOE methane data has been interpolated in the extratropics to derive monthly means.

A time-latitude contour plot of the continuous field for ozone, based on data from the MLS instrument at 50 hPa after interpolation, is shown in Figure 3.2. There is an ozone minimum in the tropics and higher values at the poles where downwelling brings ozone-rich air from higher in the stratosphere. These extratropical maxima in the ozone mixing ratio have a distinct annual cycle in each hemisphere, which will be further discussed below. Evidence of the Antarctic springtime "ozone hole" can be seen at high latitudes in the southern hemisphere during October and November. The simultaneous retrieval (in a monthly mean sense) of the same species by two or more instruments provides an additional step for validation of the reported mixing ratios. Such comparisons are more fully treated in the references in Table 3.1. Intercomparisons in this paper will be confined to differences in the integrated mass flux calculated by using trace gas mixing ratio fields from different instruments. While random errors do not affect the resulting mass flux, biases between instrument records will affect the resulting mass flux calculations and add an additional degree of uncertainty.

3.2 Results

The mixing ratio data are combined with the stream function using Equation 3.3 and integrated separately for the whole globe, for each hemisphere, and for those

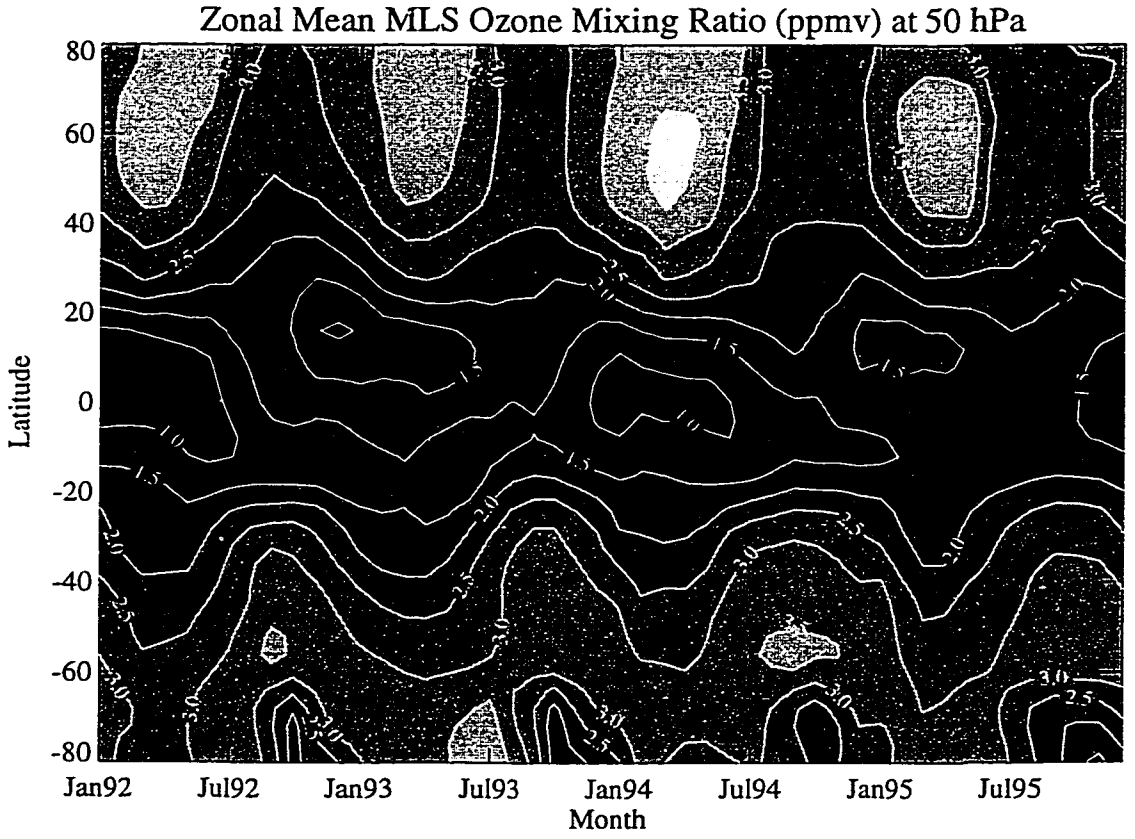

Figure 3.2: Time-latitude plot of zonally averaged ozone mixing ratio in parts per million by volume at 50 hPa from Microwave Limb Sounder (MLS) data.

regions of extratropical downward motion, and tropical upward motion. Mass flux estimates will be reported for the isobaric surface of 50 hPa, which is approximately the lowest level where full UARS coverage of good quality is available. Mass flux estimates are thus available from isobaric surfaces that represent the lower portion of the stratospheric overworld but not its lower boundary. Fluxes in the tables are reported as annual averages of the monthly zonal means shown in the figures. Annual means are constructed by integrating the flux using Equation 3.3 over all latitudes for each month and then averaging the monthly integrated flux over the 48 months of the data record. Monthly fluxes are reported in kilograms per second, but for comparability with other studies, annual averages of monthly fluxes will be converted to teragrams (Tg) per year. Average mass fluxes for nitrous oxide and CF_2Cl_2, derived from CLAES data, are an average of four running 12-month means because of the short 16-month time series.

Mass flux results for each gas will be discussed separately, beginning with ozone. A simple box model is used to infer the flux of ozone at 100 hPa, using estimates of mixing and photo-chemistry. The 100 hPa surface is approximately contiguous with the upper mean boundary of the lowermost stratosphere. In this formulation the flux across this level approximates the level at which stratosphere-troposphere exchange occurs. The estimation of the ozone flux across the 100 hPa surface uses the knowledge that the tropical ozone mixing ratio at 100 hPa is an order of magnitude lower than at 50 hPa, low enough to neglect the upward flux across 100 hPa, where the residual circulation is highly uncertain. A similar analysis is not possible for those species such as methane, nitrous oxide, and CF_2Cl_2 which have sources that are almost exclusively in the troposphere. Their upward flux in the tropics cannot be neglected. Following results for ozone fluxes, the 50 hPa fluxes for nitrous oxide, methane, and CF_2Cl_2 are presented for comparison with other work. CF_2Cl_2 flux estimates are also converted to a transient stratospheric lifetime estimate for comparison with other studies. In this region of the atmosphere, it is expected that the temporal and meridional distribution

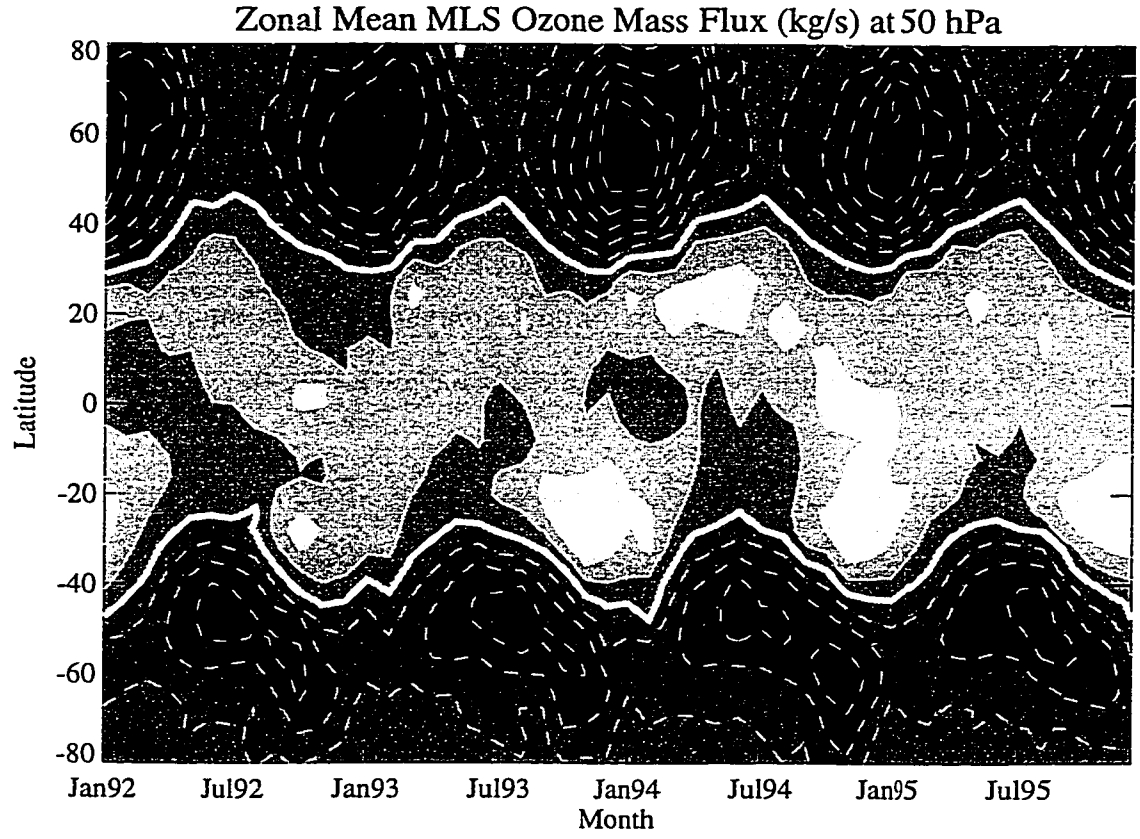

Figure 3.3: Zonally averaged ozone mass flux at 50 hPa from Microwave Limb Sounder (MLS) data and residual circulation in kilograms ozone per second (kg O_3/s). Contour interval of 1.8 x 10^{-4} kg O_3/s. Dotted contours indicate negative (downward) fluxes. Zero contour plotted as a thick white line.

of the flux will be dominated by variations in the circulation rather than chemical production or loss (Brasseur and Solomon, 1986).

3.2.1 Ozone Fluxes

The mass flux of ozone as a function of latitude and calendar month calculated using mixing ratios from the MLS instrument at the 50 hPa level is illustrated in Figure 3.3. An annual cycle is clearly evident at most latitudes, with maximum upward ozone fluxes in the subtropical summer hemisphere and maximum downward fluxes corre-

sponding to the winter season in the extratropics. A comparison of the ozone mixing ratio (Figure 3.2), and the ozone mass flux (Figure 3.3) at 50 hPa, clearly shows that the annual cycle in ozone mixing ratio, particularly in midlatitudes, lags the annual cycle in ozone mass flux by 2-3 months. The lag is consistent with transport of ozone-rich air from higher altitudes. If the annual cycle in ozone mixing ratio at 50 hPa were dominated by photochemical production then the maximum concentration would occur closer to summer at high latitudes and not lag the annual cycle in the ozone flux.

The meridional variability of the ozone mass flux also appears to be regulated primarily by meridional dependence of the residual circulation, rather than meridional variations in the ozone concentration itself. Figure 3.4 shows the average over 4 years of the "amplitude" of the annual cycle in mass flux, which can be defined as the maximum monthly value minus the minimum value (for each latitude) during a 12-month annual cycle. The annual cycle of ozone mass flux has a peak amplitude in midlatitudes (Figure 3.4a), which is strongly correlated with the peak amplitude of the annual cycle in air mass flux (Figure 3.4b). Large amplitudes in the annual cycles in air mass and ozone flux extend significantly farther poleward in the northern hemisphere than in the southern hemisphere. This pattern does not correspond to any pattern of ozone production.

Estimates of the mass flux of ozone integrated over the tropical upwelling region are presented in Figure 3.5a for various instruments. There is good agreement between HALOE and MLS both in the time variation and absolute value of the upward tropical mass flux. However, the two spectrometer channels on CLAES (designated here CLAES 1 and CLAES 2) give results which are generally higher (CLAES 1), or lower (CLAES 2), than for other instruments. Ozone mass fluxes in the tropical upwelling region calculated by using HALOE data are virtually identical to a similar calculation made with MLS data. When integrated for all latitudes (Figure 3.5b), the CLAES channels indicate a smaller integrated downward mass flux than MLS, indicating

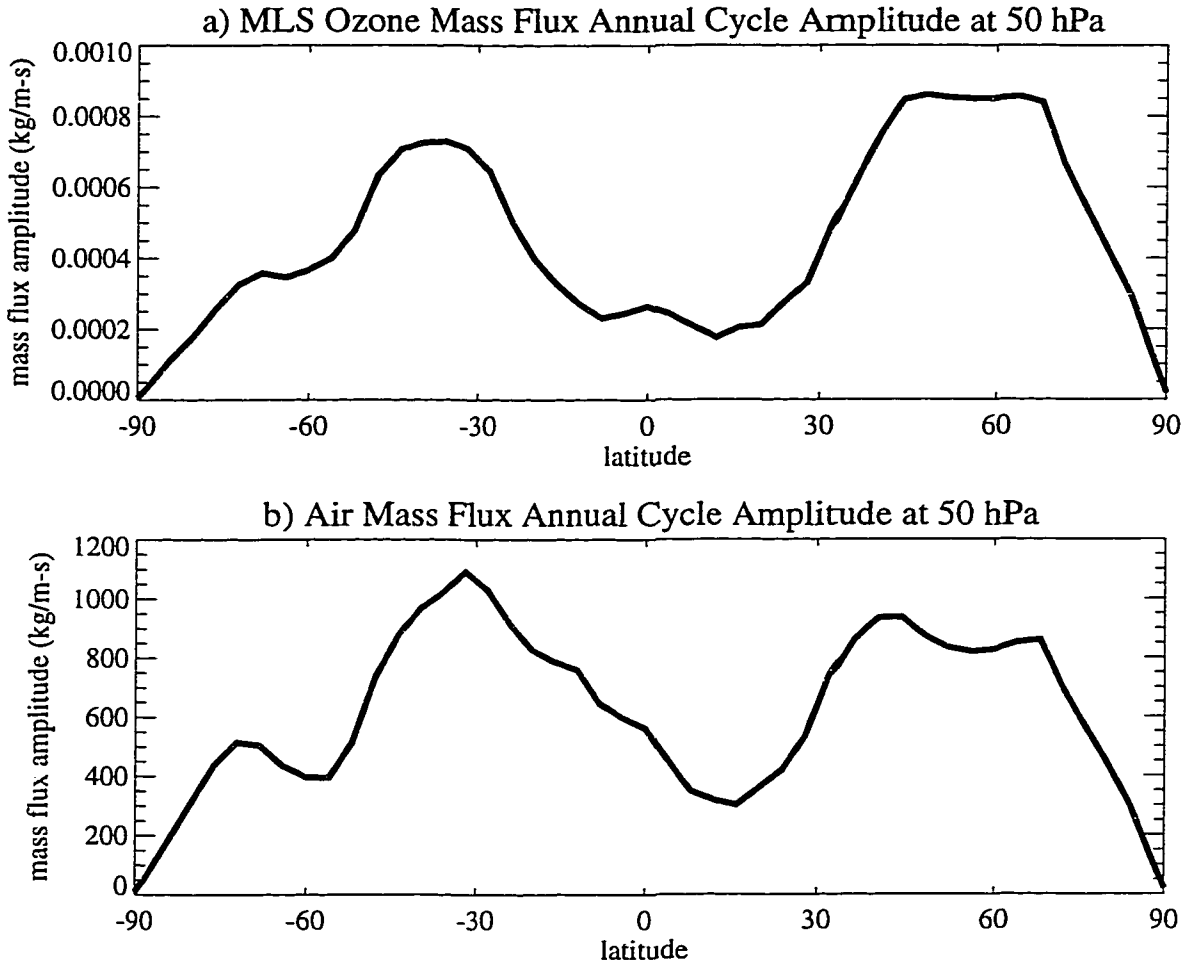

Figure 3.4: Zonally averaged amplitude of annual cycle of mass flux in kilograms per second (kg/s) as a function of latitude averaged over 4 years. (a) Microwave Limb Sounder (MLS) ozone mass flux in kilograms ozone per second (kg O_3/s) (b) air mass flux in kilograms air per second (kg air/s).

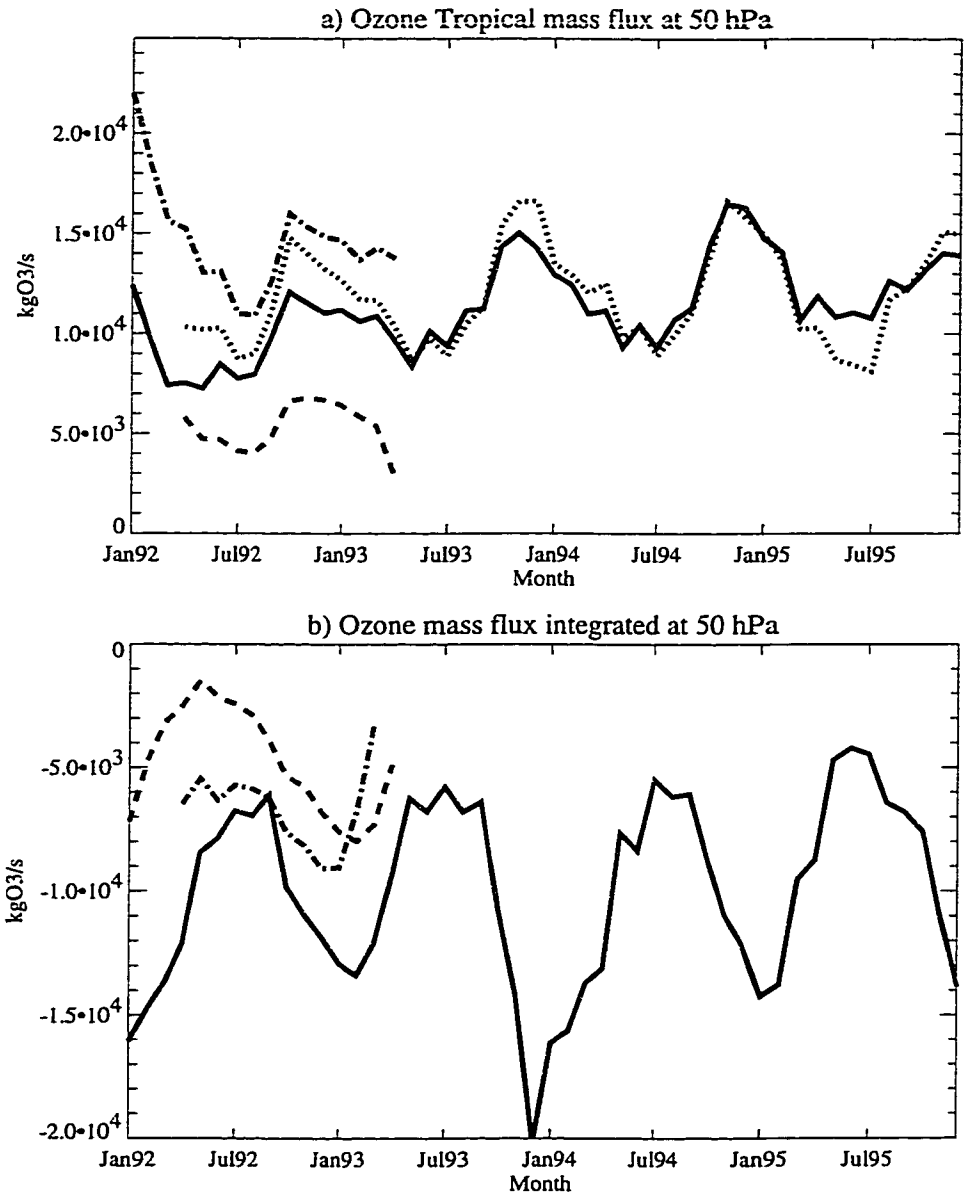

Figure 3.5: Ozone mass fluxes at 50 hPa from Microwave Limb Sounder (MLS) (solid), Halogen Occultation Experiment (HALOE) (dotted). Cryogenic Limb Array Etalon Spectrometer (CLAES) channel 1 (dotted-dashed) and CLAES channel 2 (dashed). (a) Integrated over the tropical upwelling region. (b) Globally integrated.

Table 3.2: Ozone Mass Flux (in Teragrams per year)

Pressure (hPa)	SH Extratropics	Tropics	NH Extratropics	Net Mass Flux
67	-280	330	-350	-300
50	-290	360	-380	-310
32	-350	700	-330	-20
20	-380	970	-360	230

SH, Southern Hemisphere; NH, Northern Hemisphere.

differences in the extratropical flux estimates. HALOE mixing ratios have insufficient coverage of high latitudes to estimate global mass fluxes.

Quantitative estimates of the total mass flux of ozone are taken from MLS, which has the longest available time series with global coverage. MLS-derived ozone mass fluxes show virtually no linear trend over the short data period. The gross upward and downward fluxes and globally integrated net fluxes for several pressure levels are presented in Table 3.2. The estimated average net downward flux of ozone is 310 Tg ozone per year at the 50 hPa level. Integrated mass flux estimates at 50 hPa in the stratosphere show a strong cancellation between upwelling in the tropics and downward transport in the extra-tropics. Table 3.2 also illustrates that tropical fluxes increase rapidly with altitude, reflecting the increasing ozone concentration due to net production in that region. Table 3.2 also illustrates that extratropical fluxes (particularly in the northern hemisphere) vary relatively slowly with height. At 20 hPa there is a net upward ozone flux, even though the maximum ozone concentration is near 10 hPa (Brasseur and Solomon, 1986).

The net mass flux (at 50 hPa) is the net of a large downward extratropical flux of approximately -670 Tg O_3/yr and an upward flux of 360 Tg O_3/yr. The fact that the net flux at 67 hPa is nearly equal to that at 50 hPa might suggest that by simple extrapolation the net flux across the 100 hPa surface from the overworld into

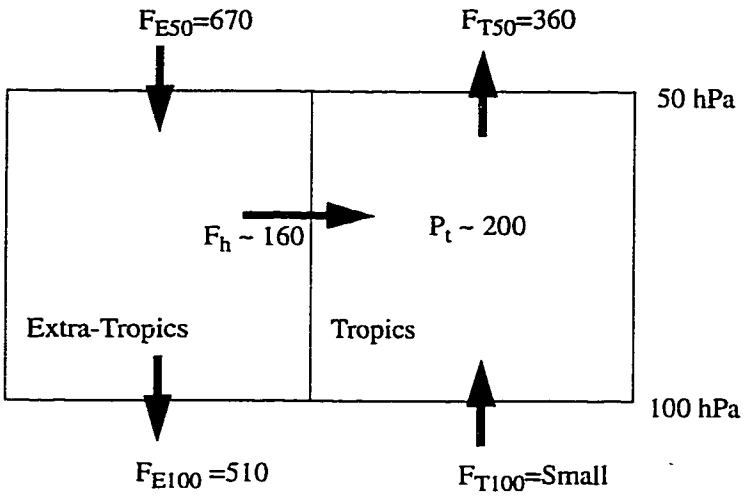

Figure 3.6: Two box model of the 50 to 100 hPa layer showing the ozone budget. Numbers show our best estimate of fluxes and net production in units of Tg O_3/yr.

the lowermost stratosphere must be about -300 Tg O_3/yr. However, because ozone mixing ratios at 100 hPa in the tropics are very small (~0.1 ppmv), the upward flux at 100 hPa must be very small. There is considerable mixing between midlatitude and tropical air in the lower few kilometers of the stratosphere above 100 hPa (Rosenlof et al., 1997). Furthermore, the MLS ozone data have large error bars at 67 hPa, so that the flux values at that level are less certain, which also argues for use of the 50 hPa level as the primary reference level for vertical fluxes. Part of the error is due to the fact that the 67 hPa level is interpolating data between 50 hPa and 100 hPa. However, it would be useful to estimate the net flux of ozone at a level closer to the lower boundary of the stratospheric overworld. Such an analysis will now be performed using a simple two-box model.

The model is pictured in Figure 3.6. In this model the mass of the atmospheric layer between 50 and 100 hPa is divided into two equal parts, a tropical box representing the air equatorward of 30° latitude and an extratropical box representing the air poleward of 30° in both hemispheres. If we assume that the flux of ozone across the 100 hPa surface in the tropics can be neglected, then the flux F_{T50} across the 50

hPa surface in the tropics is given by:

$$F_{T50} = P_T + F_h \tag{3.4}$$

where P_T designates the net production (difference between production and loss, see equation 3.7 and discussion thereafter) in the tropical box, and F_h designates the horizontal flux into the tropics from the extratropics. For the extratropics the mass budget can be expressed as:

$$F_{E50} = F_{E100} - F_h \tag{3.5}$$

where F_{E50} and F_{E100} designate the fluxes across the 50 and 100 hPa surface in the extratropics, respectively (negative values for downward fluxes). We have neglected chemical production and loss in the extratropical box since this layer is transport dominated except in the summer when fluxes are very weak.

From Equation 3.5 it is clear that the maximum possible downward flux across the 100 hPa surface occurs if there is no horizontal mixing into the tropics across the subtropical "transport barrier." In that case the mass fluxes at 50 and 100 hPa must be equal. Furthermore, in an annual average the ozone transfer from the lowermost stratosphere into the troposphere must be equal to the transfer into the lowermost stratosphere from the overworld. Thus the maximum possible transfer of ozone into the troposphere according to our analysis is 670 Tg O_3/yr of which 57% (380 Tg O_3/yr) is in the northern hemisphere extratropics and 43% (290 Tg O_3/yr) is in the southern hemisphere extratropics.

It is known, however, from analysis of the vertical profiles of long-lived tracers in the tropics (Minschwaner et al., 1996; Mote et al., 1996) that there is significant transport and mixing of extratropical air into the 50-100 hPa layer in the tropics. Thus the above estimate cannot be correct. The contribution from horizontal mixing can be estimated by assuming that:

$$F_h = M(\chi_E - \chi_T)/\tau_{mix} \tag{3.6}$$

Here M (= 1.3×10^8 Tg air) designates the mass of the tropical box; χ_T and χ_E designate, respectively, the ozone mass mixing ratios in the tropical box, and in the latitude range of 30°-40°in the extratropics (which is assumed to be the region from which mixing into the tropics occurs); τ_{mix} designates the timescale for this mixing.

If we let the 70 hPa level represent the mean for the 50-100 hPa layer, then from ER-2 observations and model results quoted by Murphy et al. (1993), the mean ozone mass mixing ratio in the tropical box is 0.8×10^{-6} and in the extratropics is in the range of 1.6-2.4 $\times 10^{-6}$.

Minschwaner et al. (1996) give a range of 9-18 months for τ_{mix}, with a best estimate of 12 months. Volk et al. (1996) give a similar range of 11-16 months with a best estimate of 13.5 months. Using the wider range from Minschwaner et al. (1996) and Equation 3.6, we then can derive a best estimate F_h = 160 Tg O_3/yr and a range of 70-280 Tg O_3/yr.

The possible range of values of F_h can be further narrowed with the aid of Equation 3.4. To do so we need to estimate the net production (P_T). We define the gross photochemical production rate as:

$$P_{gross} = M\chi_T/\tau_p \tag{3.7}$$

where τ_p is the chemical replacement time for ozone in the tropical box. According to Ko (1993) the range of τ_p near 70 hPa in the tropics for several two-dimensional models is 1/3 - 2/3 year. From Equation 3.7 this yields a range for P_{gross} of 160-310 Tg O_3/yr. However, according to Ko (1993), chemical loss rates in the same region are about 10% of gross production. Thus the net production P_T = 140-280 Tg O_3/yr. Substituting into Equation 3.4, we find that F_h must lie in the range of 80-220 Tg/yr, which is compatible with the best estimate of F_h derived from Equation 3.6. Using our best estimate of F_h, F_{E50} and the 50 hPa flux from Table 3.2 gives an estimate which implies an annual downward flux of ozone across the tropopause of 510 Tg O_3/yr with a range of 450-590 Tg O_3/yr. This estimate is compared with similar results

Table 3.3: O_3 Flux to Troposphere in Teragrams/year (10^{10} molecules $cm^{-2}s^{-1}$)

Source	Value	Range	Method (Altitude if Known)
This study	510 (4.0)	450-590 (3.5-4.6)	residual circulation (100 hPa)
Roelofs and Lelieveld (1996)	459 (3.6)		3-D model[a]
Murphy (1994)	450 (3.5)	200-870 (1.5-6.8)	N_2O-O_3 correlation
World Meteorological Organization (1986) (GCM estimates)		320-850 (2.5-6.6)	3-D models
Holton and Lelieveld (1995)	528 (4.1)		3-D model (100 hPa)
Danielsen and Mohnen (1977)	1000(7.8)		PV - ^{90}Sr - O_3 correlation

[a]Roelofs and Lelieveld (1996) use a dynamical definition of the tropopause as 3.5 PVU in the extratropics and a thermal definition of the tropopause in the tropics.

from previous work in Table 3.3. Recent estimates of the stratosphere-troposphere exchange of ozone using models (Roelofs and Lelieveld, 1996; Holton and Lelieveld, 1995) and correlations (Murphy, 1994) agree well with the range of estimates provided by this method. In particular, the estimate of the ozone exchange is in good agreement with calculations of Holton and Lelieveld (1995) across the same isobaric surface.

3.2.2 Methane

Methane is a greenhouse gas whose concentration in the atmosphere is increasing (World Meteorological Organization, 1994), and understanding the cycle of methane is important for fixing the changing radiation balance of the Earth. Methane sources are exclusively terrestrial (Brasseur and Solomon, 1986) and significantly affected by human activity. The source strengths and distribution are still highly uncertain (World Meteorological Organization, 1994). The primary sink for methane in the troposphere and stratosphere is reaction with the hydroxyl radical (OH). Because of uncertainties in the global distribution of OH and the rate constants of the reaction with OH, the strength of this sink is still uncertain. The net difference between

the methane fluxed up from the source regions in the troposphere through tropical upwelling and the methane mass returned from the stratosphere in the extratropics provides an estimate of the loss of methane above that surface. The net methane flux across an isobaric surface into the stratosphere should then be positive and is equivalent to the stratospheric sink.

The stratospheric destruction of methane is a small fraction of the total estimated loss in the troposphere due to reaction with OH, which is estimated to be 450 $\pm$ 100 Tg/yr (Crutzen, 1991). In the stratosphere, reactions with excited oxygen ($O(^1D)$) and free chlorine (Cl) are of secondary and tertiary importance, respectively. Photolysis is not significant below the stratopause (Brasseur and Solomon, 1986). Comparison between calculations and photochemical model estimates of the stratospheric methane sink (largely due to reaction with OH) can help constrain the reaction rates between OH and methane, and further constrain the total annual loss of methane, an important greenhouse gas.

Methane fluxes can be calculated with mixing ratio data from both the HALOE and the CLAES instruments. Fluxes estimated with CLAES methane mixing ratios are significantly lower than those estimated with HALOE data, as illustrated in Figure 3.7. The monthly tropical (Figure 3.7a) agreement is good, but when integrated between the poles (Figure 3.7b), there is a distinct bias between the two calculations, a result of higher CLAES mixing ratios in the extratropics and thus a stronger estimate of the extratropical downward flux in the winter season in each hemisphere when mixing ratios from the CLAES instrument are used. The longer time series of HALOE data permits better evaluation of the annual cycle (Figure 3.7b). Using Equation 3.3, mixing ratios from the HALOE instrument are combined with the stream function to estimate the latitudinal distribution of the methane flux in Figure 3.8. The timing and the meridional distribution of the methane flux in Figure 3.8 shows marked similarity to that of the ozone flux in Figure 3.3, further evidence that latitude and time variations of the residual circulation rather than of the tracer mixing ratio control the

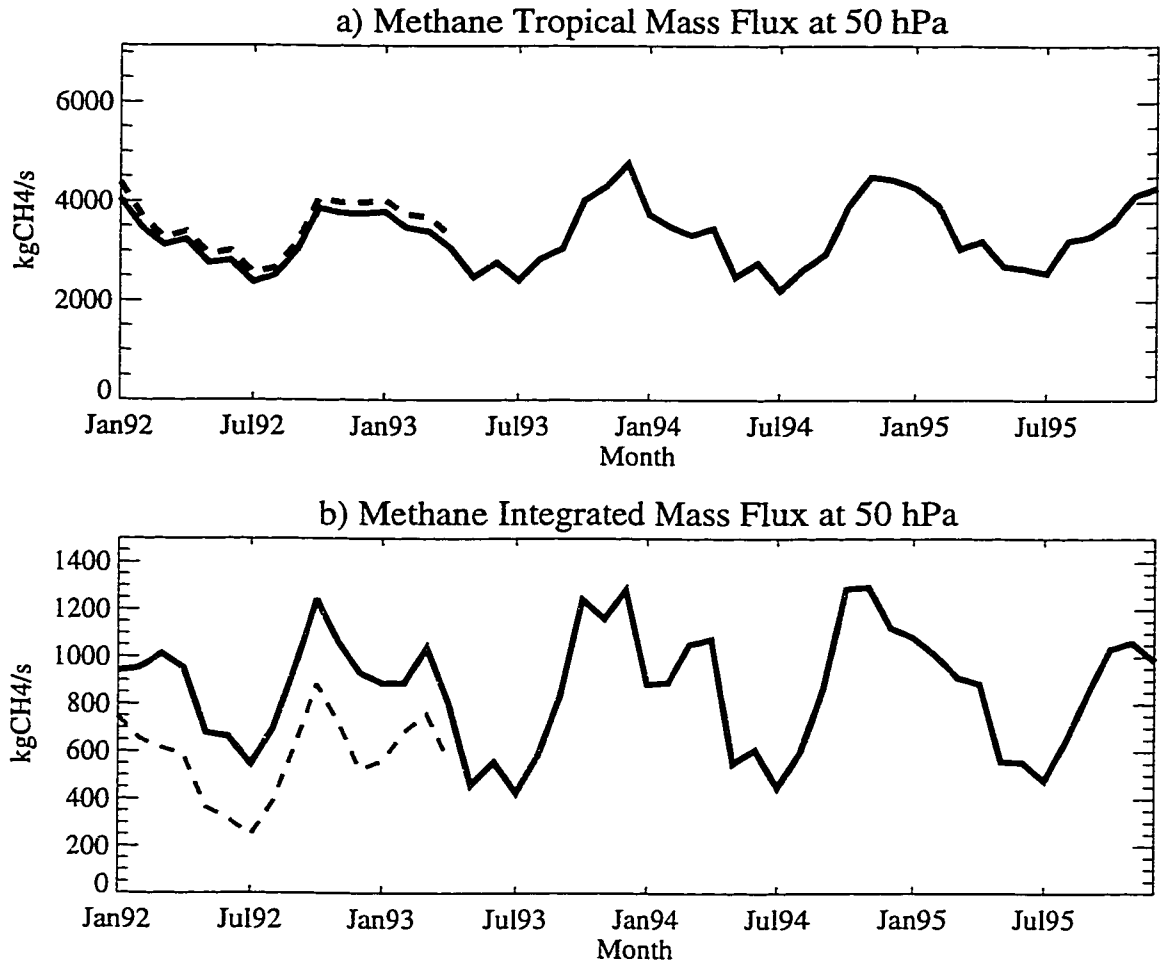

Figure 3.7: Methane mass fluxes at 50 hPa from HALOE (solid) and CLAES (dashed). (a) Integrated over the tropical upwelling region. (b) Globally integrated.

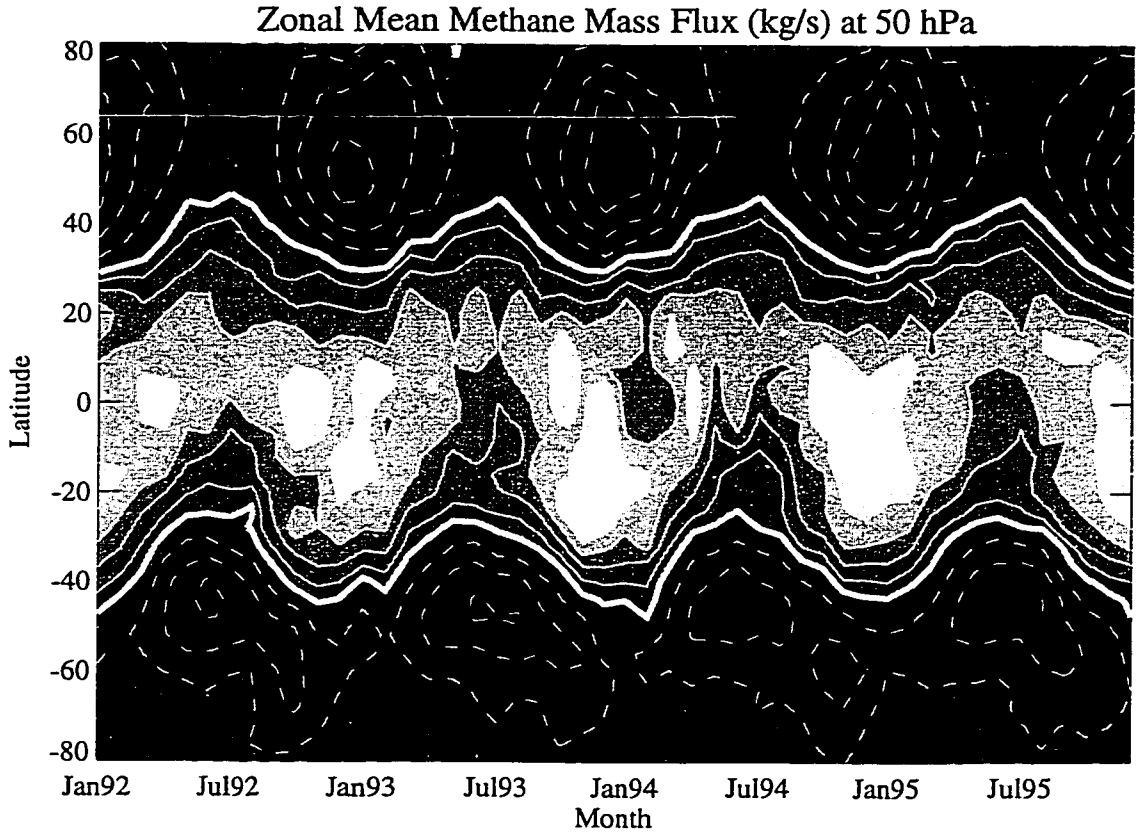

Figure 3.8: Zonally averaged methane mass flux using HALOE mixing ratios and residual circulation at 50 hPa. Contour interval of 2.7 x 10^{-5} kg CH4/s. Dotted contours indicate negative (downward) fluxes. Zero contour plotted as a thick white line.

variation of the flux.

Summing the flux over all latitudes and taking an annual average over the 4-year period of the data record yields an estimate for the 50 hPa flux using HALOE mixing ratio data of 27 Tg CH_4/yr. Other estimates shown in Table 3.4 give a range of values for the stratospheric loss of methane from 10 to 47 Tg CH_4/yr, mostly based on photochemical reaction rates and models. Note that the flux estimate presented here is altitude dependent and is based on a 50 hPa reference level. Other studies may have a similar altitude dependence. Altitudes were not reported in the literature.

Table 3.4: Methane Mass Flux in Teragrams of Methane per year

Source	Strat Loss	Range	Method
This study HALOE (50hPa)	27		residual circulation
Crutzen (1983)	47		data & photochemical model
WMO (1994)[a]	40	25-55	Unknown
Khalil et al. (1993)	16		photochemical model
Crutzen (1991)	10	5-15	photochemical model
Fung (1991)	33		3D Model

[a]WMO = World Meteorological Organization

Nonetheless, this estimate provides an observational check on calculated and modeled estimates of the methane loss in the stratosphere.

3.2.3 Nitrous Oxide

The sources of nitrous oxide are almost exclusively terrestrial, and the main sinks are photolysis in the stratosphere (Jaffe, 1992). As with methane, the net flux (upward minus downward) across an isobaric surface in the stratosphere is equivalent to the loss above that surface. The mass flux of nitrous oxide across 50 hPa isobaric surface using Equation 3.3 is presented in Figure 3.9. The available record of mixing ratios from the CLAES instrument is only 16 months from January 1992 to April 1993. The temporal scale is the same as the other time-latitude plots previously presented for ozone (Figures 3.2 and 3.3) and methane (Figure 3.8). The latitudinal distribution of the N_2O flux is broadly similar to that for ozone and methane, indicating again the primacy of latitude-time variations in the residual circulation. Summing the flux in Figure 9 over all latitudes for each month and taking a running 12-month average over the 16-month record yields an annual upward flux into the stratosphere of 8 Tg

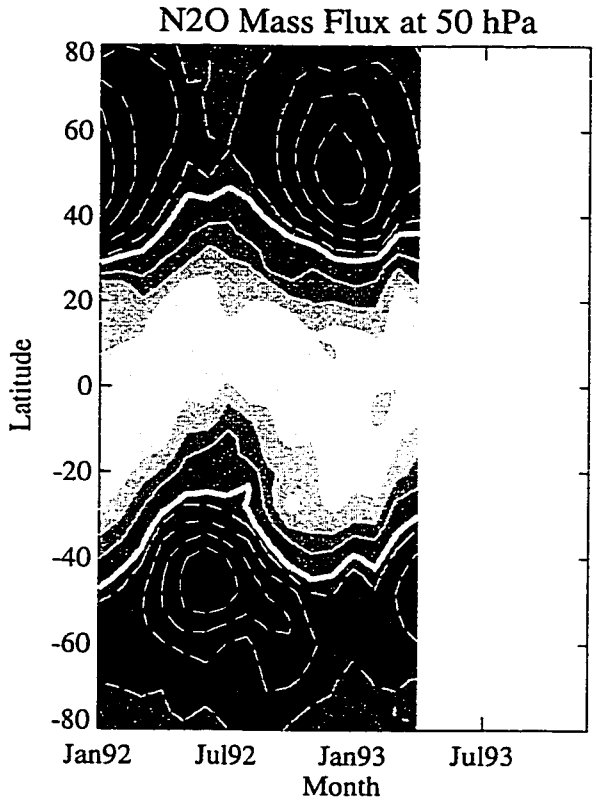

Figure 3.9: Zonally averaged N_2O mass flux using CLAES mixing ratios and residual circulation at 50 hPa. Contour interval of 1.2 $\times 10^{-5}$ kg N_2O/s. Dotted contours indicate negative (downward) fluxes. Zero contour plotted as a thick white line.

N/yr. The nitrous oxide flux is stated in mass units of nitrogen rather than nitrous oxide for ease of comparison to other work.

Many estimates of the flux of nitrous oxide from the troposphere into the stratosphere have been made from models, correlated or calibrated with observations. Estimates of N_2O mass flux using the residual circulation and mixing ratios from the CLAES instrument (Table 3.5) are within the range of estimates of Crutzen (1983) using photochemical rates constrained by observations but generally lower than estimates published by World Meteorological Organization (1994) and Ko et al. (1991) using models. The altitudes of these estimates are unknown, but any discrepancy

Table 3.5: N_2O Mass Flux in Teragrams of N per year

Source	Mass Flux	Range	Method
This study (50hPa)	7.7		residual circulation
WMO (1994)[a]	12.3	9-17	2-D models
Ko et al. (1991)		13-17	2-D model photochemical rates
Crutzen (1983)		6.8-10	observations & photochemical rates

[a]WMO = World Meteorological Organization

should be small, as there is little photochemical destruction of N_2O below 50 hPa. For comparison with these estimates, World Meteorological Organization (1994) reports total N_2O sources of 6.2–19.2 Tg N/year (of which 2.1–6.3 Tg N/year is anthropogenic and is 4.1–12.2 Tg N/year is natural). The large range is due to uncertainty in the oceanic and terrestrial soil sources. The atmospheric increase of N_2O is 3.1–4.7 Tg N/year (World Meteorological Organization, 1994).

3.2.4 CF_2Cl_2

The artificial chlorofluorocarbon compound CF_2Cl_2 has been a serious concern as a source of free chlorine to catalyze ozone destruction, particularly through heterogeneous chemistry in the Antarctic springtime stratosphere. As for nitrous oxide, CF_2Cl_2 has a tropospheric source and mainly stratospheric photolytic sinks. The net flux across the 50 hPa surface can be used to estimate the stratospheric sink term. A detailed view of the annual and meridional flux of CF_2Cl_2 calculated by using Equation 3.3 is presented in Figure 3.10. The annual cycle has a similar shape to that of the other species observed here, with a broad tropical maximum in the northern hemisphere fall/winter season. The distribution of the CF_2Cl_2 flux in latitude and season is very similar to that observed for methane (Figure 3.8) and nitrous oxide

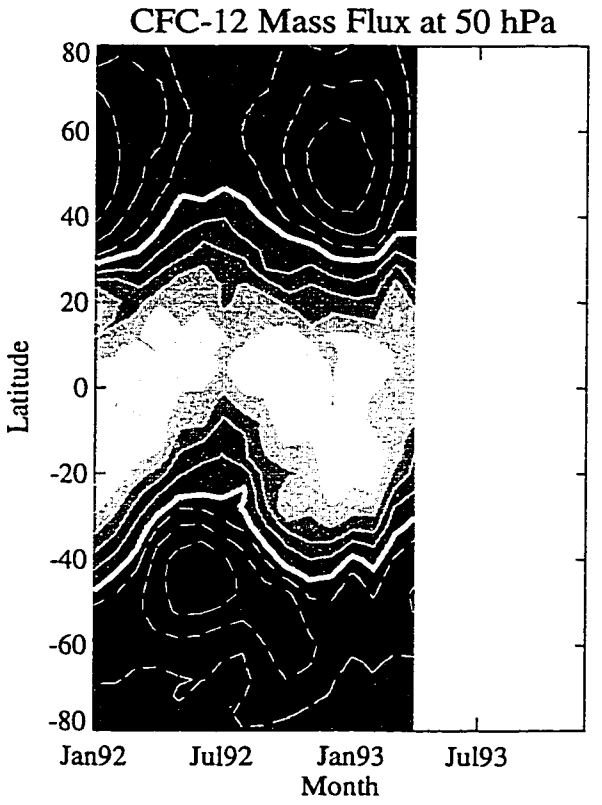

Figure 3.10: Zonally averaged CFC-12 mass flux using CLAES mixing ratios and residual circulation at 50 hPa. Contour interval of 4.1 $\times 10^{-5}$ kg CF_2Cl_2/s. Dotted contours indicate negative (downward) fluxes. Zero contour plotted as a thick white line.

(Figure 3.9). Summing the flux over latitude yields a monthly integrated flux, and averaging that flux with running 12-month means results in an annual flux of 0.081 Tg CF_2Cl_2/yr.

Concern over ozone depletion through anomalous chlorine chemistry has led to many estimates of the atmospheric residence time or "lifetime" of CF_2Cl_2 (e.g., Bloomfield, 1994). The lifetime is the expected (average) time that a molecule remains in the atmosphere before being removed. In the case of CF_2Cl_2, removal is generally by photolysis at wavelengths below 215 nm (Brasseur and Solomon, 1986).

The lifetime can be much longer than the age of air in the stratosphere because a molecule may pass across the tropopause many times before it gets above the ozone maximum and is photolyzed. For a more thorough discussion of atmospheric lifetimes see Rodhe (1992). A longer lifetime implies a longer time horizon for concern over the chlorine-catalyzed destruction of ozone. For CF_2Cl_2, whose major sink is photolytic destruction in the stratosphere, knowledge of the net mass flux across a pressure surface can be used, with some caveats, to infer a chemical lifetime. The lifetime can be calculated assuming that the only significant sink is photolytic destruction above a pressure surface. The chemical lifetime above a pressure surface (τ_p) can then be written as

$$\tau_p = B/F_p \tag{3.8}$$

where B is the mass (burden) of tracer below a pressure p, and F_p is the integrated mass flux across the pressure surface p, corresponding to a net loss above the surface p. The lifetime can be estimated using the estimated flux and the present tropospheric concentration of CF_2Cl_2 of ~500 parts per trillion by volume (pptv) (Elkins, 1993). This relationship is dependent upon the altitude chosen. If significant photolysis or other chemical destruction exists below the altitude at which the flux is calculated, then the estimated lifetime (τ_p) may be too long for the stratosphere as a whole. This lifetime is a transient lifetime for a species whose concentration in the troposphere is changing.

Using Equation 3.8, the lifetime estimate (τ_{50}), from a flux of 0.081 Tg CF_2Cl_2/yr at 50 hPa is 1.2×10^2 years. This "lifetime" estimate at 50hPa compares favorably with other lifetime estimates as illustrated in Table 3.6. Extreme caution should be taken in comparing "lifetime" estimates using different approaches. The literature is often unclear on the methodology employed, and the calculations may be estimating different things. In the case of Bloomfield (1994) and World Meteorological Organization (1994), the lifetime is calculated using a formulation of Equation 3.8 in which F_p is the source of the species and not the sink, which defines a "steady state" life-

Table 3.6: CFC-12 "Lifetime" Estimate in Years

Source	Value	Range	Method
This study (50hPa)	120		residual circulation
WMO (1994)[a]	102		Unknown
Weisenstein (1992)	105		2D photochemical model
Ko et al. (1991)	95		2D model & satellite data
Bloomfield (1994)	122	85-213	source estimates & observed trends

[a]WMO = World Meteorological Organization

time. A steady state lifetime presumes that the sources and sinks are in balance, an assumption which is probably not the case for CF_2Cl_2. The source of CF_2Cl_2 has declined since its use was regulated by the Montreal Protocol. The growth of mass of CF_2Cl_2 rate has declined from 16–20 pptv (0.35–0.44 Tg/yr) in the 1980's to 11 pptv (0.24 Tg/yr) in 1993 (World Meteorological Organization, 1994). Differences in the lifetime estimate are expected. It is most useful to observe that calculations based on sources and sinks are approaching similar ranges as Table 3.6 indicates. Studies using models, however, such as that of Ko et al. (1991), indicate shorter "lifetimes" for CF_2Cl_2. No actual flux numbers were published for these models.

3.3 Summary and Discussion

UARS instruments provide data necessary to evaluate global trace gas mass fluxes in the lower stratosphere for species such as ozone and for longer-lived species such as methane, nitrous oxide and CF_2Cl_2. Analysis of ozone mass fluxes across the 100 hPa surface, using a simple box model calculation, constrains the net ozone flux from the stratosphere into the troposphere to between 450 and 590 Tg O_3/yr. Estimates of methane, nitrous oxide, and CF_2Cl_2 fluxes at 50 hPa yield estimates of net fluxes that

are within the range of other estimates using independent methods. The meridional distribution of upward and downward fluxes of all these species, and the similarity in the annual cycle of fluxes, provides strong confirmation that the meridional and temporal patterns in the mass flux are controlled by meridional and temporal patterns in the residual vertical velocity. The range of uncertainty is largely a function of potential uncertainty in the calculation of the residual circulation.

The methodology used here for species other than ozone will have greater value if the results can be extended to the "lowermost" stratosphere below the 400 K isentrope (approximately 100 hPa), where meridional mixing along isentropes and across isentropes leads to an exchange of mass and chemical constituents between the stratosphere and the troposphere. Continued refinement of the low-altitude (100 hPa and below) observations from the UARS instruments used in this study for mixing ratios and calculation of the residual circulation, as well as use of other data, would be necessary for these estimates. However, there exist several potential limitations and sources of further error. It may be impossible to constrain heating rates sufficiently to get reliable residual circulation estimates using a transformed Eulerian mean formulation at 100 hPa. Second, good quality global mixing ratio data from the lowermost stratosphere may not be available, and coverage may be limited. Finally, asymmetric zonal distribution of trace species on a pressure surface in the lowermost stratosphere near the tropopause may introduce significant errors below 50 hPa. Alternative approaches may be necessary.

Chapter 4

ASSIMILATION DATA AND MODELING TOOLS

In subsequent chapters, the Stratosphere-Troposphere Exchange (STE) of shorter lived species (such as nitrogen oxides) will be considered at the tropopause. At the tropopause the assumption of zonal symmetry made in Chapter 3 at 100 hPa and above is no longer valid, and other approaches will be considered. This chapter more fully describes some of the data and modeling tools used in the remainder of this study. First, an assimilated data set is compared to other assimilated products and observations with respect to those quantities important to stratosphere-troposphere exchange: temperature, the tropopause and the general circulation. A three dimensional chemical transport model and an isentropic trajectory model are also described, and some brief experiments discussed to understand model performance.

4.1 GEOS Data Overview

The dynamical (wind and temperature) fields governing both the transport of chemical constituents and description of the tropopause in the remainder of this study are mostly derived from the Goddard Earth Observing System Data Assimilation System (GEOS-DAS, hereafter GEOS). The GEOS 'analysis' is used to estimate the tropopause in Chapter 5. It also provides the background circulation for the transport studies described in Chapter 6 and the transport and thermodynamic information for the simulation of water vapor in Chapter 7. Tropopause level data from the GEOS system is also analyzed at length in the diagnostic presented in Chapter 8. This Chapter provides a basic description of the GEOS data as well as comparison of the

GEOS fields to other data sets.

In data assimilation, as described by Schubert et al. (1993), an objective analysis scheme is used to input wind and temperature data from an observational network into a General Circulation Model (GCM) of the atmosphere. The resulting output is a set of dynamically consistent 'analyzed' or 'assimilated' fields. The stratospheric version of the GEOS-GCM is more fully described by Coy and Swinbank (1997). This chapter will analyze the performance of the assimilation wind, temperature and derived tropopause fields for studies of stratosphere-troposphere exchange only. For a more exhaustive comparison of GEOS output fields consult Schubert et al. (1995).

The GEOS data employed in this study is officially termed the GEOS-1 assimilation system, and the runs cover the general period from 1995-1998 in support of the Stratospheric Tracers of Atmospheric Transport (STRAT) aircraft campaigns. Data is available on a 2.5° longitude by 2° latitude grid with a maximum time resolution of 6 hours. For many of the applications in this study, daily time resolution has been used. The vertical resolution of GEOS data varies with the application. The chemical transport model (see Section 4.5) has been run with either 29 or 46 level assimilated data from the surface to about 0.1 hPa, which is output directly from the GEOS GCM (see section 4.5).

For the diagnostic analyses in the following Chapters, GEOS fields are available on 18 pressure levels (model inputs use different levels) in the vertical from the surface to 0.4 hPa. Potential vorticity and potential temperature fields are used for the analysis of tropopause height in Chapter 5 and Chapter 6, while wind data interpolated to the tropopause is used in Chapter 8. In Sections 4.2 and 4.3 GEOS temperature and tropopause height will be compared to other assimilation data products from the United Kingdom Meteorological Office (UKMO) assimilation system (Swinbank and O'Neill, 1994) and the assimilation system operated by the National Centers for Environmental Prediction (NCEP). UKMO and NCEP data are available on the same levels as GEOS data. In Section 4.4 the general circulation of the GEOS winds and

Table 4.1: GEOS Assimilation Vertical Levels

Pressure (hPa)	Log-Pressure Height (km)	Press (hPa)	Log-P Height (km)
1000.0	0.0	100.0	16.1
850.0	1.1	70.0	18.6
700.0	2.5	50.0	21.0
500.0	4.9	30.0	24.5
400.0	6.4	10.0	32.2
300.0	8.4	5.0	37.1
250.0	9.7	2.0	43.5
200.0	11.3	1.0	48.4
150.0	13.3	0.4	54.8

residual circulation important for transport in analyzed. The implications of these transport differences are explored with a trajectory model in Section 4.7

Vertical levels for the 18 level GEOS data (and other assimilation data) are illustrated in Table 4.1 along with their log-pressure height. The resolution of the GEOS data around the tropical tropopause is about 2km, and 1.5 km at the altitude of the extratropical tropopause. Comparisons of wind, tropopause and temperature fields performed below in Sections 4.4, 4.3 and 4.2 use this 18-level data, on the same grid for all assimilation data.

4.2 Temperature

The temperature structure in the assimilation data is used to calculate the potential vorticity fields (and hence place the tropopause). The temperature fields are also important for their basic interaction with the general circulation through the thermal wind relation (Holton, 1992). The temperature of the tropical tropopause region is

also critically important in defining the stratosphere-troposphere exchange of water vapor (see for example, Mote (1995); Mote et al. (1996) and Newell and Gould-Stewart (1981)), a topic more fully developed in Chapter 7. In this section, the temperature structure of the GEOS assimilation will be studied in relation to several other assimilation products. In particular, the GEOS temperature reproduces the key features in the upper troposphere and lower stratosphere, as indicated in Figure 4.1 (solid contours). There is a strong temperature gradient from the mid-troposphere into the stratosphere, and the tropics are warmer than the midlatitudes at a given pressure level up to 200 hPa. The minimum of the temperature field in the tropics is found at about 100 hPa, around or slightly above the tropical tropopause. Note that the cold point is usually not at 100 hPa, but on average slightly above (Reid, 1998), as indicated in the zonal mean snapshot of Figure 4.1a.

It is instructive to focus on the location of the coldest point in the lower and middle atmosphere, which generally occurs near or just above the tropical tropopause (Reid, 1998). This minimum temperature is critical for determining the water vapor distribution into the stratosphere (see Chapter 7). A comparison of the zonal mean monthly temperature structure between GEOS and NCEP data in Figure 4.1b clearly indicates that the minimum (cold point) temperatures in the GEOS analyses are on average 1–2°K warmer than NCEP reanalysis temperatures, but that the distribution and altitude of the cold point is similar to NCEP and radiosonde data (Reid, 1998). As depicted in Figure 4.1b, the difference is largest in the tropics from October to January, but is larger than 1°K throughout the year. Schubert et al. (1995) have performed a similar comparison with fields from the European Center for Medium Range Weather Forecasts (ECMWF) and found that GEOS fields in the tropics from 200 hPa to 100 hPa are 2° K warmer in the climatological average than ECMWF temperature fields in both Northern Hemisphere winter (December, January and February) and summer (June, July and August) (see Schubert et al., 1995, figures 10b and 11b).

There are also differences in the upper troposphere below the cold point. While

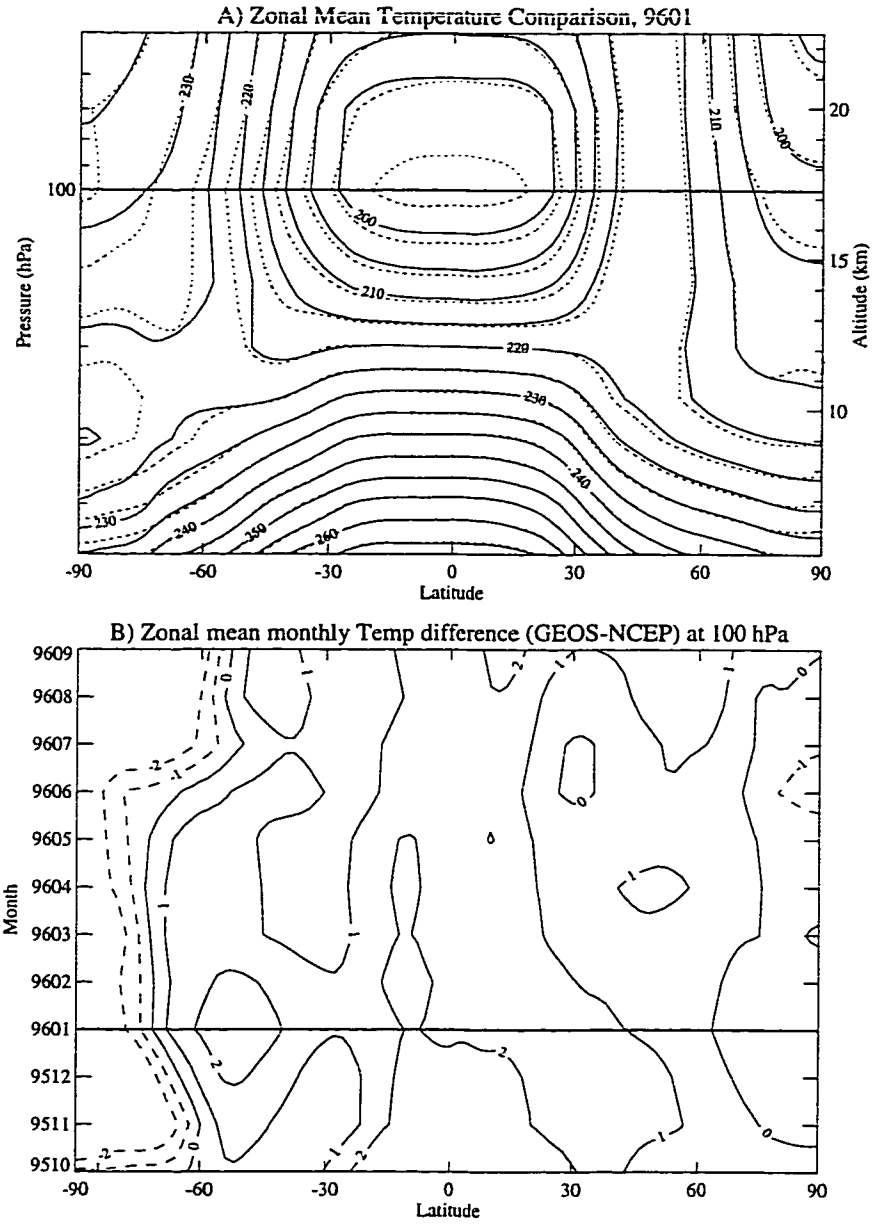

Figure 4.1: Zonal monthly mean temperature comparison between GEOS and NCEP data. Solid- GEOS, Dotted- NCEP. A) By height in the upper troposphere and lower stratosphere for January 1996. B) Difference plot GEOS-NCEP at 100 hPa..

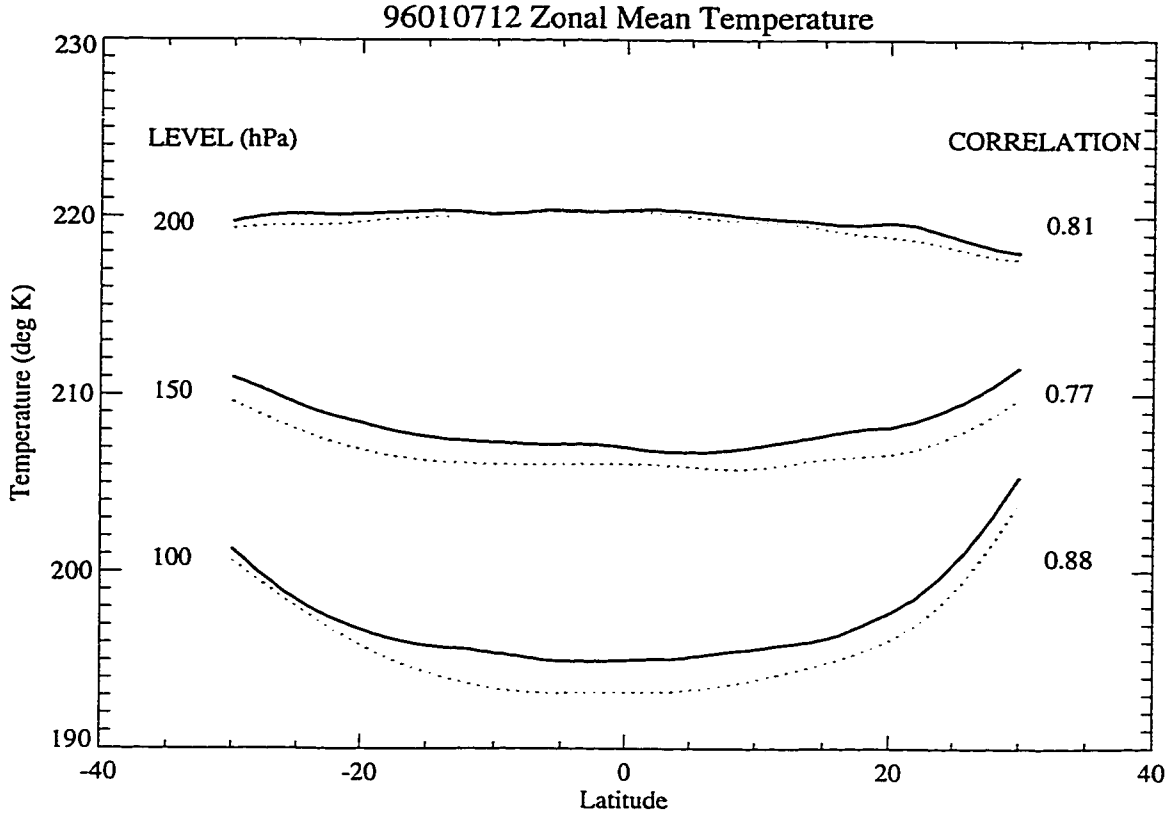

Figure 4.2: Zonal mean temperature for 12z January 7, 1992. Plotted for tropics at 200 hPa, 150 hPa and 100 hPa. Correlations on right are latitude and longitude spatial correlations in the tropics ($|lat| < 30°$). Solid- GEOS, Dotted- NCEP.

temperatures compared well with NCEP data at altitudes up to 220 hPa from 200 hPa to 100 hPa the GEOS warm bias is present in the tropics at several levels. The bias is clear in the zonal mean temperature at a particular time, illustrated in Figure 4.2. The spatial correlations between individual NCEP and GEOS data points in longitude and latitude (on the right side of Figure 4.2) indicate that the point-to-point temperature variability of the assimilation data are correlated. The correlation is statistically significant (see Devore, 1987, pg. 490) given that it is taken at each latitude and longitude location in the tropics (over 4000 points). GEOS data is 2–3° K warmer than NCEP data at 100 hPa, a bias which increases from virtually identical mean

temperatures at the 200 hPa level. This temperature bias may have some profound effects with regard to stratosphere-troposphere exchange, as it indicates differences in the saturation vapor mixing ratio (SVMR) of water vapor of 2 ppmv or nearly 40% (using the algorithm of Marti and Mauersberger (1993) at 193K and 100 hPa: $SVMR(T_{NCEP}) = 5.45$, $SVMR(T_{GEOS}) = 7.55$). Schubert et al. (1993) note that GEOS climatological averages are also 2°K warmer around the tropical tropopause than a similar ECMWF climatology.

While the GEOS temperature structure generally agrees with other data, there are some potential discrepancies between different data sources. As a check on much of the analysis in this work, the tropopause height analyzed with GEOS data will be examined to see if it exhibits any differences with other assimilation products.

4.3 Tropopause

The GEOS assimilation system produces a tropopause which is nearly coincident with the tropopause analyzed in two other assimilation data products. Figure 4.3 illustrates the zonal mean analyzed tropopause height for GEOS, UKMO and NCEP data sets in January and July. The tropopause is calculated using an isosurface of Ertel's potential vorticity (Equation 2.1) and a potential temperature surface in the tropics (see Chapter 2). These data sets have different meridional grid spacing (2° latitude for NCEP and GEOS and 2.5° for UKMO), but the same vertical levels. Figure 4.3 illustrates that the calculated zonal mean dynamic tropopause surface for all three data sets is nearly coincident (3 PVU shown, the result holds for all surfaces). Figure 4.3 only indicates where the mean of one data set is biased against another, and not whether they contain similar variability about the temporal and zonal means.

A detailed analysis of the 3D structure at a single time, and of the seasonal evolution of the tropopause height, indicates that the only differences between data

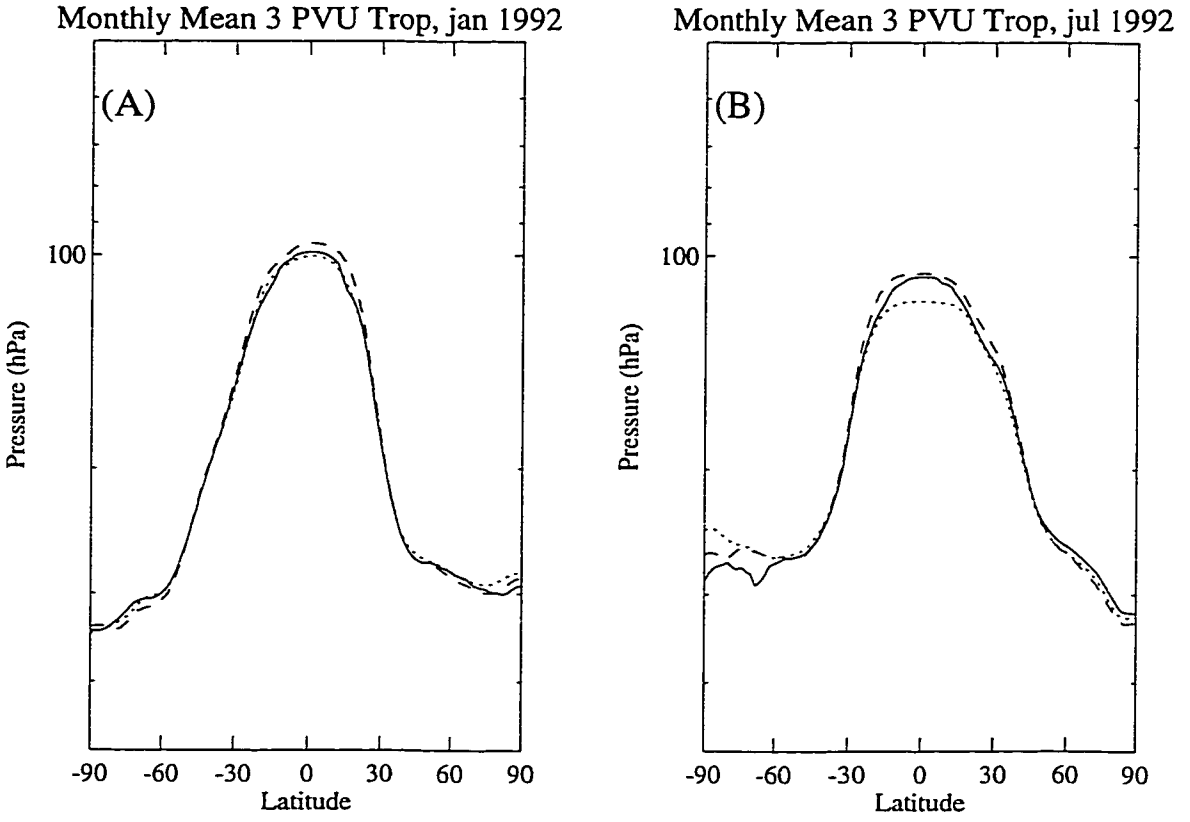

Figure 4.3: Monthly zonal mean dynamic tropopause pressure for (A) January and (B) July 1992 on the 3 PVU (and 380K θ surface in the tropics) tropopause surface calculated with various assimilated data sets. Solid- NCEP, Dotted- GEOS, Dashed- UKMO.

sets exist at the tropical tropopause (shown in Figure 4.3) and in high latitudes of the southern hemisphere in winter, and are less than 10 to 20 hPa (100–200m). The differences in the tropics are to be expected based on the different thermal structure noted in Section 4.2, which would tend to shift the height of the 380 K potential temperature surface. GEOS data is slightly warmer than NCEP data, so the height of the analyzed tropopause (the 380K surface) is lower than NCEP data. The difference in mean tropical tropopause pressures over the equator is up to 4 hPa in January (96 hPa NCEP, 100hPa GEOS) and 10 hPa in July (106 hPa NCEP, 116hPa GEOS).

4.4 General Circulation

The zonal mean wind in the GEOS analyses compares well with observations of the gradient wind in the extratropics (Coy et al., 1994). The zonal mean wind analysis compares well to the zonal mean wind derived by the United Kingdom Meteorological Office (UKMO) assimilation system (Coy and Swinbank, 1997). The Transformed Eulerian Mean (TEM) circulation (see Chapters 2 and 3) derived directly from the GEOS analysis, compares well with the vertical component of the TEM residual circulation estimated from UKMO analyses (Coy and Swinbank, 1997). Using a formulation of the TEM circulation calculated from the diabatic heating and the temperature tendency (Rosenlof, 1995), the residual circulation implied by the GEOS data as illustrated in Figure 4.4, (also see Douglass et al., 1996, Figure 1b) compares well with a residual circulation estimated from UARS data (Rosenlof, 1995). The GEOS residual vertical velocity matches both the magnitude and direction of the UARS residual vertical velocity to the lower limit of observations (105hPa). The residual circulation appears significantly different only above 5 hPa. Douglass et al. (1996) note differences between a direct and a thermodynamic calculation of the residual circulation, and inconsistencies in the residual circulation estimated from the GEOS analysis.

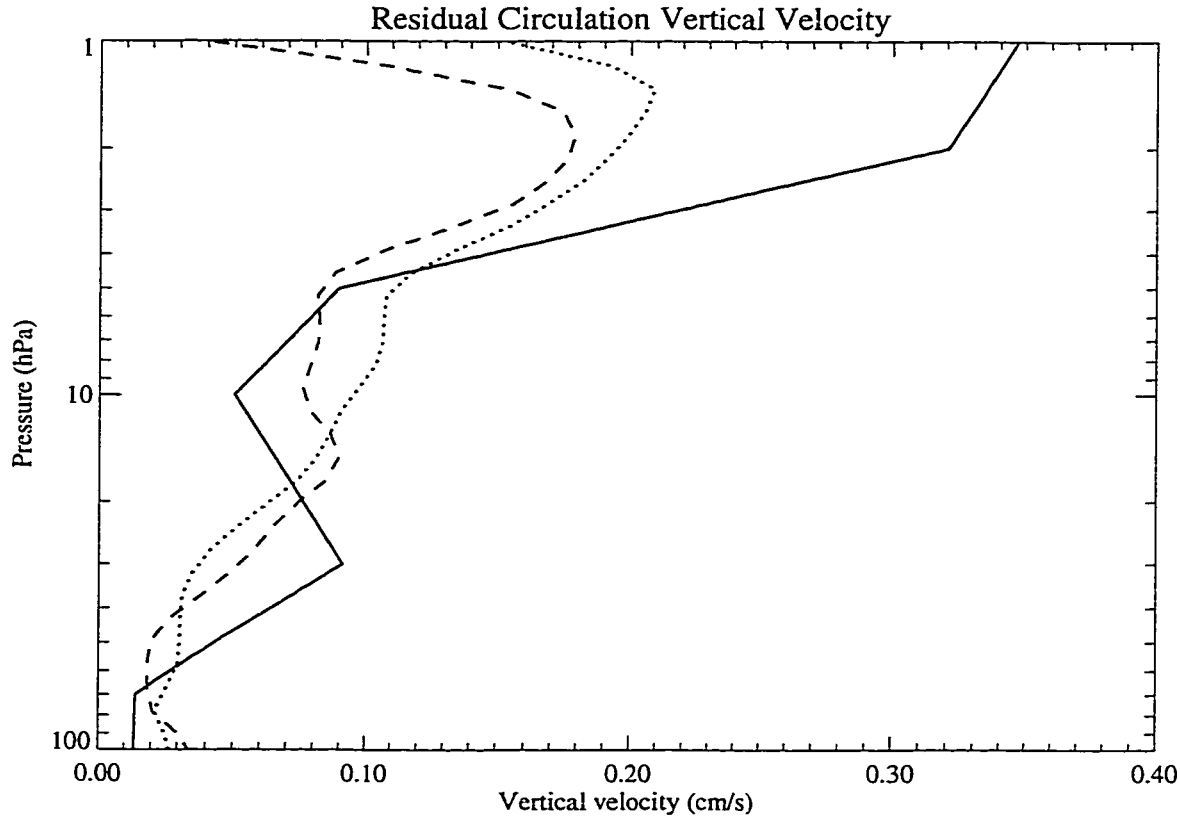

Figure 4.4: Monthly mean residual circulation ($\bar{w}^*$) over the equator in cm/s. Dotted- Rosenlof (1995) January 1993, Dashed- Rosenlof (1995) January 1994, Solid- GEOS January 1996.

Coy and Swinbank (1997) perform a more detailed comparison of the GEOS general circulation and the UKMO assimilation system. Some differences in magnitude are noted, but both analyses capture the seasonal variation of the Hadley cell and the polar stratospheric circulations well. Some transport anomalies have been noted in the subtropical lower stratosphere, where anomalous convergence in the windfields appears to lead to excessive vertical mass fluxes into the lower stratosphere (L. Coy personal communication, 1997). Otherwise the general circulation of the GEOS data compares favorably to other global data sets and observations.

4.5 Goddard Chemistry and Transport Model (CTM)

The GEOS-1 wind and temperature data (see sections 4.2 and 4.4) are used to drive the transport in an 'off-line' Chemical Transport Model developed in the Laboratory for Atmospheres at the NASA Goddard Space Flight Center. Hereafter this model will be designated the Goddard CTM or GCTM. In a chemical transport model, chemical constituents are advected by winds, and chemical reactions are determined based upon a set of specified equations. In an 'off-line' model, the winds and temperatures driving the transport of constituents are fixed, and not affected by feedbacks from radiatively active species (such as ozone). Douglass et al. (1996) note two benefits of this method over a full General Circulation Model (GCM) with chemistry and feedbacks; the ability to use temperatures that are closer to those of the actual stratosphere than in most GCM's, and to appropriately simulate interannual variability and perturbations.

Several versions of the GCTM model described by Douglass et al. (1996) will be used in this study. The basic version of the transport model uses a 2° x 2.5° grid with 46 sigma levels up to 1 hPa. The vertical grid can be modified to fit different assimilation data sets, or to study different processes. The full chemistry package and the use of the model is described by Crum (1996). The transport core of the model is based on a semi-Lagrangian transport scheme (Lin and Rood, 1996), which has the

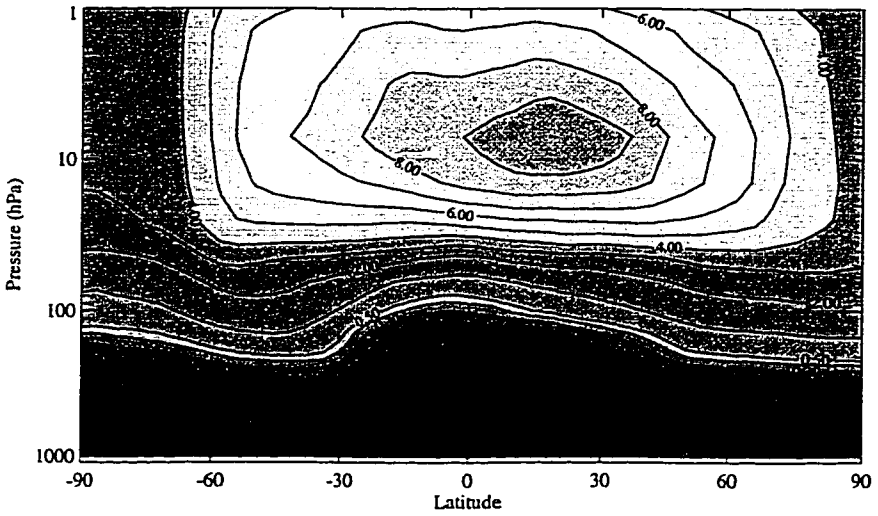

Figure 4.5: Zonally averaged ozone mixing ratio from GCTM full chemistry simulation for August 1992 in ppmv.

advantage of being monotonic (in the form used), conserving mass, and preserving tracer-tracer correlations, which are vital for transport. Transport is derived from assimilated winds (section 4.4) and temperatures (section 4.2). GEOS temperatures and wind inputs to the transport model are taken directly from 46 sigma level GCM data, not the 18 level archived product described earlier (Table 4.1). 18 level data are used for diagnoses and trajectory calculations only. 46 level data is used for the transport calculations using this model in Chapters 6 and 7. Horizontal transport is derived directly from input winds. Vertical transport is calculated based on the convergence and divergence of the horizontal wind. This yields a very vertical wind field with high spatial and temporal variability.

The GCTM has been shown by Douglass et al. (1996) to be able to simulate the annual cycle of ozone in the stratosphere quite well, including synoptic scale events. The ozone distribution after a full chemistry run of 10 months is illustrated in Figure 4.5. The model ozone distribution has a maximum near 10 ppmv around 10 hPa in the tropics, and a sharp gradient in ozone near the tropical and extratropical

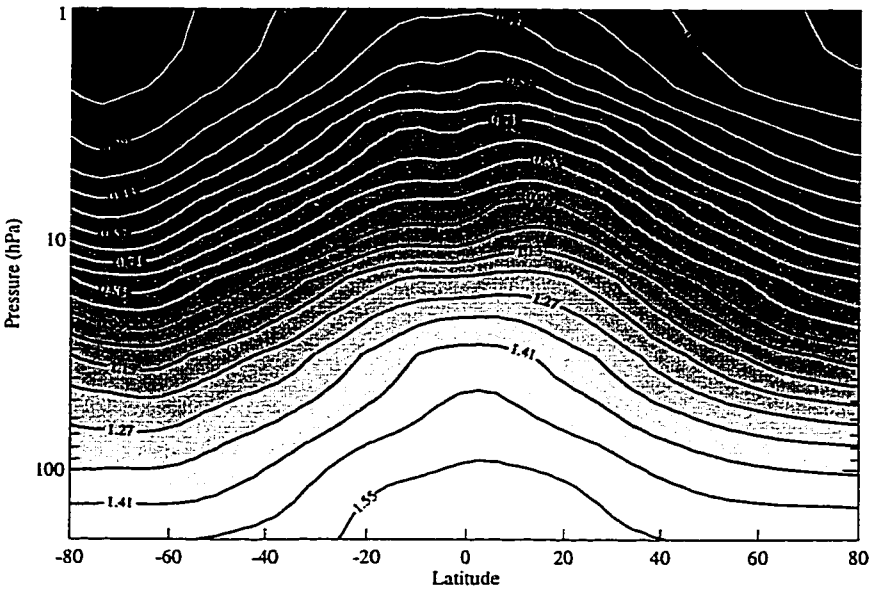

Figure 4.6: Annual zonal mean methane mixing ratio from GCTM full chemistry simulation in ppmv. Compare to Figure 2.2.

tropopause. The GCTM has also been used by Weaver et al. (1996) to simulate the distribution of NO_x from a projected supersonic High Speed Civil Transport (HSCT) fleet in the stratosphere. Both studies have noted potential problems in the simulation of large scale gradients; the meridional gradients in column ozone are too strong (less tropical ozone and more in midlatitudes), based on comparing modeled column ozone with TOMS data (Douglass et al., 1996) and the subtropical transport barrier in the stratosphere is weak in the model and allows too much mixing above 50 hPa (Weaver et al., 1996). The difference is clearly evident in the zonally averaged distribution of a long lived tracer such as methane, illustrated in Figure 4.6. While the model does accurately simulate many of the gross features of the methane distribution (tropical upwelling and lower methane values near the poles), the meridional gradients in the mid-stratosphere are small compared to the HALOE observations in Figure 2.2. Figure 4.6 also indicates that the observed methane distribution from HALOE has

sharper meridional gradients around the boundary of the stratospheric overworld than found in the GCTM simulations. Further analysis of the mixing processes in the lowermost stratosphere and upper troposphere using GCTM tracer experiments will be a focus of the following chapters.

The GCTM has been used to study the upper troposphere as well as the stratosphere. Rood et al. (1997) have demonstrated the ability of the GCTM to resolve midlatitude synoptic scale extratropical cyclones and associated stratosphere-troposphere exchange. Allen et al. (1996) have shown that the GCTM with a convective parameterization and a parameterized surface source of radon (^{222}Rn) compares favorably with observations. The radon distributions of Allen et al. (1996) also compare favorably with 2D and 3D models examined by Jacob et al. (1997) throughout the depth of the troposphere, particularly in the upper troposphere. The GCTM has also been used to study meridional mixing in the model troposphere by comparing a GCTM simulation of the upper tropospheric 'aircraft' tracer of Jacob et al. (1997) with other tropospheric chemistry models running the same simulation. These later models include convective parameterizations, so the tracer comparison will be a good test of GCTM performance in the upper troposphere. The tracer is injected continuously in the northern hemisphere midlatitudes from 400 hPa to 200 hPa, with a decay time (half life) of 3.8 days. The resulting zonal average for the northern hemisphere summer season is illustrated in Figure 4.7, which compares favorably to the distributions of other two and three dimensional transport models examined in Figure 6 of Jacob et al. (1997). In particular, the vertical gradient of the tracer distribution resembles other models, and there is isolation between the lowermost stratosphere and the upper troposphere. There is significant inter-hemispheric transport but only in the upper troposphere. However, the vertical transport is on the order of 0.2 cm/s calculated from the upward propagation of tracer concentrations. This velocity is faster than typical residual vertical velocities in the lower stratosphere (Rosenlof, 1995; Coy and Swinbank, 1997), even those produced by the GEOS assimilation from which the

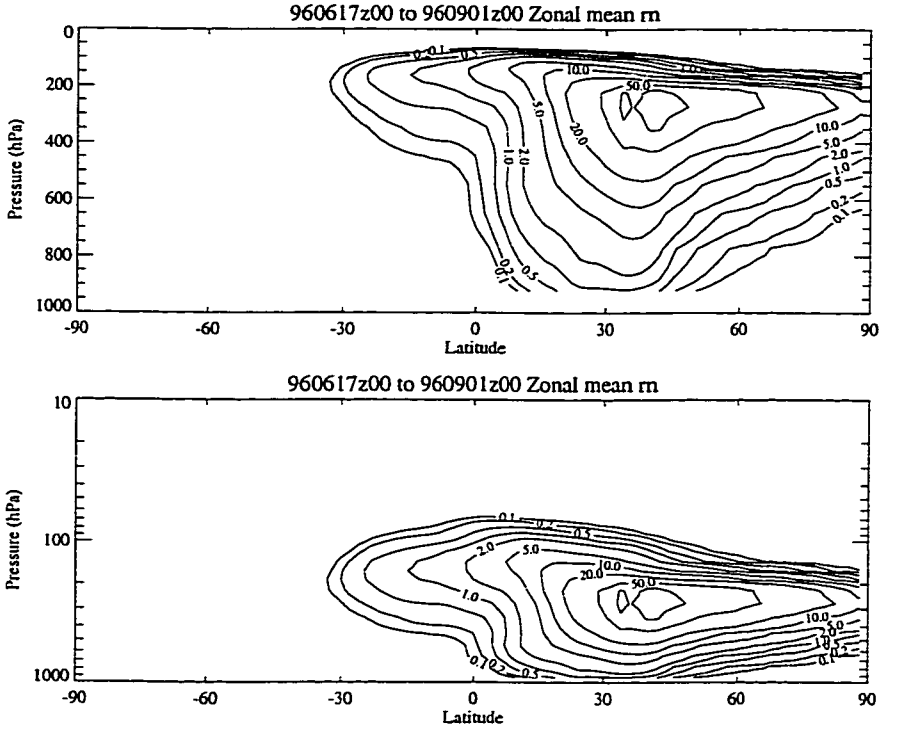

Figure 4.7: Zonally averaged '^{222}Rn' tracer between June 17 and September 1. units of 10^{-21} mol/mol. Top panel vertical axis is linear in pressure (for comparison to Jacob et al. (1997), Figure 6), bottom panel is logarithmic in pressure.

transport winds are derived (see Figure 4.4). The vertical tracer transport in the simulated stratosphere thus appears to be much too rapid.

The GCTM has also been used to study the evolution of a passive subsonic aircraft tracer, both on seasonal timescales by Gettelman (1998) and on annual timescales for comparison to other 2-D and 3-D models (Danilin et al., 1998). These simulations will be discussed further in Chapter 6. The GCTM has also been used by Cerniglia et al. (1999) to evaluate stratosphere-troposphere exchange using the distribution of ozone around the tropopause. The GCTM is particularly good at simulating transport in individual synoptic events, as illustrated by the synoptic scale simulations of Rood et al. (1997) and the comparison of modeled ozone with ozonesonde observations by Cerniglia et al. (1999). The GCTM has also been used to simulate the distribution of carbon dioxide in the upper troposphere and lower stratosphere by Strahan et al. (1998) and will be used in Chapter 7 to simulate the distribution and stratosphere-troposphere exchange of water vapor.

4.6 Goddard Trajectory Model

Trajectory models provide Lagrangian estimates of transport and are a useful tool for testing chemical models. The Goddard trajectory model (Schoeberl and Sparling, 1994) can be run either as an isentropic (adiabatic) model, or using heating rate data in a 'diabatic' mode, in which case the model still transports isentropically, but uses heating rate data to derive diabatic motion. The trajectory model uses assimilated winds and temperatures as inputs for driving model transport. Trajectory models provide a tool for doing detailed chemistry to test chemical models (or chemical modules of chemical transport models). They can also be used to trace the history of a series of parcels (Rood et al., 1997). Using a large ensemble of parcels, trajectory models can provide statistics of parcel transport (Eluszkiewicz, 1996), in a similar manner to the use of passive tracers in chemical transport models described previously.

Sparling et al. (1995) have used the trajectory model developed by Schoeberl and Sparling (1994) to simulate emissions from aircraft in the lower stratosphere and compare it to a simulation using a chemical transport model. Schoeberl et al. (1998) have used the trajectory model to estimate the lifetime of supersonic aircraft emissions in the stratosphere. In Chapter 6, the Goddard trajectory model will be used in a variety of contexts to supplement the transport studies with the GCTM.

4.7 Stratosphere-Troposphere Exchange

The general circulation and the tropopause are combined information that can be used to evaluate stratosphere-troposphere exchange (STE). The Goddard trajectory model (see Section 4.6), can be used to evaluate the effects of different assimilation datasets on simulated transport between the stratosphere and the troposphere. Differences between assimilation winds at the tropopause level may be significant even if the tropopause evolution (Section 4.3) and the general circulation (Section 4.4) are comparable. To test the robustness of STE estimated with different assimilation systems, the exchange of mass on an isentropic surface crossing the tropopause is evaluated using an ensemble of trajectories advected by different assimilated wind data sets. This experiment is similar to the trajectory model experiments of Eluszkiewicz (1996) and Chen (1995). GEOS, UKMO and NCEP assimilated data sets have been used to drive an ensemble of parcels initialized on an equidistant 4° grid (every 4° latitude and 450 km in longitude) for 28 days in February. Isentropic trajectories as well as a diabatic experiment using NCEP heating rates are analyzed. The zonal mean parcel distribution function is not very sensitive to the density of the ensemble mesh (number of parcels) used, or to the time-step of the integration. However, the different datasets yield slightly different distributions after 28 days of integration. Table 4.2 shows the fraction of parcels, initialized every 4° in latitude and every 450 km in longitude on the 350K potential temperature surface, exchanged between: (1) the

Table 4.2: Parcel Exchange between the stratosphere and the troposphere, parcels initialized on 350K potential temperature surface in February 1992. Fraction of parcels exchanged after 28 days is shown. Last column is the summer hemisphere to winter hemisphere (S/W) ratio. Tropopause surface is 3 PVU.

Data Source	Troposphere to Stratosphere	Stratosphere to Troposphere	Strat to Trop S/W Ratio
GEOS-DAS	0.09	0.19	1.8
UKMO	0.06	0.16	1.7
NCEP	0.16	0.10	4.7
NCEP-Diabatic	0.03	0.41	4.9

troposphere and stratosphere, (2) the stratosphere and the troposphere and (3) the ratio of the exchanged parcels between the summer (Southern) and winter (Northern) hemispheres. The 350K potential temperature surface is in the troposphere in the tropics, and the extratropical lowermost stratosphere (middleworld) in the extratropics. STE along this surface is 'quasi-isentropic' exchange as discussed in Chapter 2.

The values in Table 4.2 indicate the fraction of parcels in the original region crossing the dynamic tropopause after 28 days. For all analyses (including diabatic analyses where heating rates are included), isentropic exchange into the troposphere is more vigorous than exchange into the stratosphere. Some exchange into the stratosphere on isentropic surfaces does occur. When diabatic effects are included in the NCEP data, the fraction of parcels from the stratosphere crossing the tropopause rises significantly, and the fraction of parcels moving from the troposphere across the tropopause decreases. This is not surprising given the strength of the downward branch of the residual circulation in February (Rosenlof, 1995; Appenzeller et al., 1996).

In February the troposphere-stratosphere exchange occurs only in the northern

hemisphere, at subtropical to mid latitudes. For all analyses, exchange into the troposphere is more vigorous in the summer than the winter hemisphere (experiments were run in both February and August), in agreement with Lagrangian calculations of Chen (1995) and Eluszkiewicz (1996). GEOS and UKMO data have a similar hemispheric ratio, while the NCEP data indicates significantly more summer exchange into the troposphere. This exchange is related to the 'permeability' of the subtropical tropopause break, which the 350K surface bisects. Thus according to this transport simulation, all three of the assimilation data sets predict that quasi-isentropic exchange does occur. Stratosphere-Troposphere exchange estimated with GEOS winds is similar in aggregate to UKMO estimated exchange, while the exchange estimated with NCEP winds has noticeable differences in the vigorousness of the exchange between summer and winter hemispheres. Differences in the tropical temperature structure at the tropopause level between assimilation data (see section 4.2) might affect the permeability of the tropopause by changing the meridional temperature gradient and hence the meridional wind shear. While the effect is of the right sense to cause differences here, it is probably not that dramatic. Rather, differences may be due to limitations of the NCEP data in the tropics. In the trajectory simulations driven by NCEP winds, parcels appear to 'stall' in tropical regions, a result of the fact that the balanced wind assumption used in the NCEP data fails at the equator (where the coriolis force goes to zero), so that anomalous winds are generated in the tropics on a regular basis. The UKMO and GEOS winds are expected to be more robust in this region.

4.8 Summary

In summary, the GEOS temperature structure compares favorably to other studies, with some differences at the tropical tropopause and the cold point in the lower tropical stratosphere. The structure and distribution of the tropopause also compares

favorably to other analysis products, with slight differences at high southern latitudes, and at the tropical tropopause. The latter are understandable from differences in the thermal structure. Both the mean circulation and the mean residual circulation in the stratosphere are well represented when compared to other data sources and assimilation products, lending confidence to the applicability of the analysis for driving tracer studies. The corresponding simulated STE with a trajectory model appears similar between the GEOS and UKMO analysis winds. All these factors lend confidence to the use of GEOS system winds and temperatures for studies of stratosphere-troposphere exchange.

The good correspondence between assimilation systems is not surprising given that assimilation systems have generally common physics, common data and similar methodologies for handling input data. However, this similarity also means that errors and biases may still be present. It is particularly true in regions of sparse data coverage and less than certain physical processes. These conditions are particularly true of the tropical tropopause region (critical for the analyses in Chapter 7), and the nonconservative processes at the extratropical tropopause (which are important for the discussion in Chapter 8).

Chapter 5

DEPOSITION OF SUBSONIC AIRCRAFT EMISSIONS INTO THE STRATOSPHERE

5.1 Introduction

Concerns about the possible effects of subsonic and supersonic aircraft emissions have been raised periodically over the past 25 years. The effects of possible future supersonic aircraft on stratospheric ozone have been reviewed recently (Stolarski et al., 1995). The effects of subsonic aircraft emissions have recently become of concern in both Europe (Fabian and Kärcher, 1997; Brasseur et al., 1998) and the United States (Friedl, 1997). Emissions from the commercial aircraft fleet are composed mostly of water vapor (H_2O) and carbon dioxide (CO_2). Trace species also include nitrogen oxides (NO_x=NO + NO_2), carbon monoxide (CO), sulfur, carbon soot and unburned hydrocarbons (HC). The ratio of these species to total fuel burned is usually described by an emission index (EI) for each species (Baughcum et al., 1996), which will vary with engine type and power setting.

Commercial air traffic spends the majority of its time in the 9–13 km altitude band. Thus, much of the emissions occur near the tropopause in a region where transport processes are not generally well treated by either stratospheric or tropospheric chemical transport models used in assessment calculations. Emissions from aircraft have different effects depending on altitude. The residence time of emissions in the atmosphere is different depending upon whether emissions are in the troposphere or the stratosphere (Holton et al., 1995; Gettelman, 1998). For NO_x emissions the difference translates into different chemical evolution and removal pathways, with

effects on ozone (O_3) production and loss. Furthermore, differences in the relative amounts of background trace species (such as O_3, H_2O, and CO) and resulting radicals (OH, HO_2, and NO_x) between the troposphere and the stratosphere have profound effects upon the chemistry and resulting ozone production or loss (Wennberg et al., 1994).

Previously, Hoinka et al. (1993) have investigated aircraft emissions in the North Atlantic Flight Corridor (NAFC) and reported that 44% of aircraft cruising time occurred in the lower stratosphere. Baughcum (1996) has estimated that 17% of global aircraft emissions occur in the lower stratosphere, on the basis of an annually averaged inventory. That study concluded that approximately 16% of the total fuel burned occurs within 1 km of the tropopause and 29% of the total fuel burned within 2 km.

In this chapter, we evaluate the direct deposition of aircraft emissions into the lower stratosphere using two recently available three-dimensional global aircraft emissions inventories. The sensitivity of the results to the choice of meteorological data set is tested using temperature and potential vorticity fields from three data assimilation systems over the period from 1983 to 1996. The sensitivity of the results to tropopause definition is tested using both the thermal lapse rate and dynamical definitions of the tropopause.

5.2 Methodology

Daily global assimilated meteorological data are used to define the tropopause using different definitions. This surface is used to determine whether subsonic aircraft emissions from a gridded inventory are in the stratosphere or the troposphere by comparing the daily analyzed tropopause pressure with an aircraft emissions inventory on a standard atmosphere pressure grid. Two different sources of the emissions inventory are used, as is described in section 5.3. Three different sources of daily meteorolog-

ical data are used, also described in section 5.3. The definition of the tropopause is discussed in section 5.4. Transport of deposited emissions is considered in Chapter 6.

Section 5.5 will present results of sensitivity tests on the stratosphere-troposphere distribution of emissions. The results are discussed with regard to the fraction of emissions in the stratosphere (section 5.5.1), variations in the tropopause height (section 5.5.2), the effect of interannual variability of the tropopause height (section 5.5.3), analyses by region (section 5.5.4), and projections of future emissions (section 5.5.5). The temperature of deposition will be used to analyze the potential for contrail formation at deposition in section 5.6. In section 5.7 we summarize the analyses and present conclusions.

5.3 Data Description

Three-dimensional inventories of fuel use and emissions (NO_x, carbon monoxide, and hydrocarbons) for each month of 1992 for the global current aircraft fleet have been developed for the National Aeronautics and Space Administration (NASA). The inventory of scheduled air traffic emissions has been developed by Baughcum et al. (1996). An inventory for non scheduled air traffic (charter, military, general aviation, and former USSR and China) has been developed by Metwally (1995) and updated and revised by Mortlock and van Alstyne (1998). The total annual fuel burn for the present fleet is estimated at 139 Tg yr^{-1} for this inventory (henceforth, the "NASA" inventory). Emissions of carbon dioxide and water vapor can be derived by scaling the quantity of fuel burned by factors of 3.16 kg CO_2 per 1 kg fuel and 1.24 kg H_2O per 1 kg fuel.

A similar data set for four months of 1991–1992 was developed in Europe as part of the Abatement of Nuisances Caused by Air Traffic (ANCAT) program of the European Civil Aviation Conference (ECAC). The original database was described by Gardner et al. (1997) and has subsequently been updated (Gardner, 1998) with signif-

icantly lower estimates of fuel burned and NO_x emissions (henceforth, the "ANCAT2" inventory). A database using the same air traffic pattern has also been developed by Schmitt and Brunner (1997). The ANCAT2 emissions data are available for July 1991, October 1991, January 1992, and April 1992. The total annual fuel emissions for the ANCAT2 inventory are 131 Tg yr^{-1}. Total emissions from the ANCAT2 inventory are lower than the NASA inventory owing to differences in the air traffic databases and methodologies as well as a slightly earlier time period. The ANCAT2 data begin in October 1991, while the NASA inventory begins in January 1992.

Both inventory databases include scheduled commercial traffic (including the supersonic emissions of the Concorde), civil aviation, and cargo traffic, as well as estimates of military traffic. For these analyses both data sets are interpolated from a 1° latitude by 1° longitude grid in the horizontal to the meteorological data grid. The vertical resolution of the data is 1 km (pressure altitude). Emissions are separately derived for mass of total fuel, nitrogen oxides (NO_x), carbon monoxide and hydrocarbons for the NASA data set and for fuel and NO_x for the ANCAT2 data.

The total fraction of aircraft NO_x emissions deposited into the stratosphere closely resembles the emissions fraction from fuel burned because the emission index of NO_x at cruise conditions does not vary greatly with changes in cruise altitudes. For hydrocarbon and carbon monoxide emissions, the emission indices are much higher at low power settings (e.g., taxi operations and descent), so a larger fraction of the emissions are concentrated in the boundary layer. Consequently, the fraction of these constituents deposited in the stratosphere is much lower than that for fuel burned or NO_x. Assessment calculations (Stolarski et al., 1995; Friedl, 1997) have indicated that aircraft emissions of hydrocarbons and carbon monoxide will not make significant contributions to stratospheric ozone chemistry. The bulk of this analysis will thus focus primarily on the mass of fuel and NO_x deposited above the tropopause.

The NASA fuel data for January are plotted in Figures 5.1 and 5.2. Figure 5.1 illustrates the concentration of emissions in the midlatitude upper troposphere and

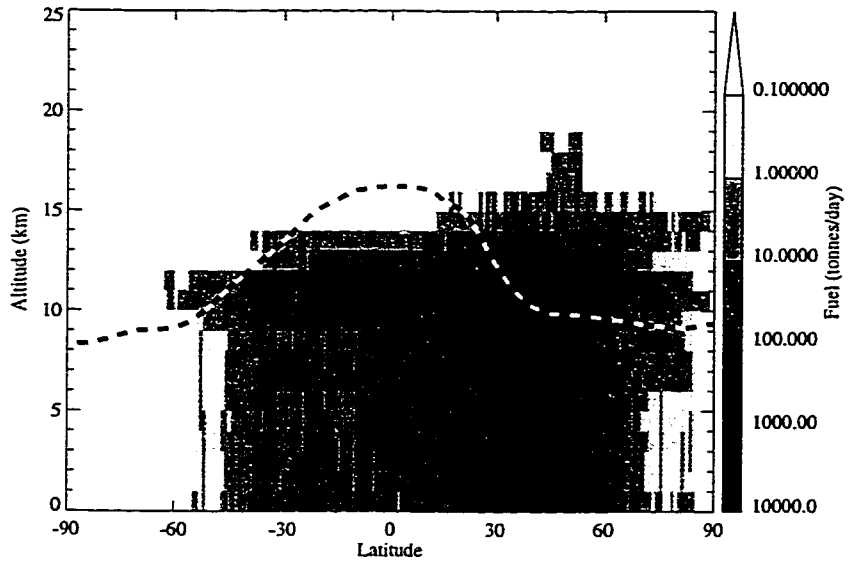

Figure 5.1: Zonally integrated aircraft emissions from NASA inventory in metric tons of fuel per day (10^3 kg d^{-1}) for January 1992. A 1° latitude by 1 km altitude grid is used. Heavy dashed line is the monthly mean dynamic tropopause of 3 Potential Vorticity Units (PVU) and 380 K potential temperature surface in the tropics (see text for details).

lower stratosphere of the Northern Hemisphere relative to the tropopause. The greatest quantity of emissions on a zonally integrated basis (Figure 5.1) occurs in the midlatitudes, between 30° and 60°N. The fuel distribution is a slowly varying function over the year, with a maximum in July of 4.2 x 10^8 kg d^{-1} (kg per day) and a minimum in January of 3.7 x 10^8 kg d^{-1}. Since fuel varies only slowly, we treat it as a step function with constant emissions over each calendar month. The tropopause is discussed more fully in section 5.4. Aircraft emissions are zonally asymmetric, as is illustrated in Figure 5.2. Emissions are largest over North America and Europe.

Meteorological data are used to define the tropopause height and temperatures. Data is taken from a variety of sources to examine the sensitivity of the result to different input data and resolutions. Table 5.1 illustrates the details of the three re-

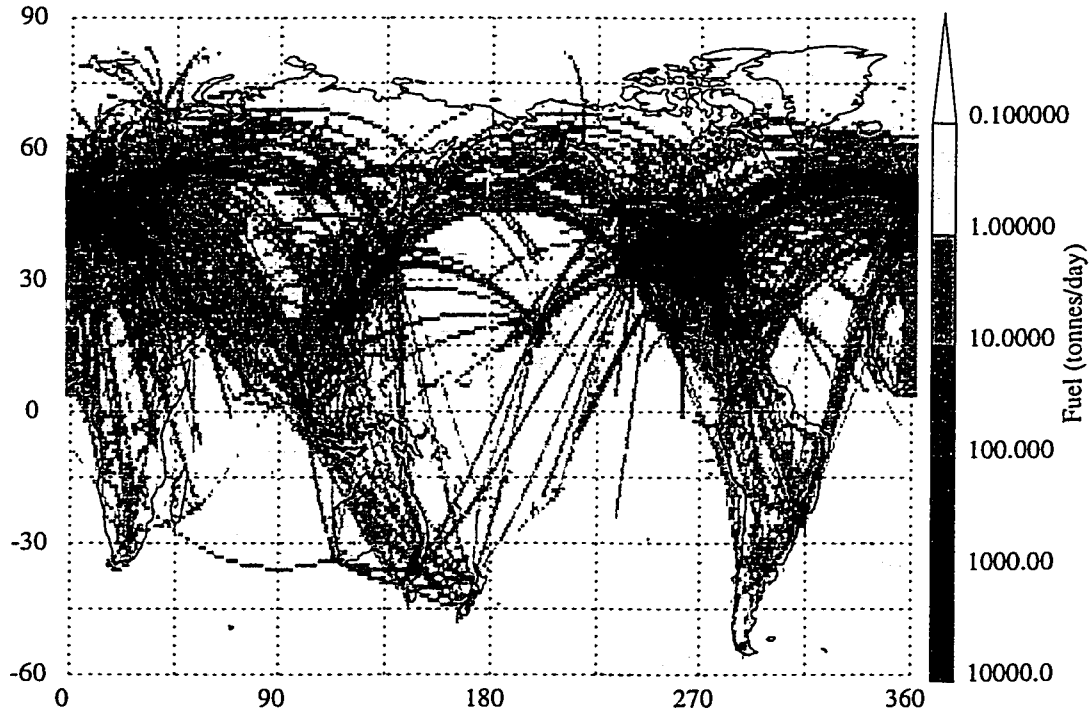

Figure 5.2: Integrated column emissions from NASA inventory in metric tons of fuel per day (10^3 kg d^{-1}) for January 1992. A 1° longitude by 1° latitude grid is used.

Table 5.1: Meteorological Data used for calculations

Source	Resolution (lon x lat)	Years	Reference
NCEP	5° x 2°	1983–1993	Kalnay et al. (1996)
UKMO	3.75° x 2.5°	1992–1996	Swinbank and O'Neill (1994)
GEOS	5° x 4°	1992	Schubert et al. (1993)
GEOS	2.5° x 2°	1996	Schubert et al. (1993)

analysis data sets from the National Centers for Environmental Prediction (NCEP), the United Kingdom Meteorological Office (UKMO), and the Goddard Earth Observing System (GEOS), Data Assimilation System. All three assimilations are utilized on the same 18 level vertical grid from the surface to 1 hPa (see Table 4.1) with a vertical resolution of 1–2 km around the tropopause. Meteorological data are analyzed once daily at 0000 UTC for NCEP and GEOS data and at 1200 UTC for UKMO data.

5.4 The Tropopause

The tropopause marks the boundary between the stratosphere and troposphere. The zonal mean tropopause height is high in the tropics (approximately 100 hPa) and below 300 hPa near the poles, as is discussed in Chapter 2 and indicated by the tropopause surface for January 1992 in Figure 5.1. The tropopause has a highly variable structure in three dimensions. While Figure 5.1 presents a zonal mean picture for clarity, all analyses are conducted using three-dimensional daily tropopause surfaces which are zonally asymmetric. For this analysis, the tropopause is defined in several ways to test the sensitivity of the results to varying tropopause definitions.

The tropopause is conventionally defined as the beginning of the change in vertical

stratification that marks the lower limit of the stratosphere using either a "thermal" or "dynamic" definition (see Chapter 2). In most of the analysis in this chapter, unless noted, PV refers to the absolute value of Ertel's Potential Vorticity (equation 2.1) in units of K kg^{-1} m^2 s^{-1}. For convenience, a Potential Vorticity Unit (PVU) is defined such that 1 PVU = 10^{-6} K kg^{-1} m^2 s^{-1}.

PV has a strong cross-tropopause gradient in midlatitudes but not in the tropics because PV normally goes to zero at the equator. In this chapter the tropical dynamic tropopause is defined as the 380 K potential temperature surface (located near 100 hPa), as discussed in Chapter 2. Because there is no single accepted value for the tropopause and a maximum in the aircraft emissions deposition occurs very close to the tropopause, several different values of PV are used for a sensitivity analysis of the dynamic tropopause height. These analyses use a range of PV values between 1 and 4 PVU in the midlatitudes (and 380 K potential temperature in the tropics), calculated from the meteorological wind and temperature data to define four different dynamic tropopause surfaces. The temporal variation and latitudinal structure in the zonal mean tropopause height have recently been discussed in more detail by Appenzeller et al. (1996).

Figure 5.3 illustrates the height of the four different dynamic tropopause surfaces in January and July. For clarity, Figure 5.3 presents zonal mean monthly averaged tropopause heights, converted from pressure using the U.S. Standard Atmosphere (National Oceanic and Atmospheric Administration, 1976). In the Northern Hemisphere, the difference between the 1 and 2 PVU surface is 2–3 km increasing toward high latitudes. Between the 2 and 3 PVU surface the height difference is 1–2 km, also increasing toward the pole, and between the 3 and 4 PVU surface the height difference is only about 700 m, with little latitudinal gradient. In general, the 1, 2 and 3 PVU surfaces are separated by at least one grid box in the vertical resolution of the analysis data. Given the depth of the tropopause region bounded by these different PV surfaces, the determination of the tropopause has a significant effect on

the fraction of emissions estimated to occur in the stratosphere.

The dynamic tropopause is compared to the tropopause surface defined using a thermal definition in Figure 5.3. A much more thorough treatment of the comparison between the thermal and dynamic tropopause definitions can be found in the work of Hoerling et al. (1991). The zonal mean 3 PVU surface is nearly coincident with the zonal mean thermal definition for both January and July. An examination of the three dimensional (3-D) tropopause fields indicates that the relationship in Figure 5.3 holds in three dimensions as well. There are some differences in tropopause height in the tropics and around the subtropical summertime break in the summer hemisphere (owing to a slightly different latitudinal gradient), both in January (Figure 5.3a) and in July (Figure 5.3b). The high dynamic tropical tropopause does not spread as far from the equator as the thermal tropopause does. While the 380 K surface is nearly coincident with the tropical tropopause in January (Figure 5.3a), the difference between the two tropopause surfaces in July may be significant (Figure 5.3b). Since both surfaces are estimated using the same data set (NCEP data) on the same grid, the differences in the subtropics are a real feature of the two definitions and not just an aliasing artifact or a data set bias. Because the Northern Hemisphere midlatitude tropopause cuts through the region of maximum emissions (see Figure 5.1), slight differences impact the pattern of deposition of aircraft emissions in July (Northern Hemisphere summer) but do not have an impact in January.

A detailed analysis of the 3-D structure of the tropopause at a single time, and of its seasonal evolution as discussed in Chapter 4 (Figure 4.3), indicates that the tropopause height is not sensitive to the meteorological data set used to define it. The only differences between data sets exist at the tropical tropopause and in high latitudes of the Southern Hemisphere in winter, and are less than 10–20 hPa (100–200 m) as described in section 4.3 (Figure 4.3). The effect of these differences will be analyzed as part of the discussion of results. Since neither location has significant aircraft emissions near the tropopause, the differences should have little effect on

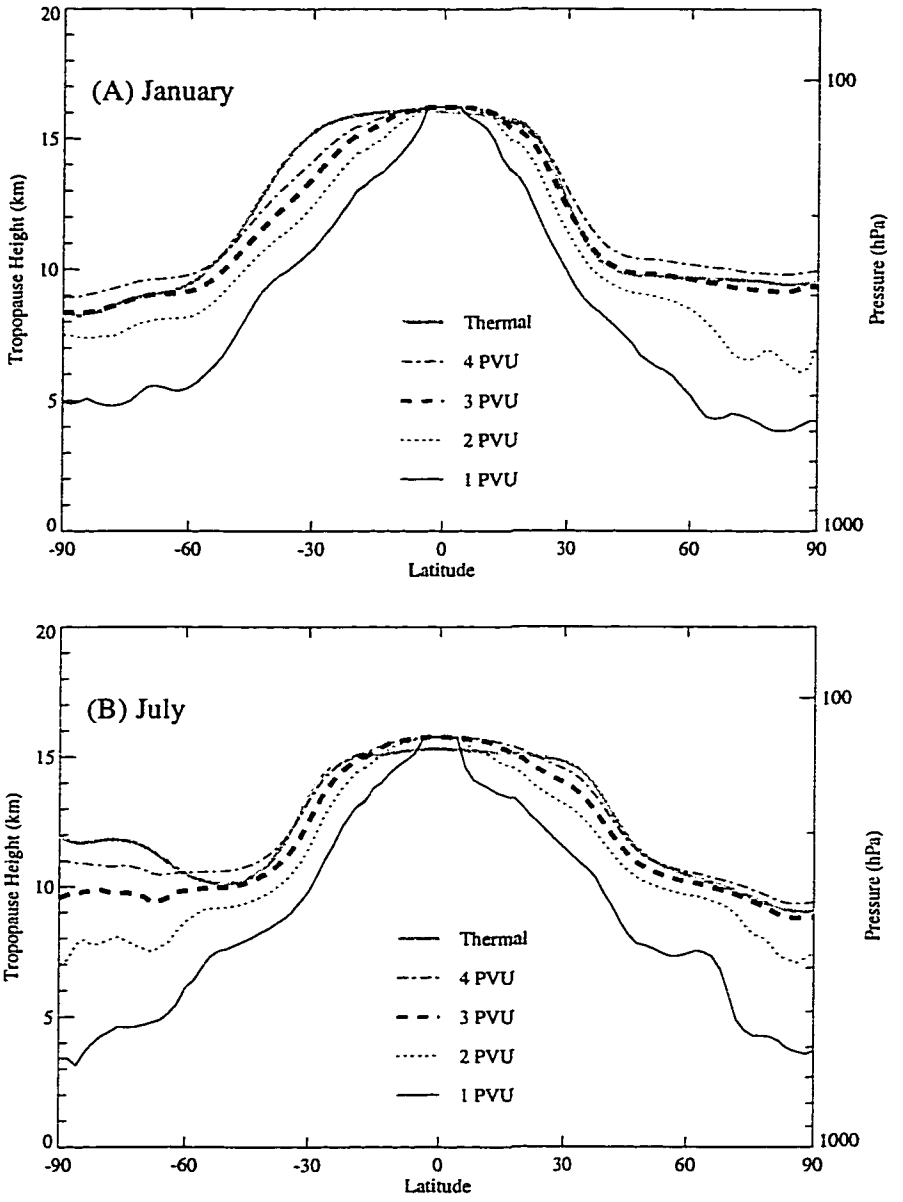

Figure 5.3: Monthly average tropopause height (log-pressure height) and pressure for different potential vorticity surfaces in (A) January and (B) July, using 1992 NCEP tropopause data.

stratospheric emissions.

5.5 Results

5.5.1 Stratospheric Fraction

The basic analysis used for comparison in the sensitivity studies is the NASA inventory analyzed with the NCEP meteorology and a dynamic tropopause for 1992. This "scenario" is chosen as a baseline for the sensitivity studies because monthly emissions data are available, and the meteorological data corresponds to the actual time of emissions. For this analysis, two different interpolation schemes were tried and found to be nearly identical. The first method assumes that all emissions within the grid box where the tropopause falls and below were in the troposphere. The second method divides the emissions within the grid box where the tropopause lies between the troposphere and stratosphere on the basis of a linear interpolation. The globally integrated difference in stratospheric emissions diagnosed between the two methods is less than 0.07% of total emissions (where the linear interpolation results in slightly higher stratospheric emissions), or 3 x 10^5 kg d^{-1} of fuel, and is not significant for this analysis.

Figure 5.4 illustrates the daily diagnosed fraction of fuel (Figure 5.4a) and NO_x (Figure 5.4b) deposited in the stratosphere from this scenario for all four dynamic tropopause surfaces. As expected, there is significant variability in the day to day deposition of emissions. Note that the emissions vary only monthly, so the high-frequency variability is entirely due to variability in the tropopause height relative to the emission data. The annual average fraction of fuel diagnosed as deposited in the stratosphere ranges from 18 to 44% depending on the PV value chosen for the dynamic definition of the tropopause (Table 5.2). The corresponding annual average fraction of fuel analyzed as deposited in the stratosphere using a thermal definition of the tropopause is 20% (Table 5.2). Again analyzing the emissions using the thermal

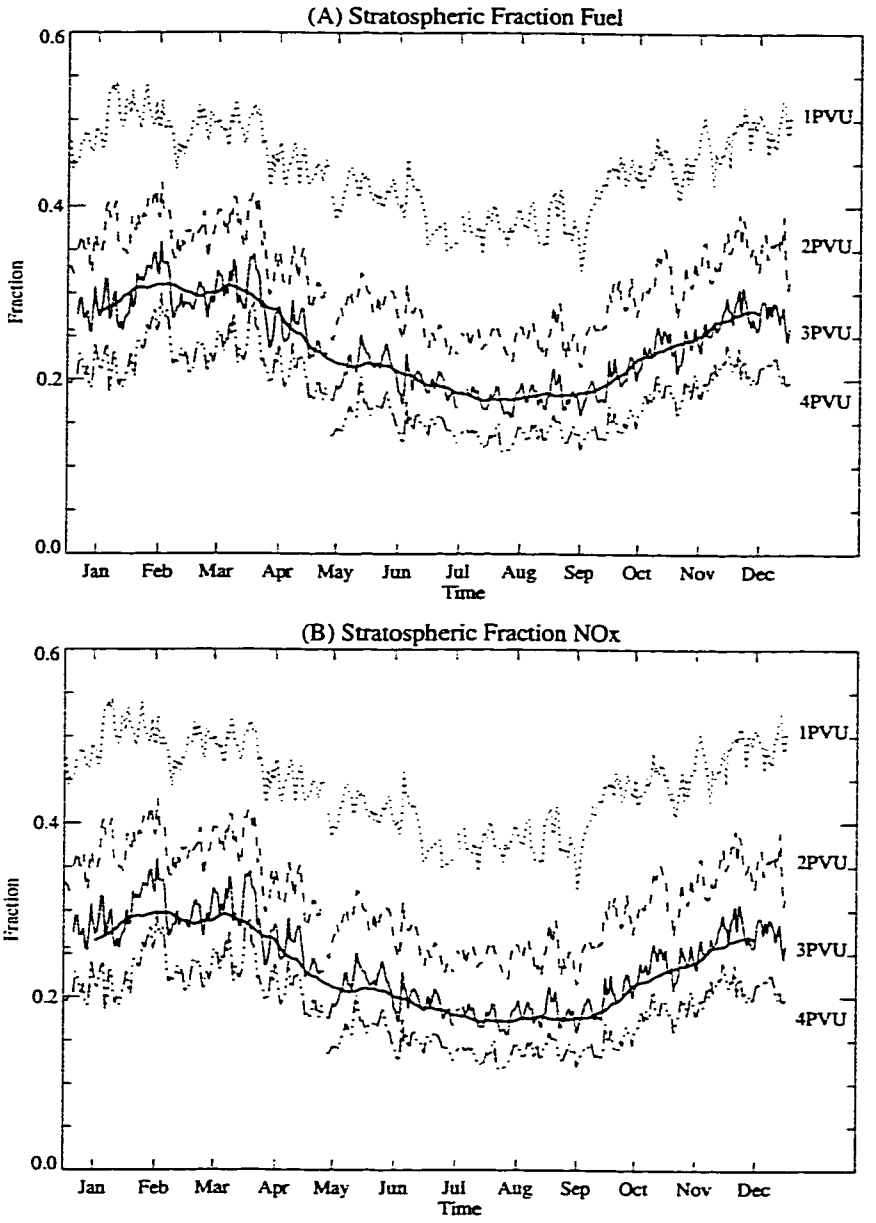

Figure 5.4: Daily fraction of emissions deposited in the stratosphere at 1 PVU (dotted lines), 2 PVU (dashed lines), 3 PVU (solid lines), and 4 PVU (dash-dotted lines) in 1992 using NCEP dynamic tropopause and NASA emissions inventory for the stratospheric fraction of (A) Fuel and (B) NO_x. Heavy line through 3 PVU tropopause is the 30 day running mean.

Table 5.2: Annual average fraction of fuel in the stratosphere calculated from 1992 tropopause data

Input Data		Tropopause Definition				
Meteorology	Inventory	4PVU	3PVU	2PVU	1PVU	Thermal
NCEP	NASA	0.18	0.24	0.31	0.44	0.20
GEOS	NASA	0.17	0.23	0.32	0.44	
UKMO	NASA	0.16	0.22	0.30	0.43	
NCEP	ANCAT2	0.14	0.19	0.26	0.39	

definition of the tropopause, the corresponding annual average fraction deposited in the stratosphere is 18% for NO_x, 9% for CO, and 12% for HC. The H_2O and CO_2 fractions are the same as that of fuel, and the mass can be found by scaling the fuel emissions (Baughcum et al., 1996). The fraction of NO_x deposited in the stratosphere is almost identical to that of fuel deposited in the stratosphere, and the fractions of CO and HC are significantly lower than the fraction of fuel, as was previously noted by Baughcum (1996). Since the daily deposition of NO_x is highly correlated with that of fuel (Figure 5.4), the remainder of the discussions will concentrate on fuel burned but are equally applicable to NO_x, CO_2 and H_2O.

Even though peak emissions occur in the summer, the fraction and mass of emissions in the stratosphere are higher in Northern Hemisphere winter than in summer, consistent with the lower midlatitude tropopause height (see Figure 5.3) in winter. For the 3 PVU surface the fraction of emissions emitted into the stratosphere is around 30% in February and less than 20% in August. This 10% range of the annual cycle is found through the various tropopause surfaces chosen. There is slightly less variability in the total mass between summer and winter than there is in the fraction. This is to be expected because the total emissions in Northern Hemisphere summer are

higher than those in Northern Hemisphere winter. Note that Table 5.2 also indicates that 26% of the current fleet emissions fall between 1 and 4 PVU in the extratropics.

The effect of using different meteorological data sets is also summarized in Table 5.2. Differences of 2% or less are seen in the fraction of emissions calculated in the stratosphere for the various data sets. NCEP analyses indicate slightly higher emissions in the stratosphere (lower tropopause height) than either the GEOS or UKMO analyses do. Generally, the variability in the daily mass fraction in the stratosphere is highly correlated between the data sets, with a correlation coefficient of 0.97 or greater. A slight systematic difference persists between the data sets, which may be due to either the different horizontal resolution or slight differences in PV calculated from the meteorological data, but in general the use of different meteorological data sets does not significantly influence the fraction of fuel deposited in the stratosphere.

The difference between the calculated global fraction for the thermal and 3 PVU dynamic tropopause definitions is 4% of annual average total emissions (Table 5.2). The result is understandable owing to differences in the summertime position of the tropopause in the Northern Hemisphere subtropics between the thermal and dynamic tropopause definitions, as is illustrated in Figure 5.3b. Figure 5.5 illustrates the daily global mass of emissions estimated using the 3 PVU dynamic tropopause and the thermal tropopause. In January the daily fraction of emissions into the stratosphere is nearly identical, but in July the slightly more poleward thermal tropopause (see Figure 5.3a) results in a lower mass of emissions in the stratosphere by about 25%, or 3×10^7 kg d^{-1}.

Table 5.2 also illustrates the effect of using different emissions data sets. The ANCAT2 data are only available for 4 separate months, so in Table 5.2 the annual average ANCAT2 data are used to compute the annual fraction. Figure 5.6 compares the daily globally integrated stratospheric deposition for 4 months of available ANCAT2 data, with the deposition using NASA data for the same tropopause surface (3 PVU). While the individual daily variability and seasonal variation are highly cor-

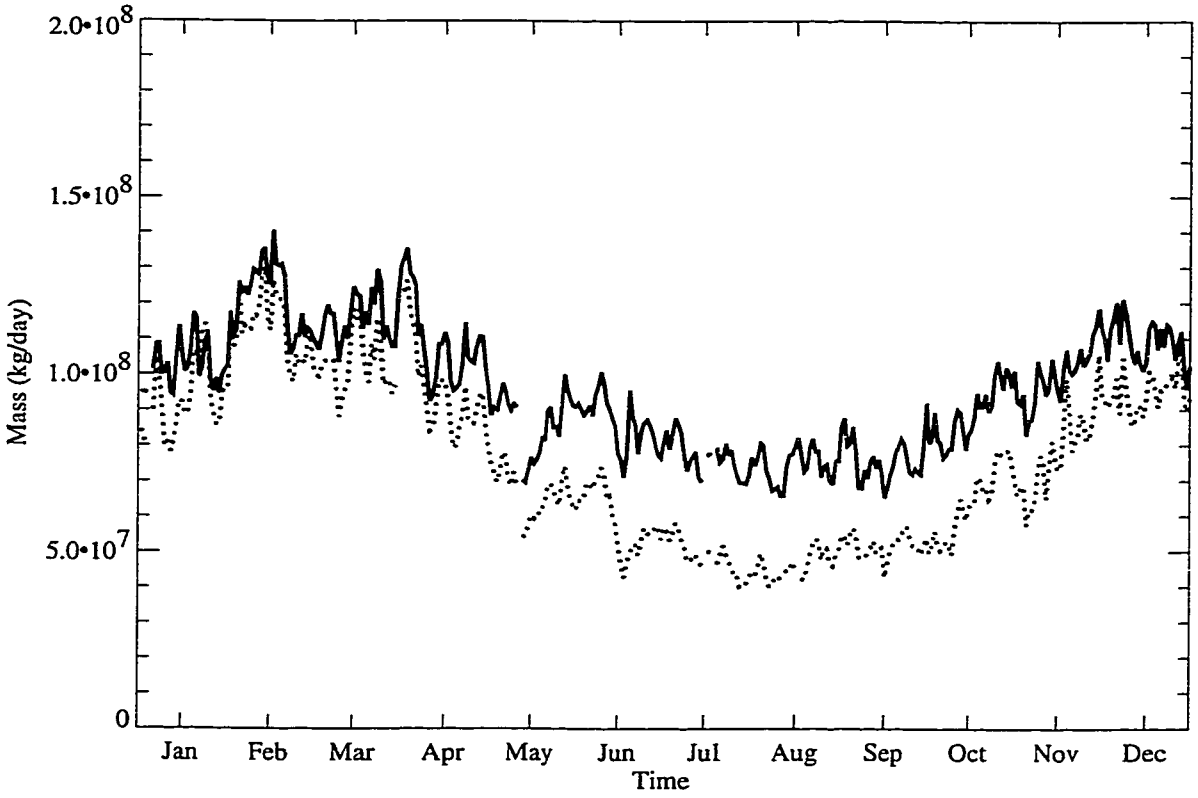

Figure 5.5: Mass of stratospheric fuel emissions for 1992 NCEP tropopause data. NASA 1992 emissions data are for the dynamic 3 PVU tropopause (solid line) and the thermal tropopause (dotted line).

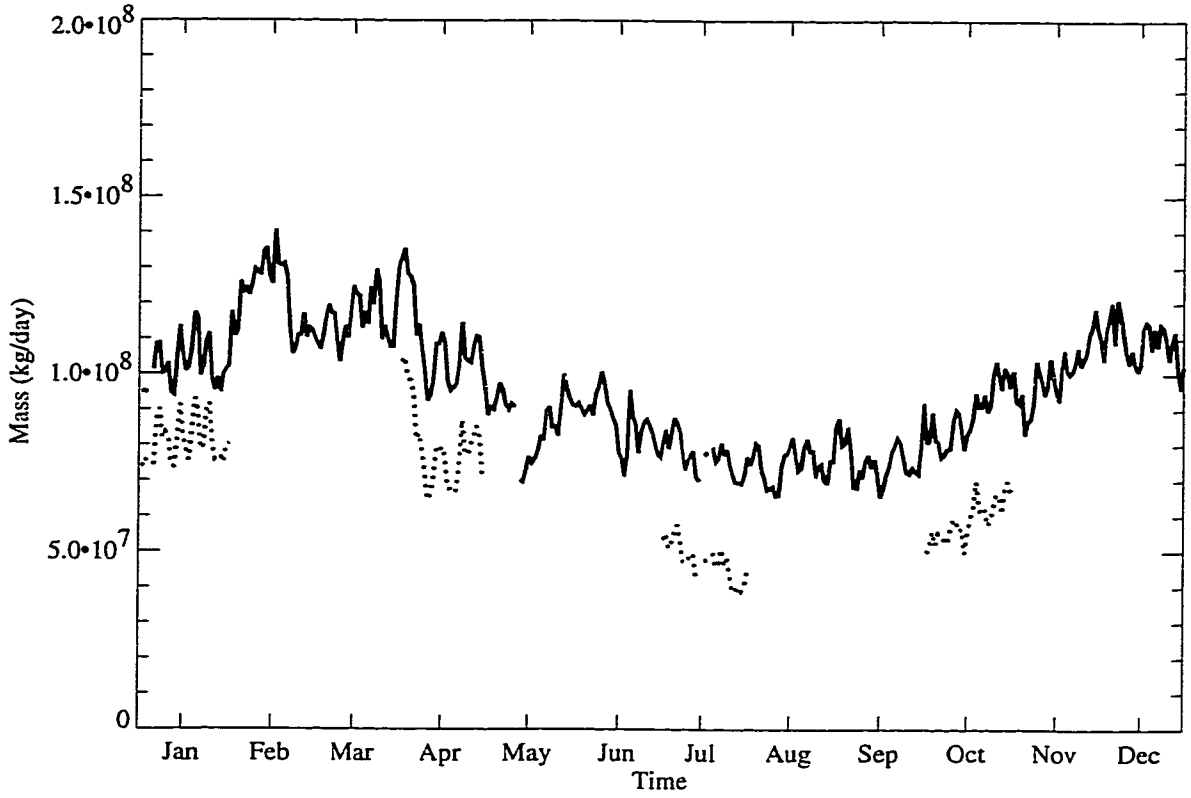

Figure 5.6: Mass of stratospheric fuel emissions for 1992 NCEP dynamic 3 PVU tropopause. Emissions data include NASA emissions data (solid line) and ANCAT2 emissions data (dotted line).

related, the ANCAT2 data show a consistently lower mass of stratospheric emissions (Figure 5.6) and lower fraction (Table 5.2). The ANCAT2 database has a slightly lower mass of total annual emissions (131 versus 139 Tg yr^{-1} for NASA), which may account for some of the difference in mass. As noted in section 5.3, the remainder of the differences are likely due to the lower cruise altitudes and different geographical distributions of the ANCAT2 data set.

Table 5.3: Fraction of NASA 1992 emissions in stratosphere with the tropopause changed by indicated height for two definitions of the tropopause using NCEP data.

Δ Tropopause, km	3 PVU	Thermal
-2	0.44	0.39
-1	0.35	0.30
0	0.24	0.20
+1	0.14	0.11
+2	0.06	0.05

5.5.2 Altitude Variation

In addition to sensitivity to the height of the tropopause, the quantity of aircraft emissions in the stratosphere is also a function of the assumed aircraft flight altitude. Such an analysis is conducted here as that in the work of Baughcum (1996) by varying the height of the dynamic (3 PVU) and thermal tropopause, relative to the aircraft emissions. The sensitivity can be assumed as an uncertainty in the flight altitudes or the tropopause heights. The aircraft emission inventories assume certain payloads and optimum flight profiles in their calculations. Actual usage and air traffic control constraints may be different. Table 5.3 illustrates the fraction of emissions in the stratosphere as the tropopause height is changed. Table 5.3 also indicates that nearly 38% of emissions are within 2 km of the 3 PVU dynamic tropopause (34% within 2 km of the thermal tropopause) and that 21% of emissions are within 1 km (19% are within 1 km of the thermal tropopause).

5.5.3 Interannual Variability

To discern the effect of interannual variability of the tropopause surface, 11 years of 3 PVU dynamic and thermal tropopause data (1983–1993) from NCEP reanalyses and

5 years of UKMO dynamic tropopause analyses (1992–1996) were used to analyze the mass of fuel burned in the stratosphere, using the 1992 NASA emissions inventory as the input for each year. The only differences between each year are due to the meteorology. Figure 5.7 illustrates the mean monthly fraction and standard deviation for 11 years of emissions calculated with the thermal tropopause. The result is not very sensitive to either the source of the meteorological data or the exact year of meteorological data chosen. The annual cycle is virtually identical for each year. The standard deviation of the monthly means is only 2% of total emissions in August and 3% in February. A similar result is obtained with NCEP or UKMO dynamic tropopause data. The range of maxima and minima on any given day for the 11 years of NCEP data in Figure 5.7 is approximately 10% of total emissions, but because of the long lifetime of emissions in the stratosphere, these daily variations are averaged out. The total expected interannual variability is thus smaller than the sensitivity to the definition of the tropopause height.

5.5.4 Regional Differences

The global picture of aircraft emissions can also be broken down into a regional picture, recognizing that emissions are not distributed evenly across the globe. The latitude of emissions is an important factor in determining the subsequent transport of emissions either within the stratosphere or between the stratosphere and the troposphere. Emissions deposited in the stratosphere at midlatitudes are unlikely to be transported significantly above the tropopause and are likely to be rapidly exchanged into the troposphere. Emissions at tropical latitudes, however, may be lofted higher into the stratosphere with the rising branch of the residual circulation (Holton et al., 1995).

Figure 5.8 presents the annually averaged fraction (Figure 5.8a) and mass (Figure 5.8b) of stratospheric emissions in the Northern Hemisphere estimated using four different dynamic tropopause heights. The fraction of emissions in the stratosphere

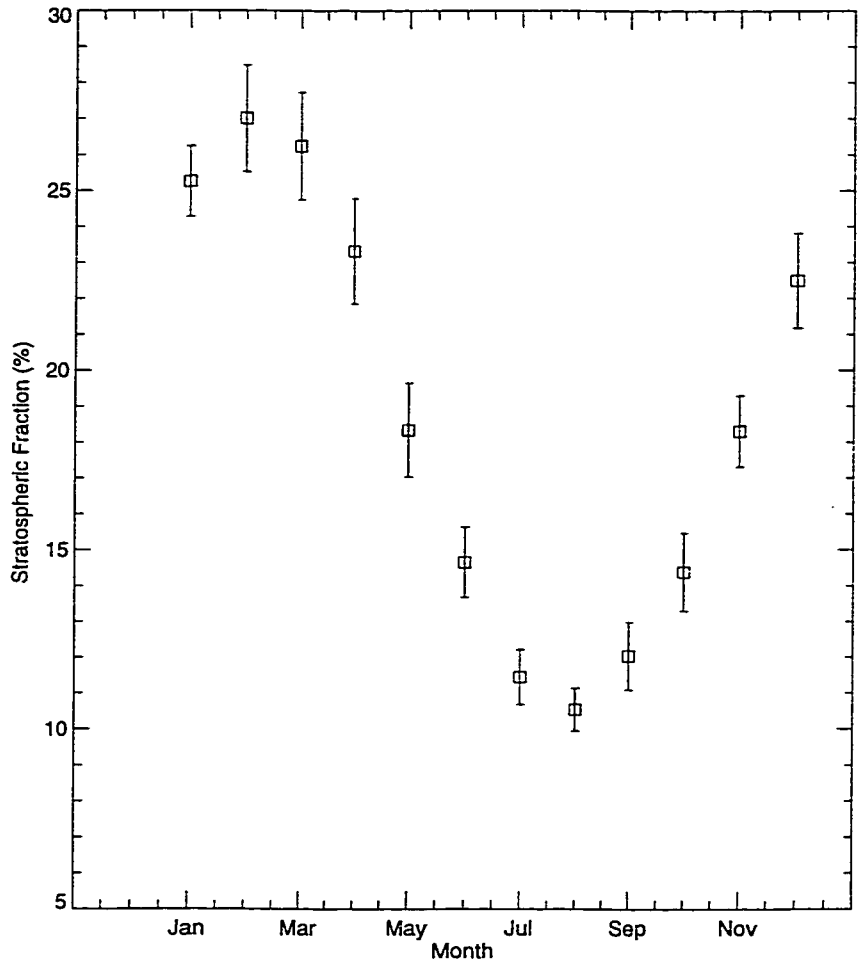

Figure 5.7: Monthly fraction of fuel in the stratosphere for 1983–1993 NCEP thermal tropopause and NASA inventory. Error bars indicate 1 standard deviation.

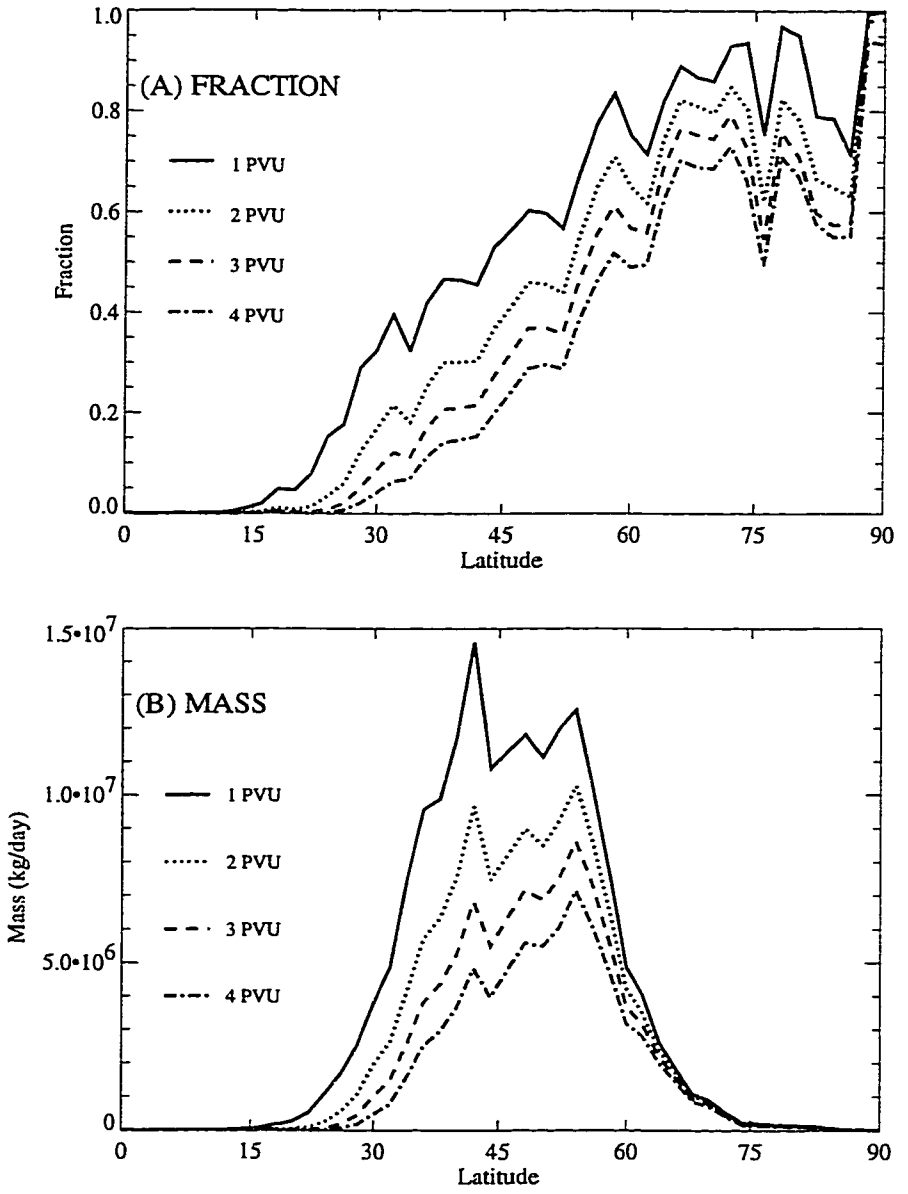

Figure 5.8: Annual average stratospheric fuel deposition for NASA inventory with 1992 NCEP dynamic tropopause in the Northern Hemisphere by latitude for (A) fraction and (B) mass.

climbs rapidly poleward of the subtropical jet. While a significant fraction (Figure 5.8a) of emissions in polar regions (70°–90°N) are in the stratosphere, the actual mass deposited in the stratosphere in these regions is not significant relative to deposition into the stratosphere at midlatitudes (Figure 5.8b). The greatest mass of emissions into the stratosphere occurs in a broad band from 45°–60°N corresponding to the latitudes of transatlantic and transpacific flight routes, as well as the latitudes of Europe (see Figure 5.2). As with the globally averaged emissions (Figure 5.4a) there is a spread of approximately a factor of 2 between emissions deposited above 1 PVU and emissions deposited above 4 PVU.

The average fraction by latitude may be affected by whether flight routes (large fraction in stratosphere) or major cities (low fraction in stratosphere owing to landings and takeoffs) are present in a particular latitude band, as is illustrated by the variability in the average fraction of emissions (Figure 5.8a) at high latitudes where the total stratospheric emissions are small (Figure 5.8b). It is important then to treat regional estimates with some caution.

A comparison with previous work illustrates some of the problems with regional analyses. Hoinka et al. (1993) estimate that 44% of aircraft cruising time is in the stratosphere, using a definition of the North Atlantic Flight Corridor (NAFC) of 45°–65°N and 50°–10°W. Using our methodology for total emissions and a definition of the tropopause from Hoinka et al. (1993) (1.6 PVU minus a 30 hPa pressure correction), we calculate a stratospheric fraction of fuel use in this region of 68% for the same years and the same NAFC region as Hoinka et al. (1993), with a range of 62–74% from 11 years of meteorological analyses. The higher fraction in our analysis is probably due to differences in the description of aircraft altitudes between the NASA inventory and the inventory used by Hoinka et al. (1993). The NASA inventory assumes ideal flight routing (great-circle routes) and altitudes, while Hoinka et al. (1993) use reported way points and flight levels, which are generally lower than optimal levels. Given this difference the results in the NAFC are not inconsistent. Note that while the

global fraction is insensitive to the interannual variability of the tropopause height, individual regions can be more sensitive. Furthermore, the estimated fraction of emissions in the stratosphere over the North Atlantic (68%) is significantly higher than the estimated global fraction of emissions in the stratosphere of 31% for a 2 PVU tropopause (Table 5.2). One major factor in this difference is that the North Atlantic region defined by Hoinka et al. (1993) is limited to aircraft at cruise altitudes, while the global average includes landings, takeoffs, climbs, and descents.

5.5.5 Future Projections

Both NASA and ANCAT2 inventories provide estimates of emissions from the total fleet in 2015. For a detailed discussion of how the growth of emissions has been determined, see Baughcum et al. (1998) and Mortlock and van Alstyne (1998) (NASA) and Gardner (1998) (ANCAT2). The future fleet growth projections are highlighted in Table 5.4, both by fraction and mass. The emissions scenarios analyzed for 2015 from both the NASA and the ANCAT2 inventories are annual averages (invariant over the course of the year). The 3 PVU tropopause surface of the NCEP 1992 meteorological data is used to analyze the stratospheric emissions. The 2015 stratospheric emissions are projected to be around 125% higher than current stratospheric emissions for both emissions inventories, which is proportional to the increase in total fuel emissions. The important conclusion from Table 5.4 is that the average fraction of fuel deposited in the stratosphere is projected to be similar for 1992 and 2015. The annual cycle of emissions and the distribution of fuel in the stratosphere by latitude are not qualitatively different between 1992 and 2015 in either emissions data set.

5.6 Temperature of Deposition

Several chemical processes in the upper troposphere and lower stratosphere, most notably contrail formation and heterogeneous chemistry on ice or hydrate surfaces

Table 5.4: Average annual emissions into the stratosphere for different tropopause definitions in 1992 and projected in 2015. Units of 10^7 kg d^{-1} for mass. Analyzed with 1992 NCEP data.

Emissions Data		Tropopause Definition							
		1 PVU		2 PVU		3 PVU		4 PVU	
Inventory	Year	Mass	Fract	Mass	Fract	Mass	Fract	Mass	Fract
NASA	1992	17.4	0.44	12.3	0.31	9.5	0.24	7.3	0.18
NASA	2015	39.3	0.46	27.7	0.32	21.0	0.24	15.8	0.18
ANCAT2	1992	13.7	0.39	9.1	0.26	6.7	0.19	4.9	0.14
ANCAT2	2015	30.3	0.39	20.3	0.26	15.0	0.19	11.0	0.14

(which regulate ozone production and loss), are strongly temperature dependent. Meteorological temperature analyses can be used along with aircraft emission inventories to explore the mass of emissions deposited at or below specific critical temperatures. One application of this analysis is to estimate the regions where contrails may form. Contrails may have an important radiative effect on the atmosphere. Boucher (1999) has recently noted the increase in cirrus cloud frequency co-located with aircraft emissions, and speculated that the local increase in cloud radiative forcing over land from 1982–1991 was 0.7 Wm^{-2}.

Contrails form from aircraft exhaust when the ambient air temperature is below a certain threshold value, as described initially described by Appleman (1953). The threshold is dependent on pressure, background water vapor content (humidity), and the engine heat and water vapor emissions. Coleman (1996) generalized the result for water vapor mixing ratio and Miake-Lye et al. (1993) and Busen and Schumann (1995) have noted that vortex dynamics and the propulsion efficiency of the aircraft can raise the threshold temperature above that predicted by theory. Busen and Schumann (1995) noted that the modified theory for threshold temperature simulates well the

observed contrail formation conditions behind a research aircraft. A key aspect of the theory is that because of the non-linear nature of water vapor saturation curves, mixing processes can lead to contrail formation in sub-saturated air. For a typical mid-latitude "dry" atmosphere (sub-saturated conditions), Coleman (1996) notes a contrail "threshold" temperature of 223°K at 9km and 215°K at 13km. For the theory of Appleman (1953) the corresponding critical temperatures for zero relative humidity and typical aircraft exhaust are 221°K at 9km and 215°K at 13km. This theory does not concern the *persistence* of contrails, which are dependent on super-saturated conditions, but merely the initial deposition environment and whether contrails form at all. Persistent contrails are generally only possible in the troposphere where the environmental humidity is high enough. To achieve a rough estimate of the "contrail potential" in the troposphere, 220°K is chosen as a threshold value, and the total mass of emissions deposited in the troposphere at temperatures lower than this is examined.

Figure 5.9 is the resulting contrail potential showing the mass of emissions deposited in the troposphere at temperatures less than 220°K when immediate contrails would be expected to form almost always, although they may dissipate rapidly in regions where the atmosphere is very sub-saturated. Figure 5.9a shows zonally integrated daily emissions and Figure 5.9b illustrates the monthly total emissions at low temperature by latitude and longitude for one month. The largest mass deposited at low temperatures is centered around 45°N (coincident with the emissions maximum in Figure 5.8b) and occurs mostly in the Northern Hemisphere winter season, with a lower mass in the Northern Hemisphere summer. In the Southern Hemisphere the contrail potential maximum is closer to the equator at around 30°S, and occurs in the fall (March to June). The total mass at NCEP temperatures below 220°K is 30 Tg yr^{-1}, which is 21% of annual total emissions (estimated with NCEP 1992 3 PVU tropopause data and NASA emissions scenario). Figure 5.9b indicates that emissions in the troposphere at low temperatures in January occur predominately over Europe,

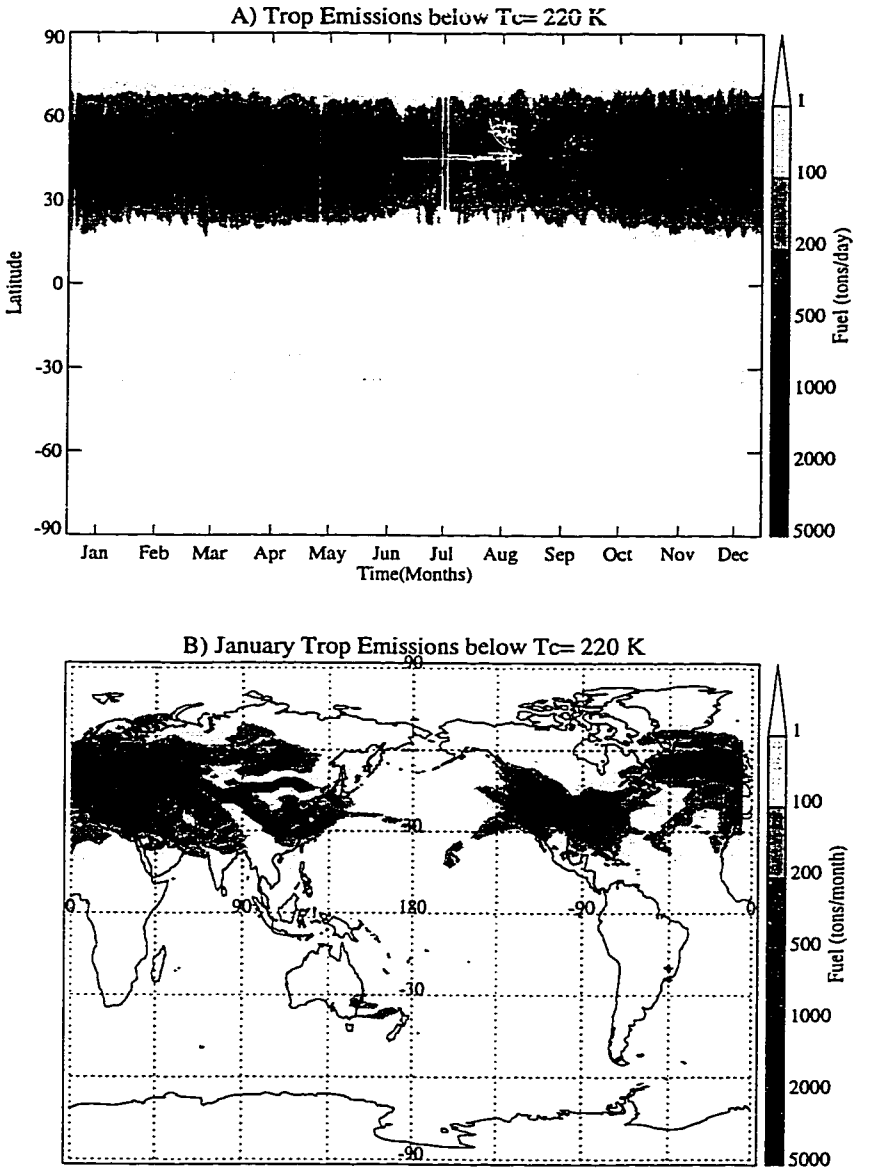

Figure 5.9: Metric tons (10^3 kg) of aircraft emissions from NASA 1992 inventory deposited in the troposphere (3 PVU Tropopause) at NCEP temperatures below 220°K for 1992 Meteorology. A) Zonally integrated per day by latitude for each day of 1992. B) By month for January 1992.

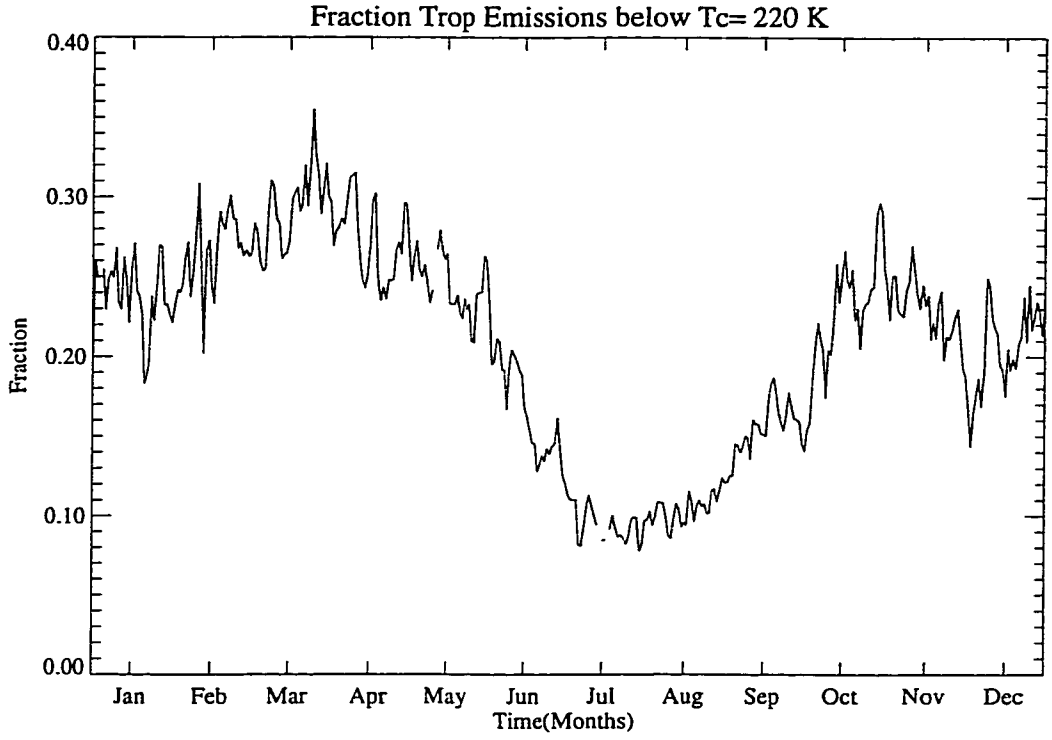

Figure 5.10: Fraction of daily aircraft emissions per day from NASA 1992 inventory deposited in the troposphere (3 PVU Tropopause) at NCEP temperatures below 220°K for 1992 Meteorology.

the North Atlantic, and Western North America. The fraction of daily emissions occurring below these temperatures is plotted in Figure 5.10. There is a strong annual cycle with the maximum fraction of emissions deposited at or below typical contrail formation temperatures occurring in March and the minimum in July. These contrail potential plots in space and time are only approximate. The critical temperature depends on details of the engine performance (Coleman, 1996). To determine the persistence of contrails, ambient water vapor measurements are vital. This analysis then is only a boundary condition exercise. It does not consider persistence of upper tropospheric contrails (so the fraction cannot be converted into a sky cover), which is dependent also upon local ambient humidity. Some gross comparisons from this

boundary condition exercise with previous studies are possible. The seasonal cycle of contrail coverage found by Sausen et al. (1997) is higher in January than July in agreement with the analysis here. Combining this data with humidity data would enable an estimate of contrail frequency and fractional sky coverage. This would then allow a direct comparison with the coverage experiments of Sausen et al. (1997) and the radiative forcing experiments of Ponater et al. (1996).

5.7 Conclusions

Analysis indicates that stratospheric emissions from the current world aircraft fleet are concentrated in Northern Hemisphere midlatitudes as expected from air traffic patterns and the latitudinal variation of tropopause height. Emissions into the stratosphere are higher in January than in July because of the lower tropopause heights in the Northern Hemisphere midlatitudes in winter, despite slightly higher total emissions in July. The maximum deposition of emissions into the stratosphere occurs in February, and the minimum occurs in August. Emissions of NO_x track closely the emissions of fuel, which is not the case for CO and hydrocarbons, which have a lower fraction of total emissions deposited into the stratosphere.

The annual average stratospheric emissions fraction from the current fleet is between 18–44% of the total fuel burned. The range of estimates is derived from different dynamic tropopause heights, defined using potential vorticity. An alternate way of approaching these estimates is to note that 26% of total aircraft fuel loading is emitted between 1 and 4 PVU or 21% of total fuel loading is within $\pm$ 1 km of the 3 PVU tropopause, 38% within $\pm$ 2 km of the 3 PVU tropopause. The tropopause definition is critical for estimating the total stratospheric burden of aircraft emissions.

Further tests on the results indicate sensitivity to several factors beyond just tropopause height and insensitivity to others. The meteorological data set used to estimate the tropopause height makes little difference in the results. In midlatitudes

where the results are most sensitive to tropopause height, the tropopause surfaces estimated from different assimilated data fields are virtually coincident. While the thermal tropopause is nearly coincident with the 3 PVU surface, there exist slight differences in the tropics and in the structure of the summer hemisphere tropopause "break." The height of the tropical tropopause does not affect the emissions deposited into the stratosphere. However, the difference in structure of the subtropical tropopause break between the thermal and dynamical definitions does lead to higher annual average emissions when the tropopause is defined dynamically. The interannual variability of the tropopause is a less significant factor in estimating the quantity of emissions into the stratosphere than the variability in tropopause height is.

When different emissions data sets are used in the analysis, there are consistent differences in the fraction and mass of emissions deposited in the stratosphere. The mass is expected to be slightly different due to differences in total emissions between methods of the order of 5–10%. However, the ANCAT2 inventory has higher emissions at lower altitudes than the NASA inventory does (resulting in fewer stratospheric emissions). The seasonal evolution and latitudinal distribution of both data sets are very similar. The results are sensitive to the assumed flight altitudes. Both inventories have been developed assuming optimum performance for an estimated aircraft payload (passengers plus cargo). Air traffic control constraints and heavier payloads may result in lower flight altitudes.

The results of this analysis compare favorably with those of previous studies (Baughcum et al., 1996; Hoinka et al., 1993). However, care must be taken in comparing regional analyses with global analyses, as the results can be quite different depending upon the exact region chosen. For global analyses fractions are convenient, but they can be misleading for regional analysis. Because the residence time of emissions in the stratosphere is of the order of 1–2 months (Gettelman, 1998), regional analyses are not appropriate for studies of transport and chemistry in the lower stratosphere.

Estimates are also available for emissions from the future (2015) subsonic aircraft fleet. Though the absolute magnitude of emissions into the stratosphere is expected to more than double, the increased deposition is not expected to significantly alter the annual fraction and latitudinal distribution of mass in the stratosphere. Most of the aircraft that will be flying in 2015 have already been designed and their flight characteristics are unlikely to change significantly. As a result, the fraction of total aircraft emissions into the stratosphere is unlikely to vary drastically from the present fraction by 2015. In addition, future traffic growth projected by these inventories (Baughcum et al., 1998) is expected to remain strongest in the Northern Hemisphere midlatitudes, not significantly changing the latitude of maximum emissions.

One fifth of emissions are deposited in the troposphere at temperatures where momentary contrails might form, with a maximum in Northern Hemisphere winter and a minimum in Northern Hemisphere summer. The present analysis is not able to ascertain whether these contrails will persist, which is necessary for them to have a climatic impact. Persistence requires information on the water vapor mixing ratio (specific humidity) in the upper troposphere and lower stratosphere, as characterized by Sausen et al. (1997).

In summary, the deposition of emissions from the current aircraft fleet into the stratosphere is most strongly dependent upon the definition and altitude of the tropopause and the assumed flight altitudes. The sensitivity has important implications for model studies of the effect of these emissions once deposited. The transport characteristics of the upper troposphere and lower stratosphere are quite different (Holton et al., 1995). Emissions can be cleansed from the troposphere much more rapidly than emissions in the stratosphere can.

Our conclusions strongly suggest that chemical transport model studies of the effect of aircraft emissions need a realistic description of the tropopause altitude and nearby regions of both the stratosphere and the troposphere, including tracer transport within such regions. Since a significant fraction of emissions are deposited within

1 km of the tropopause, correctly treating the deposition altitude and the transport processes near the tropopause is critical for diagnosing subsequent buildup and accumulation of aircraft emissions and their chemical impact. Chemical transport models may require higher resolution or better formulation of tracer transport in the region around the tropopause for such studies.

The most appropriate definition of the tropopause is probably dependent upon the type of analysis desired. In general, defining the tropopause using the dynamic definition allows a greater analysis of the sensitivity to stratospheric deposition. For the calculation of transport and chemical effects of emissions using models, it is probably wise to diagnose the tropopause using a range of definitions in the absence of a better method of judging the ability of models to capture stratosphere-troposphere exchange. Such estimates in the literature range from 1.6 to 3.5 PVU. This approach has been used by Gettelman (1998) with these emissions scenarios and a transport model to estimate the lifetime of deposited emissions in the stratosphere, discussed next in Chapter 6.

Chapter 6

THE EVOLUTION OF AIRCRAFT EMISSIONS IN THE STRATOSPHERE

Aircraft emissions deposited in the lower stratosphere will have a longer residence time than tropospheric emissions, and in many cases qualitatively different radiative or chemical effects, as Wennberg et al. (1994) noted for nitrogen oxide (NO_x) emissions. An accurate assessment of the effects of the present and future fleet of subsonic aircraft thus requires a careful consideration of the exchange of trace constituents between the stratosphere and the troposphere. As described by Holton et al. (1995) and in Chapter 2, exchange across the tropopause can occur by both diabatic processes and through quasi-adiabatic processes along a constant potential temperature surface (an isentrope). The dominant tendency in the tropics is for cross isentropic exchange from the troposphere to stratosphere driven by the global scale diabatic or residual circulation. In the extra-tropics, both isentropic and cross-isentropic exchange are important (Danielsen, 1968), and the global net tendency is for exchange from the stratosphere to the troposphere.

Previous studies of subsonic aircraft have either focused on the chemical effects of emissions (Brasseur et al., 1996) or concentrations of constituents (van Velthoven and Kelder, 1996). A large literature exists on the stratospheric residence time from the higher altitudes of a proposed supersonic fleet Stolarski et al. (1995). Estimates of the residence time of emissions in the stratosphere range from 13 months for supersonic emissions at 50 hPa (Weaver et al., 1996) to 0.5 months for parcels at 11 km (Schoeberl et al., 1998). This Chpater will use more realistic descriptions of the sub-

sonic emissions distribution and the tropopause region to estimate the stratospheric residence time of emissions from the current fleet, and to analyze transport pathways between the stratosphere and troposphere. We will also examine the burden of aircraft emissions in the atmosphere, based on continuous emission and parameterized loss, and the temperature distribution of emissions after deposition.

Emissions will be simulated in a transport model as a conserved tracer. The residence time of emissions in the stratosphere is estimated by tracking the evolution of emissions in the stratosphere and troposphere. The transport model is described below, followed by the methodology and datasets used. Finally, results and conclusions are presented.

6.1 Model Description

The transport model of the laboratory for atmospheres at the Goddard Space Flight Center is used for this analysis. The model is discussed more fully in Chapter 4, and only a brief description is provided here. The model has previously been used to examine projected NO_y emissions from supersonic aircraft (Weaver et al., 1996), and is capable of accurately simulating synoptic features in chemical tracers on a global scale (Douglass et al., 1996).

The three-dimensional flux form semi-Lagrangian transport code (Lin and Rood, 1996) uses winds from the Goddard Earth Observing System (GEOS) Assimilation System (Schubert et al., 1993). Model resolution is 2° latitude by 2.5° longitude with 46 sigma levels in the vertical from the surface to 0.1 hPa. The model sigma levels are spaced approximately 1.5 km apart around the mid-latitude tropopause. Input winds are interpolated to a 900 second timestep from 6 hourly data. Explicit convective transport is not included in the base case. These simulations use data from January through September 1996.

The analysis also incorporates trajectory simulations using the trajectory model

developed by Schoeberl and Sparling (1994). The isentropic model is also run in diabatic mode by applying heating rates to the trajectories at each time step. The trajectory model is discussed more fully in Section 4.6 and has been used in a similar study of aircraft emissions by Schoeberl et al. (1998).

6.2 Methodology

The sub-sonic aircraft emissions inventories developed by NASA (Baughcum et al., 1996) and the ANCAT/EC group (Gardner et al., 1997), which are discussed in more detail in Chapter 5, are interpolated to the model grid, and one day of emissions (in kilograms) is converted to mixing ratio. The concentration is then advected as a passive tracer starting in January and July for 90 days. The tracer mass conservation in the model is better than 95% over 90 days. Most of the mass change is an adjustment occurring at the lowest model level, and does not effect the analysis in the upper troposphere and lower stratosphere.

The residence time of aircraft emissions is defined as the 'e-folding' or response time (Rodhe, 1992). For a system relaxing from a state χ_0 the residence time is computed from:

$$\chi_t = \chi_0 e^{-kt} \tag{6.1}$$

where k^{-1} is the e-folding time.

Simulations were also conducted using only stratospheric or tropospheric fractions of the emissions dataset. To examine how well the dynamical information is represented in the assimilation winds, a conserved tracer is also initialized equal to the absolute value of potential vorticity. Discussion of a simulation in which convective mass fluxes are included is also presented. Finally, simulations performed by Danilin et al. (1998) using continuous emissions and a sink in the troposphere are analyzed to estimate the atmospheric burden of emissions.

For this analysis, it is logical to divide the stratosphere into two regions, following

Holton et al. (1995) as discussed in Chapter 2. Recall that the 'overworld' is that region of the stratosphere which lies completely above the potential temperature of the tropical tropopause (approximately 380 Kelvin), and the 'lowermost stratosphere' is that region of the stratosphere between this surface and the tropopause. Exchange between the overworld and the troposphere requires diabatic motion, whereas exchange between the lowermost stratosphere and troposphere can occur along an isentropic surface.

For analyzing the stratosphere-troposphere exchange of mass and constituents a dynamical definition of the extratropical tropopause based on Ertel's potential vorticity (PV) is superior to the usual thermal definition (Holton et al., 1995). The tropopause is analyzed daily as a set of material surfaces by constructing a map of the tropopause height using a range of coordinate values of potential vorticity in the extra-tropics and a potential temperature surface in the tropics. PV values for the tropopause are generally in the range of 1.6 PVU to 3.5 PVU (Hoskins, 1991) where 1 PVU=10^{-6} $Kkg^{-1}m^2s^{-1}$. Values examined are 2, 3 & 5 PVU. The temperature and wind data used to construct the tropopause surface are taken from the same assimilation as the winds used to drive the transport model.

6.3 Results and Discussion

Figure 6.1 presents the zonal mean of the initial concentration of aircraft fuel. The distribution is the same as Figure 5.1 interpolated to the model grid and converted from daily total mass in kilograms to mixing ratio evenly distributed over a model grid box. Overplotted are three different analyzed tropopause surfaces showing their approximate vertical separation, and the 380K potential temperature surface, marking the boundary between the 'overworld' and the 'lowermost stratosphere'. The majority of emissions occur in the northern hemisphere. The highest concentration of emissions is situated near the latitude and altitude of the northern hemisphere mid-latitude

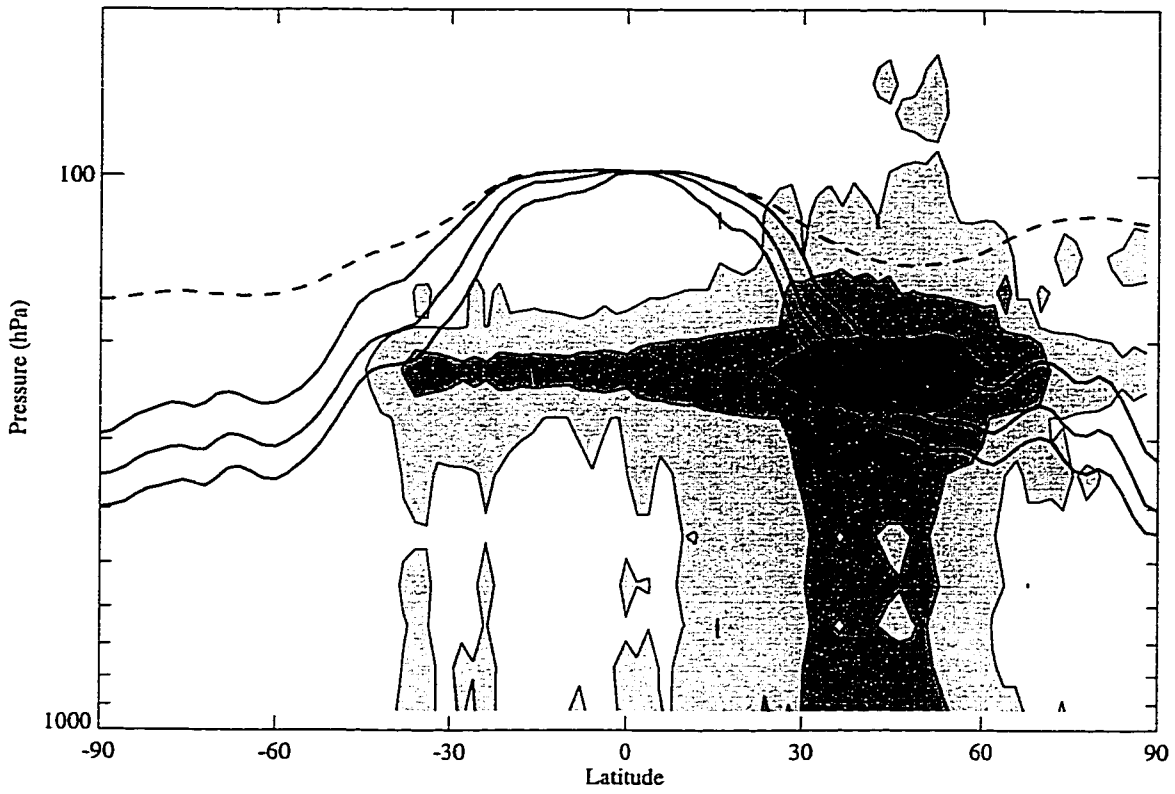

Figure 6.1: Zonal mean initial condition of aircraft emissions. Contours are 0.01, 0.1 and 1 ppbv of fuel. Thick solid lines represent the zonal mean tropopause for 0000 UTC on January 1, 1996 at 3 PV surfaces (2,3 & 5 PVU). The dashed line indicates the 380 K potential temperature surface.

tropopause 'break'. The initial fraction of aircraft fuel in the stratosphere in January and July is given in Table 6.1. The total mass of aircraft emissions is 14% larger in July than in January, but the fraction and absolute mass deposited into the stratosphere is larger in January as noted in Chapter 5 (Gettelman and Baughcum, 1999). These estimates are not substantially affected by the inventory data set, tropopause data source or interannual variability of tropopause height as discussed in Chapter 5.

The global mass of emissions relative to the analyzed tropopause surfaces is computed daily. The resulting mass of emissions in the troposphere, lowermost strato-

Table 6.1: Fraction of fuel in the stratosphere (NASA92 emissions database)

Tropopause	2 PVU	3 PVU	5 PVU
January	0.35	0.29	0.17
July	0.24	0.18	0.10

sphere and stratospheric overworld using the ANCAT emissions dataset is plotted for January-March in Figure 6.2 and for July-September in Figure 6.3. The decline of emissions in the lowermost stratosphere is gradual and is well described by an exponential decay, indicated by the thin solid lines. The *e*-folding residence times calculated using Equation 6.1 are presented in Table 6.2. Alternative emissions data sets (NASA data), or meteorological time periods (1995), do not substantially affect the estimates. The residence time is in the range of 40 days in January and 50 days in July, and decreases as the tropopause height increases. Figure 6.2 and Figure 6.3 indicate that after 60 days the rate of decay begins to slow. The initial faster rate of decrease is likely the advection of the initial distribution in the stratosphere into the troposphere. The subsequent slower decay is likely emissions from the troposphere slowly transported into the stratosphere and then exchanged back into the troposphere. The change in rate could also be a separation of the transport regime at different levels in the lower stratosphere. Chen (1995) found that transport between the stratosphere and the troposphere was more vigorous below the 350K potential temperature surface than above it.

An exponential decay has also been found by Schoeberl et al. (1998) in trajectory simulations of parcels in the overworld. Schoeberl et al. (1998) parameterize removal from the stratosphere when parcels pass a given pressure surface, which does not fully capture tropopause variability. The residence time is shorter than the 200 day residence time for a tracer just above the tropopause estimated with a 2-dimensional

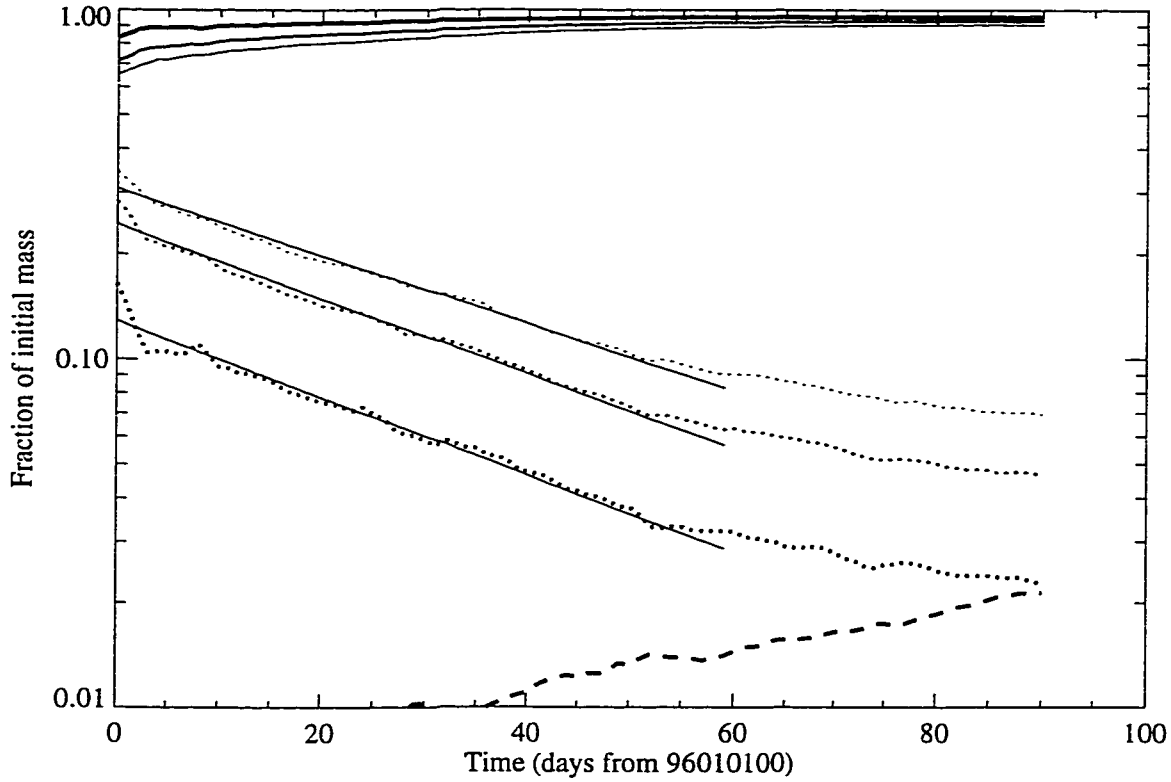

Figure 6.2: Evolution of aircraft emissions starting 1 January 1996 from ANCAT emissions inventory. Solid lines - tropospheric component, dotted lines- lowermost stratosphere and dashed line - stratospheric overworld. Thicker lines indicate a higher PV tropopause surface - 2,3 & 5 PVU shown. Thin solid lines are exponential fits to the mass of emissions in the lowermost stratosphere.

model by Niedermeier and Fabian (1994). The estimated residence time is also longer than a rough estimate of 30 days from the Eulerian diabatic heating in this region (-1K day^{-1}), and the change in potential temperature from the emissions altitude to the tropopause (320K to 290K).

The residence time estimates are similar to those estimates produced by other models, as illustrated in Table 6.3. The estimates from the conservative tracer and estimated using heating rates are comparable to similar calculations using a suite of global atmospheric models. The method used for the other model calculations

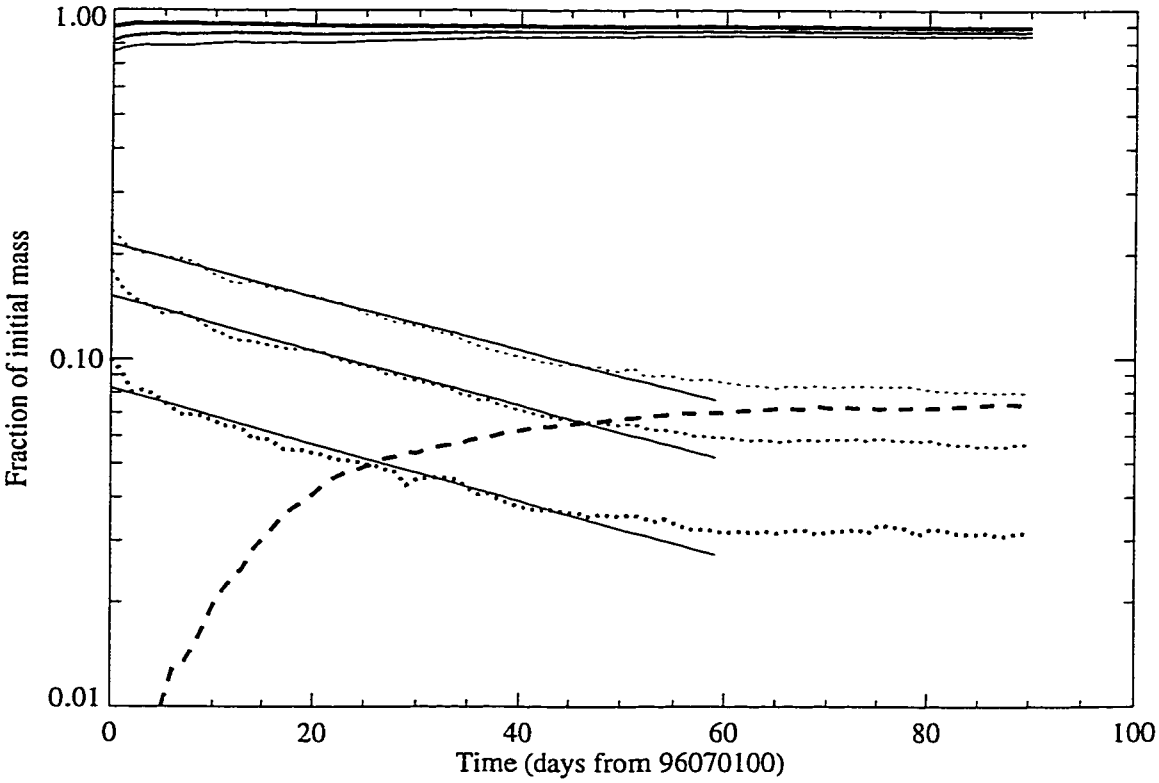

Figure 6.3: Same as figure 2 but starting 1 July 1996.

Table 6.2: *e*-folding residence time of emissions in the lowermost stratosphere (ANCAT data- 1996) in days

Tropopause	2 PVU	3 PVU	5 PVU
January	45	40	38
July	57	55	53

Table 6.3: Residence times of subsonic aircraft emissions in the lower stratosphere for a variety of models. First three rows (conservative tracer, and heating rate calculation) are from this analysis (Gettelman, 1998). Two dimensional (2D) and three dimensional (3D) model values are taken from Danilin et al. (1998) and Fahey and Schumann (1999).

Model		Residence Time (days)	Range (days)
Conserved	JULY	55	53-59
Conserved	JAN	40	38-45
Diabatic Heating		30	20-40
2D	AER-2D	38	
	GSFC-2D	62	
	LLNL-2D	65	
	UNIVAQ-2D	23	
3D	ECHAM3	22	
	GSFC-3D	52	
	KNMI/TM3	21	
	UCI/GISS	27	
	UIO	29	
	UMICH	45	
	UNIVAQ-3D	25	

(described by Danilin et al. (1998)) is slightly cruder than that here as it does not detail the tropopause and does not include a sensitivity analysis (as defined by the error bars for the conservative tracer and heating rate estimates). However, note that the 'GSFC-3D' model in Table 6.3 is the same model as that used here, indicating that the results are comparable.

The three-dimensional aircraft emission tracer spreads throughout the mid-latitude tropopause region, and in the tropics is lofted to the base of the stratospheric overworld. Most extratropical emissions in the lowermost stratosphere remain at low potential temperatures. While there is evidence of exchange from the tropics into the mid-latitudes at higher potential temperatures in the summer hemisphere, little such exchange is evidenced in winter, in agreement with the isentropic simulations of Chen (1995).

To detail quasi-isentropic exchange between the stratosphere and the troposphere, the tropopause was used to separate the initial emissions into a stratospheric and tropospheric component. Each component was advected separately for 30 days. In a schematic zonal mean format, Figure 6.4 illustrates the initial and final mass fractions, and the adjustment over 30 days. In July, quasi-isentropic transport into the lowermost stratosphere accounts for half of the mass remaining, while in January, it is a much lower fraction of stratospheric emissions, and is confined to lower potential temperatures. In 90 days almost all the original lowermost stratosphere emissions have entered the troposphere.

Figures 6.2 and 6.3 also show the buildup of aircraft emissions in the stratospheric overworld, mostly by transport through the tropical tropopause. Aircraft emissions in the stratospheric overworld are 7% in July and 2% in January at the end of the 90-day period examined. In July tropical emissions are 10% higher and a significant quantity of emissions are lofted into the stratospheric overworld near the subtropical edge of the tropical tropopause. The pathway has been verified using a diabatic trajectory model with independent wind analyses. Transport experiments with other tracers

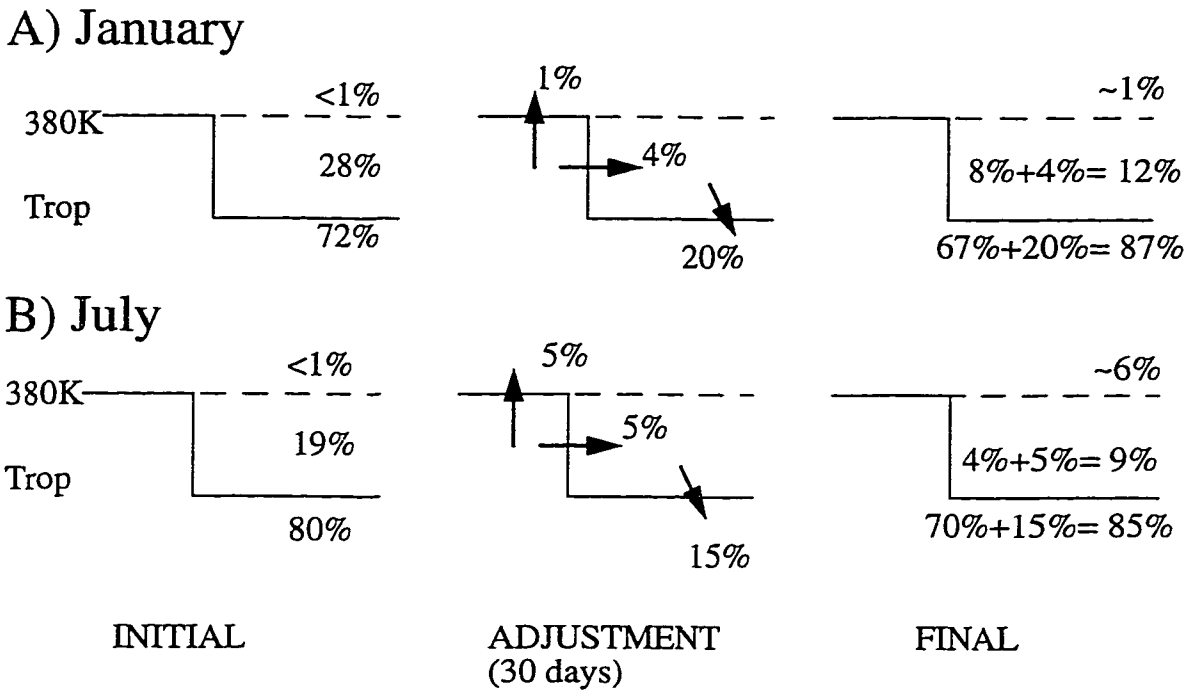

Figure 6.4: A)January and B)July mass fractions in the troposphere, stratospheric overworld and extratropical lowermost stratosphere. Solid lines are the tropopause, and dashed lines the 380K potential temperature surface. Equator is on the left, the pole is on the right. Left to right panels show initial mass fractions, net adjustment and final mass fractions as the sum of remaining plus advected mass.

such as CO_2 (Strahan et al., 1998) and water vapor (Chapter 7) indicate that vertical transport in the overworld using this model is much faster than observed. Thus the estimated concentration of emissions transported to the overworld in 90 days may be high.

A tracer was also initialized whose mixing ratio gradient is everywhere equal to the potential vorticity gradient. Over 30 days, a correlation map on a pressure surface in the lowermost stratosphere (223 hPa) indicates that correlation coefficient between a potential vorticity tracer and analyzed potential vorticity in mid-latitudes averages 0.85. Since in the absence of significant diabatic processes potential vorticity is approximately conserved, the strong correlation indicates that simulated transport accurately reflects the dynamics of the lower stratosphere.

The decay rates illustrated in Figures 6.2 and 6.3 are remarkably steady given the variability of the tropopause surface. A closer analysis of a single point or latitude band indicates significant daily variability in the tropopause height. Several tropopause folding events are observed during the period of the simulation where air with high tracer concentrations is cut off from stratospheric air and remains in the troposphere, increasing local tropospheric tracer concentrations. Throughout the simulations, steep tracer gradients are maintained between the stratosphere and the troposphere. Even with this realistic behavior, it is possible that the model is unable to resolve significant local processes that lead to greater variability in the integrated rate of stratosphere-troposphere exchange.

The simulations described thus far do not consider convective fluxes. Because aircraft emissions are predominately deposited in the upper troposphere, convective transport will not bring significant emissions from the lower troposphere. Also, aircraft generally avoid convective updrafts, and fly in regions of subsidence surrounding convection. Convection might however entrain aircraft emissions and carry some upward. Simulations with convective fluxes (C. J. Weaver, 1998, personal communication) indicate that including convective mass fluxes reduces upper tropospheric

concentrations, consistent with the results of transport simulations by van Velthoven et al. (1997). Reducing upper tropospheric concentrations would also tend to reduce the quantity of emissions in the overworld and reduce the estimated residence time of emissions in the stratosphere, by decreasing the troposphere to stratosphere transport. The residence time estimates should thus be considered as upper bounds.

6.4 Trajectory Model Analysis

The Eulerian transport study can also be supplemented with a Lagrangian viewpoint by using a trajectory model to evaluate the dispersion of parcels along aircraft flight tracks. Such an analysis with supersonic emissions has been performed by Sparling et al. (1995). Here the analysis is repeated in a limited way with subsonic emissions to examine the region and temperature to which aircraft emissions are transported after the deposition considered in Chapter 5.

For this analysis, a limited set of flight tracks is constructed based on the optimal routes that aircraft would fly given atmospheric conditions, chiefly headwinds. Aircraft do not necessarily fly great circle routes as assumed in the development of emissions inventories (Baughcum et al., 1994). A more realistic set of routes was derived from the JEPPSEN commercial flight planning service using actual flight path parameters and climatological winds. Most notably, a strong winter jet stream over the North Pacific results in flight routings to very high northern latitudes over northern Alaska and Siberia on San Francisco to Hong Kong westbound routings. While these routings may not be fully realistic[1], they provides an interesting exercise on the potential for deposition and transport.

A simulated parameter-space for aircraft fuel emissions for 21 days after initial emission during February on four sample routes between cities in the North Pacific (San Francisco and Hong Kong), North Atlantic (New York and London), Central

[1]Air traffic over Siberia is still restricted and commercial traffic routings are not permitted there (S. L. Baughcum, 1997, personal communication)

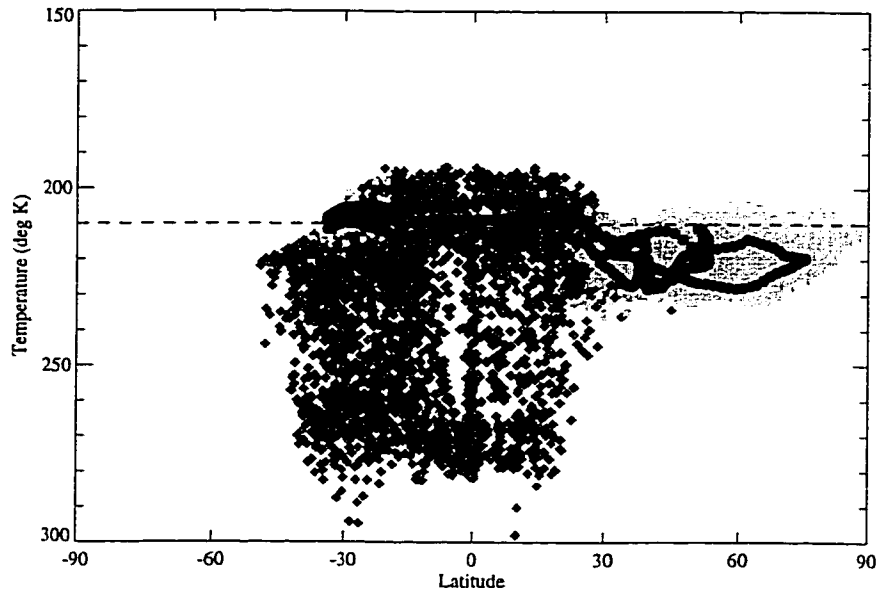

Figure 6.5: Temperature of aircraft emissions as a function of latitude though 21 day trajectory evolution. Positions of 475 trajectories every day for 21 days. February 1992 NCEP meteorology. Black circles: initial positions. Dark grey diamonds: Position of parcels in Troposphere. Light grey squares: Position of parcels in stratosphere. Dotted line is 210°K. Tropopause is the 3 PVU surface and 380K in tropics.

Pacific (San Francisco and Sydney) and Western Pacific (Hong Kong and Sydney) is illustrated in Figure 6.5. Parcel potential vorticity, temperature and potential temperature are tracked along trajectories, and the latitude of the parcels are displayed along with their temperature and location in the stratosphere or troposphere each day for 21 days. The potential temperature range for the initial emissions is 343-384K. Parcels in the tropics mostly remain in the troposphere. A few tropical parcels have risen into the stratosphere in the tropics and subtropics. Parcels in the stratosphere are generally descending (decreasing potential temperature is not shown), but have not significantly entered the troposphere after 21 days, consistent with the longer residence time indicated by the transport model simulations. In the subtropics, quasi-isentropic exchange across the tropopause does occur for a few parcels.

Figure 6.5 also indicates that routes in the northern hemisphere may deviate significantly into very high latitudes (up to 75°N), as a consequence of attempting to avoid regions of strong headwinds. Temperatures on these trajectories in high latitudes are as low as 210°K–205°K (-63°C to -68°C) where aerosol mediated reactions may increase ozone loss rates (Solomon et al., 1997), and formation of Polar Stratospheric Clouds in aircraft plume conditions are possible (Schumann, 1994). Deposition occurs at temperatures above this, but parcels are transported in 21 days to higher latitudes with colder temperatures. For the trajectory calculation in Figure 6.5, 9% of parcels beginning above 45°N end up at temperatures below 210°K in 21 days. 23% of parcels on these four flight routes encounter temperatures below 210°K poleward of 45°N over this period.

Thus while significant deposition may not occur at low temperatures, subsequent evolution (again, with an anomalous condition—in this case the flight routing) might transport significant NO_x or aerosol emissions to low temperature regions. It is not likely (given the global analysis discussed in Chapter 5) that this will be a significant effect in the near future. However, if deviations of the Northern Hemisphere jet stream conditions associated with low temperatures at flight altitudes are associated with deviations of aircraft flight paths into these regions then the quantity of emissions deposited at these temperatures might be larger than implied by analyses of deposition using great circle routes (Chapter 5). One way to approach this question is to examine aircraft reported flight level temperature data.

6.5 Atmospheric Loading

Given the residence time of emissions derived here, it is reasonable to attempt to put this problem in perspective and ask if the distribution and residence time of emissions will generate significant effects. While this issue has been addressed in more complex coupled chemical transport model experiments (for a review see Fahey

and Schumann (1999) and references therein), the analysis here will simply attempt to frame the problem. To perform this analysis, the transport simulations have been run using the aircraft emissions with a continuous emission (rather than just a momentary emission) and a sink in the troposphere, using otherwise identical model parameters. These runs were performed by C. J. Weaver as part of an intercomparison study by Danilin et al. (1998). Simulations of the total mass of fuel were run for 5 years, using the same meteorology each year, with and without convective mass fluxes.

Convective mass fluxes reduce the total quantity of emissions in the atmosphere, as noted previously. If convective mass fluxes are included in the continuous simulation, the mass of emissions remaining in the overworld is decreased by 70% (from 7 x 10^9 kg to 2 x 10^9 kg), and the summertime mass in the northern hemisphere middleworld is reduced by 25%. The mass of emissions in the troposphere is reduced by 1/3. Similar reductions in the atmospheric loading of aircraft emissions with convection have also been noted in simulations by van Velthoven et al. (1997). To estimate the potential effect of emissions, the loadings with convection and without convection will be examined for nitrogen oxides, sulfur, and soot.

The NASA 1992 emission inventory was used as input to this analysis. The total fuel loading can be multiplied by the emission index (EI) to generate maps of total mass or concentration. Zonal mean NO_x concentrations due to present (1992) aircraft emissions in January and July when convection is included are illustrated in Figure 6.6. Maximum NO_x concentrations due to the current aircraft fleet in 1992 are estimated at about 150 parts per trillion by volume (pptv), centered in the Northern Hemisphere lowermost stratosphere. If convective mass fluxes are not included in the simulation, the distribution of emissions (in the zonal mean) is nearly identical to Figure 6.6, but the maxima in January and July are about 200 pptv (1/3 higher than with convective fluxes). In both seasons (January and July) for both cases (with and without convection), NO_x loadings are higher in the stratosphere due to the longer residence time (this simulation includes a lower tropospheric sink of emissions, simu-

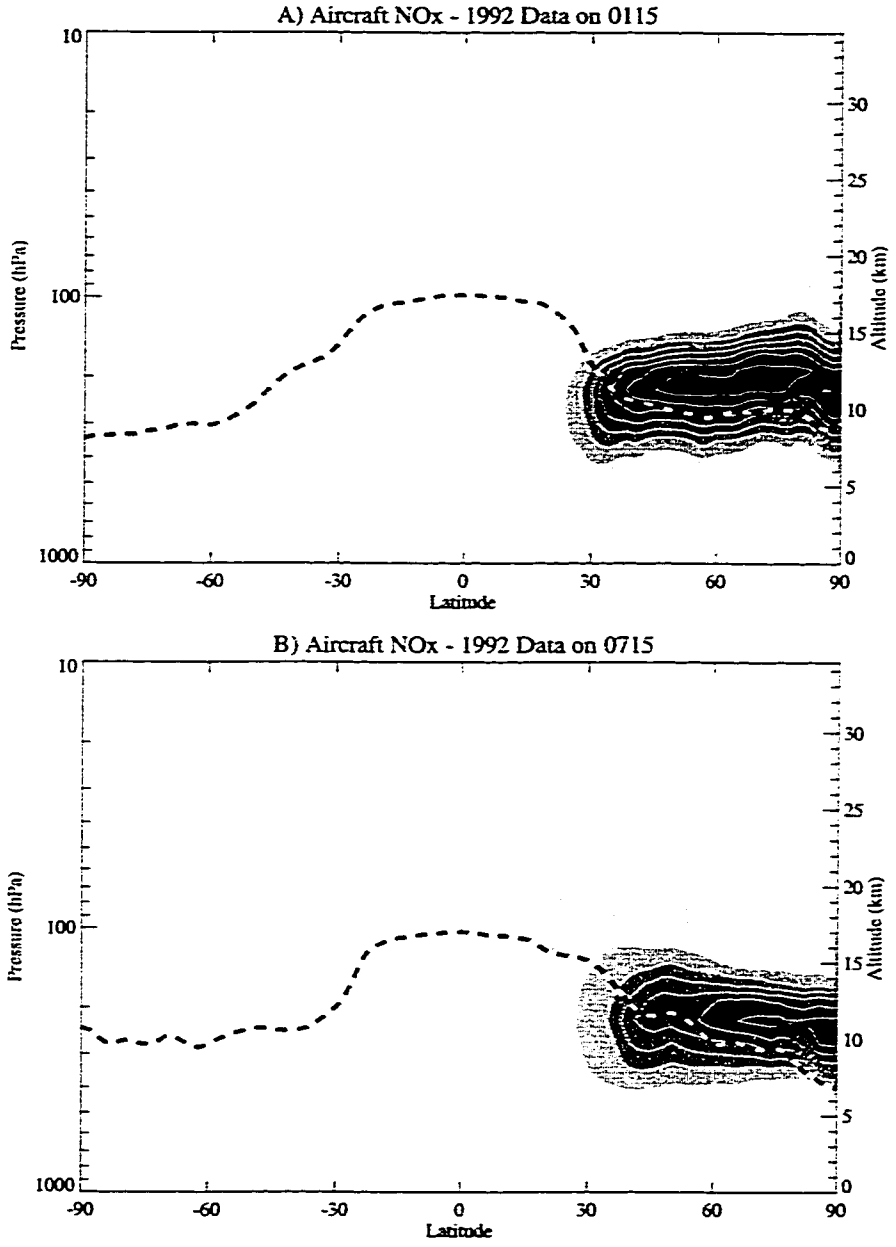

Figure 6.6: Zonal Mean NO_x concentration for 1992 aircraft emissions for A) January 15 and B) July 15, in parts per trillion (PPTV). Heavy dashed line is the daily zonal mean 3 PVU tropopause

lating rainout). Concentrations are higher in January (Figure 6.6a) because the mass of aircraft emissions deposited in the stratosphere is higher (Chapter 5). Maximum concentrations in both seasons are almost a factor of 2 larger than those predicted by van Velthoven et al. (1997) for passive transport of present day emissions, with a parameterized loss shorter than the stratospheric residence time in these simulations. Simulated NO_x loadings are also 50% larger than those modeled by Wauben et al. (1997) using a transport model with detailed ozone and carbon monoxide chemistry.

Based on NO_x observations by in-situ aircraft by Weinheimer et al. (1994), the average NO_x concentrations at mid-latitudes in the northern hemisphere lowermost stratosphere are around 100 pptv, and in a range generally from 40 pptv to 130 pptv. Such values indicate that the concentration loadings from aircraft NO_x in Figure 6.6 is probably high, as the average concentration from aircraft appears higher than the background. Such a result is not surprising given that the simulation accounts only for transport and not chemical removal process of NO_x. Nonetheless, it appears as if aircraft NO_x is a significant contributor to the NO_x concentration of the lowermost stratosphere. As noted in Chapter 5 the distribution of aircraft emissions in the stratosphere in 2015 is projected to be very similar to present day emissions in total fraction. Thus stratospheric emissions in the near term appear to scale with total fuel burn. Thus the NO_x concentration for the future fleet of aircraft is expected to have the same distribution as in Figure 6.6 but with concentrations approximately 125% higher (maximum of $\sim$360 pptv). This loading may have significant chemical effects on the lowermost stratosphere (for example, resulting in ozone production as in the simulations of Wauben et al. (1997)).

For aircraft sulfur emissions the total loading can be again estimated from the emission index (EI) of sulfur (0.4 g/kg Fuel) and the total fuel loading. However, since sulfur is often in aerosol form in the stratosphere (as liquid sulfuric acid), the total mass is a more appropriate unit than concentration. Estimating that 30% of emissions are deposited in the stratosphere (Chapter 5, Table 5.2), the total annual deposition of

sulfur into the lowermost stratosphere and stratospheric overworld is about 0.02 Tg/S per year. The distribution, being a function of deposition and transport identical to NO_x, should have the same distribution as the transport calculated NO_x emissions in Figure 6.6. The annual loading of naturally oxidized sulfur from Carbonyl Sulfide (COS or OCS) is about 0.05 Tg/S per year (Chin and Davis, 1995). Thus, the aircraft deposition of sulfur into the stratosphere is about 40% of the natural background source (not including volcanic eruptions). As with NO_x emissions, sulfur loading in the stratosphere is projected to increase by over 100% in 2015 with the total fuel loading, assuming that the EI remains the same. This effect is swamped by the natural injection of volcanic sulfur emitted sporadically into the stratosphere, but aircraft sulfur in certain regions may represent a significant fraction of the background of sulfur in the stratosphere. Sulfur from aircraft is concentrated in the Northern Hemisphere lowermost stratosphere (as is the NO_x distribution in Figure 6.6), where it may be larger than the natural background source due to OCS.

Aircraft emissions of soot (black carbon) may also increase aerosol surface area in the stratosphere and contribute to ozone loss. The transport of soot should be similar to that for sulfur or NO_x species (neglecting differences due to the sedimentation of solid soot particles), and so the hypothesized distribution of soot has a maximum cincentration in the NH lowermost stratosphere (12 km) from 40°N to 60°N of about 0.4-1.5 ng/m^3 for emission indices of 0.02 g/kg to 0.1 g/kg (see Bekki (1997)). Without explicit convective transport the soot concentration is 0.5-2.5 ng/m^3. The concentration compares favorably to the observed soot distributions in the lowermost stratosphere reported by Blake and Kato (1995) of about 0.05 to 3.4 ng/m^3 at these latitudes and aircraft flight altitudes, with a wide variance. Accepting that the transport of soot particles will be reduced by sedimentation, it appears that aircraft emissions represent a significant fraction of the black carbon in the lowermost stratosphere. Concentrations are similar to those simulated using a two-dimensional model including settling velocities by Rahmes et al. (1998). For these concentrations

Rahmes et al. (1998) found no significant radiative forcing on climate from soot. Effects on chemistry may be significant though. Hofmann et al. (1998) have estimated that aircraft emissions between 8–12 km may contribute to 10% of total condensation nuclei (a large fraction being sulfate) over Wyoming. Bekki (1997) has illustrated that aircraft enhancement of stratospheric aerosol surface area (by sulfur and soot) may be contributing significantly to midlatitude ozone loss.

6.6 Summary

The residence time of aircraft emissions in the lowermost stratosphere has been deduced from simulations using a chemical transport model and aircraft emissions inventories. The model transport preserves dynamic structures and potential vorticity on the timescale of 30 days, despite a classically noisy vertical velocity field. The residence time of aircraft emissions in the stratosphere is on the order of 50 days. Exchange between the stratosphere and troposphere is dominated by episodic descent of emissions across the extratropical tropopause, and rise across the tropical tropopause. Transport between the tropical troposphere and the mid-latitude lowermost stratosphere is always confined to potential temperature surfaces near the tropopause in the winter, but occurs at up to 380K in the summer hemisphere. Transport into the overworld in the summer hemisphere also occurs in the subtropics. Some net transport from the troposphere to the stratosphere may occur in the extra-tropics, but the emissions are mostly confined to the tropopause region below 5 PVU. The transport pathways and quantities appear consistent with previous work, and are consistent with Lagrangian trajectory simulations of parcels along aircraft flight tracks. A limited analysis of realistic aircraft flight tracks indicates that high-latitude emissions may evolve towards colder temperatures where heterogeneous chemistry may become important. Derivations of atmospheric concentrations of NO_x from this work indicate concentrations higher than observations of the natural background or other model

studies, perhaps because of the lack of chemistry incorporated into these estimates. Sulfur and soot (black carbon) emissions from aircraft are found to be a potentially significant fraction of total sulfur and black carbon in the background (non-volcanic) atmosphere. The estimates here tend to overstate the effect of NO_x and soot in particular because certain removal processes in the stratosphere (conversion to nitric acid for NO_x and sedimentation for soot) are not considered. These estimates are only order of magnitude exercises.

Nonetheless, the residence time estimates of represent a substantial refinement of estimates that do not explicitly consider the details of the tropopause or of the pattern of emissions, and should improve assessments of current aircraft impacts on the atmosphere, and enable further estimates of the loadings of different species to be determined.

Chapter 7

SIMULATED DISTRIBUTIONS OF WATER VAPOR IN THE LOWER STRATOSPHERE AND UPPER TROPOSPHERE

Because aircraft emissions are concentrated in the midlatitudes, the discussion in Chapters 5 and 6 dealt mostly with the extratropics. In this chapter, details of Stratosphere-Troposphere Exchange (STE) in the tropics are considered. The distribution of water vapor in the upper tropical troposphere and lower stratosphere is studied in an attempt to better understand the processes important for STE in the tropics.

7.1 Introduction

Water vapor in the upper troposphere and lower stratosphere is an important radiatively active trace species. As a greenhouse gas, water vapor is important for determining the radiative balance of the upper troposphere, particularly in the tropics. This has implications for local diabatic heating, and for feedbacks to climate radiative forcing (Sun, 1993; Inamdar and Ramanathan, 1998). Water vapor is one of the few atmospheric gases to reach saturation at atmospheric temperatures and pressures. Because it has few sources and sinks in the stratosphere it is also important as a tracer for stratospheric transport.

The processes that control water vapor in the stratosphere have been understood in broad terms since Dobson et al. (1929) hypothesized the large scale circulation of the stratosphere from extratropical water vapor measurements. As discussed in Chap-

ter 2, the water vapor distribution in the stratosphere is controlled by cold temperatures at the tropical tropopause. The motion of air across the tropical tropopause is affected by a variety of processes, discussed in Section 2.4.2. These processes include: the large scale residual circulation in the stratosphere (Rosenlof, 1995), overshooting convective turrets which penetrate the tropopause (Danielsen, 1993), sub-visible cirrus clouds which may influence the diabatic heating at the tropopause (Rosenfield et al., 1998), and Kelvin and gravity waves forced from the troposphere which may also affect diabatic processes and mix air into the stratosphere (Pfister et al., 1993). The relative importance of these processes for stratosphere-troposphere exchange in the tropics, and their effect on water vapor in this region, are still uncertain.

This uncertainty stems from the lack of sufficient observations in the upper tropical troposphere and lower stratosphere. Observations of water vapor in the upper tropical troposphere and lower stratosphere have been increasing in recent years, but coverage is far from accurate or complete. The major sources of data are radiosondes and satellites. Radiosonde moisture measurements are often unreliable in the extreme dryness of the upper troposphere and lower stratosphere (Gaffen, 1999). Satellites have better quality, but coarse horizontal and especially vertical resolution, often sampling layers 1–3 km thick. Satellite data include the Stratosphere Aerosol and Gas Experiment II (SAGE II) (Pan et al., 1997), the Microwave Limb Sounder (MLS) (Read et al., 1995; Newell et al., 1996) on the Upper Atmosphere Research Satellite (UARS) and the Halogen Occultation Experiment (HALOE) (Rosenlof et al., 1997) also on UARS. Observations of high quality and spatial resolution are also available from in-situ aircraft (Boering et al., 1995; Hintsa et al., 1998) and balloons (Ray et al., 1999), but these platforms provide limited temporal sampling. Modeling studies of water vapor (Mote et al., 1994; Mote, 1995) have elucidated some important aspects of the stratospheric circulation, namely the imprint of tropical temperatures on water vapor — the 'Tropical Tape Recorder' (Mote et al., 1996).

In this chapter, we will simulate the water vapor distribution in the lower strato-

sphere and upper troposphere. We will attempt to identify the dominant processes of STE in the tropics, and their importance in the transition region between stratospheric "control" (above 80 hPa) and tropospheric control (below 200 hPa), discussed in Section 2.4.2. Specifically, we will focus on the importance of thermodynamic processes and the large scale windfield. Convective turrets and small scale waves will not be included in the simulations. Vertical motions will be calculated in the transport model based only on the convergence and divergence of the assimilated winds. The significance of convection and gravity waves can be judged indirectly by their absence from the simulations. Good correspondence between simulations without these processes and observations will indicate that large scale transport is more important, while systematic deviations between the simulations and observations indicate that other processes, not represented, are important. The approach attempts to build upon the modeling work of Mote et al. (1994) and Mote (1995). These studies used an integrated GCM which included feedbacks, while here we seek an approach which limits the number of simulated processes to better determine their relative importance.

The focus is on three regions. (1) The lower stratosphere between 380K and 500K, approximately from the highest isentrope that does not lie in the tropical troposphere (Holton et al., 1995; Hoskins, 1991) to the lower boundary of the 'tropical pipe' region (Plumb, 1996), (2) The 'extratropical lowermost stratosphere' (Holton et al., 1995) also known as the stratospheric portion of the 'middleworld' (Hoskins, 1991), which lies between the extratropical tropopause and the isentrope whose level is equal to the tropical tropopause (380 K) and (3) the upper tropical troposphere. Transport between the stratospheric overworld (1) and the troposphere (3) occurs only across an isentrope (diabatic motion) while transport between the lowermost stratosphere (2) and the troposphere (3) may occur along an isentrope (quasi-isentropic motion). For a complete review see Holton et al. (1995) and Chapter 2.

The transport model is fully described in Section 4.5. The simulation constraints and parameters are described in Section 7.2. Details of the temperature distribu-

tion are given in Section 7.3. The simulated distributions of water vapor in the stratospheric overworld (above 380K), in the middleworld and in the upper tropical troposphere are detailed in Section 7.4. Detailed comparisons with observations are presented in Section 7.5. The stratosphere-troposphere exchange of water vapor is discussed in Section 7.6. Discussion and conclusions are contained in Section 7.7.

7.2 Description of Model & Constraints

The Chemical Transport Model (CTM) of the laboratory for atmospheres at the Goddard Space Flight Center (GSFC), as described in Chapter 4, is used for this analysis. As discussed in Chapter 4, the model has previously been used to examine projected emissions from supersonic (Weaver et al., 1996) and subsonic (Gettelman, 1998) aircraft. It is capable of accurately simulating synoptic features in chemical tracers including ozone (Douglass et al., 1996) and carbon dioxide (Strahan et al., 1998).

A brief description of the CTM is repeated here from the information in section 4.5. The three-dimensional flux form semi-Lagrangian transport code (Lin and Rood, 1996) uses 46 sigma level winds from the Goddard Earth Observing System (GEOS) Assimilation System (Schubert et al., 1993). Model resolution is 2° latitude by 2.5° longitude with 46 sigma levels in the vertical from the surface to 0.1 hPa. The model sigma levels are spaced approximately 1km apart near the tropical tropopause. The model is run in an off-line mode, so the tracer concentrations do not feedback to affect the winds and temperatures. Input winds and temperatures are interpolated to a 900 second timestep from 6 hourly data. Explicit convective transport is not included. Vertical motion is calculated from the convergence or divergence of the horizontal wind between levels. Douglass et al. (1996) note two benefits of this method over a full General Circulation Model (GCM) with chemistry and feedbacks; the ability to have temperatures more representative of the actual stratosphere than those

in most GCM's, and to appropriately simulate synoptic scale perturbations. Both of these benefits are critical to the simulations as described below and distinguish this analysis from other studies using GCM's (Mote et al., 1994). Chen et al. (1998) have compared GEOS assimilation water vapor to MLS observations, and found good synoptic agreement but systematic overestimation of water vapor in the upper troposphere. The conclusion is expected in the work of Chen et al. (1998) since the GEOS specific humidity data used are calculated incorrectly from saturation vapor mixing ratio over liquid in the upper troposphere. For comparison of the simulation with observations, a variety of assimilated and observed datasets are used. These datasets are discussed more fully as each is introduced; they range from global assimilation systems to individual radiosondes.

Several simulations of water vapor were performed. The results here are mostly drawn from an experiment in which a tracer was initialized with a source of 5% of atmospheric concentration (50,000 ppmv) at the surface, and a 7 day e-folding lifetime (sink) from the surface to 400 hPa. Simulated tracer in the upper troposphere and above is not sensitive to the concentration at the ground using this parameterization of water vapor. From 400 hPa to 80 hPa, the tracer is checked against the Saturation Vapor Mixing Ratio (SVMR) of water over ice at each time step using the algorithm of Marti and Mauersberger (1993). If the tracer concentration is larger than the SVMR, the tracer value is reduced to the saturation value. This process is analogous to the "dehydration" of water vapor when it passes from the vapor phase into either liquid or solid phase and then precipitates, and occurs when the "relative humidity" in the simulation is 100%. In this work, we will repeatedly use the term "Relative Humidity". Relative Humidity or "RH" is defined as:

$$RH = \frac{\chi_t}{SVMR(t,p)} \times 100 \tag{7.1}$$

where χ_t is the model tracer value and the saturation vapor mixing ratio ($SVMR$) is a function of the temperature t and pressure p according to Marti and Mauersberger

(1993).

In another simulation which will be referred to as the "tropical" or "saturated" simulation, the tracer mixing ratio was fixed at the SVMR from 157 hPa to 94 hPa in the region from 10°S to 10°N with the tropospheric sink described above, but with no surface source. This simulation tests the condition of a fully saturated upper troposphere and region of entry of air into the stratosphere.

The tracer, while referred to as the 'water vapor tracer', is not necessarily comparable to the water vapor mixing ratio in the atmosphere. It will be comparable only if the major process affecting water vapor are 'dehydration' and transport. In particular there is no source of water in the upper stratosphere, as results in the atmosphere from the oxidation of methane (Brasseur and Solomon, 1986). An accurate simulation of water vapor in the middle and upper stratosphere should include this source. Supersaturation is not permitted in the simulation. Processes that occur in and around clouds, such as re-evaporation of falling liquid or solid H_2O are also not treated. Differences between the simulation and observations will be discussed in light of these missing processes where appropriate.

The model is run for three years starting October 1, 1995 and repeating meteorology from October 1, 1995 to October 1, 1996 each year. In the region of the atmosphere being studied (below 500K) the transport lifetimes are generally 1 year or less, as shown by Schoeberl et al. (1998), and the annual cycle appears to repeat itself each year. There is a continual secular increase in mixing ratios in the stratosphere which is evident in the overworld mass budgets for water vapor. The increase is expected given the transport lifetimes in the stratospheric overworld. Since this analysis concerns itself with the lower stratosphere only (below the tropical pipe region at about 500K), the 3 year duration should be sufficient. Most analyses here will use only the third year of data from the simulations, to compare with observations from the period October 1995 to October 1996.

7.3 Temperature Comparison

The only sink for water vapor outside of the lower troposphere in the simulation is a thermodynamic constraint that the tracer concentration be below the saturation vapor mixing ratio (SVMR) of water over ice. The SVMR is uniquely determined by the temperature and pressure, following the algorithm of Marti and Mauersberger (1993), and the SVMR is typically close to the water vapor concentration in the tropical upper troposphere. Temperature is thus a critical parameter for determining the water vapor distribution in the lower stratosphere and upper troposphere. For the simulation to represent the water vapor distribution correctly, accurate temperatures are a prerequisite. As discussed in section 4.2, GEOS temperatures near the cold point at the tropical tropopause are biased warm by about 2°K when compared to other reanalysis data. The GEOS analyses place the tropical cold point at the 94 hPa or 79 hPa model level, in general agreement with the average cold point pressure of 96 hPa noted by Reid (1998). Increasing the temperature by 2°K would change the SVMR significantly. For a sample location at 192°K and 100 hPa, increasing the temperature by 2°K will increase the SVMR by nearly 40% (4.6 to 6.4 ppmv). For temperatures as high as 200°K a 2°K the change in temperature represents a 20% difference in the SVMR.

The zonal temperature distribution in the tropics becomes important for discussions of regions where there is preferential upward mass flux, the 'stratospheric fountain' hypothesis of Newell and Gould-Stewart (1981). There is a zonal asymmetry in upper tropical tropospheric temperatures, specifically at 94 hPa, the level of maximum simulated dehydration in the NH winter season. In NH winter, minimum temperatures generally occur from 100°E to 160°W longitude and from 20°N to 10°S, with the coldest values for both NCEP and GEOS temperatures around 150°E to 180°E. These temperatures are 2°K–3°K colder than other regions. In the NH summer from May to September, there is generally less than 1°K difference in zonal temperatures

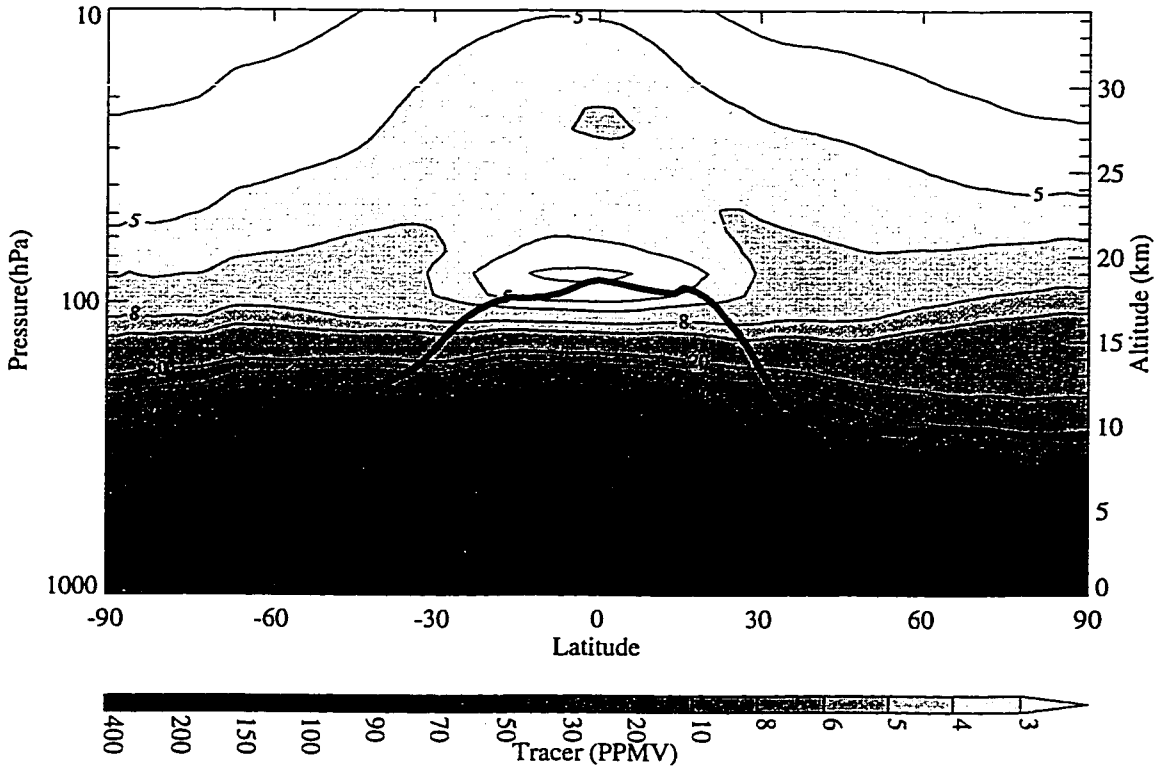

Figure 7.1: Zonal mean tracer for January, 1996 in PPMV. Thick solid line is the monthly mean tropopause.

at the cold point over the tropics. The zonal asymmetry extends down to 190 hPa in the analysis, but the seasonality and amplitude are muted. This discussion will be important background for understanding the water vapor distribution.

7.4 Simulated Water Vapor Distribution

The monthly averaged zonal mean simulated water vapor tracer approximately duplicates the water vapor concentration of the lower stratosphere and upper troposphere as depicted in Figure 7.1 for January, 1996. There is a minimum in the tracer concentration just above the tropical tropopause where cold temperatures dehydrate the

air. The tracer concentrations are high in the tropics and lower in the extratropics in the middle stratosphere. The meridional gradients in the lowermost stratosphere (below 100 hPa) are very flat, and there is a sharp jump in the tracer concentration in the extratropics just below the tropopause. The Southern Hemisphere (summer) middleworld has slightly higher concentrations than the Northern hemisphere (winter) middleworld. The tracer concentration decreases steadily with altitude from the surface source.

A focus on the entry of air into the stratosphere is presented for the three years of data in Figure 7.2. There is a maximum in the tropics in September in each hemisphere, which takes 3–4 months to propagate to high latitudes. The tropical maximum is more pronounced in the northern hemisphere. The tropical maximum does not appear to propagate as readily into the high latitudes of the southern hemisphere. The annual cycle in the high latitudes in the southern hemisphere is partly due to the annual cycle of temperatures in this region. The high values are also probably a consequence of very low surface pressures which affect the conversion of tracer mixing ratio from sigma coordinates to pressure coordinates.

It is perhaps more useful in dynamic terms to examine the transport on a potential temperature surface. Figure 7.3 illustrates the tracer mixing ratio interpolated to the 390K potential temperature (θ) surface. While in the tropics the pressure of the 390K surface is close to 94 hPa, in the extratropics the surface may be as low as 160 hPa and as high as 79 hPa. The distribution in Figure 7.3 does not replicate the pattern of HALOE observations of water vapor on 390 K (Rosenlof et al., 1997, Plate 6), but resembles the deviation of pressure on the 390K surface; low pressure in the tropics in spring and high pressure at the poles in summer and fall in each hemisphere. The observed mixing ratio on an isentropic surface appears to be a function of the altitude (pressure) on that surface. Transport in the simulation thus appears to be less isentropic than observations, which may be a result of the noisy vertical velocity field, and the coarse (1.5km) vertical resolution of the transport model.

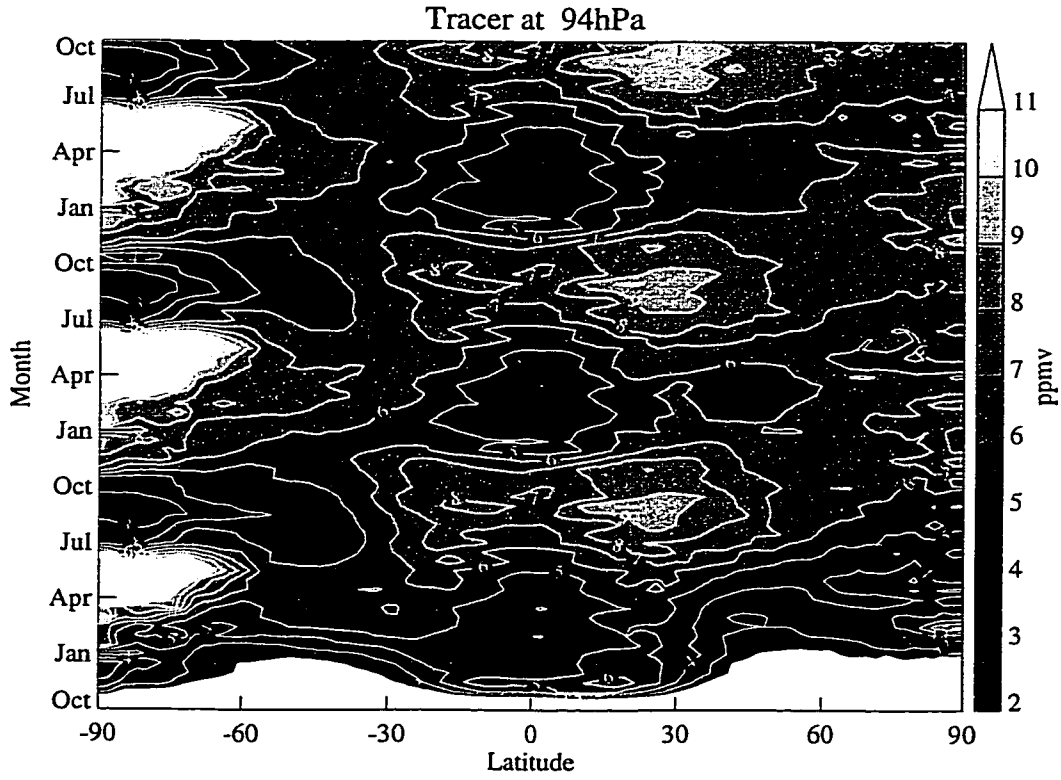

Figure 7.2: Zonal mean tracer at 94 hPa for three years, in PPMV.

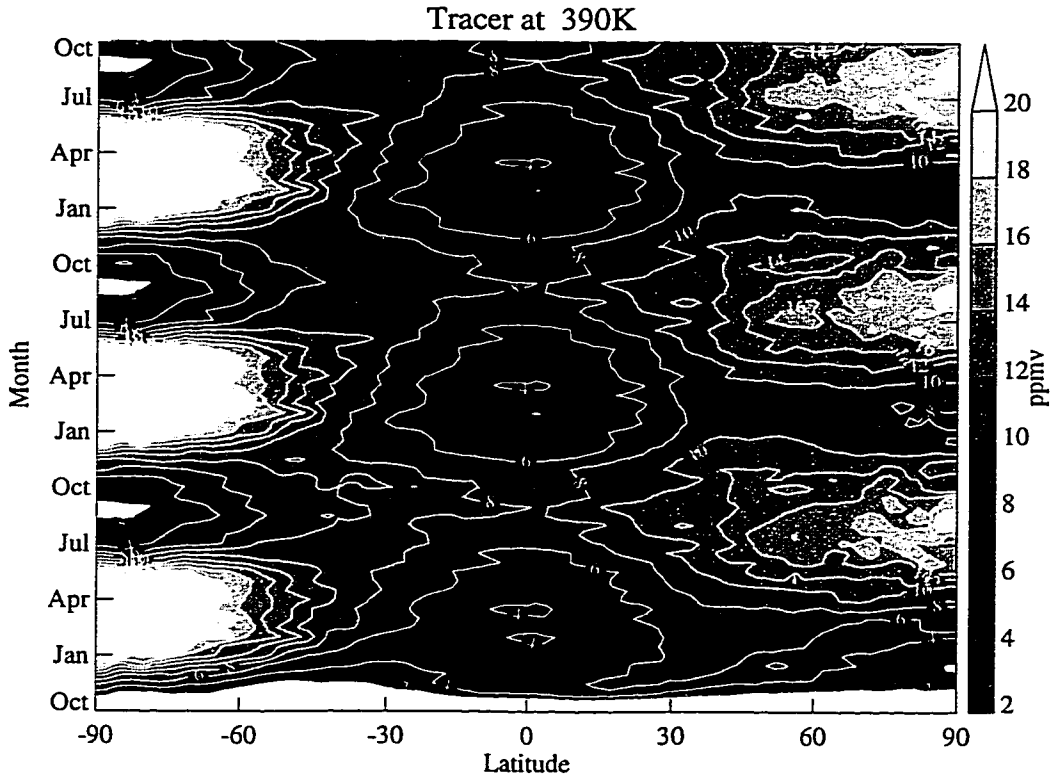

Figure 7.3: Zonal mean tracer at 390K for three years, in PPMV.

7.4.1 Tropical Tape Recorder

The tropical stratospheric "Tape Recorder" discussed by Mote et al. (1996) is also present in the water vapor simulation. The tape recorder signal is easily seen in the zonal mean water vapor concentration at the equator, presented in Figure 7.4. The annual cycle of the water vapor tracer at 94 hPa seen in Figure 7.2, which corresponds to the annual variation in cold point temperatures, propagates vertically in the stratosphere. In the simulation the speed of the tape recorder (vertical transport) is much too rapid. The propagation time of the signal from 100hPa to 50hPa is less than 3 months. The observed tape signal as illustrated by Mote et al. (1996) with data from MLS or HALOE (both on UARS) takes on the order of 6 months to transit this region. Rapid vertical transport using GEOS winds was also noted by Strahan et al. (1998) for a simulation of CO_2 in the stratosphere.

The seasonality of the source function is approximately correct. The highest observed tracer values are seen in August to October and the lowest values in January to April (compare to Figure 7.2). The minimum tracer concentrations occur above 100 hPa, at approximately the same altitudes as minima observed from satellite data (Mote et al., 1996). The amplitude of the tape recorder signal (Figure 7.4b) of 4 to 5 ppmv is larger than observed with UARS instruments (2.5 to 3 ppmv). The maximum amplitude is simulated at approximately the correct altitude (just above 100 hPa). The simulated tape recorder appears to well represent the 'recording head' at the tropical cold point, recognizing the warm bias to temperature, while the signal propagation in the vertical appears too fast. The signal attenuation is also too rapid compared to observations. A visible signal in water vapor is clearly evident to at least 30km. Since the signal is attenuated too fast, it implies that there is more meridional mixing in the stratosphere in the simulation than in observations.

The propagation of the water vapor signal in the stratosphere has implications for the transport of aircraft emissions discussed in Chapter 6. Vertical transport in

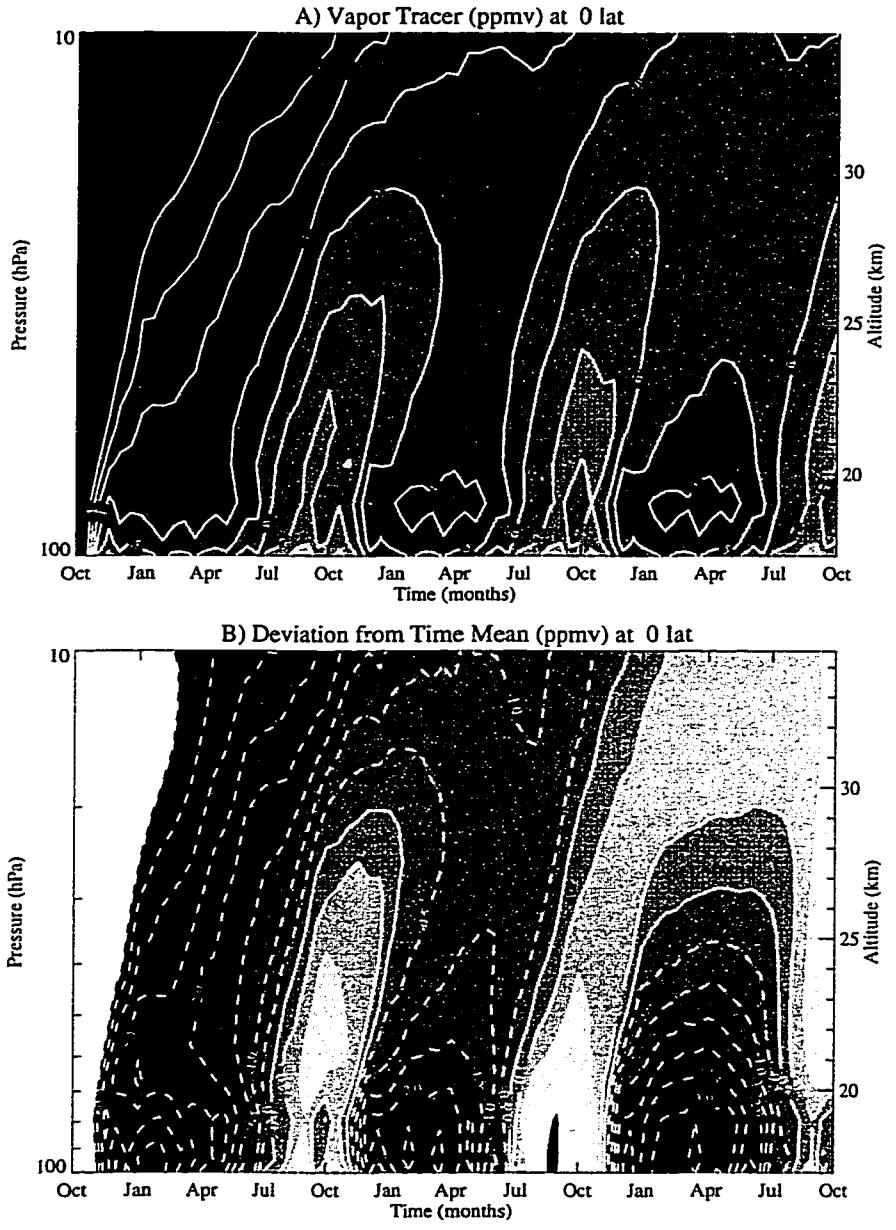

Figure 7.4: Equatorial tracer mixing ratio in ppmv. A) Zonal mean tracer mixing ratio and B) Deviation from time mean.

the tropical stratosphere which is too rapid would tend to make the stratospheric burden of emissions anomalously high. Actual transport of aircraft emissions into the stratospheric overworld would then be lower than noted in Chapter 6.

7.4.2 Water Vapor Mass Budgets

Budgets for the Southern Hemisphere (SH) the Northern Hemisphere (NH) and the tropics are calculated by converting the tracer mixing ratio into mass at each location (using surface pressure to interpret sigma levels and the size of each grid cell), and then fractionating the tracer mass using potential vorticity and potential temperature surfaces from archived 18 level GEOS assimilation data. The tropics are again defined by latitude (ϕ) such that $|\phi| < 20°$. The mass of water vapor tracer in the lower stratospheric overworld (380–500 K), the middleworld (Tropopause–380 K) and the tropical troposphere is illustrated in Figure 7.5. In this figure, data is evaluated for two days each month (biweekly). With the exception of the tropical troposphere (Figure 7.5c), the mass budgets change slowly over the year.

In the lower stratosphere (Figure 7.5a) the seasonal cycles of the tracer budget in the NH and SH extratropics are out of phase, and both hemispheres have their largest mass of water vapor tracer in the late summer (February-March in the SH, August in the NH) and minima in winter (August in the SH, January in the NH). A linear trend from the continued increase of tracer in the lower stratosphere is apparent in the budget, a rise of less than 10% over the year as the stratosphere continues to adjust towards equilibrium from the initial zero distribution. The annual average budget in the NH has 10% more water vapor than the southern hemisphere. A 'wetter' NH is consistent with generally higher tracer concentrations in the Northern Hemisphere, caused by a warmer tropics in NH summer when the tropical upwelling region is north of the equator (see Figure 7.2) and a larger annual cycle in high latitudes of the Southern Hemisphere (a result of dehydration in the SH under cold temperatures). This interpretation is consistent with the findings of Rosenlof et al. (1997).

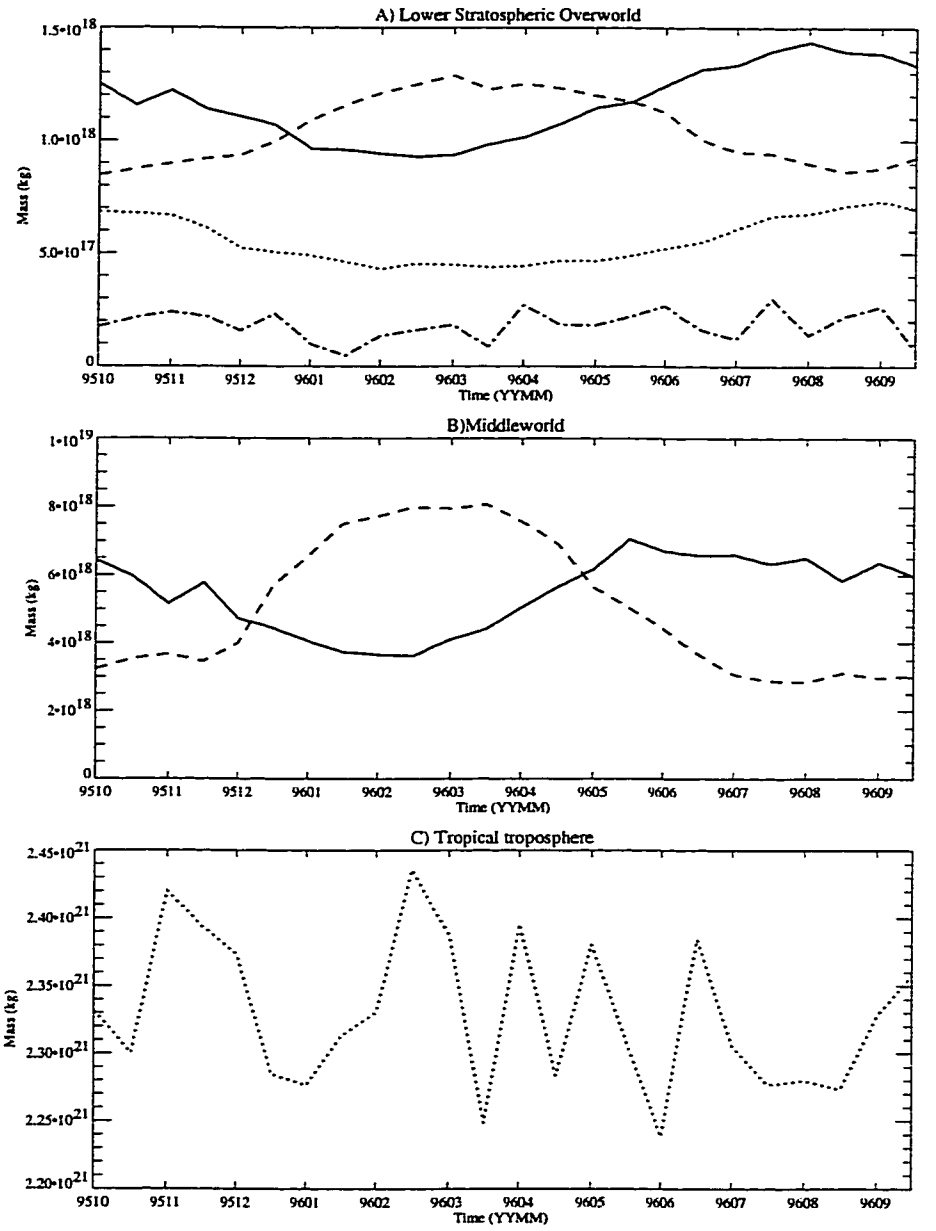

Figure 7.5: Hemispheric mass budgets for water vapor tracer in the Northern Hemisphere (20°N–90°N) (solid lines), Southern Hemisphere (20°S–90°S) (dashed lines), and the tropics (20°S–20°N) (dotted lines). A) Lower stratosphere between 380K and 500K. Dot-Dashed line is the tropics directly above the tropical troposphere. B) Extratropical Lowermost stratosphere between 3 PVU tropopause and the 380K surface. C) Tropical Troposphere from 400 hPa to the tropopause between 20°S and 20°N

The tropical budget ($|\phi| < 20°$) in the lower stratosphere (Figure 7.5a, dotted line) is in approximate phase with the northern hemisphere budget. The budget of water vapor tracer is lowest in NH winter and highest in NH late summer (August-September). This agrees with the cycle of mixing ratios noted when discussing the tape recorder in Section 7.4.1. If we only consider the tropical region directly above the tropical troposphere (the dot-dashed line in Figure 7.5a), where the tropopause is defined by the 380K potential temperature surface and the middleworld mass at these latitudes is zero, then the seasonal variation in this smaller tropical region is reduced. Above the tropical tropopause there is a slight minimum in the annual cycle in NH winter. This region is a small subset of the tropical region defined by the dotted line in Figure 7.5a. The defined annual cycle in the tropics and the lack of such a cycle at the tropical tropopause implies that vertical transport through the middleworld is important to the mass budget of the lower stratospheric overworld.

The budget of water vapor in the extratropical lowermost stratosphere (Figure 7.5b) indicates in the annual average that the NH has 10% more tracer mass than the SH. This convolves the size of the middleworld with the concentration. The annual cycle of middleworld mass is simpler in the SH where the annual mass of the middleworld does not change much over the year (Appenzeller et al., 1996). The SH middleworld mass of tracer is high in summer (January to March) and low in winter (July to October). The NH middleworld tracer budget is a maximum in June and a minimum in February. The middleworld mass works against this trend, being low in July to September and high in December to March.

The tracer mass in the tropical troposphere (Figure 7.5c) shows significant variability in all seasons. There is little evidence of a defined annual cycle. No distinct evidence of the South Asian or other monsoon circulations is evident in the tropical upper troposphere. The lack of a signal may also be simply due to the latitude banding applied to the analysis.

7.4.3 Relative Humidity

The distribution of 'Relative Humidity' (see Equation 7.1), shows that the maximum humidities away from the surface source occur around the tropopause and in the lower winter polar vortex (Figure 7.6). Note that dehydration is still occurring at levels when the zonal mean humidity is less than 100% since the zonal mean is an average. The zonal mean picture is a convenient way to examine where saturated conditions for the simulated tracer occur. In the winter polar regions dehydration occurs in both hemispheres. Colder temperatures in the southern hemisphere result in dehydration at up to 40 hPa (Figure 7.6b) while in the northern hemisphere dehydration occurs mostly below 100 hPa (Figure 7.6a).

The zonal mean RH of the tracer at 94 hPa in tropics is typically 65% in August and 70% in February. Air is closer to saturation in February (NH winter) than August, consistent with the annual cycle of tropical temperatures (Yulaeva, 1994). The standard deviation of the Relative Humidity in the tropics at this level is about 20%. The relative humidity is also high in all seasons around the altitude of the extratropical tropopause. In this simulation, the maximum RH in the tropics corresponds to the maximum removal of tracer due to concentrations higher than the local SVMR. The maximum RH (Figure 7.6) occurs around 180 hPa in the summer hemisphere, though significant regions of saturated conditions occur up to the cold point at 94 hPa or 79 hPa (especially in February). Air in this simulation reaches saturation well below the cold point.

The analysis indicates that in the simulation tracer mixing ratios are often below the SVMR for air entering the stratosphere in the tropics. This condition was further tested by simulating the condition of fully saturated air (tracer equal to SVMR) at 94 hPa. Results from this simulated tracer experiment (not shown) indicate tracer concentrations in the stratospheric overworld on the order of 8–10 PPMV in the tropics, much higher than observed, indicating that the air cannot be uniformly saturated.

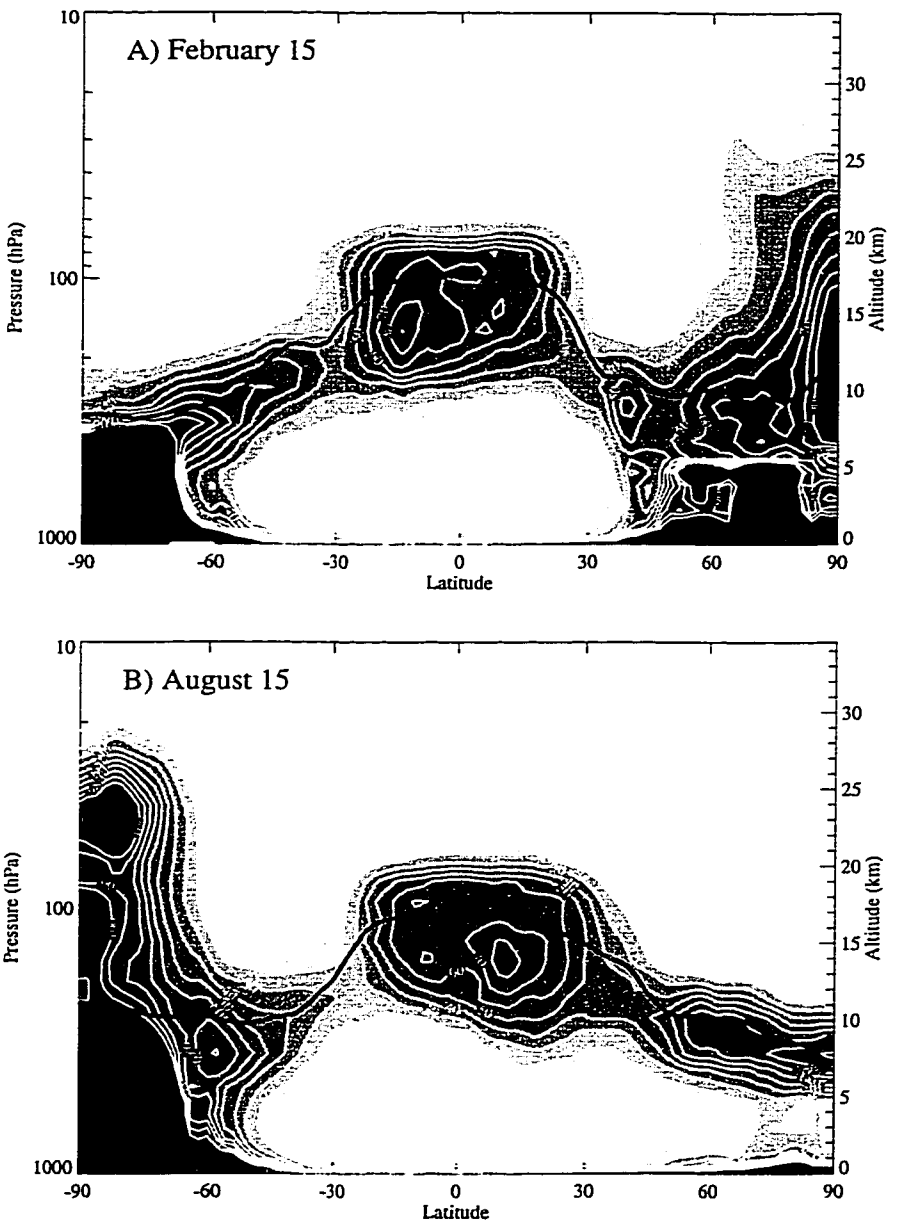

Figure 7.6: Zonal mean tracer 'Relative Humidity' (see Equation 7.1) in percent (%) for A) February 15th and B) August 15. Solid Black Line is the zonal mean daily 3 PVU tropopause surface.

In the lower tropical stratosphere (the tropics are defined by latitude, ϕ, such that $|\phi| < 20°$), the zonal distribution is illustrated in Figure 7.7a at 94 hPa. Relative humidity of the simulated tracer is generally between 70% and 90% with a NH winter maximum near the dateline (180° longitude) and over South America. The month of November has some anomalously high humidities close to 100%. In the upper troposphere (Figure 7.7b), the zonal distribution of RH is not as symmetric and ranges from 20% in the Eastern Pacific (180° to 270° longitude) to 60%-80% over the Maritime Continent (90° to 130° longitude). In the upper troposphere, the pattern is consistent with the tropical Walker circulation (Bjerknes, 1969) of rising air over Indonesia and South America, and sinking air (from drier regions above) over the Eastern Pacific.

7.4.4 Isentropic Surfaces

Examination of potential temperature surfaces does not present as clear a picture as comparisons on pressure surfaces, since as noted in the overworld (Figure 7.3) transport does not appear to be isentropic. However, it is still useful to evaluate simulated tracer concentrations in dynamical isentropic space for comparison with similarly fit observations. In Figure 7.8, tracer values are interpolated to theta surfaces in the stratosphere (these surfaces may occasionally intersect the tropopause). The Northern hemisphere tracer concentrations are generally higher than southern hemisphere values at high latitudes. The annual cycle in the Southern Hemisphere is slightly larger than the Northern Hemisphere. The absolute values of tracer concentration in the middleworld are much higher than either the SAGE II (Pan et al., 1997), HALOE (Rosenlof et al., 1997), or MLS (Figure 7.12 c and d) in this region, and even up to 450K in the extratropics. While some of the satellite data may have large errors in this region, aircraft data (Hintsa et al., 1998) generally agree with satellite data. Tracer values at 350K in midlatitudes of 20–50 ppmv are 50%–100% higher than expected from satellite or aircraft data. Selecting points only in the stratosphere does

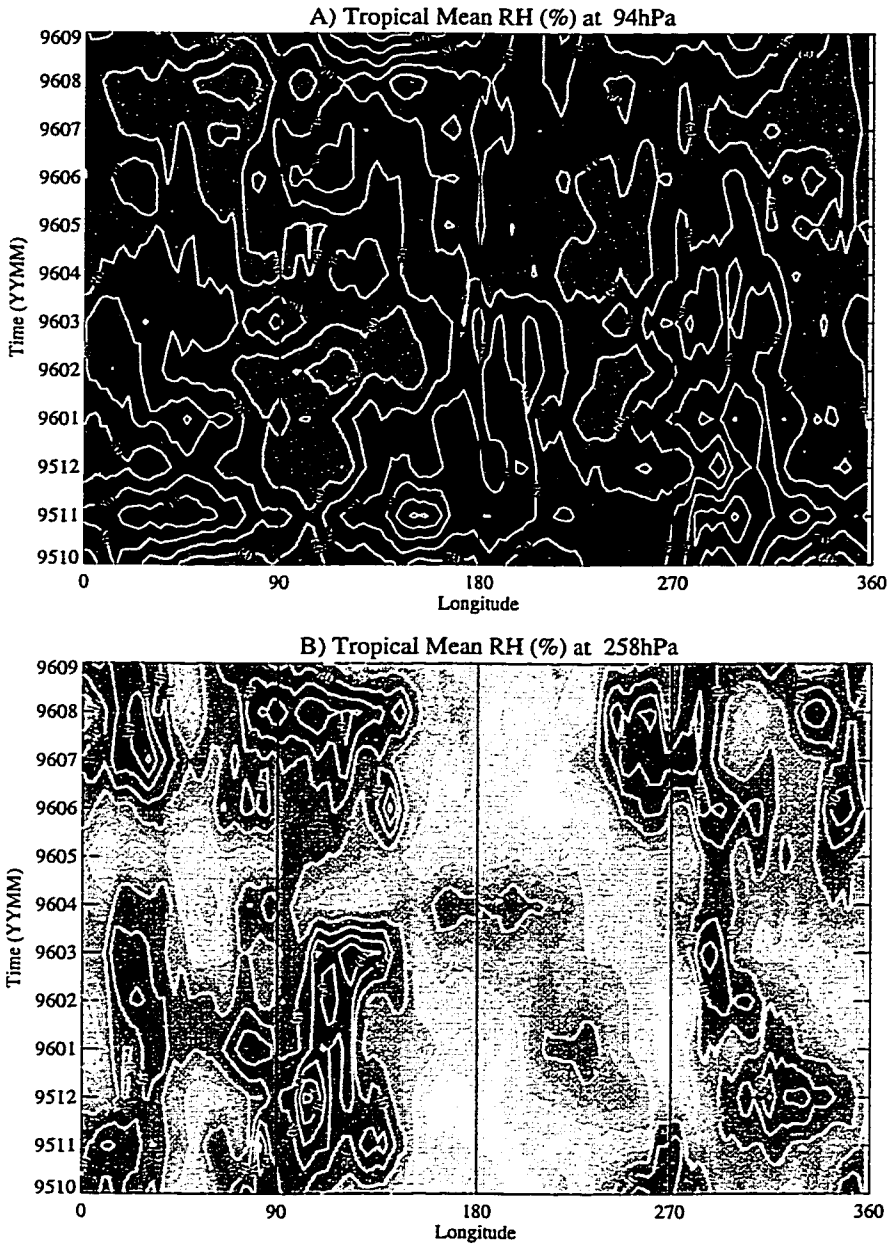

Figure 7.7: Monthly mean tracer 'Relative Humidity' (see Equation 7.1) in percent (%) averaged over tropical latitudes ($|\phi| < 20°$) for A) 94 hPa and B) 258 hPa.

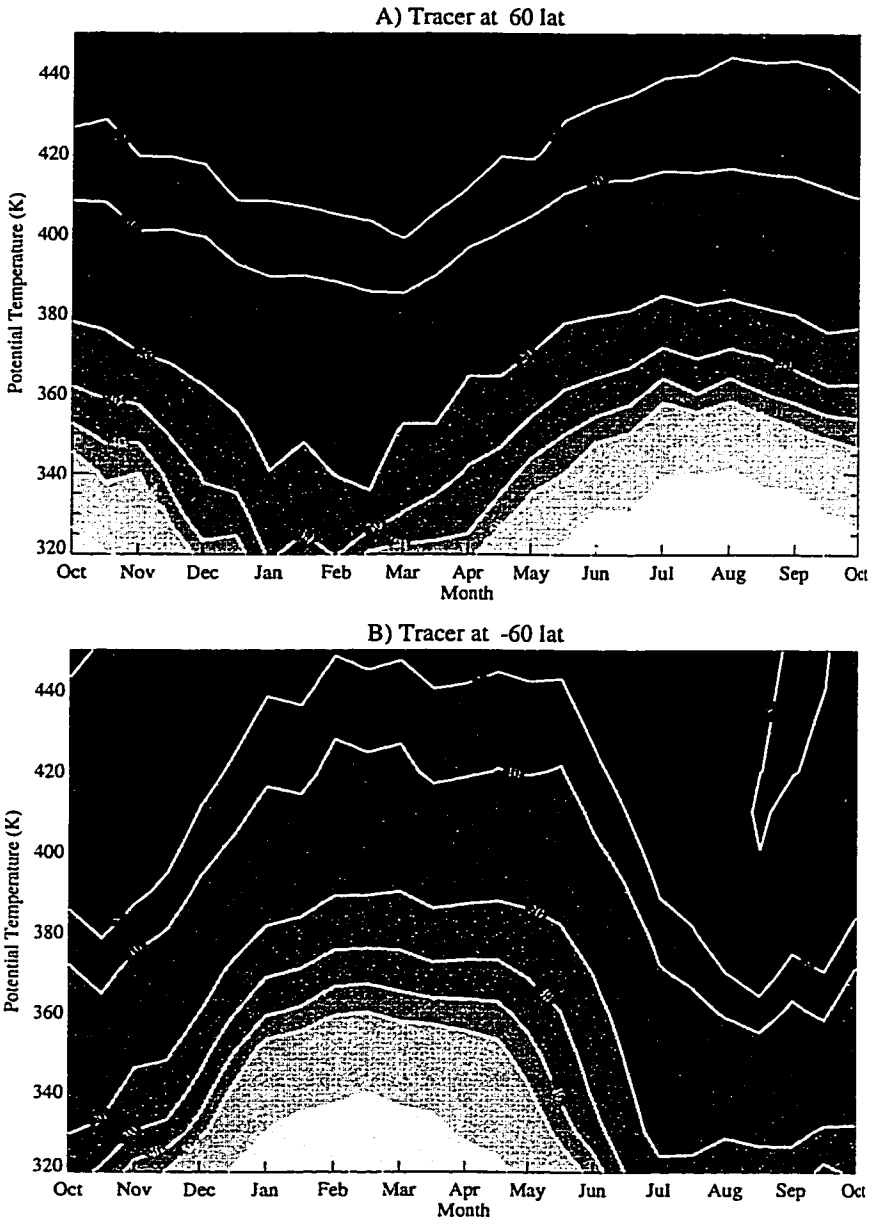

Figure 7.8: Simulated tracer mixing ratio on potential temperature surfaces in the middleworld and lower stratosphere at A) 60°N and B 60°S in PPMV.

not substantially affect the comparisons. As noted previously, high values may be a result of interpolating between vertical levels spaced 1.5 km apart in a region of strong gradients, with the result that model transport is not isentropic (as illustrated in Figure 7.3).

The Northern Hemisphere is wetter than Southern Hemisphere, at least in midlatitudes, both in mixing ratio and in the mass budget of the vapor tracer as discussed in Section 7.4.2. The increased water vapor is particularly noticeable in summer, when there is a significant plume of tracer advected from the surface into the upper tropical troposphere, and then quasi-isentropically into the middleworld due to the monsoon circulation, which injects a large mass of water vapor tracer into the NH middleworld. Without this plume of air (analyzed in a separate "tropical" simulation without a surface source of water vapor), the Southern Hemisphere middleworld has higher tracer concentrations than the Northern Hemisphere. The monsoon penetrates more into midlatitudes in the Northern Hemisphere summer upper troposphere. The monsoon circulations are thus important for the annual cycle of water vapor in the lowermost stratosphere, as noted by Rosenlof et al. (1997).

In addition, dehydration occurs at high latitudes in the middleworld, similar to that noted on 94 hPa and 390K in Figures 7.2 and 7.3 and in Figure 7.6. Dehydration occurs especially in the southern hemisphere winter from July to October. Saturation reduces water vapor throughout the southern hemisphere as it is transported to lower altitudes. Thus the variation over a year of the water vapor mixing ratio simulated in the southern hemisphere middleworld is larger than in the northern hemisphere. As discussed in Section 7.4.2, the variation in the total size of the NH middleworld also reduces the annual cycle of water vapor mass (but not necessarily concentration).

The zonal distribution of water vapor tracer in the upper troposphere (220 hPa) has generally high values over South America and over the Maritime continent, and low values over the eastern Pacific, consistent with the Walker circulation. Hovemuller plots (Figure 7.9) of longitude and time at various latitudes in the tropics

have an annual cycle which is particularly clear over the western Pacific, with high concentrations north of the equator (Figure 7.9) in NH summer and high concentrations south of the equator (not shown) in SH summer. These patterns, also noted in 215 hPa MLS water vapor data by Clark et al. (1998), are expected based upon the annual cycle of the convergence zones in the tropics. Zonal sections also show eastward propagation of high and low anomalies with periodicity of 30 days or so (Figure 7.9). Similar patterns and signals in the MLS water vapor data have been noted by Clark et al. (1998), which they attribute to the Madden-Julian Oscillation (MJO). There is also some evidence of westward propagating anomalies from the region of high water vapor associated with the summer monsoon from 90–0°E, which may be related to Rossby-gravity wave activity (Gill, 1982, pg. 452) associated with monsoon convection.

7.5 Comparisons with Observations

Because the simulation has no source of stratospheric water vapor the tracer concentration decreases with height in the stratosphere, whereas in the atmosphere the oxidation of methane (CH_4) is a source of water vapor. Accordingly, only the lower stratospheric overworld and below can be compared to observations. In this section, a variety of satellite and radiosonde water vapor data are used for comparison.

A direct comparison of simulated tracer concentrations in the stratospheric overworld and water vapor data from the HALOE instrument on UARS (Randel et al., 1998) is illustrated in Figure 7.10. The minimum value in the simulated tracer falls at 79hPa in the tropics, while the HALOE minimum is at 100 hPa. At 100 hPa, the lowest value of the simulated tracer in the lower stratosphere is generally higher than the observed water vapor concentration by approximately 1–2 ppmv in NH winter and nearly 3 ppmv in NH summer. Given the possible temperature biases discussed in Section 7.3, this difference is not surprising. There is a clear annual cycle of mix-

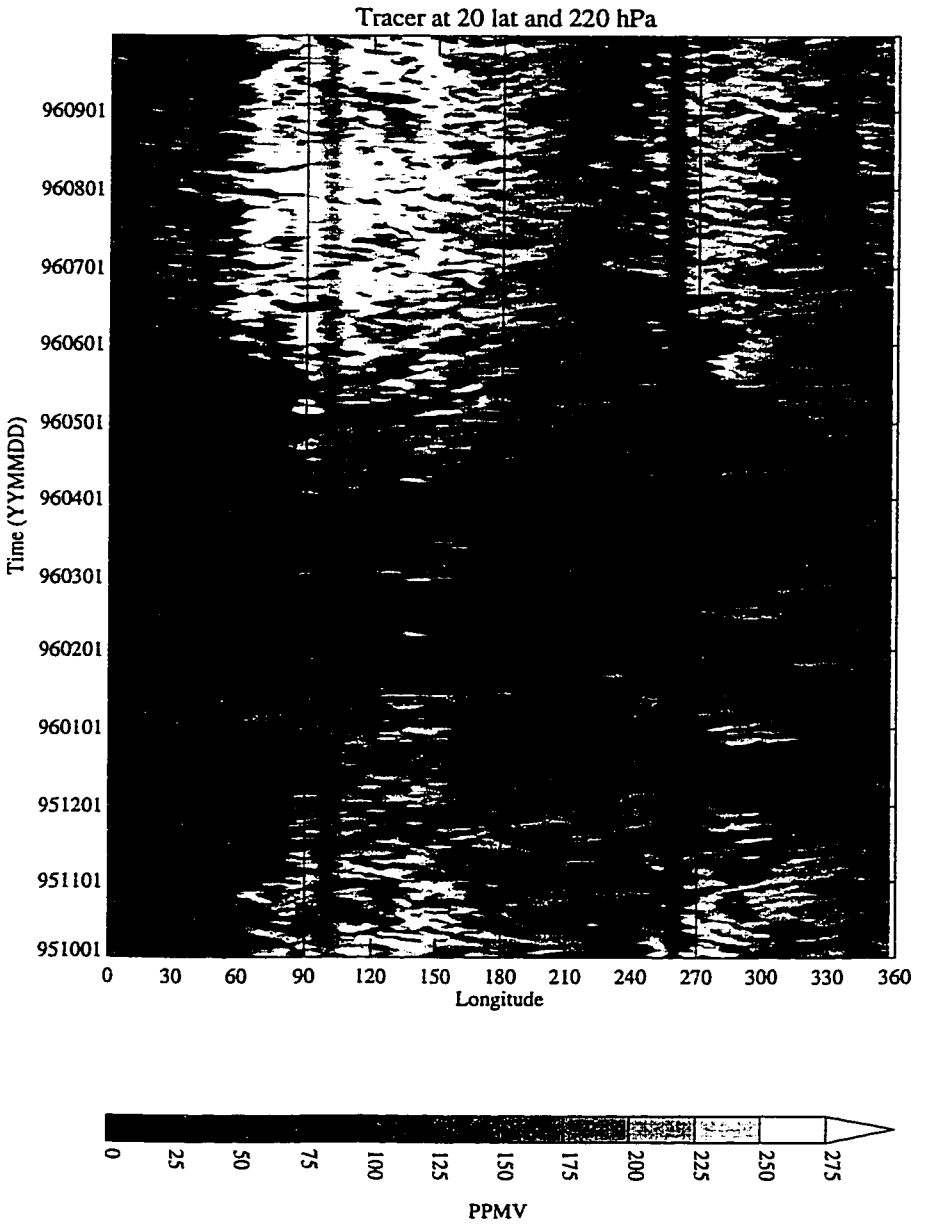

Figure 7.9: Hovemuller plot of Tracer at 20°N for one year in PPMV.

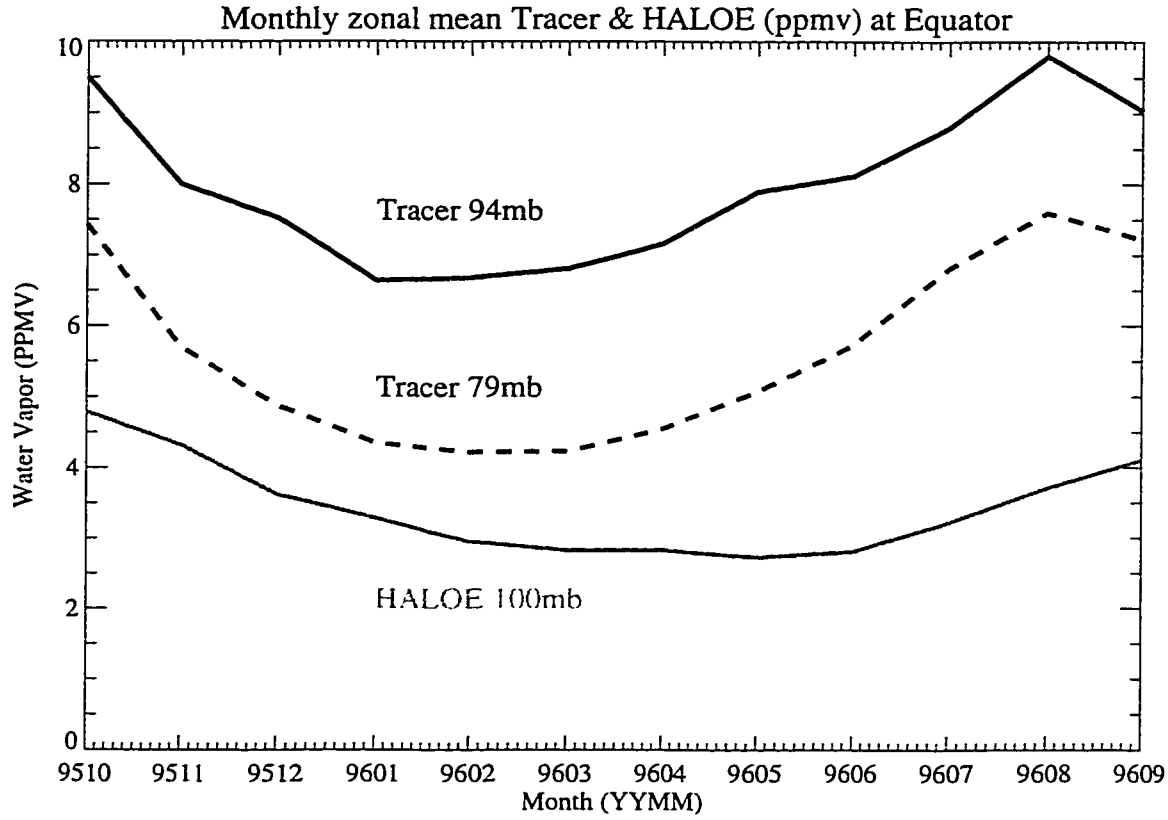

Figure 7.10: Monthly zonal mean HALOE water vapor and simulated tracer measurements in PPMV at the equator. Tracer at two levels: 94 hPa–solid black line, 79 hPa–dashed black line. HALOE data at 100mb–solid grey line. HALOE data are fully described by Randel et al. (1998).

ing ratio in the simulation illustrated in Figure 7.10. The minimum in the simulated equatorial concentration of water vapor at 94 hPa appears in March while the HALOE data has a minimum at 100 hPa in May. The tropical maximum in HALOE water vapor occurs in September or October, but in the tropical maximum in the simulated tracer occurs in August. The difference may be due to the vertical weighting function of the HALOE data over about 2km in the vertical, or due to differences in vertical transport in the simulation, which is discussed in Section 7.4.1. It is difficult to compare the high latitude data due to lack of HALOE coverage. Analysis of the HALOE data by latitude (not shown) indicates that at 100 hPa the NH polar minimum occurs in June, 3 months after the tropical minimum at 100 hPa, and slightly slower than in the simulation at these altitudes (Figure 7.2).

The absolute values of the simulated water vapor tracer in the middleworld (Figure 7.11a) are also generally larger than observed from satellites and aircraft. Higher mixing ratios than observed implies either a temperature bias, and/or differences in transport and coupling to the troposphere. The distribution of tracer in latitude and in time does however resemble observations. Figure 7.11b presents MLS data for the same meteorological year (Oct 1995-Aug 1996) at 215 hPa. Figure 7.11a illustrates that the maximum mean tracer value in the tropics migrates seasonally and is a maximum in summer and fall in each hemisphere, in agreement with MLS observations (Figure 7.11b). The seasonality of maxima in midlatitudes is also simulated correctly relative to the MLS observations at 215 hPa. The pattern is similar at 146 hPa.

Differences in high latitudes are more easily seen in line plots at various latitudes in Figure 7.12. Both model and MLS data indicate minimum water vapor concentrations at NH midlatitudes in February at 30°N (Figure 7.12c). MLS data is a minimum at 62°N in May while the simulated tracer has a minimum at 62°N in February (Figure 7.12a). The minimum tracer concentration is 20%-30% of the equatorial upper troposphere concentration at 215 hPa in January to April and 80% in July to September. At 215 hPa the simulation appears to reproduce well the magnitude and phasing

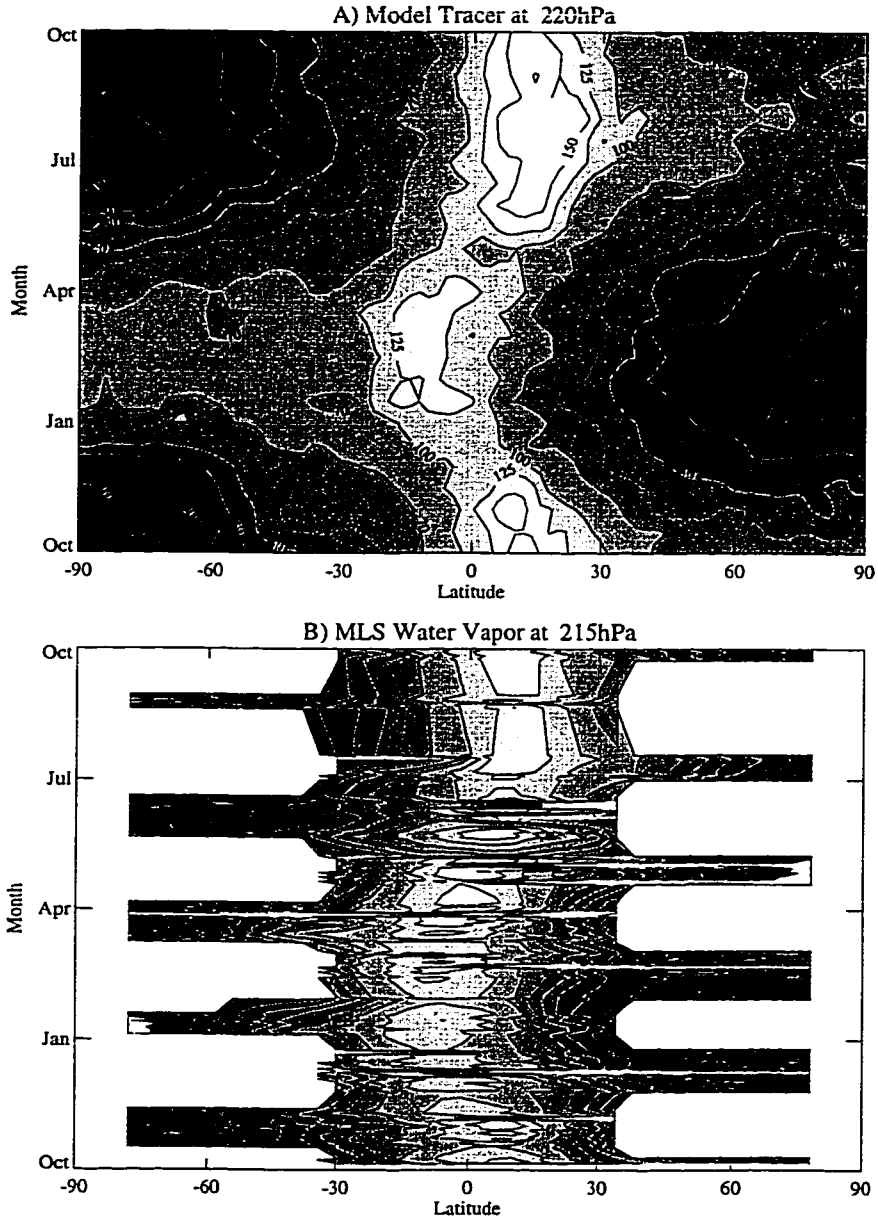

Figure 7.11: Time-Latitude plot of A) simulated tracer mixing ratio (PPMV) at 220 hPa and B) MLS water vapor mixing ratio (PPMV) on 215 hPa. The third year of the simulation is displayed. Color scale is the same for each plot.

of the annual signal at 30°N and 30°S (Figure 7.12c and 7.12d). The phasing of the concentration maximum appears to be nearly synchronous between the simulation and MLS at 30°N, but is harder to discern at 30°S. At 62°N and 62°S (Figure 7.12a and 7.12b), the simulation captures the phase of the signal (with larger amplitude). At 146 hPa agreement is not as good as 215 hPa. The simulation produces good agreement with equatorial MLS tracer values, both in magnitude and in simulating the variability over the course of the year (Figure 7.12e). This indicates that in the tropics at these altitudes the water vapor concentration is likely controlled by the thermodynamics (temperature), while in the lowermost stratosphere it is likely transport and an isolation from the troposphere that keeps the water vapor concentration low. This transport barrier does not appear to be perfectly represented in the simulation. Chen et al. (1998) have compared upper tropospheric water vapor from the GEOS assimilation with MLS data at 215 mb and found fair agreement but a tendency towards overestimation, especially in summer.

The synoptic agreement with observations in the upper tropical troposphere and lowermost stratosphere is generally quite good. Figure 7.13 shows a scatterplot of gridded MLS data and simulated tracer binned to the same grid for one day. MLS data in the extratropics often indicate low values of water vapor, and so the plot is restricted to points where the mixing ratio is greater than 10 ppmv. This eliminates many extratropical points. On this day, the MLS data cover only the Northern Hemisphere extratropics, a result of the satellite orientation. The simulation is generally biased a bit high relative to MLS data in the upper tropical troposphere, although generally agreement is quite good. The linear correlation coefficient between MLS and simulated tracer for this day (February 15, 1996) 0.70 in the tropics.

Simulated tracer concentrations can also be compared to radiosonde observations. Since radiosonde observations of humidity in the upper troposphere and lower stratosphere are not of research quality (Gaffen, 1999), radiosonde temperature measurements were converted to Saturation Vapor Mixing Ratio (SVMR) and compared to

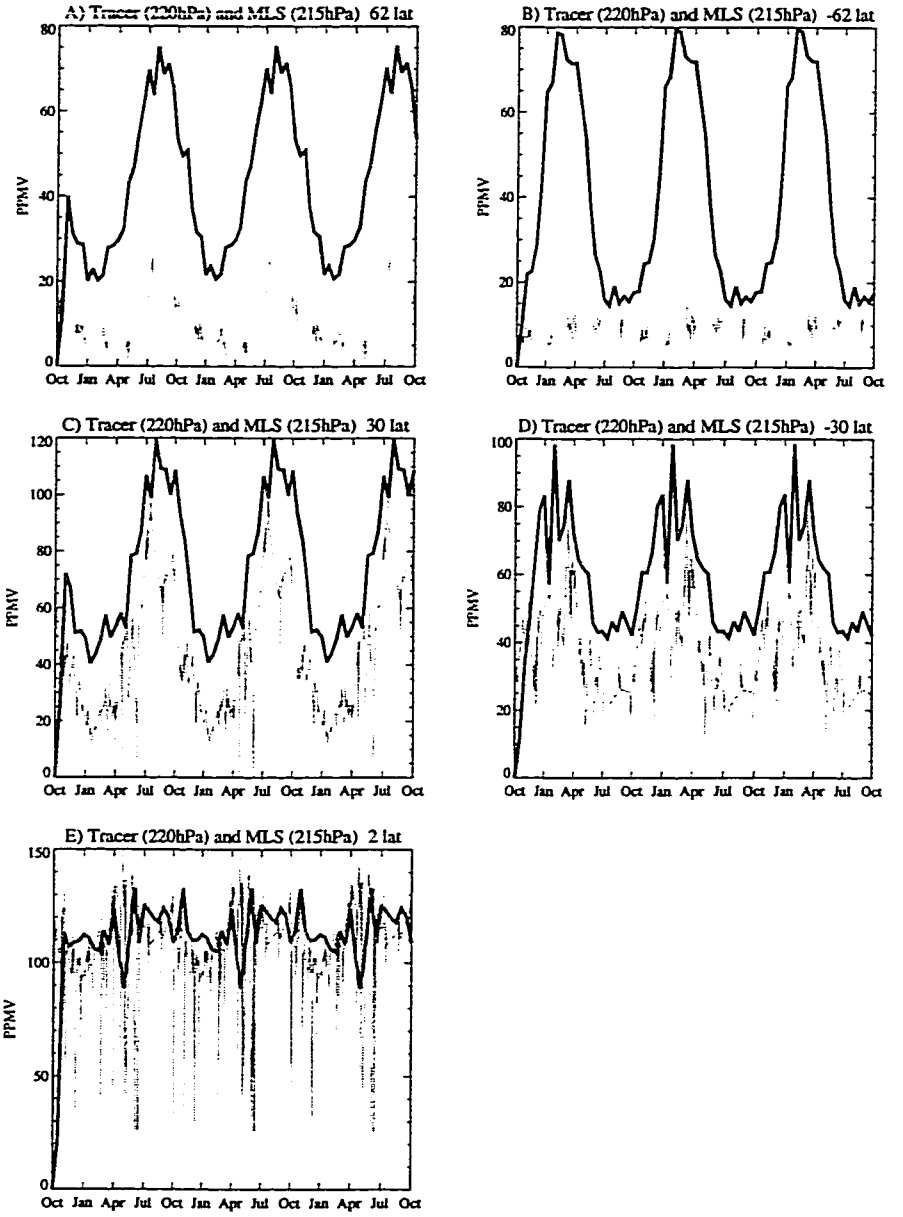

Figure 7.12: MLS water vapor mixing ratio (PPMV) on 215 hPa (grey lines) and simulated mixing ratio at 220 hPa (black lines) at various latitudes: A) 62°N, B) 62°S, C) 30°N, D) 30°S and E) 2°N

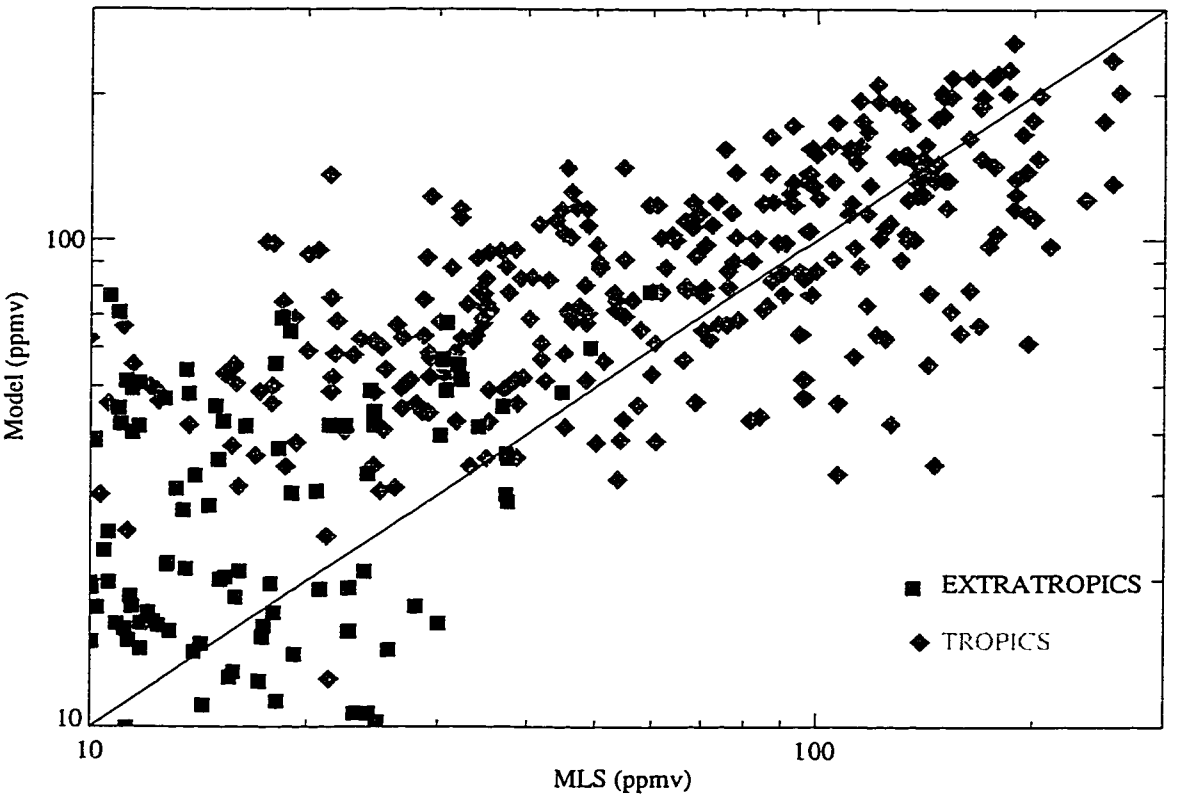

Figure 7.13: Scatterplot of MLS water vapor mixing ratio (PPMV) on 215 hPa for February 15, 1996 versus simulated mixing ratio at 220 hPa. Black squares indicate a point outside of the tropics ($|\phi| > 30°$), while grey diamonds are tropical points ($|\phi| < 30°$).

simulated SVMR and simulated tracer values. Figure 7.14 presents an analysis for Koror, an island station in the Western Pacific (8°N, 135°E). Several tropical stations at other longitudes (Diego Garcia in the Indian Ocean, and Barbados in the Atlantic) were examined and found to have similar results. Model fields for SVMR and tracer were interpolated to mandatory reporting levels for radiosonde data for comparison. Generally, the simulated SVMR is able to reproduce the annual cycle at Koror from 80–250 hPa. The SVMR calculated using radiosonde temperatures and using assimilated temperatures both have similar ranges. The simulated relative humidity (tracer nearly equal to SVMR) is highest at 150 and 200 hPa, consistent with Figure 7.6. At 150 hPa (Figure 7.14b) and 200 hPa (Figure 7.14c) the simulated SVMR is significantly higher than SVMR estimated using radiosonde temperatures throughout the year, consistent with the warm bias of assimilation temperatures at the cold point discussed in Section 7.3. But at 80 hPa (Figure 7.14a) and 250 hPa (Figure 7.14d) the simulated and observed SVMR are quite similar. The differences are consistent with the vertical distribution of assimilation temperature biases discussed in Sections 7.3 and 4.2. The result is higher simulated tracer values in the upper tropical troposphere, as noted in comparisons with MLS data (Figure 7.12).

Daily maps of the relative humidity as defined by Equation 7.1 and 300 hPa upper tropospheric humidity (UTH) fields from the NCEP/NCAR Reanalysis (Kalnay et al., 1996) also indicate good agreement between the simulated and observed synoptic scale (1000's of km) features. The best agreement for 300 hPa UTH fields occurs in the simulation at 220 hPa, where the temperature field constrains the tracer by dehydration. At 300 hPa, particularly in the extratropics, the simulation has lower RH than assimilated UTH data because it has not yet reached saturation temperatures.

Tracer concentrations can also be compared to Outgoing Longwave Radiation (OLR). Minima in OLR indicating the presence of high clouds and deep convection, correspond to some of the lowest tracer values in the Western Pacific near the equator (interpolated OLR data provided by the NOAA-CIRES Climate Diagnostics Center).

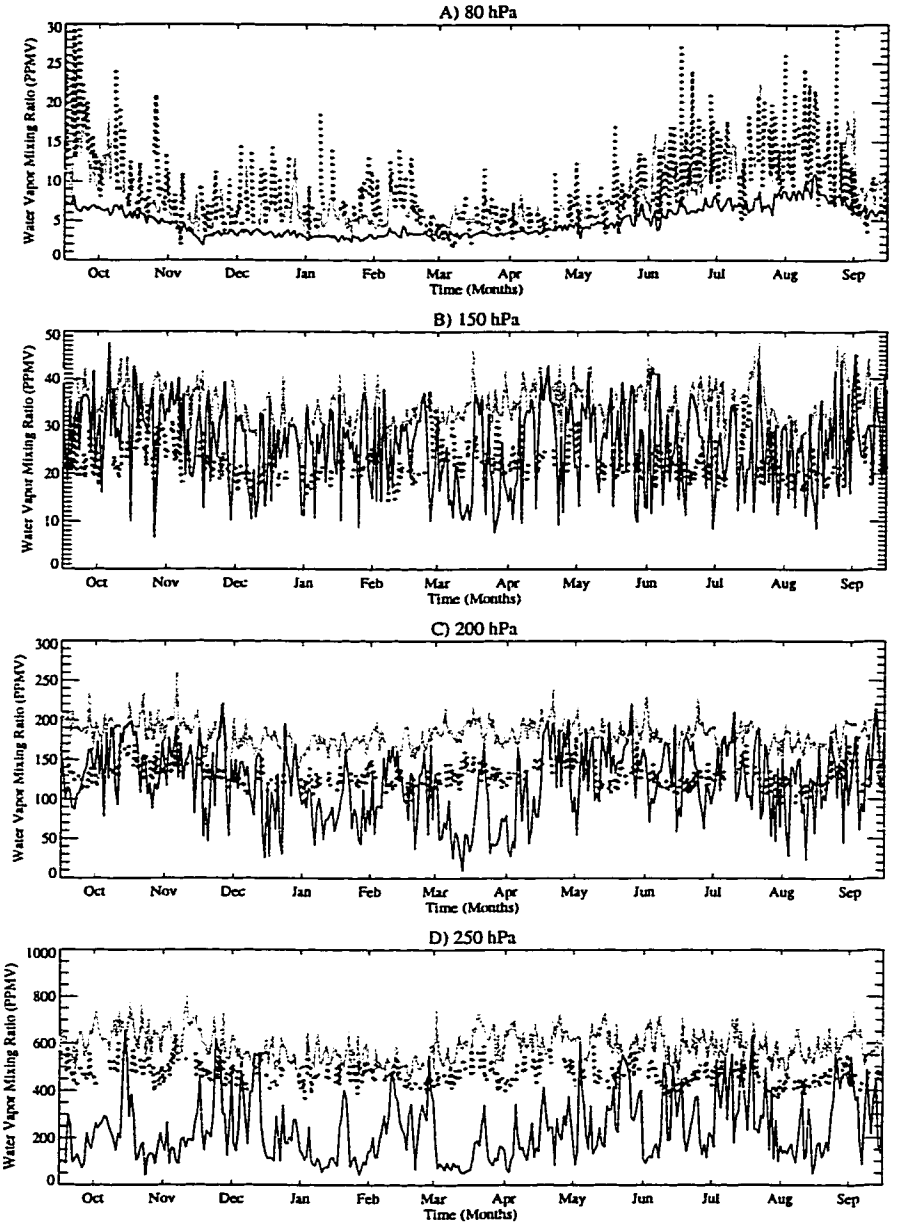

Figure 7.14: Simulated SVMR (thick grey line), radiosonde SVMR (black dotted line) and simulated tracer (thin solid line) at Koror (8°N, 135°E) in PPMV. Plots at different altitudes for one year of data. Model temperature and tracer data are interpolated to radiosonde standard levels at: A) 80 hPa, B) 150 hPa, C) 200 hPa, and D) 250 hPa.

In NH winter tracer values are a minimum around the cold point (79mb), in the central and eastern Pacific. These regions of low tracer correlate with low OLR values. By September, low values in the eastern Pacific again form just north of the equator, and as in winter these are correlated with minima in OLR. OLR and UTH data illustrate that above 200 hPa or so, the processes controlling water vapor in the upper tropical troposphere are largely regulated by large scale advection and thermodynamics. Such a conclusion is also consistent with the presence of a propagating signal similar to the MJO in the water vapor distribution (Figure 7.9). Such large scale regulation of humidity is also noted in reconstructed humidity fields using trajectory calculations by Salathé and Hartmann (1997) and Pierrehumbert and Roca (1998).

However, there are some tracer concentrations in the stratospheric overworld which do not correlate well with observations. In July, high values of water vapor up to 8–10 ppmv are found well into the stratosphere at 94 hPa and 79 hPa, and at latitudes of 30°N to 40°N. The high values occur from 120°E to about 60°W, and are not correlated strongly with the monthly mean OLR. It appears as if there is significant upward transport into the lower stratosphere from the middleworld that does not pass through the cold point in the summer season. This transport "short-circuits" the cold point tropopause. It has been seen in previous simulations using this assimilation data, and is potentially a problem in the GEOS-1 assimilation. (Coy 1998, personal communication). This might account for high mixing ratios in the extratropical lower stratospheric overworld.

7.6 Stratosphere-Troposphere Exchange of Water Vapor

The simulated water vapor tracer, coupled with complete and consistent vertical velocity fields from the transport simulation, can also be used to examine details of the tropical cold point (the minimum in the vertical temperature profile) and the entry of water vapor into the stratosphere. The mass flux of water vapor into the

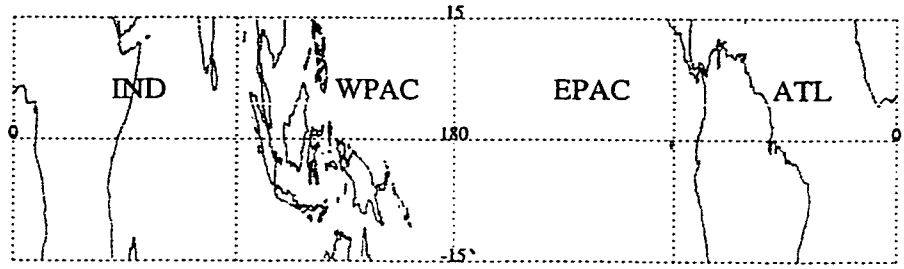

Figure 7.15: Tropical Sectors: Indian (IND), Western Pacific (WPAC) Eastern Pacific (EPAC), Atlantic (ATL).

stratosphere can yield insights into whether the entry of air into the stratosphere is only through certain longitudinal regions (the 'stratospheric fountain' hypothesis of Newell and Gould-Stewart (1981)) or whether water vapor is injected into the stratosphere at all longitudes (Dessler, 1998).

Fluxes of tracer across pressure (sigma) surfaces were estimated by saving the pressure vertical velocity (omega—in mb/day) at each timestep the tracer was saved. The vertical velocity is not an input meteorological variable. Rather, it is derived in the transport model from the convergence or divergence implied by the large scale wind field. The vertical velocity contains significant variability on the smallest simulated time and space scales (6 hours and 100's of km). In the following discussion the tropics will be broken into four regions by longitude defined as follows: the "Indian" (IND) sector from the Greenwich meridian (0°W) to 90°W, the "Western Pacific" (WPAC) sector from 90°W to the dateline (180°W), the "Eastern Pacific" (EPAC) from the dateline to 90°E and the "Atlantic" (ATL) sector from 90°E to the Greenwich meridian. These sectors are graphically illustrated in Figure 7.15. The Indian sector includes tropical African land regions, the Western Pacific includes the maritime continent and the Atlantic sector includes tropical South America and part of Africa.

Generally in the lower stratosphere, the extratropical tracer flux is downward, and

the tropical flux is upward. The simulation cannot provide accurate flux results above the point where the oxidation of methane, not parameterized in the simulated tracer, begins to contribute to the water vapor concentration significantly. As a consequence of the high variability in the vertical velocity field, mass fluxes and also tracer fluxes are generally noisy. At the altitude of the cold point (79 hPa or 94 hPa and about 18 km), there is generally upward motion in the tropics and downward motion in the extratropics, but with lots of zonal variability. Downward extratropical fluxes in the winter hemisphere are larger than the corresponding fluxes in the summer hemisphere.

To better examine whether a tropical 'stratospheric fountain' (a longitudinal region of preferential vertical transport) is present, the flux can be broken down into various regions in longitude. The tracer flux represents a convolution of the tracer concentration with the air mass flux, so the average tracer concentrations are presented in Figure 7.16 (averaged over the tropical sectors illustrated in Figure 7.15). Note that the separation of the levels is about 1.3 km. Analysis is performed for February (dotted lines in Figure 7.16) and August (solid lines in Figure 7.16). There is zonal symmetry in tracer concentrations in the lower stratosphere (67 hPa and 79 hPa) in both August and February. Around the cold point (located at either 79 hPa or 94 hPa), and below, average tracer concentrations vary significantly (by $\sim$20%) between the different sectors as illustrated in Figure 7.16. Tracer concentrations are significantly higher in August than February in the tropics. In February, tracer concentrations are lowest in the Western Pacific sector at all levels from 132 hPa to 67 hPa. In August the concentrations are lowest in the Indian sector (except at 67 hPa).

The tracer fluxes by sector (Figure 7.15) are illustrated in Figure 7.17 for model levels in the upper tropical troposphere and lower stratosphere. In the tropics, there are sectors where the monthly averaged mass flux is downward, and these are indicated in Figure 7.17. Downward fluxes are found mostly in February, and most consistently in the Eastern Pacific (including through the cold point at 79 hPa and 94 hPa). In the upper troposphere these fluxes may be plausibly related to the descend-

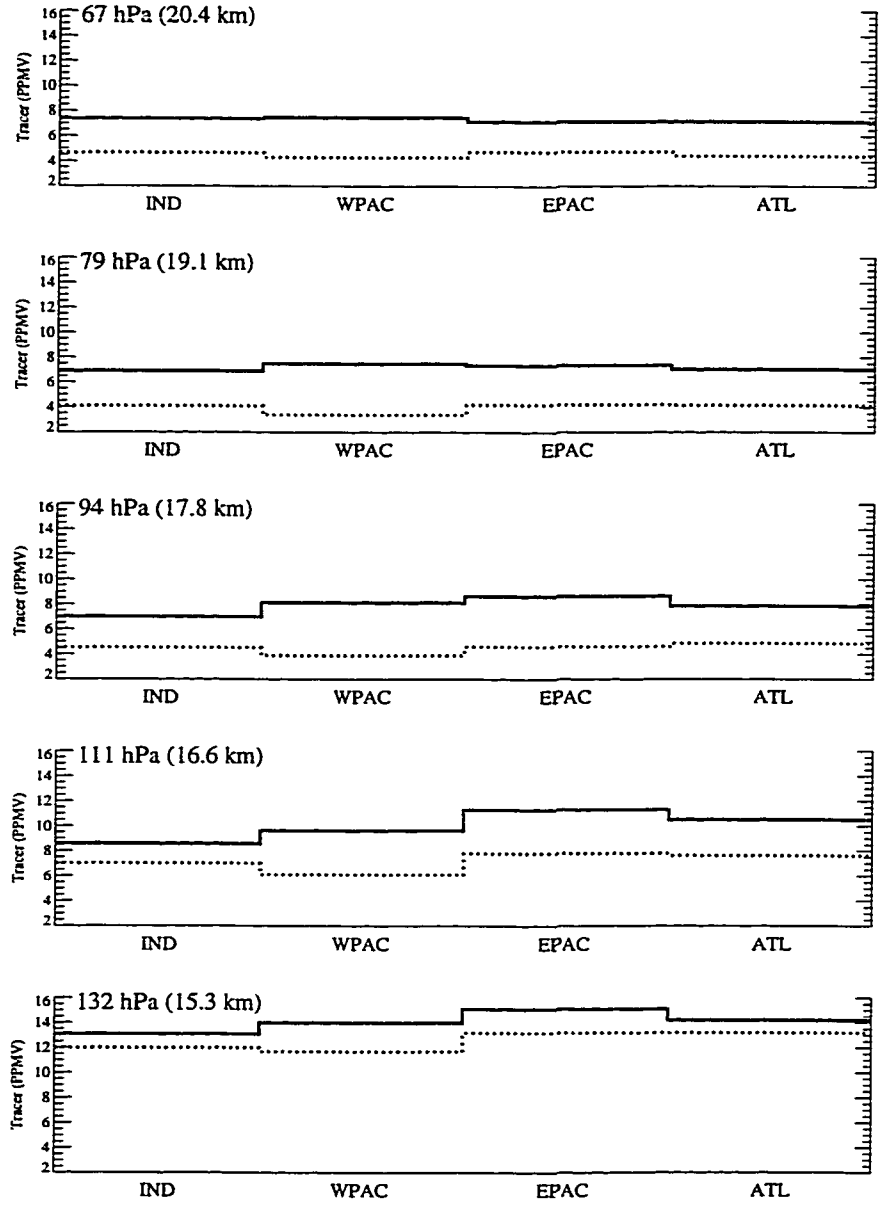

Figure 7.16: Average tracer mixing ratio (PPMV) averaged over tropical ($|\phi| < 15°$) sectors: Indian (IND), Western Pacific (WPAC) Eastern Pacific (EPAC), Atlantic (ATL). 5 different pressure levels shown (log-pressure altitude in parentheses) for August (solid lines) and February (dotted lines).

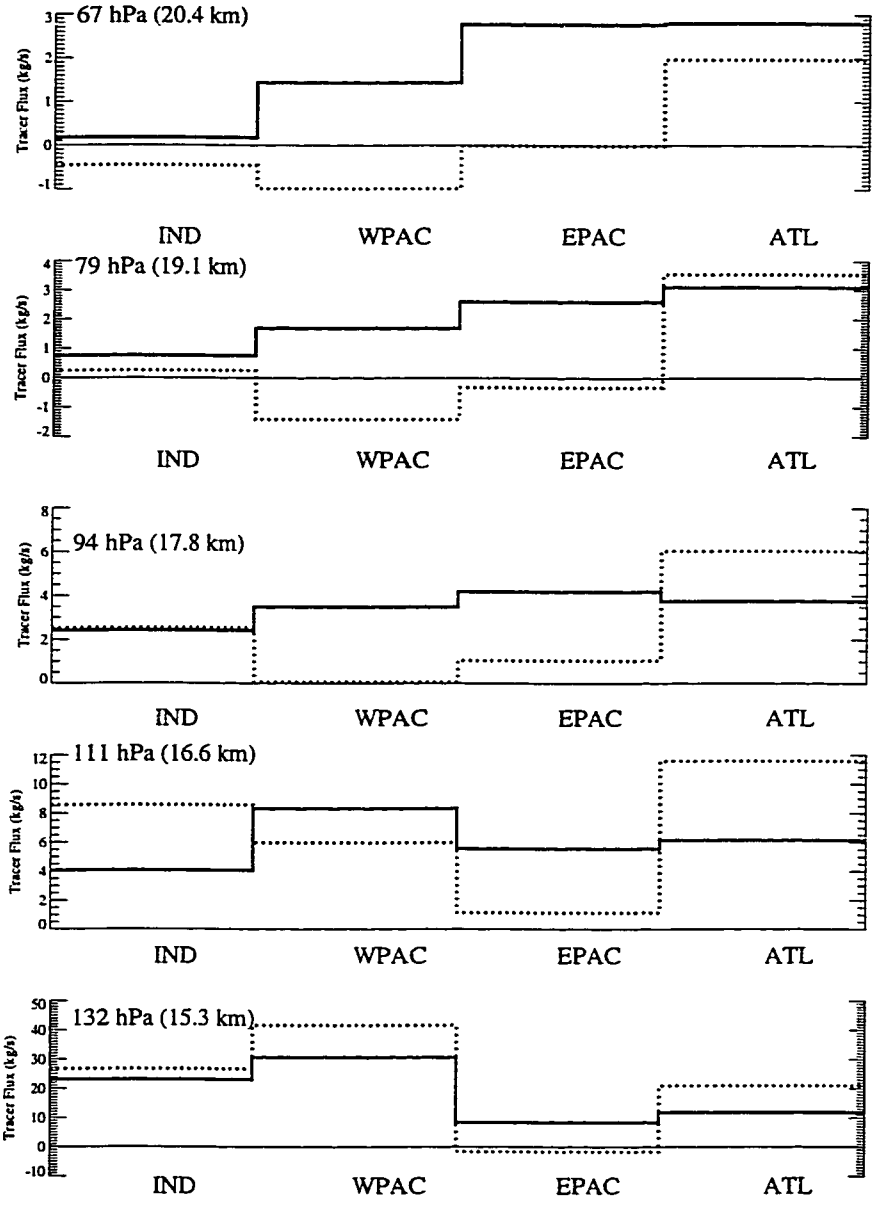

Figure 7.17: Average tracer mass flux (kg/s) averaged over tropical ($|\phi| < 15°$) sectors: Indian (IND), Western Pacific (WPAC) Eastern Pacific (EPAC), Atlantic (ATL). 5 different pressure levels shown (log-pressure altitude in parentheses) for August (solid lines) and February (dotted lines). Zero line is plotted as a thin solid line.

ing branches of the Walker circulation in the tropics (Bjerknes, 1969) or influences from the descending branch of the Hadley cell in the subtropics. However, because larger tracer concentrations are found at lower levels, even if the net air mass flux is downward the net tracer flux may still be upward (positive). Mass fluxes are more consistently upward in August. Tracer mass fluxes are stronger and more variable by sector in February than in August. Note that the tropical upwelling region may extend outside of the latitudes of the deep tropics analyzed here, as indicated in Figure 3.3 for the ozone mass flux at 50 hPa. The tracer mass flux in February around the cold point (111 hPa to 79 hPa) is strongest upward over the Atlantic sector, containing the Amazon basin in South America.

The tropical upward tracer flux is larger in NH summer than in NH winter, as illustrated in Figure 7.17—driven more by the cycle in tropical mixing ratios than tropical upward air mass flux, which is greater in NH winter. The tropical mass flux is largest in the Western Pacific sector at 132 hPa in both February and August (and extending up to 111 hPa in August). At the cold point the largest upward tracer flux is over the Atlantic sector (South America). The absence of a water vapor 'fountain' at the cold point in the Western Pacific where temperatures are coldest is different from the model simulations of Mote et al. (1994). The simulation here is consistent with the findings of Mote et al. (1994) that additional resolution reduced the presence of the fountain, and raised the altitude (and lowered the temperature) of the cold point. A 'fountain' (preferential regions or sectors where air enters the stratosphere) is not necessary, as noted by Dessler (1998), to explain the low water vapor mixing ratios in the stratosphere. Here we find generally higher averaged simulated tracer concentrations than observations of water vapor, but this is consistent with the temperature differences discussed in Section 7.3.

The exchange of water vapor between the stratosphere and the troposphere does not occur simply across the tropical tropopause into the overworld. As discussed in Chapter 2, there is significant quasi-isentropic exchange from the upper tropical tro-

posphere into the extratropical lowermost stratosphere, and vice versa. This exchange occurs when synoptic events create 'tropopause folds' which significantly deform the tropopause structure (Holton et al., 1995) and eventually result in 'cut-off' cyclones and the deposition of stratospheric air into the troposphere, and vice versa. Postel and Hitchman (1999) have characterized this exchange as Rossby wave breaking and analyzed the climatology of such events on the 350K surface. The preferred locations for such events noted by Postel and Hitchman (1999) correspond to the planetary wave 'ducts' of westerly winds in the tropics (Webster, 1983; Webster and Holton, 1982). These events occur preferentially in the summer hemisphere, at different longitudes in each hemisphere. Analysis of daily tracer maps on a pressure surface near 350K (187 hPa) from the simulation yields a similar preferential distribution of high average monthly tracer values in longitude in both hemispheres during summer. These averages are found to be the result of discrete 'Rossby wave breaking' events that transport air horizontally between the tropical troposphere and the extratropical lowermost stratosphere (and vice versa).

Another way of analyzing this exchange is by analyzing the transit time of water vapor from the tropical troposphere to high latitudes on a pressure or theta surface which spans the tropopause. The meridional transit times in the middleworld from the tropics into the high midlatitudes can be estimated by analyzing a single pressure level in time (Figure 7.11a). It takes about 1–3 months for the signal to propagate from the tropics into high latitudes (Figure 7.2). Transit times appear slightly longer for MLS water vapor (Figure 7.11b). On a theta surface the transport is less clear, and appears to be driven by fluctuations in altitude of the theta surface (Figure 7.3). Using a virtually identical model, Strahan et al. (1998) found rapid transport of the CO_2 signal from the tropics to midlatitudes in the lowermost stratosphere, and of coupling of the lowermost stratosphere directly to the extratropical upper troposphere. This is consistent with the coupling and the short delay indicated in this data. Little difference is found in the annual cycle of tracer concentrations throughout the mid-

dleworld in the vertical. A delay of only 1–2 months exists between the arrival of the minimum concentration on 330 K and 370 K at midlatitudes (not shown), consistent with the findings in the CO_2 simulation of Strahan et al. (1998). Fast transport from the surface to the middleworld (1.5 months) is recorded by Ray et al. (1999) in analyzing SF_6 measurements on balloon flights, similar to the transport times diagnosed by Strahan et al. (1998), and consistent with the rapid transport from tropical troposphere to the middleworld illustrated in the water vapor tracer analyzed here.

7.7 Discussion and Conclusions

A global transport model with parameterized thermodynamics has been used to simulate the distribution of water vapor in the upper troposphere and lower stratosphere. A simulation with crudely parameterized water vapor removal and saturation reproduces the general pattern of water vapor in the upper troposphere and lower stratosphere, and many of the details of the water vapor distribution. This correspondence indicates that the large scale forcings are the primary drivers for water vapor in the stratospheric overworld. Differences between the simulation and observations in the upper tropical troposphere indicate that small scale processes are important in the upper tropical troposphere.

Detailed comparisons with observations of water vapor have been performed to examine the limits of the simulation. The temperature structure in the assimilation system used to drive the simulation approximately represents the height of the tropical cold point, but the temperature of the cold point is 2°K warmer than the cold point in other assimilation data sets. The bias will increase the water vapor concentration of the stratosphere. Indeed, the tracer concentrations simulated in the lower stratosphere above the 380K potential temperature surface are generally 2–3 ppmv higher than water vapor observed by HALOE or radiosondes. The seasonal cycle of water vapor mixing ratio is well represented on pressure surfaces in the stratospheric overworld

and the extratropical lowermost stratosphere, but less well simulated on isentropic surfaces. Model transport does not appear to be isentropic in the middleworld. The simulated stratospheric overworld also has a well defined 'tropical tape recorder' signal of varying water vapor mixing ratios which propagate vertically. Vertical transport of water vapor in the stratosphere is too rapid when compared to observations, a result which has been noted previously for this transport model. Significant dehydration of the lower stratosphere occurs in the polar vortices in winter.

Simulated water vapor in the upper troposphere and lower stratosphere also compares well to the synoptic scale distribution of water vapor from satellite constituent data and radiosondes. In particular, there is good correspondence in the tropics between the simulated tracer and observed MLS water vapor concentrations. Simulated tracer concentrations also correspond to observed upper tropospheric humidity distributions, and monthly mean outgoing longwave radiation.

In the upper troposphere, the South Asian monsoon circulation is found to be responsible for moistening the northern hemisphere lowermost stratosphere. The higher concentrations of simulated water vapor in the northern hemisphere are found to be a result of this monsoon circulation as well as the spreading of dehydrated air in the southern hemisphere, consistent with the work of Rosenlof et al. (1997) using satellite observations in the stratospheric overworld.

The simulated tracer with its crude parameterization indicates that much of the distribution of water vapor in the upper troposphere and lower stratosphere can be understood through the temperature structure and through transport. Details of microphysical processes or even of sub-grid scale convection are not explicitly necessary to generate a large scale picture of water vapor in this region of the atmosphere. In particular, the simulation is able to recreate propagating regions of high and low water vapor which resemble wave driven phenomena such as the MJO using only the large scale observed horizontal wind fields and temperatures. However, the temperature structure in the upper tropical troposphere deviates significantly from other assimi-

lation datasets and radiosonde observations at 150 hPa. It is suggested that at this level convective processes may be much more important for determining the water vapor distribution than large scale processes. This may also impact the water vapor distribution in the middleworld through quasi-isentropic exchange which has been shown to be a transport mechanism for water vapor into the middleworld, consistent with analyses of Dessler et al. (1995).

In this simulation it does not appear that there is a tropical fountain of air entering the stratosphere over the Western Pacific when temperatures are cold (NH winter). There is evidence of such a fountain at lower levels (132 hPa) and in August. The largest tracer mass flux into the stratosphere at the cold point is over South America and the tropical Atlantic Ocean. Air is dehydrated at levels up to 94–79 hPa, the cold point, but at this level it appears as if there is uplift at all longitudes, or at longitudes with higher temperatures than that of the 'fountain region'. The simulation does imply lower mixing ratios in the Western Pacific, consistent with lower temperatures there. The simulation without a fountain duplicates tropical water vapor to within the range expected from a warm bias to the cold point, leading to differences in SVMR of 2–3 ppmv. This agrees with the recent work of Dessler (1998) suggesting that a fountain is not necessary to account for the low water vapor mixing ratios in the stratospheric overworld. The lack of a fountain is also consistent with the lack of zonal variation in high, cold (convective) cloud fraction in analysis of geostationary satellite brightness temperature data by Zhang (1993).

Transport of high tropical tracer values between the tropics and the middleworld occurs episodically, and is consistent with the zonal climatology of planetary wave breaking noted by Postel and Hitchman (1999). This quasi-isentropic exchange is more vigorous in the summer hemisphere, also in agreement with climatologies from Postel and Hitchman (1999), and isentropic exchange noted by Chen (1995). Higher than expected middleworld tracer values are coupled to higher than observed tropical water vapor tracer values and/or excessive exchange between the tropics and mid-

latitudes during these wave breaking events. It takes approximately 1–3 months for maxima and minima in the water vapor distribution to propagate meridionally from the tropical upper troposphere to the high latitudes in the stratospheric middleworld by this exchange pathway. Unlike the work of Strahan et al. (1998) there does not appear to be a difference in the seasonal cycle of water vapor on midlatitude pressure levels in the lowermost stratosphere and upper troposphere. Since the water vapor signal for both regions in this simulations originates in the tropics, a difference should not be expected in the timing of the signal, especially if there is rapid meridional transport in the middleworld as well as in the upper troposphere. In both regions water vapor is a maximum in late summer and fall (in both hemispheres).

It is interesting to compare the conclusions of this simulation with those from Mote et al. (1994), who found a fountain present at 'low' vertical resolution (2.2 km around the cold point), but not at 'high' vertical resolution (1.1 km around the cold point), more similar to this simulation. Generally Mote et al. (1994) consider the stratosphere-troposphere exchange characteristics of the high resolution simulation 'worse' than the low resolution case. In this simulation we find a similar lack of a stratospheric fountain at the cold point present at 'high' resolution. We do find a fountain at lower altitudes in the tropics in the Western Pacific. One difference between this study and that of Mote et al. (1994) is that we do not include convection, but derive vertical motion via convergence and divergence, while the GCM simulations of Mote et al. (1994) have an explicit convective parameterization scheme. It does not appear that an explicit representation of convection or a water vapor fountain as postulated by Newell and Gould-Stewart (1981) is necessary to explain the cycle of air entering the stratosphere which gives rise to the tropical 'tape recorder' (Mote et al., 1996). From these simulations it appears that the mass flux due to convective regions over the maritime continent (Indonesia) in February tops out well below the cold point.

These simulations have presented an overall picture of the water vapor distribution

in the upper troposphere and lower stratosphere using a detailed model and some very crude parameterizations. The resulting realizations of the water vapor distribution imply that large scale transport and thermodynamics are of primary importance for the stratosphere-troposphere exchange of water vapor. Future work in this area should include comparison with other transport simulations using similar tracer formulations. Future work with this particular set of model tools should include the incorporation of a realistic convective mass flux scheme. Especially valuable would be a convective scheme which can be modified to vary the maximum height of the convective flux. Similar simulations may also help in the validation and comparison of such schemes. Finally, a study of the interannual variability of the water vapor distribution is an important extension of this work which has not yet been performed.

Chapter 8

DIRECT DIAGNOSES OF STRATOSPHERE-TROPOSPHERE EXCHANGE

In the preceding chapters we have examined in detail the stratosphere-troposphere exchange of air and trace constituents, including: ozone, nitrous oxide, and CF_2Cl_2 in Chapter 3, aircraft fuel emissions and components in Chapter 6 and water vapor in Chapter 7. For most of this discussion, quantitative discussion of the exchange of air or constituent mass across the tropopause has not been analyzed at the tropopause surface, but at levels in the stratospheric overworld (Chapter 3), pressure and theta surfaces in the lowermost stratosphere (Chapter 7) or as mass budgets of the lowermost stratosphere (Chapters 6 and 7). For some long lived species this method provides useful data, but for other short lived species it is desirable to know the fluxes at the tropopause. In this chapter a method for deriving these fluxes at the tropopause is analyzed in detail. There are two goals to this analysis. First, to understand quantitative information about mass and tracer fluxes at hourly to interannual timescales in. Secondly, we seek to understand the limits of current methods in the absence of a more complete description of the non-conservative processes that cause stratosphere-troposphere exchange.

8.1 Motivation

In order to understand the physics and chemistry of the upper troposphere and lowermost stratosphere, quantitative information on the mass and property transports between these two regions is required. While important aspects of the circulation of

mass between the troposphere and the region of the middle atmosphere known as the "overworld" (Shaw, 1930; Hoskins, 1991) are fairly well constrained (Holton et al., 1995), this does not imply a similar level of certainty concerning actual property fluxes across the tropopause. Recently, several studies have performed calculations intended to remedy this lack of quantitative knowledge, using the method described by Wei (1987) (hereafter "the Wei method"). This method, in principle, allows both upward and downward components of the cross-tropopause mass flux to be separately determined. Some other commonly used methods only constrain the net mass flux, which is in general inadequate to determine fluxes of chemical species. This study applies the Wei method to assimilated fields from the Goddard Earth Observation System (GEOS) data set. One aim is to provide results for comparison with similar calculations using other data sets. A second aim is to perform calculations which test the robustness of the Wei method, particularly when a typical global assimilated data set is used and quantitative results are desired. We find that while the method is a useful tool for some purposes, it places severe demands on the quality of the input data. Because of this, the method may be ill-conditioned in practice when used to obtain quantitative results from data of realistic quality. Our analysis suggests that better results might be expected when the diagnostic is applied to output from free-running model simulations, but in fact problems similar in nature to those discussed here are reported by Wirth and Egger (1999) even with a free-running model.

Throughout this paper we will use the term Cross Tropopause Flux (CTF) to refer to the exchange of mass across a surface defined as separating the stratosphere and troposphere. The CTF may be instantaneous or averaged. Where appropriate, we will specify what type of averaging, if any, has been applied; if no averaging is mentioned, instantaneous CTF is meant. The CTF may be reversible, in the sense that an air parcel may cross the surface in one direction and then cross back again soon after, without undergoing true mixing.

We first describe conceptual issues related to two-way exchange and the results

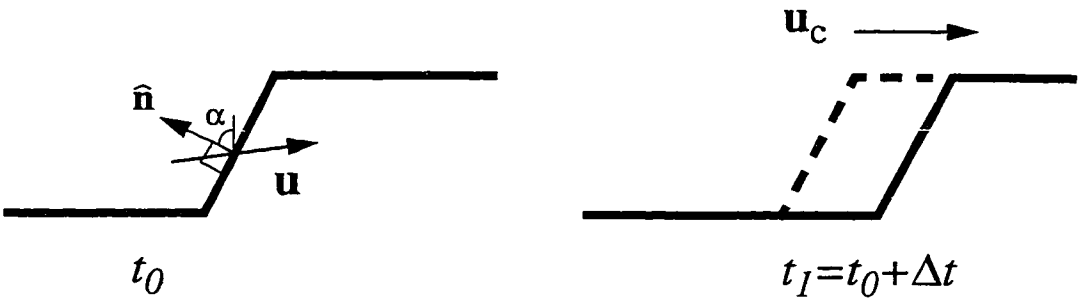

Figure 8.1: Schematic of motion of across the tropopause. Left panel is time t_o and right panel is a later time t_1 illustrating the motion of the tropopause ($\mathbf{u}_c$) and the 3D wind ($\mathbf{u}$) with the normal to the tropopause ($\hat{\mathbf{n}}$) and the angle between $\hat{\mathbf{n}}$ and the vertical (α) also shown.

of previous studies in Section 8.2. We then describe our implementation of the Wei method in Section 8.3, and present results from these calculations in Section 8.4. The results are broken into a discussion of mass budgets in Section 8.4.1, instantaneous snapshots in Section 8.4.2, monthly integrated results in Section 8.4.3 and globally and annual integrated results in Section 8.4.4. We discuss the effect of errors in the input data in Section 8.5, and present conclusions in Section 8.6.

8.2 Basic concepts and results of previous studies

Consider a two-dimensional surface defining the tropopause. At every point on the surface the mass flux across it per unit surface area can be written:

$$\tilde{m} = \rho(\mathbf{u} - \mathbf{u}_c) \cdot \hat{\mathbf{n}} \tag{8.1}$$

where $\mathbf{u}$ is the three-dimensional fluid velocity, $\mathbf{u}_c$ is the velocity of the surface itself, ρ is the density, and $\hat{\mathbf{n}}$ is the unit vector normal to the surface (positive upward). Equation 8.1 is graphically illustrated in Figure 8.1. As is typical in previous studies,

we will for most purposes use the quantity

$$m = \frac{\tilde{m}}{\cos\alpha} \tag{8.2}$$

where α is the angle between $\hat{n}$ and the vertical, assumed less than 90°. m is the mass flux across the surface per unit horizontal area rather than per unit surface area. When the surface is the tropopause (however defined) we will call m the "instantaneous CTF" (positive upward).

The Wei method is equivalent in principle to the direct application of (8.1) and (8.2). The more complex expressions in Wei's paper result from taking the surface to be an isosurface of potential vorticity (PV) and expanding the terms, resulting in expressions such as (8.5) below. More detailed presentations of the manipulations involved can be found in Wei (1987) and Wirth and Egger (1999).

In some studies, the instantaneous, local mass flux $m(x, y, t)$ is presented only after having been submitted to some integration or averaging, in time as well as either zonally or over large areas. While this may be instructive, it obscures the information which is most directly relevant for making inferences about the fluxes of material properties, such as trace gases, since these depend directly on the extent to which a given net mass flux is made up of canceling components of opposite sign.

To understand the two-way aspects of stratosphere-troposphere exchange, we can integrate the positive and negative components of $m(x, y, t)$ separately. That is, we can integrate over longitude, time, etc., but perform the integral twice, first including only points where m is positive, and then only those where it is negative. Call the resulting "upward" and "downward" integrated mass fluxes M_u and M_d respectively, with the sign built into the definition so that both are positive numbers. M_u and M_d will be collectively referred to hereafter as "gross" fluxes. The net mass flux is simply the difference of these,

$$M = M_u - M_d$$

where we have defined positive upwards.

The relevance of M_d and M_u to tracer fluxes is most easily illustrated by considering the idealized case of a trace gas, q, which has uniform mixing ratio q_1 just below the tropopause and q_2 just above, with a discontinuity at the tropopause. In this case, the flux of q across the surface is

$$F_q = M_u q_1 - M_d q_2 \tag{8.3}$$

There is no way to infer F_q from the total mass flux M alone. (8.3) can be rewritten

$$F_q = M q_2 + M_u (q_1 - q_2) \tag{8.4}$$

So that in this case the flux of tracer has a one-way part, which depends only on the tracer mixing ratio above the tropopause, and a two-way part, which depends on the difference in the mixing ratios above and below the tropopause and is zero if $M_u = 0$.

Downward control theory (Haynes et al., 1991; Holton et al., 1995), and radiatively derived estimates of the residual circulation (Rosenlof, 1995; Eluszkiewicz et al., 1996), do not provide any direct information on tracer fluxes, because they constrain only M. Additional assumptions, such as taking $M_u = 0$ at some surface well above the tropopause, can make M useful for analyzing the cross-tropopause fluxes of long-lived constituents, provided the chemical lifetimes of the constituents are longer than the transit time through the region between the chosen upper surface and the tropopause. In that case the cross-tropopause tracer flux is computed as a residual from the total budget of tracer for that intervening region. This approach has been used to calculate the cross-tropopause flux of ozone using the zonally and temporally averaged residual circulation (Chapter 3 and Gettelman et al. (1997)) and using transport models (Lelieveld and Crutzen, 1994; Tie and Hess, 1997). For shorter-lived species, this approach is invalid.

The major advantage of the Wei method, then, is that in principle it allows the direct computation of M_u and M_d. Spaete et al. (1994), Lamarque and Hess (1994), Siegmund et al. (1996) and Wirth and Egger (1999) have separately computed M_u and

M_d using the Wei method or variants of it. The four studies used different data sets. Lamarque and Hess (1994), and Spaete et al. (1994) used mesoscale model simulated data over regional domains and periods of four days and one day respectively, while Siegmund et al. (1996) used forecast data from the European Center for Medium-Range Weather Forecasting (ECMWF) for the extratropical northern hemisphere for an entire month. Wirth and Egger (1999) use ECMWF GCM model data over a regional domain for 3 days. For these studies the values of the ratio M_u/M_d were 0.24 (Wirth and Egger, 1999), 0.4 (Spaete et al., 1994),0.79 (Lamarque and Hess, 1994), and 0.97 (Siegmund et al., 1996). The spread in these values, a factor of four, implies widely differing patterns of stratosphere-troposphere exchange in the different studies. When M_u/M_d is close to unity, it implies that the exchange is mostly two-way, with the net mass flux M being a small residual of much larger upward and downward fluxes. When the same ratio is small compared to unity, it implies a more nearly one-way transport, so that tracer fluxes will be to a greater extent determined by the net mass flux M (see equation (8.4)). This effect can alternately be quantified by the ratio M_u/M, which measures the relative importance of the second term in (8.4) relative to the first, in the case $q_1 = 0$ (a reasonable first approximation for, e.g., ozone). For the above-mentioned studies this ratio is -0.3 (Wirth and Egger, 1999),-0.67 (Spaete et al., 1994), -3.67 (Lamarque and Hess, 1994), and -32.33 (Siegmund et al., 1996). This makes the studies look still more different and, in particular, makes Siegmund et al. (1996) appear to be a more extreme outlier relative to the others.

For the studies of Wirth and Egger (1999), Spaete et al. (1994) and Lamarque and Hess (1994), the process studied is in each case a particular synoptic-scale midlatitude cyclone. Siegmund et al. (1996) applied the Wei method over an entire hemisphere and an entire month. Still, one expects that the largest transport events will involve synoptic-scale systems bearing some resemblance to those in the other studies, and this expectation is supported by the results of the present study. However, the largest value of either M_u/M_d or (in absolute magnitude) M_u/M was obtained by Siegmund

et al. (1996) from an assimilated data set, while the others were obtained from free-running model simulations.

Two hypotheses suggest themselves for the difference between the results of Siegmund et al. (1996) and the other three studies (the substantially smaller differences among those other three presumably being explainable by differences in the particular events studied). One is that most of the gross flux occurs in small events, which would be sampled by Siegmund et al. (1996), but not by the others due to their focus on particular individual systems of relatively large amplitude. The other is that the Wei method for some reason yields different results depending on whether the input data come from a free-running model or an assimilated data set. The results of the present study support both hypotheses to some extent. Much of the gross flux in our calculations does appear to be due to small amplitude events, but a simple order-of-magnitude calculation (see Section 8.5) suggests that these small events might reasonably be explained as artifacts caused by errors in the input data.

8.3 Implementation

We have implemented the Wei method with the numerical modifications developed by Siegmund et al. (1996). These modifications, referred to by Siegmund et al. (1996) as the "advection method", are intended to reduce errors associated with the practical problems of time and space differencing. In finite difference terms, the advection method seeks to rationalize the addition of space and time differentials by selectively averaging the space terms over time. Since the temporal averaging is accomplished along wind vectors, it is "advective". Siegmund et al. (1996) fully discuss the mathematics and the reduction of spurious noise which results.

As input data we have used the GEOS Assimilation data set, version 1 (Schubert et al., 1993). These data are available on a 2.5° longitude by 2° latitude by 18 pressure level grid (see Table 4.1), at 6 hourly time spacing. The vertical resolution is 50

hPa (approximately 1.5 km) around the extratropical tropopause and the uppermost level is 0.4 hPa. 37 months of data from May 1995 through May 1998 are used in this analysis, with a focus on January 1996 for comparison with previous work. As a check, we also estimate the net CTF using a mass budget method described by Appenzeller et al. (1996). In contrast to studies which only examine the northern hemisphere extratropics in winter, we extend the analysis using the Wei method to the annual cycle over the globe.

The GEOS data have lower spatial and temporal resolution than most of the data used by Siegmund et al. (1996). However, Siegmund et al. (1996) indicate that at smaller time and space scales than those examined here, net fluxes estimated at increasing resolution begin to converge. Hoerling et al. (1993) found little quantitative difference between results computed at different horizontal resolutions. The resolution may bring an additional uncertainty into the analysis, though ideally the diagnostic should not be strongly resolution-dependent in the range of resolutions typical of assimilation data sets. The basic formulation for the instantaneous CTF per unit horizontal area, m, in pressure coordinates, is:

$$m = \frac{1}{g}\left(-\omega + V_h \cdot \nabla P_t + \frac{\partial P_t}{\partial t}\right) \tag{8.5}$$

as introduced by Wei (1987). In (8.5), g is the acceleration due to gravity, ω is the pressure vertical velocity, V_h is the horizontal wind vector and P_t is the pressure of the material surface of interest (the tropopause). Wirth and Egger (1999) show how (8.5) can be derived from (8.1).

The definition of the material surface for the Wei diagnostic is an important issue. In this case that surface is taken to define the tropopause. Grewe and Dameris (1996) addressed this issue in some detail, using both a thermal definition of the tropopause based on the lapse rate and a dynamic definition of the tropopause based on values of Ertel's Potential Vorticity (PV). We have chosen to define the tropopause using the dynamic definition, expressed in potential vorticity units (PVU), where 1 PVU = 1 x

$10^{-6} K kg^{-1} m^2 s^{-1}$. The value of potential vorticity corresponding to the midlatitude tropopause varies from about 1.5 PVU (World Meteorological Organization, 1986) to 3.5 PVU (Hoerling et al., 1991). Several analyses, (Hoerling et al., 1993, 1991) have shown that 3 or 3.5 PVU is quite close to the thermal tropopause in midlatitudes. The PV value chosen may be related to the resolution of the input data as noted by Hoerling et al. (1993). Higher resolution analyses (Lamarque and Hess, 1994) generally have used lower values of PV. Grewe and Dameris (1996) and Siegmund et al. (1996) have analyzed the sensitivity of the Wei diagnostic to the tropopause PV surface chosen. To constrain the value of the tropopause surface in the tropics where PV becomes ill-conditioned, we have used a potential temperature surface marking the lower boundary of the "stratospheric overworld" (Holton et al., 1995) of 380 K.

For exchange of air mass and constituents, the tropopause is perhaps best not defined by one surface, but by a "region", for example, bounded by PV surfaces. Fluxes out of this region may be more relevant than those across a single surface. Accordingly, a range of tropopause definitions using different PV surfaces is examined. These tropopause surfaces are described as single valued in the vertical, even in the case of a multiple valued tropopause in the vertical. When the tropopause "folds" in the vertical, an average tropopause height is used. Some analyses are also run by defining the tropopause as the highest altitude of the selected potential vorticity value ("Assumption A" of Siegmund et al. (1996)). Both an average and high definition of the tropopause in regions with a multiple valued tropopause in the vertical yield a few individual points of difference, and spatial integrals of the gross and net fluxes which are nearly identical. This may be because, perhaps due to the relatively large grid spacing, there appear to be few major tropopause folding events in the data record used here.

We will also implement the Wei method on a theta surface at the boundary between the "lowermost stratosphere" and the "overworld" (Holton et al., 1995), as a link to other work using the downward control principle (Haynes et al., 1991) and

residual circulation (Rosenlof, 1995; Eluszkiewicz et al., 1996; Gettelman et al., 1997) on surfaces above the tropopause.

8.4 Results

8.4.1 Budget Estimate

For comparison to our results obtained using the Wei method, we have calculated the monthly averaged net Cross Tropopause Flux (CTF) using GEOS data and the method used by Appenzeller et al. (1996). The net CTF (F_{out} in Appenzeller et al. (1996), equation 1) is defined as the sum of (1) the monthly average change in mass of the lowermost stratosphere, and (2) the diabatic mass flux across the upper boundary of the lowermost stratosphere calculated using the diabatic heating rates. The resulting monthly averaged net CTF by hemisphere is illustrated in Figure 8.2 for 1996-1997. The lowermost stratosphere is defined as the region between the 3 PVU tropopause surface and the 380K potential temperature surface in the extratropics. The daily and zonally averaged mass flux at the top of this surface is estimated using the daily and zonally averaged diabatic heating and static stability, and the result is then averaged monthly and meridionally from 28° to each pole (the heating rate calculation differs slightly from the method described by Appenzeller et al. (1996), Equation 3, in that they used monthly averaged heating rates from the start rather than performing the monthly average after the mass flux computation). The result is not very sensitive to the PV value of the tropopause surface or the latitude boundary of the tropics selected.

The annual cycle timing and amplitude illustrated in Figure 8.2 are comparable to those presented by Appenzeller et al. (1996). The Northern Hemisphere mass flux into the troposphere peaks in both winter and spring, a result of the winter peak in the diabatic circulation, and the shrinking of the lowermost stratosphere in spring. The difference in net mass flux between hemispheres is also captured. The average

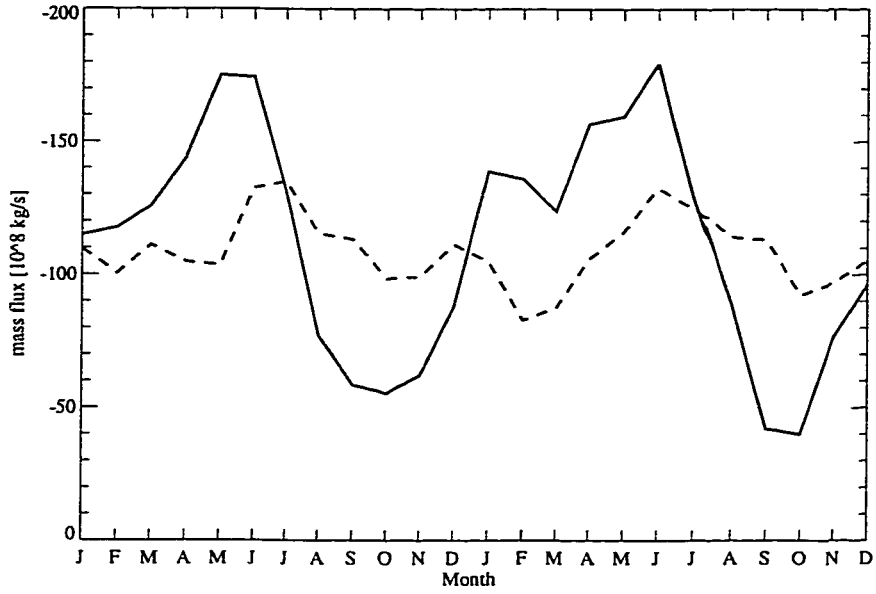

Figure 8.2: Monthly averaged net extratropical CTF by hemisphere, calculated from GEOS data, using budget method of Appenzeller et al. (1996). Northern hemisphere solid line, Southern hemisphere dashed.

Northern Hemisphere net winter mass flux (28°N to pole for December, January and February) is 1.2 x 10^9 kgs^{-1}, similar to the 1.4 x 10^9 kgs^{-1} found by Appenzeller et al. (1996). Thus in the extratropics, the GEOS data appear to capture well the long term budget of mass exchanged between the stratosphere and the troposphere as diagnosed using heating rates and seasonal variations of tropopause pressure. This provides evidence that any problems which may result when the Wei method is applied to these data cannot be ascribed to the GEOS data's being in any obvious way inferior to other data sets, such as the assimilated data from the United Kingdom Meteorological Office (UKMO) used by Appenzeller et al. (1996). There are still potential errors in any assimilation as discussed in Section 4.8.

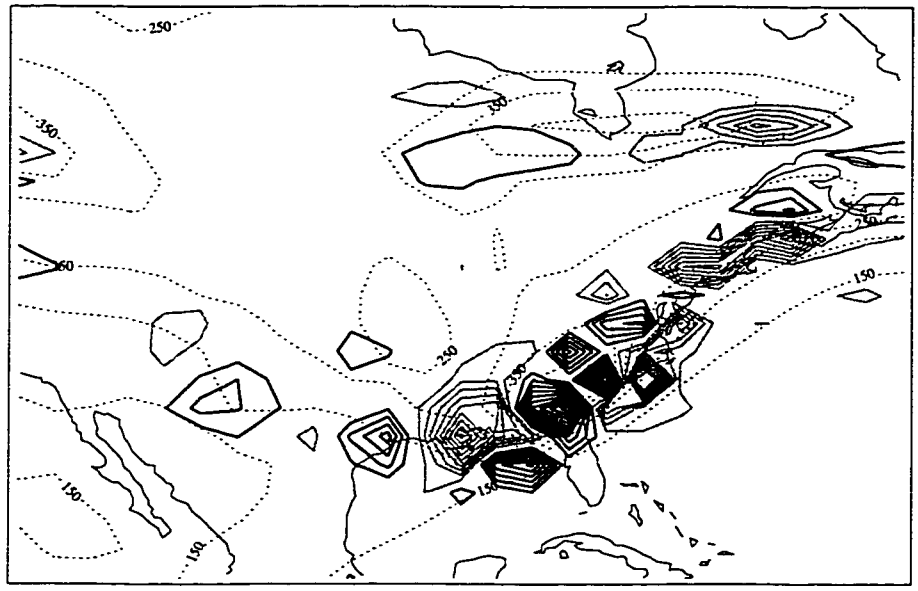

Figure 8.3: CTF at 0600 UTC 4 January 1996. Solid grey lines are downward instantaneous CTF. Solid black lines, upward CTF. Contour interval of 1x10^{-2} $kgm^{-2}s^{-1}$. Dotted lines represent the pressure on the 3PVU tropopause (in hPa).

8.4.2 Snapshots

Large CTF events may be associated with frontal systems. Figure 8.3 illustrates the application of the Wei diagnostic for a large scale frontal system over the eastern seaboard of the United States. The region of large CTF near the tropopause corresponds to a strong gradient in the tropopause height near the winter jet stream marked by strong winds. The large magnitude CTF at this time is located just west of a surface cold front indicated on surface analyses from the National Centers for Environmental Prediction (NCEP). There is significant CTF in both directions along the gradient in tropopause height.

A plot of different components of the diagnostic illustrates the situation. High wind speeds and a changing tropopause height are the most important inputs to the calculation, which yield positive and negative values of CTF in rapid succession (Fig-

ure 8.4(a)). In general, the winter storm track regions of the northern and southern hemispheres exhibit many of these canonical midlatitude cyclones, with similar features resulting in the Wei diagnostic. There appears in most cases a dipole structure to the CTF, in both time (Figure 8.4(a)) and space (Figure 8.4(b)), with components of tropopause motion and wind relative to the tropopause cancelling partially, but not completely. Similar spatial patterns are noted by Siegmund et al. (1996), Lamarque and Hess (1994) and Wirth and Egger (1999). Since this pattern typically persists for a time longer than a characteristic parcel transit time across the dipole structure, the pattern indicates that air travels "through" a region of anomalously low tropopause height, passing from troposphere to stratosphere and then immediately back again. The low tropopause just south of Hudson Bay in Figure 8.3 illustrates one case of transport into the stratosphere on the upwind (west) side and out of the stratosphere on the downwind (east) side of a low tropopause feature. A modest mismatch — such as would be caused by an error in the assimilated data — between the analyzed horizontal velocity and the translation speed of the tropopause height anomaly could cause such behavior, though we have no way of telling whether this is the case, or whether the diagnosed CTF is correct. Similar problems are noted in the case study described by Wirth and Egger (1999).

In addition to gradients in tropopause height associated with frontal systems, horizontal CTF occurs when tongues of high PV air are advected to low latitudes, and then erode into the troposphere, causing the stratosphere to troposphere exchange of mass. An example of one of these events off the western coast of North America is illustrated in Figure 8.5. In this case the structure is subsequently cut off from the stratosphere. This event and the diagnosed pattern of CTF associated with it is similar to many other cut off cyclone events in the analysis fields. The CTF in Figure 8.5 is diagnosed as being into the stratosphere as the tongue approaches, and into the troposphere as it passes. The pattern of exchange is coherent, and matches the location of the tongue. A similar pattern of exchange first into the stratosphere

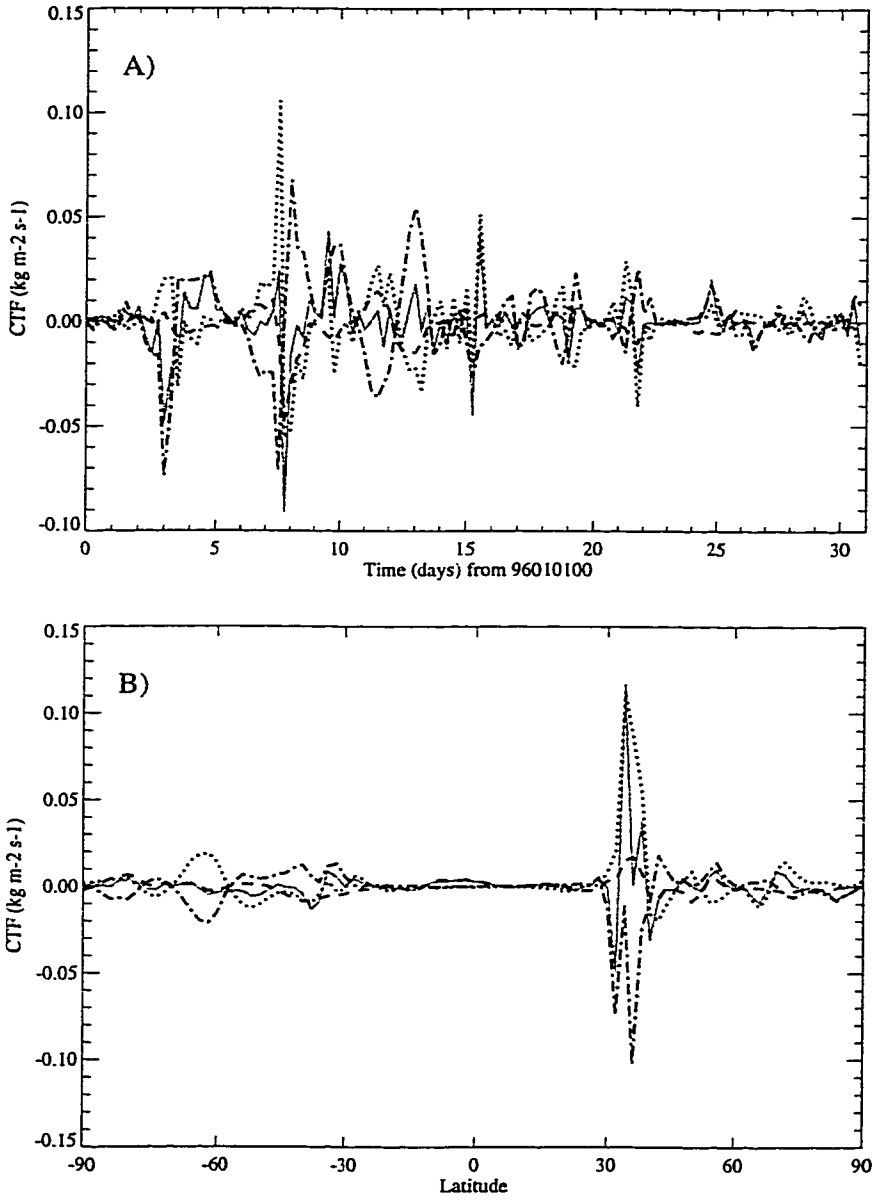

Figure 8.4: Components of the Wei diagnostic in units of $kgm^{-2}s^{-1}$. A) Time series at 32°N 80°W for January 1996. B) Latitude section at 80°W at 00 UTC 4 January 1996. Total CTF grey solid line. $-\omega$ Dashed. $V \bullet \nabla P_t$ Dot-Dash. $\frac{\partial P_t}{\partial t}$ Dotted

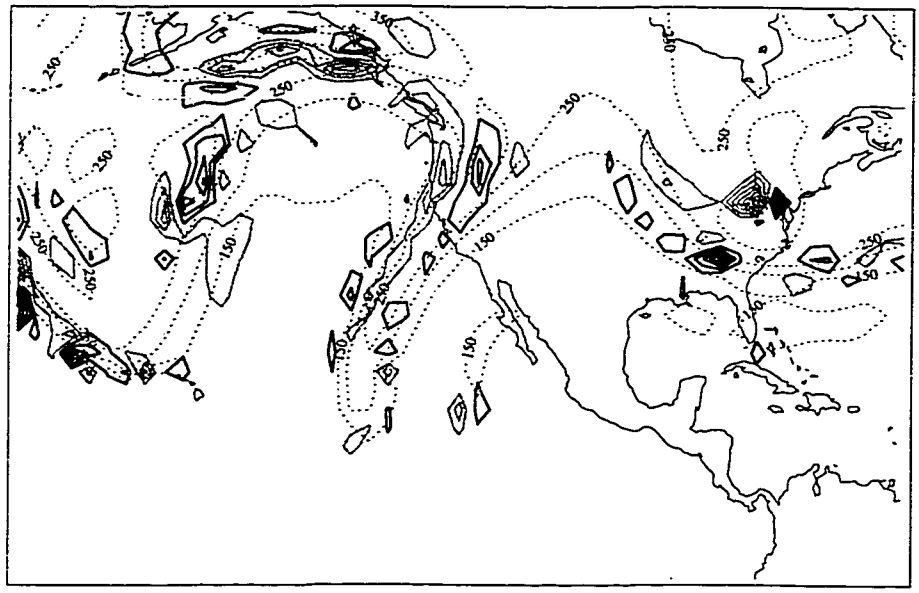

Figure 8.5: CTF on 0600 UTC 10 January 1996. Solid grey lines are downward instantaneous CTF. Solid black lines, upward CTF. Contour interval of 1x10^{-2} $kgm^{-2}s^{-1}$. Dotted lines represent the pressure on the 3PVU tropopause (in hPa).

and then back into the troposphere upstream was noted by Lamarque and Hess (1994). Again, this apparent flow through the tropopause height anomaly could be real, or could be mis-diagnosed, or at least exaggerated, by fairly small data errors. One such possible point error in tropopause height is clearly visible in Figure 8.5 at 40°N near the east coast of the United States, where a single point anomaly in the tropopause height yields significant gross (but perhaps little net) CTF. These large point errors appear infrequently and randomly in the analyses.

The two structures illustrated in Figures 8.3 and 8.5 appear at first glance to be the dominant forms of extratropical CTF. The distribution in space of the CTF over a month is illustrated in Figure 8.6 by averaging the instantaneous CTF over time. The winter hemisphere storm track experiences the greatest variability in CTF in both January (Figure 8.6(a)) and July (Figure 8.6(b)). There is still a high degree of spatial variability, with some regions showing significant average upward fluxes,

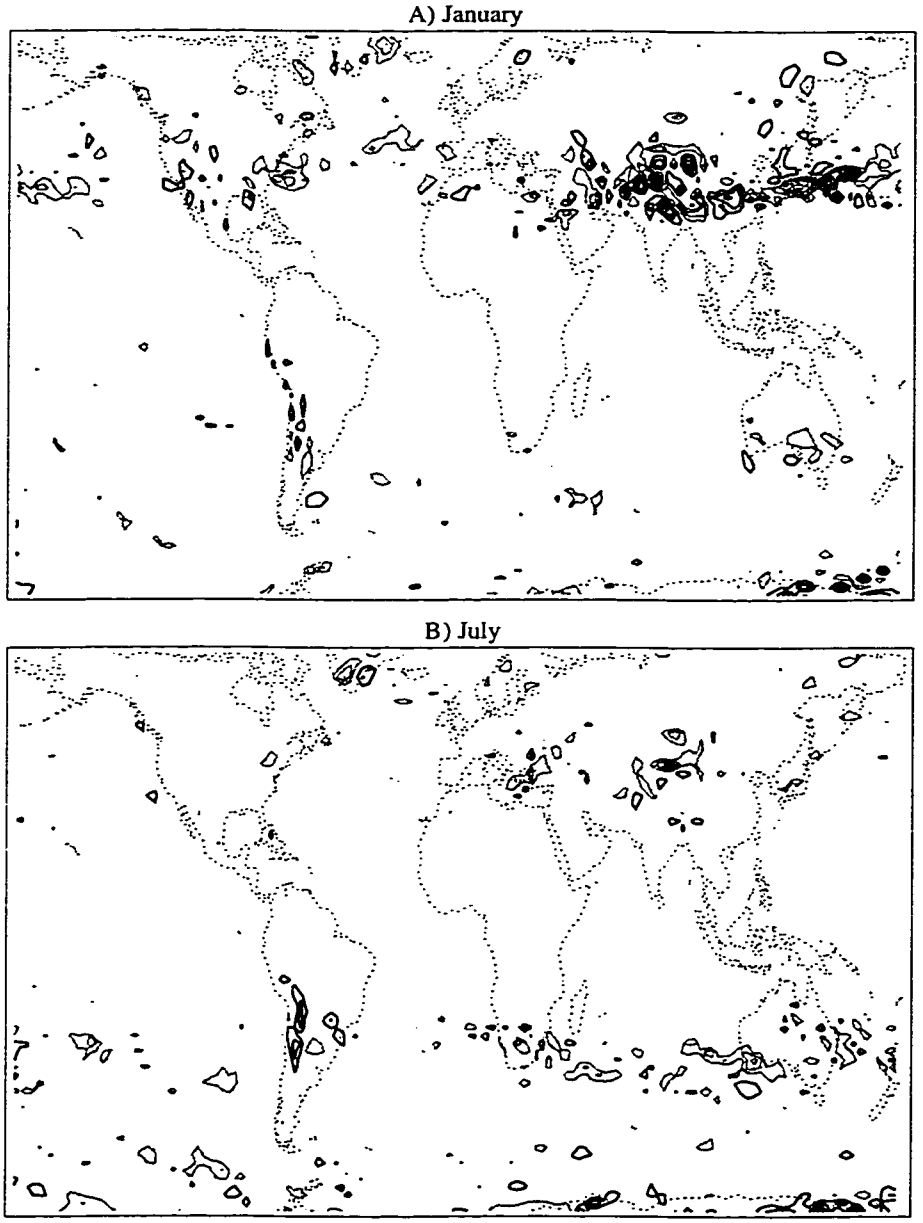

Figure 8.6: Monthly averaged CTF for A) January and B) July. Black lines are average upward CTF, grey lines are downward CTF. Contour interval of 2x10^{-3} $kgm^{-2}s^{-1}$

forming dipoles with adjacent downward average fluxes. The situation for southern hemisphere winter is similar to that in the northern hemisphere, with structures similar to those in Figure 8.3 and Figure 8.5 but of slightly lower magnitude. Most of the CTF in the northern hemisphere winter is confined to distinct portions of the storm track, primarily over the north Pacific east of Japan but also over the eastern US and North Atlantic. In the southern hemisphere winter the largest variability is seen over and around Australia. A strong jet and its associated tropopause gradient are the main features of diagnosed CTF.

In neither season is detailed structure in the instantaneous CTF found in the tropics. Tropical instantaneous CTF is generally positive, and of much lower magnitude than in high latitudes. However, there is less cancelation, so that the net mass flux into the stratosphere in the tropics ends up comparable in magnitude to that out of the stratosphere in the extratropics, as required by mass balance (though the global mass budget, as diagnosed by the Wei method, balances only very roughly, as discussed in Section 8.4.4). There appears to be little large scale organization in the tropical CTF. No patterns directly associated with the monsoon circulations are visible. It is reasonable to expect that the tropical results are more strongly affected by weaker aspects of the assimilation system, such as the convection scheme in the model used for the assimilation, than the extratropical results. For this reason we limit our attention to the extratropical results hereafter.

In midlatitudes, summertime frontal systems which generate summertime convection do have significant tropopause gradients associated with them, and to generate CTF structures similar to those noted in the winter season. However, non-frontal convective activity does not appear to generate any such structures. Convective activity over Florida in June 1996, for example, appears on several days over regions larger than the size of a grid box in the GEOS assimilation for periods longer than 6 hours according to NEXRAD radar analyses, without any evidence of significant CTF. This result is subject to the same caveat as the tropical results, that is, it may

be relatively sensitive to the diabatic parameterizations in the model.

In summary, analysis of the instantaneous CTF reveals that the midlatitude storm track regions have the highest instantaneous and temporally averaged values of CTF, and that midlatitude synoptic-scale systems and horizontal tongues of tropopause air are responsible for much of this gross exchange. Exchange from the troposphere into the stratosphere is found to occur in many of these events, though much of this is immediately compensated by exchange from the stratosphere back into the troposphere, suggesting flow "through" tropopause height anomalies rather than irreversible exchange. This phenomenon could possibly be explained by relatively small errors in the input data (as will be discussed further below) and hence its veracity may be questioned. Tropical instantaneous CTF is marked by low-magnitude upward drift, and does not have significant regional structure.

8.4.3 Monthly and seasonally integrated results

The monthly and seasonally integrated CTF are presented in this sub-section. We integrate the instantaneous CTF over time and area to generate the net flux (M) for comparison with other methods of quantifying stratosphere-troposphere exchange. Several approaches to integrating the instantaneous cross tropopause flux in space and time will be explored. The method is also extended to look at isentropic surfaces. Globally and annually integrated results are presented in Section 8.4.4.

Many of the previous analyses of stratosphere-troposphere exchange with the Wei method and others have focused on the extratropics of the northern hemisphere in winter. Accordingly, integrating the instantaneous CTF for comparison and averaging for December, January and February (DJF) of 1996 yields an average downward flux from 28°N-90°N of 387x10^8 kgs^{-1} (1x10^{17} kg/month) for a 3 PVU tropopause. The corresponding values for DJF 1996-1997 and 1997-1998 are 404x10^8 kgs^{-1} and 280x10^8 kgs^{-1} respectively (see Section 8.4.4). For January 1996, the average CTF with an extratropical tropopause defined by different PV surfaces is 334x10^8 kgs^{-1}, 314x10^8

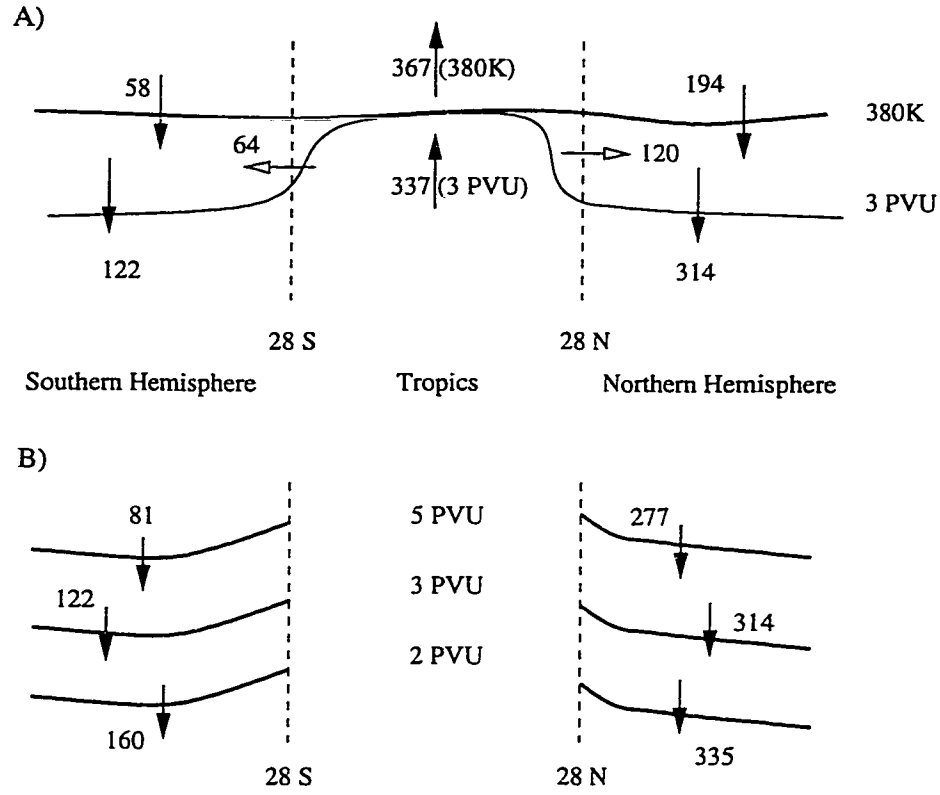

Figure 8.7: Budget calculations for January 1996 Monthly integrated net CTF in units of 10^8 kgs^{-1} in the bounded regions for A) Tropopause and 380K theta surface in the extratropics, and B) for different PV definitions of the extratropical tropopause.

kgs^{-1} and 277x10^8 kgs^{-1} for the 2, 3 and 5 PVU surfaces respectively, with a gradient of about 20x10^8 kgs^{-1} per PVU (5x10^{15} kg/month). These fluxes are presented graphically in Figure 8.7(a) and (b). The gross upward and downward fluxes (M_u and M_d) over a month for January are 10.7x10^{17} kg up and 11.6x10^{17} kg down and the ratio $M_u/M_d = 0.92$, consistent with Siegmund et al. (1996). In addition, the probability density function of instantaneous CTF over a month is virtually identical to that of Siegmund et al. (1996).

The net fluxes indicated in Figure 8.7 are highly dependent upon the latitude chosen to define the equatorward boundary of the extratropics. Figure 8.8 illustrates the integrated monthly flux by latitude for these various surfaces. The latitude 28°N

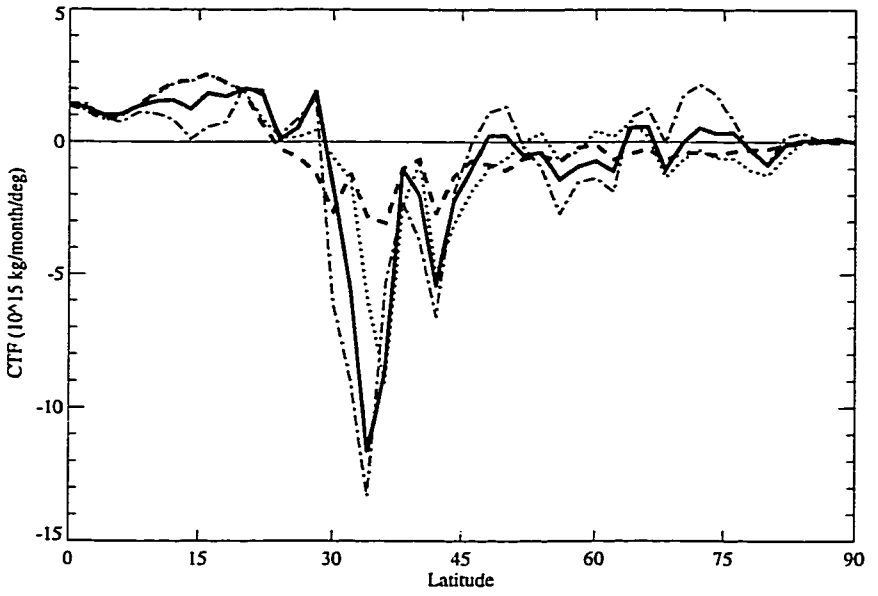

Figure 8.8: Zonally averaged monthly extratropical CTF for the Northern Hemisphere, by latitude, units of 10^{15} kg month^{-1} degree^{-1} 2 PVU Tropopause – Dot-Dash. 3PVU tropopause – Solid. 5PVU tropopause – Dotted. 380K surface – Dashed.

is taken to represent the approximate point at which the zonally averaged integrated flux becomes positive as latitude decreases towards the equator. As found by Hoerling et al. (1993) and Siegmund et al. (1996), there are latitudes in which there is net upward CTF in the extratropics over the course of a month. The upward flux arises due to the dipole structures illustrated in the average monthly flux, Figure 8.6(a). These are present because the instantaneous dipole structures, as in Figure 8.4(a), tend to recur in the same locations, and are quasi-zonally oriented, so that they do not disappear in a zonal and time average. Similar patterns have been seen in vertically folded tropopause events by Lamarque and Hess (1994).

In principle, the Wei method can be used to describe transport across any material surface in the atmosphere. While PV and potential temperature surfaces have been used here and in previous studies to define the tropopause, it is also useful in discussing stratosphere-troposphere exchange to look at exchange with the strato-

spheric overworld (Holton et al., 1995), that is, exchange across the 380K potential temperature surface. The advection method has been applied to analyses of potential temperature at this and other levels as a way of diagnosing this exchange near 100 hPa. The net extratropical downward flux from 28°N-90°N for January 1996 at 380K is 194x10^8 kgs^{-1}, as illustrated in Figure 8.7. The flux by latitude across the 380K surface is also plotted in Figure 8.8. Note that at 380K there is no upward flux in the extratropics.

The flux across 380K, along with the flux at the tropopause, implies a quasi-isentropic flux in the middleworld from the tropics (at 28°N) of 120x10^8 kgs^{-1}, as illustrated in Figure 8.7(a). In the southern hemisphere the circulation is less vigorous, with a net transport of 58x10^8 kgs^{-1} downward across the 380K surface, and 122x10^8 kgs^{-1} downward at the tropopause (3PVU), implying a net influx from the tropics of 64x10^8 kgs^{-1} at 28°S. However, the tropical fluxes do not balance this influx. Tropical fluxes imply more air rising above 380K than crossing the tropopause in the tropics which would imply net quasi-isentropic fluxes of the opposite sign to those shown in Figure 8.7(b). The maximum gross fluxes at 380K are an order of magnitude lower than those at the tropopause, while typical gross fluxes are a factor of two lower than at the tropopause. This may be due to the reduction of synoptic-scale activity with height above the tropopause. However, the net flux is still of the same order of magnitude because as for the tropopause, the smaller events dominate the net flux (see Section 8.5). These fluxes are not directly comparable to fluxes across the 100 hPa pressure surface, because the surfaces are not coincident. Especially in the Northern Hemisphere in winter, the 380K surface is significantly below the 100 hPa surface.

To compare the magnitude of the extratropical flux integrated over a month with other studies, one must be careful to apply the definition of the "extratropics" consistently. Different studies use different definitions. These studies also examine different years, so that interannual variability may cause some variation in the results. The

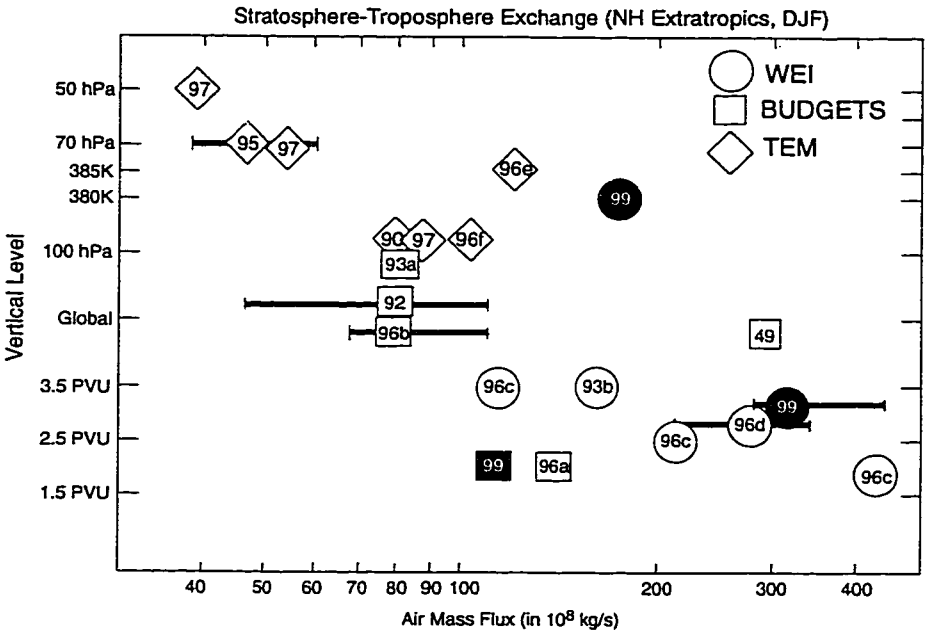

Figure 8.9: Average December, January and February extratropical CTF for the Northern Hemisphere in units of $10^8\ kgs^{-1}$. Symbols represent different methods as discussed in the text. Values in this study in black. Studies cited by year of publication as follows: Brewer (1949), Holton (1990), Follows (1992), Rosenlof and Holton (1993)a, Hoerling et al. (1993)b, Rosenlof (1995), Appenzeller et al. (1996)a, van Velthoven and Kelder (1996)b, Siegmund et al. (1996)c, Grewe and Dameris (1996)d, Yang and Tung (1996)e, Eluszkiewicz et al. (1996)f, Gettelman et al. (1997)

quantitative results presented above translate into a net downward CTF for January 1996 of 64x10^{15} kg for 14°N-90°N, 80x10^{15} kg for 24°N-90°N and 84x10^{15} kg for 28°N-90°N. The values reported here are within the range of previous estimates. Figure 8.9 puts the results here (filled points) in the context of other estimates of the Northern Hemisphere extratropical mass flux averaged over December, January and February (DJF) at various levels. Note the vertical axis is by approximate vertical level and the horizontal axis is logarithmic. Different studies are as indicated in the caption, and the different shapes indicate different methods. Ranges are indicated where known. Generally, there is an increase in the reported exchange of mass between the stratosphere and troposphere with decreasing altitude. CTF estimated using the Wei method is

generally a factor of two larger than most estimates of stratosphere-troposphere exchange of air calculated using budget methods (Appenzeller et al. (1996) and this study) or estimated using the residual circulation in the stratosphere (Rosenlof, 1995; Yang and Tung, 1996). The magnitude of the discrepancy appears to be consistent throughout the year (see Section 8.4.4). The Wei method appears to yield results that are larger than those derived by other methods, even at higher altitudes (such as the 380K potential temperature surface). Wei method calculations at the tropopause level here are within the range of other studies. Note that the CTF estimate of 1.2 x $10^9 kgs^{-1}$ using GEOS data and the mass budget approach of Appenzeller et al. (1996), as discussed in Section 8.4.1, is significantly lower than the estimate obtained from the Wei method using the same data, but comparable to the estimate of Appenzeller et al. (1996).

8.4.4 Globally and annually integrated results

In this section we present the mass flux across the tropopause using the Wei method integrated over the entire globe and a whole year. We then compare this result to an integration of the mass flux across a nearby pressure surface (300 hPa) for an entire year. In principle both calculations should give a number comparable to the annual change in mass of the stratosphere. Figure 8.10 first illustrates the annual cycle of CTF integrated from 28°N-90°N for three years from May 1995 through May 1998. The largest downward flux in the northern hemisphere midlatitudes generally occurs in January and February, with the minimum in August. The annual cycle of the diagnostic is consistent with the cycle of the residual circulation at 100 hPa (Rosenlof, 1995), lagging it by a month or two. The lag in CTF is less than that estimated in Section 8.4.1, using heating rates and the mass of the lowermost stratosphere. The magnitude of the net extratropical CTF from 28°N to 90°N throughout the year is about twice the magnitude found in Section 8.4.1 and by Appenzeller et al. (1996). The annual cycle of net CTF in the southern hemisphere extratropics has

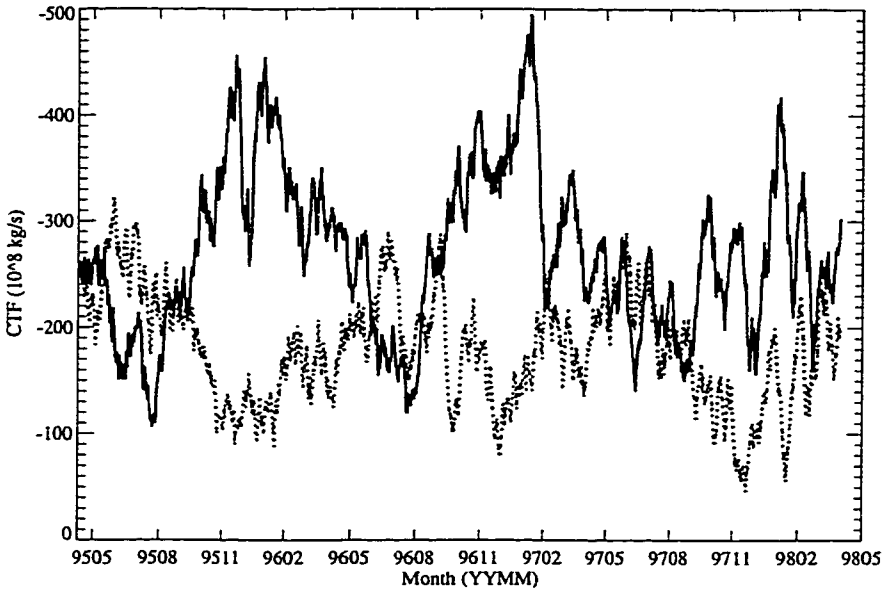

Figure 8.10: Averaged extratropical CTF from 28°–90° for the Northern (solid) and Southern (dashed) Hemispheres, in units of $10^8\ kgs^{-1}$. Data has been smoothed with a 21 day running mean filter

a smaller amplitude, and has a broad peak in July. The difference in CTF between hemispheres is larger than that previously noted by Appenzeller et al. (1996). There are significant interannual differences between years noted in Figure 8.10, particularly in the Northern Hemisphere winter CTF. The peak flux varies by nearly 25% from year to year, and the average over the winter (DJF) varies from 280 x $10^8\ kgs^{-1}$ in 1997-1998 to 404 x $10^8\ kgs^{-1}$ in 1996-1997. The causes for this variability have not been explored in detail.

The atmospheric mass above each of the surfaces across which we have computed transport changes by a relatively small fraction of its total over the course of a year. Hence if the computed net flux across a surface is a much larger fraction of the total mass above the surface, we know there is an error in the calculation whose magnitude is of the order of the discrepancy. This provides a strong check on the accuracy of the calculations, which has not been done in previous studies using the Wei method.

A global integral of the mass flux over an entire year from August 1995 to August 1996 yields a residual of -3x10^{17} kg (which averages to -95x10^{8} kgs^{-1}) at the tropopause, and +4x10^{17} kg (an average of +125x10^{8} kgs^{-1}) at 380K. With the mass of the stratosphere on the order of 11x10^{17} kg (Appenzeller et al., 1996), these fluxes are quite large. Integrating the mass flux across a pressure surface (which is simply the pressure vertical velocity, ω, divided by the acceleration due to gravity, g; the Wei method per se need not be used for this calculation) near the tropopause (300 hPa) or near the 380K surface (100hPa), yields residuals which are an order of magnitude smaller, and of the same order as potential mass changes of the stratosphere over the course of a year, i.e. a few percent or less (Appenzeller et al., 1996). Thus the errors are not caused by biases in the assimilated vertical velocities. The more likely explanation appears to be errors in the diagnoses of the PV and horizontal velocity normal to the tropopause, the same source of errors noted by Wirth and Egger (1999). The next section illustrates how what may appear to be a relatively "small" amount of noise or bias in the PV or potential temperature fields can yield relatively large errors in the CTF diagnosed by the Wei method.

8.5 Effect of input data errors

The following discussion of input data errors is derived from Gettelman and Sobel (1999). Consider the tropopause to be explicitly represented as a PV surface, and choose the sign of $\hat{\mathbf{n}}$ as positive upward so that

$$\hat{\mathbf{n}} = \frac{\nabla Q}{|\nabla Q|}.$$

where Q is the PV. We now consider the true PV, Q, to be represented by an assimilated data set subject to errors, so that the analyzed PV is

$$Q_a = Q + e$$

Clearly e should include observation errors. We argue below that it should also include the "nudging" terms in an assimilated data set.

The normal component of the analyzed PV surface velocity can then be written as

$$-\mathbf{u_c} \cdot \hat{\mathbf{n}} = \frac{\partial Q_a}{\partial t}(|\nabla Q_a|)^{-1} = (\frac{\partial Q}{\partial t} + \frac{\partial e}{\partial t})(|\nabla Q_a|)^{-1} \tag{8.6}$$

The evolution equation for the true PV is

$$\frac{\partial Q}{\partial t} = -\mathbf{u} \cdot \nabla Q + S \tag{8.7}$$

where S represents true physical sources and sinks of PV due to heating, friction, and subgrid-scale effects. Using (8.7) and (8.6) with (8.1) leads to

$$\tilde{m} = (S + \frac{\partial e}{\partial t})(|\nabla Q_a|)^{-1} \tag{8.8}$$

where we have neglected the difference between ∇Q and ∇Q_a in the advective term when substituting (8.7) into (8.6).

Equation (8.8) shows that the sensitivity of Wei's method to input data errors depends on the relative magnitudes of the true nonconservative sources and sinks of PV, and the spurious apparent source due to errors. In an assimilated data set, $\frac{\partial e}{\partial t}$ should include the "nudging" terms which force the model PV back towards observations. These terms are necessary because of inconsistencies between the PV tendencies predicted by the dynamical model used in the assimilation and the observed PV tendencies. These inconsistencies may result from observational errors, errors in the simulated PV advection, or errors in the simulated nonconservative PV sources and sinks. Therefore, the magnitude of the nudging terms must be considered representative of the magnitude of the uncertainty in both the advection and the nonconservative terms, which collectively are represented by $\frac{\partial e}{\partial t}$ in (8.8).

The approximate conservation of PV which is commonly assumed in discussions of midlatitude dynamics implies that $S \ll |\mathbf{u} \cdot \nabla Q|$. This means that the error term can be small compared to the advective term in the evolution of the analyzed PV, so that

the analyzed data can "look good" in the sense of exhibiting the expected tracer-like spatial and temporal structure in the PV field, while simultaneously $S \leq \frac{\partial e}{\partial t}$, so that the error term is significant or even dominant in mass flux calculations using the Wei method, and therefore the signal to noise ratio in the instantaneous CTF is of order unity or less. Sobel et al. (1997) discussed a similar problem with the trajectory-based "contour crossing" method, which has been used to diagnose transport across the edge of the stratospheric polar vortex.

In short, the Wei method places a very strict demand on an observed or assimilated data set by requiring that errors in the simulated PV tendency be small compared to the actual nonconservative terms, which in turn are generally small compared to advection. It is not clear that any currently available observed or assimilated data set meets this requirement.

To make the point more quantitative, consider the results of this analysis, for the northern hemisphere extratropics (28°N-90°N) in January. A typical value obtained for the instantaneous CTF is of order $\sim 10^{-2}\ kgm^{-2}s^{-1}$ or less. Assuming a typical midlatitude tropopause value for the air density of 0.3 kgm^{-3}, this corresponds to $|\mathbf{u} - \mathbf{u_c}| \sim 0.03\ ms^{-1}$. With 6-hourly data this velocity corresponds to a displacement over six hours of about 600 m, which at tropopause altitudes is less than the vertical grid spacing of the input data set. Hence spurious "jitter" in the analyzed tropopause height tendency need not even be a single vertical grid spacing per 6 hours for the results to be attributed to input data errors at the hundred percent level, as far as the instantaneous CTF is concerned. The same conclusion holds for the results of Siegmund et al. (1996), if the appropriate values from their study are inserted in the rough calculation above.

It might be plausible to suppose that when the instantaneous CTF is heavily integrated over space and time to produce a net mass flux M, the effect of the analysis errors ought to largely cancel out. However, given the lack of mass balance over the course of a year, as seen in Section 8.4.4, it appears that this is not entirely the

case. This mass imbalance suggests that the errors in the assimilated data have a persistent bias. In the case of a potential temperature surface (such as 380K), this could be caused by a persistent cold or warm bias in the model, which would lead to a spurious net heating or cooling as the model was nudged towards observations. The bias would not need to be present in the vertical integral, but only at the level of the surface in question. For a PV surface, a persistent bias in the model's potential temperature gradient (from errors in either heating or frictional terms) could cause a systematic bias in the diagnosed CTF.

In any case, spatial and temporal averaging removes much of the information relevant to two way property fluxes (M_u or M_d), which is a significant disadvantage since the potential (in principle) of the Wei method to provide this information is its main advantage over other methods. One may imagine that the error-induced component of the instantaneous flux might have short spatial and temporal time scales, as discussed to some extent by Siegmund et al. (1996), so that one could perform some sort of limited, local averaging to remove the spurious component while leaving some true, physical component behind; in fact, the results quoted for Siegmund et al. (1996) and the results reported in this study already contain a limited amount of spatial averaging using the advection method. The difficulty with such averaging is that there may be true, physical transport mechanisms with comparably short spatial and temporal scales which would also be averaged out in the process. Too little is known about the real mechanisms of stratosphere-troposphere exchange to judge how great this difficulty is, or what spatial or temporal averaging scales might be optimal.

Another way of dealing with input data errors in the diagnostic analysis is to separate large-amplitude structured CTF events (as in the snapshots described earlier), from small-amplitude events, which could be defined as "noise". A threshold value might be used to separate the small-amplitude events from large-amplitude ones. Such an analysis has been applied to the instantaneous CTF over the entire globe, and the results integrated over a month to obtain the net and gross mass fluxes including only

instantaneous fluxes larger than a given threshold in the integrating process. M_u and M_d are sensitive to the threshold value chosen. The two-way fluxes drop rapidly in absolute magnitude for higher threshold values, illustrated in Figure 8.11(a). As less of the instantaneous CTF is above the threshold, the magnitude of the net flux (M) initially increases, then begins to decrease (Figure 8.11(b)). If we were to make the *ad hoc* assumption that the two way fluxes ought to be both small in absolute magnitude and independent of the threshold chosen, this analysis would then imply that the optimum threshold value is approximately 2 x 10^{-2} $kgm^{-2}s^{-1}$, since this value does not change the net flux, but reduces M_u and M_d substantially.

This definition of noise could, however, be missing real systematic transport that simply occurs at low amplitude. Separating 'major' events from 'minor' events using a threshold value of 2 x 10^{-2} $kgm^{-2}s^{-1}$ indicates that 2/3 of the upward and downward gross fluxes occur in minor events, and only 1/3 in major events. The minor events have a fairly constant magnitude over the period of a month, with a constant level of variability. However, since the minor events are fairly evenly distributed, the total net mass flux does not change proportionately. An appropriate choice of threshold value can thus significantly change M_u and M_d without changing the net mass flux. It is unclear whether the choice of threshold value can be given a physical basis, though the curves in Figure 8.11 do have the same shape and approximately the same relationship to the threshold value in Northern Hemisphere summer (July) as in the curves shown for Northern Hemisphere winter (January), except that the flux more rapidly approaches zero as the threshold value becomes high.

8.6 Conclusions

The diagnostic formulation developed previously by Wei (1987) and other authors has been applied to examine mass fluxes across various surfaces near the tropopause. The GEOS assimilated data set has also been shown to yield net stratosphere-troposphere

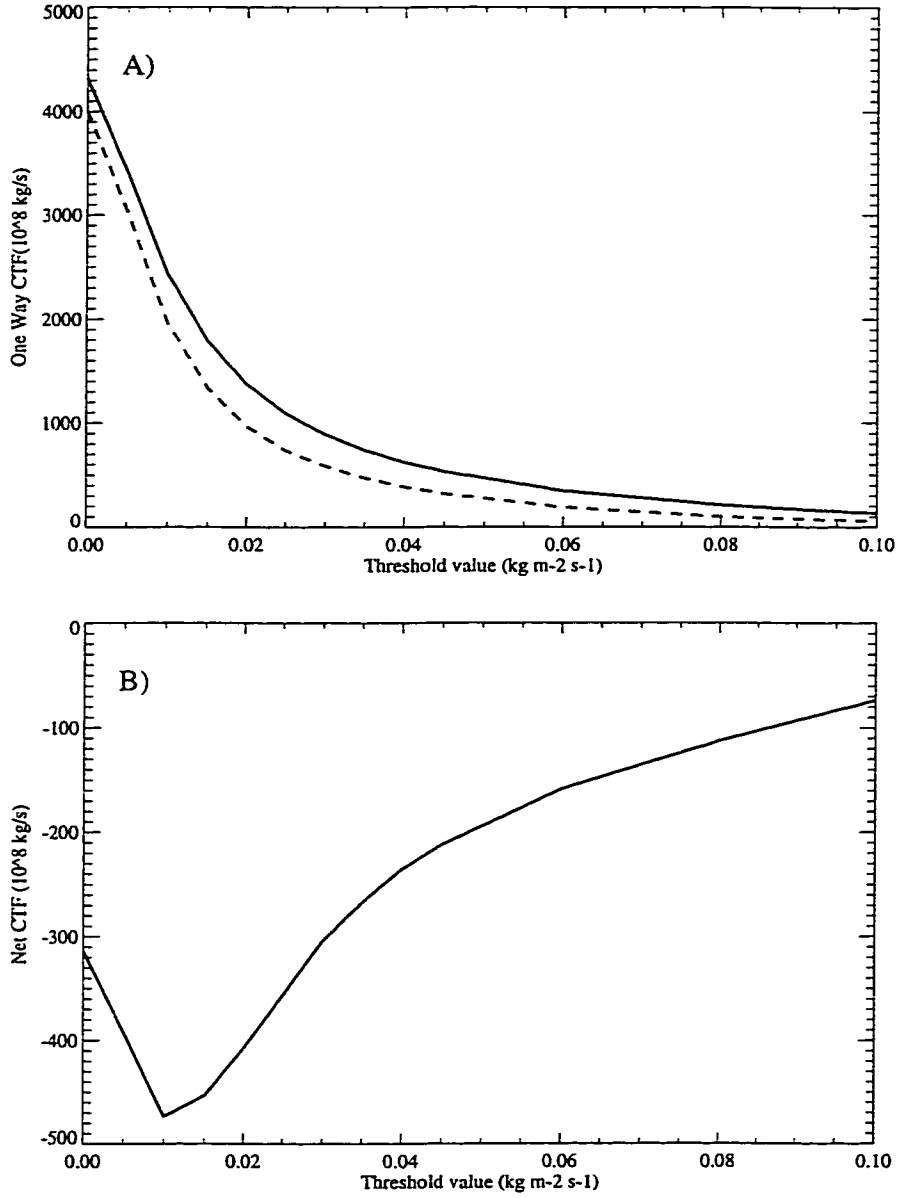

Figure 8.11: The effect of changing threshold value on A) The gross upward (M_u dashed) and downward (M_d solid) CTF and B) The net average CTF for the northern hemisphere extratropics (28°N–90°N). CTF units of $10^8\ kgs^{-1}$. Horizontal axis illustrates the threshold value in absolute magnitude below which events are treated as "noise". CTF from January 1996.

exchange estimates comparable to those obtained by Appenzeller et al. (1996) with UKMO data, using essentially the same hemispheric mass budget method used by those authors. The instantaneous results of the Wei method implemented with the GEOS data imply that the flux of mass across a tropopause surface (CTF) is an episodic process. The largest values of CTF are found in winter in midlatitudes, associated with synoptic-scale midlatitude cyclones and related processes. The diagnostic also indicates CTF associated with synoptic and mesoscale activity in the summer season at mid latitudes. Midlatitude CTF at the spatial and temporal resolution of this analysis appears to have a strong dipole structure of positive and negative exchange, especially when strong tropopause gradients are advected by the wind fields. This result is robust, and has been noted by previous authors (Lamarque and Hess, 1994) in more detailed studies of individual events. Varying the definition of the tropopause between an average height and a maximum height for a multiple valued tropopause did not significantly alter the integrated or instantaneous fluxes in this analysis, possibly because few examples of a vertically folded tropopause were found in this analysis due to the low resolution of the assimilation data set.

In the tropics, slow uplifting processes are evident in the diagnosed instantaneous CTF, which is of much lower magnitude than in the midlatitudes. Tropical instantaneous CTF does not exhibit significant large scale organization, and is nearly uniform throughout the tropics. Two possible conclusions might be inferred from this result. If the diagnostic is correct in diagnosing the magnitude of CTF in the tropics, then the method indicates that tropical CTF is dominated by slow and relatively steady diabatic motion such as that described by Wirth (1996), and the organization of convection in the tropics does not locally contribute to the flux of air across the tropopause. Alternatively, it may be concluded that perturbations associated with convection may not be diagnosed correctly at the resolution of 100's of kilometers.

The quantitative results presented here for Northern Hemisphere extratropical wintertime CTF averaged over a month agree with previous estimates using this

method, but are generally larger than comparable estimates using other methods (Figure 8.9). Some studies (Siegmund et al., 1996) reported lower quantitative estimates of the net extratropical wintertime CTF with increasing resolution, though other studies (Hoerling et al., 1993) have found no change in magnitude of the net CTF with resolution. The annual cycle of net extratropical downward fluxes predicted by the diagnostic does appear to match other estimates of stratosphere-troposphere exchange qualitatively, with a maximum in northern hemisphere winter. The average magnitude of the net CTF is larger in the northern than southern hemisphere extratropics. The annual cycle amplitude is also stronger in the northern than southern hemisphere extratropics. There is significant short term variability of the net extratropical flux which appears on top of the annual cycle, and significant year to year variability. While the annual cycle appears qualitatively reasonable, the magnitude of the CTF appears consistently large over the course of a year. Globally and annually integrated mass budgets have large errors, on the order of 30-40% of the mass of the stratosphere, which are probably due to persistent biases in the input data. Because global, annual integrals of pressure vertical velocity on pressure surfaces show much lower residuals, it appears that the errors in this heavily integrated budget are in large part due to persistent biases in the potential vorticity and/or horizontal wind fields (vertical velocity errors must surely contribute to gross fluxes, however, and hence to M_u and M_d). It should be emphasized that the Wei method is particularly sensitive to such input data errors, as also shown by Wirth and Egger (1999), so that the errors need not be "large" by other standards in order for the problems discussed here to become significant. This conclusion is supported by the quite different, and presumably more nearly correct, result obtained for the net CTF calculated using a budget method (which *assumes* a balanced mass budget) in Section 8.4.1, compared to that obtained from the Wei method.

The net CTF, even for individual synoptic events, is a residual of large upward and downward fluxes. We have argued that these are probably exaggerated by the

effect of errors in the input data, even if those errors are not large, and hence that the time integrated gross upward and downward fluxes (M_u and M_d) computed when no threshold is used are probably unrealistically large in magnitude, implying similarly exaggerated tracer fluxes. This exaggeration is reduced by applying a threshold, but there is no physical basis (at least at present) for choosing the threshold value. Hence it may be more desirable to estimate tracer fluxes by other means. For long lived constituents which behave as conserved tracers in the region of the tropopause, and which have large gradients across it (such as ozone), mass budget analyses (setting $M_u = 0$ at some surface well above the tropopause) are sufficient to determine the stratosphere-troposphere tracer flux, as shown by Tie and Hess (1997) and in Chapter 3 (Gettelman et al., 1997). However, for shorter lived species, such as nitrogen oxides, such calculations require that chemistry and two-way transport be considered explicitly. Therefore in addition to the net mass flux M, even under strong simplifying assumptions, another piece of information is required, such as M_u. In principle, the Wei method might provide useful information about these species, by enabling us to compute M_u and M_d, but its high sensitivity to relatively small errors in the input data mitigates the usefulness of this approach.

In short, the Wei method may be a useful tool for studying some aspects of stratosphere-troposphere exchange, but it should not be used as a black box. In the absence of a better mechanistic understanding of nonconservative processes occurring around the tropopause than we currently have, quantitative information obtained from this method as applied to current assimilated data sets should be interpreted with caution. Our analysis by itself suggests that the method should provide somewhat more reliable quantitative results when applied to pure model simulations, as in Lamarque and Hess (1994) and Spaete et al. (1994), though even in that case, Wirth and Egger (1999) find difficulties similar to those discussed here. Additionally, even if the noise problem is absent or ignored, it is still not entirely clear how much of the CTF represents true irreversible stratosphere-troposphere exchange and how much

may represent short-term excursions of air parcels across the tropopause and back with little attendant mixing, but this could perhaps be studied by other methods in conjunction with the Wei method. For purposes of diagnosing the cross-tropopause fluxes of long-lived trace constituents on a global or hemispheric basis, other methods are probably more trustworthy at present.

Chapter 9

SUMMARY AND CONCLUSIONS

The unifying theme of this dissertation has been stratosphere-troposphere exchange (STE). The analysis in preceding chapters presents a consistent picture of STE on scales from the global annual average to individual synoptic systems. The motivation and focus of this work has been to understand how anthropogenic perturbations to the upper troposphere and lower stratosphere are transmitted across the tropopause. These key issues are related to the exchange and transport of trace species in the atmosphere. Here the focus has been on subsonic aircraft emissions, ozone and water vapor. This work has been largely drawn from data available from instruments on the Upper Atmosphere Research Satellite (UARS) and the data assimilation products of the GEOS data assimilation system. The analysis has also drawn on modeling tools from the Atmospheric Chemistry and Dynamics Branch of the NASA Goddard Space Flight Center (GSFC). These tools have been evaluated as (see Chapter 4), and the limitations of the tools and approaches discussed as they are used.

This chapter summarizes the various conclusions of the different components of this work in an attempt at a synthesis with regard to STE and the effects of aircraft emissions. Future directions and foci for research are considered based on these conclusions.

9.1 Stratosphere-Troposphere Exchange

9.1.1 General picture

The mass flux of air and ozone from the stratosphere to the troposphere has been deduced in Chapter 3 from the large scale stratospheric circulation. Two alternate sets of estimates for the air mass flux between the stratosphere and troposphere have also been derived in Chapter 8. Both estimates in Chapter 8 use information about tropopause variability to develop STE estimates based on either budgets or a detailed diagnostic. Figure 8.9 illustrates estimates from a variety of sources. Note that the estimates in Gettelman et al. (1997) are from Chapter 3, while those marked '99' are from Chapter 8 (Gettelman and Sobel, 1999).

For long lived species the net mass flux across pressure surfaces in the stratosphere is sufficient to constrain their flux between the stratosphere and the troposphere, which is reported as 510 Tg/yr of Ozone and 0.08 Tg/yr of CF_2Cl_2. The estimate for CF_2Cl_2 corresponds to a stratospheric lifetime of 1.2×10^2 years. These STE estimates take advantage of unique aspects of these two long lived species (a negligible tropical flux into the stratosphere for ozone and the lack of a tropospheric sink for CF_2Cl_2) to constrain the flux estimates.

For shorter lived species, perhaps a better method for estimating the averaged and integrated STE on scales of a month or more is the budget approach of Appenzeller et al. (1996), which is applied to GEOS data in Chapter 8, and yields results complementary to the earlier study of Appenzeller et al. (1996). The net hemispheric exchange is well constrained by mass budget estimates.

Between about 300 hPa and 100 hPa, STE is more complicated because isentropic surfaces span the tropopause (as outlined in Chapter 2). The simulations of water vapor in Chapter 7 confirm the isolation of the extratropical lowermost stratosphere from the troposphere below with a significant drop in water vapor concentrations across the tropopause. Aircraft emissions in Chapter 6 also maintain a steep gradient

across the tropopause. Water vapor concentrations in the extratropical lowermost stratosphere just a few kilometers above the tropopause are representative of the upper tropical troposphere. Transport analyzed in Chapter 7 confirms significant exchange from the upper tropical troposphere to the middleworld. Quasi-isentropic exchange between the tropical troposphere and the middleworld is also noted in ensembles of trajectories in Chapter 4 and in analysis of the transport of aircraft emissions in Chapter 6.

Water vapor simulations in Chapter 7 highlight the importance of large scale tropical tropospheric processes and their relationship to STE. Transport with a parameterized tracer confirms the results of Salathé and Hartmann (1997) and Pierrehumbert and Roca (1998) that large scale advection dominates the water vapor distribution in the upper tropical troposphere, at least below 200 hPa. However, the analysis in Chapter 7 indicates that in the tropics, between 200 hPa and 100 hPa, simulations are less effective at reproducing the distribution of water vapor. This difference is hypothesized to indicate significant influences from local convective and wave driven processes not simulated in the modeled distribution of a water vapor tracer. Chapter 7 also indicates that in the region around 150 hPa and above, there are significant influences from the wave driven circulation in the stratosphere (Holton et al., 1995; Rosenlof, 1995), which pulls air upward rather than pushes it from below. These results are consistent with the correlation of upper tropical tropospheric temperatures above 125 hPa with stratospheric temperatures observed by Reid and Gage (1996).

The large scale transport of the water vapor tracer and the mass flux estimates in Chapter 7 suggest that no tropical 'fountain' in the western Pacific during February is necessary to explain low water vapor concentrations in the stratosphere. This conclusion confirms the hypothesis of Dessler (1998) that water vapor irreversibly enters the stratosphere at all longitudes.

9.1.2 Details of STE

As noted in Chapters 2 and 8 the detailed picture of STE at the tropopause is complex. While in theory the tropopause is a quasi-elastic transport barrier (Hoskins, 1991; Ambaum, 1997) in practice it is a region of large gradients in winds, temperatures and tracers. Diagnosing the instantaneous time and space details of STE in four dimensions is difficult. As noted in Chapters 7 and 8, downward control theory (Haynes et al., 1991; Holton et al., 1995) is no longer sufficient to constrain the gross property fluxes of short lived atmospheric constituents at the tropopause, especially in the extratropics. For many applications (as in Chapter 3), it is sufficient to use the net mass flux.

The absolute magnitude of the net mass flux across the tropopause is fairly well constrained by the diabatic limits of the residual circulation as described in Chapter 3. However, as Figure 8.9 makes clear, there are a wide range of estimates of the net mass flux (using the most common metric of the flux across the NH extratropics in winter). These estimates depend on the method used as well as the altitude chosen. The diagnostic method of Wei (1987) implies much higher net fluxes than other methods at similar altitudes.

These net fluxes are shown to be the residual of even larger gross fluxes, as detailed in Chapter 8. In Chapter 8 these gross fluxes are shown to be vastly different in different studies, even if the integrated net fluxes converge. The net flux (predicted by downward control theory) is not a constraint on the gross flux. Gross fluxes are uncertain because the amount of the cross tropopause flux which is 'reversible' is uncertain. In Chapter 8, the method introduced by Wei (1987) is critiqued and shown to have significant noise which can be interpreted as an abnormally large gross or reversible flux. The result does not however indicate physically based constraints on gross cross-tropopause fluxes. For example, it is an open question whether the gross exchange across the tropopause in frontal systems or convective overshooting is

really a large multiple of the net exchange as predicted by the Wei method.

These gross exchanges of mass across the tropopause surface are a strong function of the non-conservative terms in the potential vorticity conservation equation. In practice the only way to determine the non-conservative terms that cause the gross (partly reversible) fluxes contain coarse averaging, and the difference of two large numbers (as discussed in Chapter 8). Lagrangian trajectory models, such as the trajectory calculations described in Chapter 4, are perhaps a more robust tool at present for analyzing transport on isentropic surfaces. Trajectory models are easier to develop in isentropic coordinates, but perhaps harder to interpret in terms of a mass flux. Statistical ensembles of parcels, as used by Chen (1995) and in Chapter 4 for example, may be useful for investigating the gross or even reversible exchange across the tropopause in isentropic layers. Wirth and Egger (1999) have also recently applied a Lagrangian trajectory method to estimate the mass flux across the tropopause.

9.1.3 Next steps

Some of the most interesting and profound questions in describing the atmosphere are related to the structure and evolution of the tropopause. We still do not know some of the fundamental characteristics of tropopause variability. The interannual variability of the tropopause is unknown (W. J. Randel 1998, personal communication). The proportion of STE (net and gross) which occurs in extreme cyclonic events such as tropopause folds (Ebel et al., 1996) is uncertain. Recent studies using GCM's (Ambaum, 1997; Thuburn and Craig, 1997, 1999) and theoretical models (Haynes and Scinocca, 1997) have begun to examine the variability of the tropopause and the processes that maintain it. Recent work on individual events with models explicitly examining the non-conservative terms (Spaete et al., 1994; Lamarque and Hess, 1994; Stoelinga, 1996; Wirth and Egger, 1999) have begun to yield insights into these processes. Lagrangian studies such as trajectory experiments by Chen (1995), Eluszkiewicz (1996), Sparling et al. (1997) and Pierrehumbert (1998) are also able to

analyze detailed processes, but are hard to do as global budgets. For the foreseeable future, until understanding of tropopause processes deepens, the appropriate method for assessing STE will depend on the situation and scale examined.

With particular regard to the stratosphere-troposphere exchange of water vapor, it may be possible to apply equation 8.4 to the water vapor distribution and constrain the magnitude of the gross cross tropopause fluxes. One idea is to extend equation 8.4 using a mixing length argument (A. H. Sobel, 1999, personal communication), though applying realistic distributions to a simple equation may not be possible and is highly dependent on gradients. Another approach would be to solve equation 8.4 for multiple tracers simultaneously. Ozone, whose net flux is known (see Chapter 3, table 3.3), and water vapor, whose budget is derived in section 7.4.2 (and whose flux can be inferred from these estimates), are good tracers to use for such calculations.

The details of the temperature and trace species distribution in the tropics and its variability in space and time are more important for understanding the water vapor distribution and the processes that control it. A crude model parameterization as in Chapter 7 can only reveal the large scale picture. Current temperature records from radiosondes (Newell and Gould-Stewart, 1981; Dessler, 1998) still have uncertainties, and limited sampling. In situ aircraft measurements also have limited sampling ranges, while satellites have broad sampling ranges but limited resolution, particularly in the vertical. More observations of diverse trace species, available soon, may provide additional information, such as upper tropospheric CO measurements from MOPPIT (Wang et al., 1999) and planned or proposed tropical aircraft missions. These new observations though will suffer from many of the same resolution and sampling problems that affect current data sets.

9.2 Aircraft Emissions

While fundamental work on STE will continue, the current state of knowledge permits significant constraints to be placed on the effects that current and future commercial aircraft have on the global atmosphere. This analysis has explicitly excluded the local air quality and sound impacts from commercial aircraft. As noted in Chapters 5 and 6 the basic concerns over commercial aircraft emissions relate to (1) the emission of water vapor and aerosols (sulfur and soot), as well as (2) nitrogen oxides (NO_x). Aircraft water vapor and aerosols form contrails and may modify cirrus cloud formation, which affects the radiation balance at cruise altitudes. Sulfur and soot aerosols may increase the stratospheric aerosol loading and change the heterogeneous chemistry in the lowermost stratosphere. NO_x may increase ozone in the upper troposphere and decrease ozone in the stratosphere.

9.2.1 Basic Picture

The deposition of aircraft emissions in the atmosphere and the subsequent transport of emissions set the bounds for the possible effects the emissions may have. The basic distribution of aircraft emissions in the atmosphere is described in Chapter 5. Between 18% and 44% of emissions are deposited into the stratosphere from the present fleet. The fraction of emissions in the stratosphere is most sensitive to the height of the analyzed tropopause, and almost 40% of the total fuel burned by aircraft is emitted within 2 km of the tropopause. This result is fairly robust with regard to the meteorological or aircraft inventory dataset used. These estimates use ideal, not actual flight routings, so there are probably some discrepancies with actual deposition. Regional analyses of the fuel deposited in the stratosphere are misleading and perhaps not useful, since material is rapidly distributed zonally in the stratosphere. Zonal asymmetries may be important in the upper troposphere however because of shorter residence times and greater zonal asymmetries. In the near term (to 2015) a similar

fraction of emissions is expected to be deposited into the stratosphere, but a larger magnitude of emissions. Almost all of these emissions are deposited into the lowermost stratosphere, and a majority of these are in the northern hemisphere.

Water vapor emissions which form contrails are mostly an issue in the upper troposphere where the environmental conditions permit contrail formation. A preliminary analysis indicates the potential for formation of instantaneous (short lived) contrails for 21% of total annual aircraft emissions.

9.2.2 Transport of Emissions

In order to get a clear picture of the total effect of emissions, the residence time of emissions in the stratosphere has been determined using a transport model. The estimated residence time of emissions from the current aircraft fleet in the stratosphere is approximately 50 days, slightly longer in July than in January. About 10% of aircraft emissions are estimated to get into the stratospheric overworld, depending on how the removal of emissions is handled in simulations. As detailed in Chapter 7, subsequent analysis of model transport in the stratosphere indicates that vertical transport is too rapid in the stratosphere. Thus the fraction of emissions in the overworld is likely less than 10%. Transport pathways for the emissions agree with the stratosphere-troposphere exchange ideas developed in Section 9.1. Quasi-isentropic exchange of emissions between the stratosphere and the troposphere is found to be an important mechanism for the exchange of mass of aircraft emissions deposited into the lowermost stratosphere.

Based on this information and continuous transport simulations, the total burden or concentration of species can be determined. Loading of NO_x is not significant in the overworld for affecting the stratospheric ozone layer. But these emissions will significantly perturb (by 50%–100%) the NO_x concentration of the extratropical lowermost stratosphere, and to a lesser extent the upper troposphere (because the upper troposphere is also affected by surface sources and lightning sources of NO_x). From

the analysis in Chapters 5 and 6 it appears that little significant subsonic aircraft emissions are lofted into the stratosphere at altitudes where they will significantly affect stratospheric ozone. The conclusion is consistent with detailed chemical modeling studies (Stolarski et al., 1995). NO_x emissions will have an effect in the upper troposphere and lowermost stratosphere, increasing ozone concentrations by the order of a few percent in this region (Stolarski et al., 1995). Based on comparisons with other studies, it is likely that the NO_x concentrations predicted in Chapter 6 are high, since there are chemical losses of NO_x as well in this region which are not simulated.

Sulfur emissions from aircraft may be a significant fraction of the stratospheric source from carbonyl sulfide (as also hypothesized by Hofmann (1991)) in the quiescent (non-volcanic influenced) atmosphere. The natural soot background is still uncertain. It is likely that aircraft generated soot (black carbon) is a substantial fraction of stratospheric loadings. While Rahmes et al. (1998) have shown that no significant radiative forcing of climate will result from such loadings, Bekki (1997) has noted that there may be important chemical effects to aircraft soot.

9.2.3 Future Projections and Analysis

All of the above conclusions regarding the effects of aircraft on atmospheric chemistry appear to scale with fleet growth projections to 2015. The development of emission inventories for 2015 assumes a similar mix of aircraft engines and flight patterns, with continued growth of the number of aircraft flying. Growth is projected by both ANCAT and NASA inventories at high latitudes of the Northern Hemisphere, but over Asia rather than North America or Europe. Because the aircraft mix is projected to be similar, and the projected traffic growth occurs at the same latitudes as present emissions, the fraction of emissions deposited in the stratosphere is likely to be similar in 2015 to the present (20–40% of emissions). The mass of emissions deposited in the atmosphere is expected to roughly double. Inventory analyses to 2050 and beyond are also under development (Henderson and Wickrama, 1999; Sausen et al., 1997),

but these scenarios begin to involve a high level of uncertainty. Most of these long range scenarios to 2050 and beyond correlate air traffic growth with per capita Gross National Product (GNP), and relate this to the historical relationship in the United States and Europe over the jet age (the past 35 years or so). See Henderson and Wickrama (1999) for a complete description. For this analysis, only the results to 2015 have been considered.

9.2.4 The Bottom Line

The effects of aircraft emissions on the atmosphere are not significant enough at this time to warrant corrective or preventative action, but may become significant in the future, because total emissions and stratospheric emissions are expected to double by 2015. Aircraft are expected to increase ozone in the upper troposphere and lower stratosphere by a few percent. But, subsonic aircraft fly too low to deplete ozone in the stratosphere, and the emissions are not significantly transported to high altitudes. Contrails are mostly a tropospheric issue beyond the scope of this study, but 20% of emissions may form immediate contrails, and their local effects may be significant, especially if they do not immediately evaporate. The effects of aircraft on heterogeneous chemistry in the extratropical lowermost stratosphere are still uncertain, but the magnitude of emissions deposited at the low temperature conditions necessary for these reactions is small.

BIBLIOGRAPHY

Allen, D. J., R. B. Rood, A. M. Thompson and R. D. Hudson, 1996: Three-dimensional Radon 222 calculations using assimilated meteorological data and a convective mixing algorithm. *Journal of Geophysical Research*, **101**(D3), 6871–6881.

Ambaum, M., 1997: Isentropic formation of the tropopause. *Journal of the Atmospheric Sciences*, **54**, 555–568.

Andrews, D., J. Holton and C. Leovy, 1987: *Middle Atmosphere Dynamics.* Academic Press, New York.

Andrews, D. G. and M. E. McIntyre, 1976: lanetary waves in horizontal and vertical shear: the generalized eliassen-palm relation and the mean zonal acceleration. *Journal of the Atmospheric Sciences*, **33**, 2031–2048.

Appenzeller, C., J. R. Holton and K. H. Rosenlof, 1996: Seasonal variation of mass transport across the tropopause. *Journal of Geophysical Research*, **101**(D10), 15,071–15,078.

Appleman, H. S., 1953: The formation of exhaust condensation trails by jet aircraft. *Bulletin of the American Meteorological Society*, **34**, 14–20.

Bailey, P. L. et al., 1996: Comparison of cyrogenic limb array etalon spectrometer (CLAES) ozone observations with correlative measurements. *Journal of Geophysical Research*, **101**(D6), 9737–9756.

Baughcum, S. L., 1996: *Aircraft Emissions Deposited in the Stratosphere and Within the Arctic Polar Vortex.* NASA Contractor Report 4714, Washington, D.C.

Baughcum, S. L., S. C. Henderson, D. R. Hertel, P. S. Maggiora and C. A. Oncina, 1994: *Stratospheric Emissions Effects Database Development.* NASA Contractor Report 4592, Washington, D.C.

Baughcum, S. L., S. C. Henderson and D. J. Sutkus, 1998: *Scheduled Civil Aircraft Emission Inventories Projected for 2015: Database Development and Analysis.* NASA Contractor Report 1998-207638, Washington, D.C.

Baughcum, S. L., T. G. Tritz, S. C. Henderson and D. C. Pickett, 1996: *Scheduled Civil Aircraft Emission Inventories for 1992: Database Development and Analysis.* NASA Contractor Report 4700, Washington, D.C.

Bekki, S., 1997: On the possible role of aircraft-generated soot in the middle latitude ozone depletion. *Journal of Geophysical Research*, **102**(D9), 10,751–10,758.

Bethan, S., G. Vaughan and S. J. Reid, 1996: A comparison of ozone and thermal tropopause heights and the impact of tropopause definition on quantifying the ozone content of the troposphere. *Quarterly Journal of the Royal Meteorological Society*, **122**, 929–944.

Bithell, M., L. J. Gray and B. D. Cox, 1999: A three-dimensional view of the evolution of midlatitude stratospheric intrusions. *Journal of the Atmospheric Sciences*, **56**(5), 673–688.

Bjerknes, J., 1969: Atmospheric teleconnections from the equatorial pacific. *Monthly Weather Review*, **97**(3), 163–172.

Blake, D. F. and K. Kato, 1995: Latitudinal distribution of black carbon soot in the upper troposphere and lower stratosphere. *Journal of Geophysical Research*, **100**(D4), 7195–7202.

Bloomfield, P., 1994: Inferred lifetimes. in J. Kaye, S. Penkett and F. Osmond, editors, *NASA Report on Concentrations, Lifetimes and Trends of CFCs, Halons and Related Species*. NASA, Washington, D.C.

Boering, K. A. et al., 1995: Measurements of stratospheric carbon dioxide and water vapor at northern midlatitudes: Implications for troposphere-to-stratosphere transport. *Geophysical Research Letters*, **22**(20), 2737–2740.

Boucher, O., 1999: Air traffic may increase cirrus cloudiness. *Nature*, **397**, 30–31.

Brasseur, G. P., R. A. Cox, D. Hauglustaine, I. Isaksen, J. Lelieveld, D. H. Lister, R. Sausen, U. Schumann, A. Wahner and P. Wiesen, 1998: European scientific assessment of the atmospheric effects of aircraft emissions. *Atmospheric Environment*, **32**, 2329–2418.

Brasseur, G. P., J.-F. Muller and C. Granier, 1996: Atmospheric impact of NOx emissions by sub-sonic aircraft: A three-dimensional model study. *Journal of Geophysical Research*, **101**(D1), 1423–1428.

Brasseur, G. P. and S. Solomon, 1986: *Aeronomy of the Middle Atmosphere, Second Edition*. D. Reidel, Boston, 2nd edition.

Brewer, A. W., 1949: Evidence for a world circulation provided by the measurements of helium and water vapor distribution in the stratosphere. *Quarterly Journal of the Royal Meteorological Society*, **75**, 351–363.

Brühl, C. et al., 1996: Halogen occultation experiment ozone channel validation. *Journal of Geophysical Research*, **101**(D6), 10,217–10,240.

Busen, R. and U. Schumann, 1995: Visible contrail formation from fuels with different sulfur contents. *Geophysical Research Letters*, **22**(11), 1357–1360.

Cerniglia, M. C., A. R. Douglass, R. B. Rood, L. C. Sparling and J. E.Nielsen, 1999: Seasonal variability of middle latitude ozone in the lowermost stratosphere derived from probability distribution functions. *to be submitted to Journal of Geophysical Research.*

Chen, M., R. B. Rood and W. G. Read, 1998: Upper tropospheric water vapor from GEOS reanalysis and UARS MLS observation. *Journal of Geophysical Research*, **103**(D16), 19,587–19,594.

Chen, P., 1995: Isentropic cross-tropopause mass exchange in the extratropics. *Journal of Geophysical Research*, **100**(D8), 16,661–16,673.

Chin, M. and D. D. Davis, 1995: A reanalysis of carbonyl sulfide as a source of stratospheric background sulfur aerosol. *Journal of Geophysical Research*, **100**(D5), 8993–9005.

Clark, H. L., R. S. Harwood, P. W. Mote and W. G. Read, 1998: Variability of water vapor in the tropical upper troposphere as measured by the Microwave Limb Sounder on UARS. *Journal of Geophysical Research*, **103**(D24), 31,695–31,707.

Coleman, R. F., 1996: A new formulation for the critical temperature for contrail formation. *Journal of Applied Meteorology*, **35**, 2270–2282.

Coy, L., R. B. Rood and P. A. Newman, 1994: A comparison of winds from the STRATAN data assimilation system to balanced wind estimates. *Journal of the Atmospheric Sciences*, **51**, 2309–2315.

Coy, L. and R. Swinbank, 1997: The characteristics of stratospheric winds and temperatures produced by data assimilation. *Journal of Geophysical Research*, **102**, 25,763–25,781.

Crum, F. X., 1996: A guide to the Goddard three-dimensional chemistry and transport model: Second revision. Working Paper.

Crutzen, P. J., 1983: Chemical budgets of the stratosphere. *Planetary and Space Science*, **31**(9), 1009–1032.

Crutzen, P. J., 1991: Methane's sinks and sources. *Nature*, **350**, 380–1.

Danielsen, E. F., 1968: Stratospheric-tropospheric exchange based on radioactivity, ozone and potential vorticity. *Journal of the Atmospheric Sciences*, **25**, 502–518.

Danielsen, E. F., 1993: In situ evidence of rapid, vertical, irreversible transport of lower tropospheric air into the lower tropical stratosphere by convective cloud turrets and by larger-scale upwelling in tropical cyclones. *Journal of Geophysical Research*, **98**(D5), 8665–8691.

Danielsen, E. F. and V. A. Mohnen, 1977: Project duststorm report: ozone transport, in situ measurements and meteorological analyses of tropopause folding. *Journal of Geophysical Research*, **82**, 5867–5877.

Danilin, M. Y. et al., 1998: Aviation fuel tracer simulation: Model intercomparison and implications. *Geophysical Research Letters*, **25**(21), 3947–3950.

Dessler, A. E., 1998: A reexamination of the "stratospheric fountain" hypothesis. *Geophysical Research Letters*, **25**(22), 4165–4168.

Dessler, A. E., E. J. Hintsa, E. M. Weinstock, J. G. Anderson and K. R. Chan, 1995: Mechanisms controling water vapor in the lower stratosphere: "a tale of two stratospheres". *Journal of Geophysical Research*, **100**(D11), 23,167–23,172.

Devore, J. L., 1987: *Probability and statistics for engineering and the sciences.* Brooks/Cole, Monterey, CA.

Dobson, G. M. B., 1956: Origin and distribution of the polyatomic molecules in the atmosphere. *Proceedings of the Royal Society of London, Series A*, **236**, 187–193.

Dobson, G. M. B., D. N. Harrison and J. Lawrence, 1929: Measurements of the amount of ozone in the earth's atmosphere and its relation to other geophysical conditions part III. *Proceedings of the Royal Society of London, Series A*, **122**, 456–486.

Douglass, A. R., C. J. Weaver, R. B. Rood and L. Coy, 1996: A three-dimensional simulation of the ozone annual cycle using winds from a data assimilation system. *Journal of Geophysical Research*, **101**(D1), 1463–1474.

Dunkerton, T., 1978: On the mean meridional mass motions of the stratosphere and mesosphere. *Journal of the Atmospheric Sciences*, **35**, 2324–2333.

Ebel, A., H. Elbern, J. Hendricks and R. Meyer, 1996: Stratosphere-troposphere exchange and its impact on the structre of the lower stratosphere. *Journal of Geomagnitism and Geoelectricity*, **48**, 135–144.

Elkins, J., 1993: Decrease in the growth rates of atmospheric chloroflourocarbons 11 and 12. *Nature*, **364**(26 August 1993), 780–783.

Eluszkiewicz, J., 1996: A three-dimensional view of the stratosphere-to-troposphere exchange in the GFDL SKYHI model. *Geophysical Research Letters*, **23**(18), 2489–2492.

Eluszkiewicz, J. et al., 1996: Residual circulation in the stratosphere and lower mesosphere as diagnosed from Microwave Limb Sounder data. *Journal of the Atmospheric Sciences*, **53**(2), 217–240.

Fabian, P. and B. Kärcher, 1997: The impact of aviation upon the atmosphere. *Physics and Chemistry of the Earth*, **22**, 503–598.

Fahey, D. W. and U. Schumann, 1999: Aviation produced aerosols and cloudiness. in J. T. Houghton and D. Yihui, editors, *IPCC Special Report on Aviation and the Global Atmosphere*, Chap. 3. Cambridge Universtiy Press.

Follows, M. J., 1992: On the cross-tropopause exchange of air. *Journal of the Atmospheric Sciences*, **49**(10), 879–882.

Friedl, R. R., Ed., 1997: *Atmospheric Effects of Subsonic Aircraft: Interim Assessment Report of the Advanced Subsonic Technology Program.* NASA Reference Publication 1400, Washington, D.C.

Froidevaux, L. et al., 1996: Validation of UARS microwave limb sounder ozone measurements. *Journal of Geophysical Research*, **101**(D6), 10,017–10,060.

Fujiwara, M., K. Kita and T. Ogawa, 1998: Stratosphere-troposphere exchange of ozone associated with the equatorial kelvin wave as observed with ozonesondes and rawinsondes. *Journal of Geophysical Research*, **103**(D15), 19,173–19,182.

Fung, I., 1991: Three-dimensional model synthesis of the global methane cycle. *Journal of Geophysical Research*, **96**(D7), 13,033–13,065.

Gaffen, D. J., 1999: Radiosonde observations and their use in SPARC-related investigations. *SPARC Newsletter*, (12), 17–21.

Gardner, R. M., Ed., 1998: *ANCAT/EC2 Aircraft emissions inventories for 1991/1992 and 2015: Final Report.* European Civil Aviation Conference, European Commission, Brussles, Belgium.

Gardner, R. M., K. Adams, T. Cook, F. Deidewig, S. Ernedal, R. Falk, E. Fleuti, E. Herms, C. E. Johnson, M. Lecht, D. S. Lee, M. Leech, D. Lister, B. Masse, M. Metcalfe, P. Newton, A. Schmitt, C. Vandenbergh and R. Van Drimmelen, 1997: The ANCAT/EC global inventory of NO_x emissions from aircraft. *Atmospheric Environment*, **31**, 1751–1766.

Gettelman, A., 1998: The evolution of aircraft emissions in the stratosphere. *Geophysical Research Letters*, **25**, 2129–2132.

Gettelman, A. and S. L. Baughcum, 1999: Distribution of subsonic emissions in the stratosphere. *Journal of Geophysical Research, in press.*

Gettelman, A., J. R. Holton and K. H. Rosenlof, 1997: Mass fluxes of O_3, CH_4, N_2O and CF_2Cl_2 in the lower stratosphere calculated from observational data. *Journal of Geophysical Research*, **102**(D15), 19,149–19,159.

Gettelman, A. and A. H. Sobel, 1999: Direct diagnoses of stratosphere-troposphere exchange. *Journal of the Atmospheric Sciences, in press.*

Gill, A. E., 1982: *Atmosphere-Ocean Dynamics.* Academic Press, San Diego, CA.

Grewe, V. and M. Dameris, 1996: Calculating the global mass exhcange between the stratosphere and troposphere. *Annales Geophysicae*, **14**, 431–442.

Haynes, P. and J. Scinocca, 1997: Formation of the mid-latitude tropopause through the action of baroclinic eddies. AMS Middle Atmosphere Conference- Tacoma, WA.

Haynes, P. H., C. J. Marks, M. E. McIntyre, T. G. Shepherd and K. P. Shine, 1991: On the "downward control" of extratropical diabatic circulations by eddy-induced mean zonal forces. *Journal of the Atmospheric Sciences*, **48**, 651–679.

Henderson, S. C. and U. K. Wickrama, 1999: Aircraft emissions: Current inventories and future scenarios. in J. T. Houghton and D. Yihui, editors, *IPCC Special Report on Aviation and the Global Atmosphere*, Chap. 9. Cambridge Universtiy Press.

Highwood, E. J. and B. J. Hoskins, 1998: The tropical tropopause. *Quarterly Journal of the Royal Meteorological Society*, **124**(549), 1579–1604.

Hintsa, E. J. et al., 1998: Troposphere to stratosphere transport in the lowermost stratosphere from measurements of H_2O, CO_2, N_2O and O_3. *Geophysical Research Letters*, **25**(14), 2655–8.

Hoerling, M. P., T. K. Schaack and A. J. Lenzen, 1991: Global objective tropopause analysis. *Monthly Weather Review*, **119**, 1816–1831.

Hoerling, M. P., T. K. Schaack and A. J. Lenzen, 1993: A global analysis of stratospheric-tropospheric exchange during northern winter. *Monthly Weather Review*, **121**, 162–172.

Hofmann, D. J., 1991: Aircraft sulphur emissions. *Nature*, **349**, 659.

Hofmann, D. J., R. S. Stone, M. E. Wood, T. Deshler and J. M. Harris, 1998: An analysis of 25 years of balloon-borne aerosol data in search of a signature of the subsonic commercial aircraft fleet. *Geophysical Research Letters*, **25**(13), 2433–2436.

Hoinka, K. P., M. E. Reinhart and W. Metz, 1993: North Atlantic air traffic within the lower stratosphere: Cruising times and corresponding emissions. *Journal of Geophysical Research*, **98**(D12), 23,113–23,131.

Holton, J. R., 1990: On the global exchange of mass between the stratosphere and troposphere. *Journal of the Atmospheric Sciences*, **47**(3), 392–5.

Holton, J. R., 1992: *An Introduction to Dynamic Meteorology.* Academic, San Diego, Calif., 3rd edition.

Holton, J. R., P. H. Haynes, A. R. Douglass, R. B. Rood and L. Pfister, 1995: Stratosphere–troposphere exchange. *Reviews of Geophysics*, **33**(4), 403–439.

Holton, J. R. and J. Lelieveld, 1995: Stratosphere-troposphere exchange and its role in the budget of tropospheric ozone. in *NATO Advanced Research Workshop on Stratosphere-Troposphere Exchange.* NATO, Brussels.

Hoskins, B. J., 1991: Towards a PV-θ view of the general circulation. *Tellus*, **43AB**, 27–35.

Inamdar, A. K. and V. Ramanathan, 1998: Tropical and global scale interactions among water vapor, atmospheric greenhouse effect, and surface temperature. *Journal of Geophysical Research*, **103**(D24), 32,177–32,194.

Jacob, D. J. et al., 1997: Evaluation and intercomparison of global atmospheric transport models using ^{222}Rn and other short lived tracers. *Journal of Geophysical Research*, **102**(D5), 5953+.

Jaffe, D. A., 1992: The nitrogen cycle. in S. S. Bucher et al., editors, *Global Biogeochemical Cycles*, pp. 263–284. Academic Press, San Diego, CA.

Kalnay, E., M. Kanamitsu, R. Kistler, W. Collins, D. Deaven, L. Gandin, M. Iredell, S. Saha, C. White, J. Woollen, Y. Zhu, M. Chelliah, W. Ebisuzaki, W. Higgins, J. Janowiak, K. C. Mo, C. Ropelewski, J. Wang, A. Leetmaa, R. Reynolds, P. Jenne and D. Joseph, 1996: The NCEP/NCAR 40-year reanalysis project. *Bulletin of the American Meteorological Society*, **77**(3), 437–471.

Kelly, K. K., M. H. Proffitt, K. R. Chan, M. Loewenstein, J. R. Podolske, S. E. Strahan, J. C. Wilson and D. Kley, 1993: Water vapor and cloud water measurements over Darwin during th STEP 1987 tropical mission. *Journal of Geophysical Research*, **98**(D5), 8713–8723.

Khalil, M. A. K. et al., 1993: Methane sinks and distribution. in *Atmospheric Methane: Sources, Sinks and Role in Global Change*, Vol. 13 of *NATO ASI Series I.* Springer Verlag, New York.

Ko, M. K. W., 1993: Transport fluxes. in M. J. Prather and E. E. Remsberg, editors, *The Atmospheric Effects of Stratospheric Aircraft: Report of the 1992 Models and Measurments Workshop*, pp. N1–N43. NASA.

Ko, M. K. W., N. K. Sze and D. K. Weisenstein, 1991: Use of satellite data to constrain the model-calculated atmospheric lifetime for N_2O: Implications for other trace gases. *Journal of Geophysical Research*, **96**(D4), 7547–7552.

Lamarque, J.-F. and P. G. Hess, 1994: Cross-tropopause mass exchange and potential vorticity budget in a simulated tropopause folding. *Journal of the Atmospheric Sciences*, **51**(15), 2246–2269.

Lelieveld, J. and P. J. Crutzen, 1994: Role of deep cloud convection in the ozone budget of the troposphere. *Science*, **264**, 1759–1761.

Lelieveld, L., F. Arnold, B. Bregman, V. Burger, P. J. Crutzen, H. Fischer, P. Siegmund, P. F. J. van Velthoven and A. Waibel, 1997: Chemical perturbation of the lowermost stratosphere through exchange with the tropopshere. *Geophysical Research Letters*, **24**(5), 603–606.

Lin, S. J. and R. B. Rood, 1996: Multidimensional flux-form semi-lagrangian transport schemes. *Monthly Weather Review*, **124**(9), 2046–2070.

Mahlman, J. D., 1985: Mechanistic interpretation of stratospheric tracer transport. in S. Manabe, editor, *Issues in Atmospheric and Oceanic Modeling.* Academic Press, San Diego, CA.

Marti, J. and K. Mauersberger, 1993: A survey of new measurements of ice vapor pressure at temperatures between 170 and 250K. *Geophysical Research Letters*, **20**(5), 363–6.

Metwally, M., 1995: *Jet aircraft engine emissions database development: 1992 Military, Charter and Nonscheduled Traffic.* NASA Contractor Report 4684, Washington, D.C.

Miake-Lye, R. C., M. Martinez-Sanchez, R. C. Brown and C. E. Kolb, 1993: Plume and wake dynamics, mixing, and chemistry behind a high speed civil transport. *Journal of Aircraft*, **30**(4), 467–479.

Minschwaner, K. et al., 1996: The bulk properties of isentropic mixing into the tropics in the lower stratosphere. *Journal of Geophysical Research*, **101**, 9433–9349.

Mortlock, A. and R. van Alstyne, 1998: *Military, Charter, Unreported Domestic Traffic and General Aviation, 1976, 1984, 1992, and 2015 Emissions Scenarios.* NASA Contractor Report 1998-207639, Washington, D.C.

Mote, P. W., 1995: The annual cycle of stratospheric water vapor in a general circulation model. *Journal of Geophysical Research*, **100**(D4), 7363–7379.

Mote, P. W. et al., 1996: An atmospheric tape recorder: The imprint of tropical tropopause temperatures on stratospheric water vapor. *Journal of Geophysical Research*, **101**(D2), 3989–4006.

Mote, P. W., J. R. Holton and B. A. Boville, 1994: Characteristics of stratosphere-troposphere exchange in a general circulation model. *Journal of Geophysical Research*, **99**(D8), 16,815–16,829.

Murphy, D. M., 1994: An estimate of the flux of stratospheric reactive nitrogen and ozone into the troposphere. *Journal of Geophysical Research*, **99**(D13), 5325–5332.

Murphy, D. M., D. W. Fahey, M. H. Proffitt, S. C. Liu, K. R. Chan, C. S. Eubank, S. R. Kawa and K. K. Kelly, 1993: Reactive nitrogen and its correlation with ozone in the lower stratosphere and upper troposphere. *Journal of Geophysical Research*, **98**(D5), 8751–8873.

National Oceanic and Atmospheric Administration, 1976: *U.S. Standard Atmosphere.* Department of Commerce, Washington, D.C.

Newell, R. E. and S. Gould-Stewart, 1981: A stratospheric fountain ? *Journal of the Atmospheric Sciences*, **38**, 2789–2796.

Newell, R. E., Y. Zhu, E. V. Browell, S. Ismail, W. G. Read, J. W. Waters, K. K. Kelly and S. C. Liu, 1996: Upper tropospheric water vapor and cirrus: Comparison of DC-8 observations, preliminary UARS Microwave Limb Sounder measurements and meteorological analyses. *Journal of Geophysical Research*, **101**(D1), 1931–1941.

Niedermeier, M. and P. Fabian, 1994: Atmospheric residence times and stratospheric-tropopsheric exchange. in U. Schumann and D. Wurtzel, editors, *Impact of emissions from aircraft and spacecraft upon the atmosphere*, pp. 199–204. DLR, Koln.

Nightingale, R. W. et al., 1996: Global CF_2Cl_2 measurements by UARS Cryogenic Limb Array Etalon Spectrometer: Validation by correlative data and a model. *Journal of Geophysical Research*, **101**(D6), 9711–9736.

Olaguer, E. P., H. Yang and K. K. Tung, 1992: A reexamination of the readiative balance of the stratosphere. *Journal of the Atmospheric Sciences*, **49**(14), 1242–1263.

Pan, L., S. Solomon, W. Randel, J. F. Lamarque, P. Hess, J. Gille, E. W. Chiou and M. P. McCormick, 1997: Hemispheric asymmetries and seasonal variations of the lowermost stratospheric water vapor and ozone derived from SAGE II data. *Journal of Geophysical Research*, **102**(D23), 28,177–28,184.

Park, J. H. et al., 1996: Validation of halogen occultation experiment CH_4 measurements from the UARS. *Journal of Geophysical Research*, **101**(D6), 10,183–10,203.

Pfister, L., K. R. Chan, T. P. Bui, S. Bowen, M. Legg, B. Gary, K. Kelly, M. Proffitt and W. Starr, 1993: Gravity waves generated by a tropical cyclone during the STEP tropical field program: A case study. *Journal of Geophysical Research*, **98**(D5), 8611–8638.

Pierrehumbert, R. T., 1998: Lateral mixing as a source of subtropical water vapor. *Geophysical Research Letters*, **25**(2), 151–154.

Pierrehumbert, R. T. and R. Roca, 1998: Evidence for control of atlantic subtropical humidity by large scale advection. *Geophysical Research Letters*, **25**(24), 4537–4540.

Plumb, R. A., 1996: A "tropical pipe" model of stratospheric transport. *Journal of Geophysical Research*, **101**(D2), 3957–3972.

Plumb, R. A. and J. Eluszkiewicz, 1999: The Brewer-Dobson circulation: Dynamics of the tropical upwelling. *Journal of the Atmospheric Sciences*, **56**(6), 868–890.

Ponater, M., S. Brinkop, R. Sausen and U. Schumann, 1996: Simulating the global atmospheric response to aircraft water vapour emissions and contrails: a first approach using a GCM. *Annales Geophysicae*, **14**(9), 941–60.

Postel, G. A. and M. H. Hitchman, 1999: A climatology of Rossby wave breaking along the subtropical tropopause. *Journal of the Atmospheric Sciences*, **56**(3), 359–373.

Potter, B. E. and J. R. Holton, 1995: The role of monsoon convection in the dehydration of the lower tropical stratosphere. *Journal of the Atmospheric Sciences*, **52**(8), 1034–1050.

Poulida, O., R. R. Dickerson and A. Heymsfield, 1996: Stratosphere-troposphere exchange in a midlatitude mesoscale convective complex 1. observations. *Journal of Geophysical Research*, **101**(D3), 6823–6836.

Rahmes, T. F., A. H. Omar and D. J. Wuebbles, 1998: Atmospheric distributions of soot particles by current and future aircraft fleets and resulting radiative forcing on climate. *Journal of Geophysical Research*, **103**(D24), 31,657–31,667.

Randel, W. J., F. Wu, J. M. R. III, A. Roche and J. W. Waters, 1998: Seasonal cycles and QBO variations in stratospheric CH_4 and H_2O observed in UARS HALOE data. *Journal of the Atmospheric Sciences*, **55**(2), 163–185.

Ray, E. A. et al., 1999: Transport into the northern hemisphere lowermost stratosphere revealed by in situ tracer measurements. *submitted to the Journal of Geophysical Research.*

Read, W. G. et al., 1995: Upper tropospheric water vapor from UARS MLS. *Bulletin of the American Meteorological Society*, **76**, 2381–2389.

Reid, G. C., 1998: The tropical tropopause: Approaching a physical picture. *SPARC Newsletter*, **11**, 16–19.

Reid, G. C. and K. S. Gage, 1996: The tropical tropopause over the western Pacific: Wave driving, convection, and the annual cycle. *Journal of Geophysical Research*, **101**(D16), 21,233–21,241.

Roche, A. E. et al., 1996: Validation of CH_4 and N_2O measurements by the cryogenic limb array etalon spectrometer instrument on the Upper Atmosphere Research Satellite. *Journal of Geophysical Research*, **101**(D6), 9679–9710.

Rodhe, H., 1992: Modeling biogeochemical cycles. in S. S. Butcher, R. J. Charlson, G. H. Orians and G. V. Wolfe, editors, *Global Biogeochemical Cycles*, Chap. 4, pp. 55–72. Academic Press.

Roelofs, G. J. and J. Lelieveld, 1996: Model study of the influence of cross-tropopause O_3 transports on tropospheric O_3 levels. *Tellus, Series B*, **49**, 38–55.

Rood, R. B., A. R. Douglass, M. C. Cerniglia and W. G. Read, 1997: Synoptic scale mass exchange from the troposphere to the stratosphere. *Journal of Geophysical Research*, **102**(D19), 23,467–23,485.

Rosenfield, J. E., D. B. Considine, M. R. Schoeberl and E. V. Browell, 1998: The impact of subvisible cirrus clouds near the tropopause on stratospheric water vapor. *Geophysical Research Letters*, **25**(11), 1883–1886.

Rosenlof, K., A. Tuck, K. Kelly, J. Russell III and M. McCormick, 1997: Hemispheric asymmetries in water vapor and inferences about transport in the lower stratosphere. *Journal of Geophysical Research*, **102**(D11), 13,213–13,234.

Rosenlof, K. H., 1995: Seasonal cycle of the residual mean meridional circulation in the stratosphere. *Journal of Geophysical Research*, **100**(D3), 5173–5191.

Rosenlof, K. H. and J. R. Holton, 1993: Estimates of the stratospheric residual circulation using the downward control principle. *Journal of Geophysical Research*, **98**, 10,465–10,479.

Salathé, E. P. and D. L. Hartmann, 1997: A trajectory analysis of tropical upper-tropospheric moisture and convection. *Journal of the Atmospheric Sciences*, **10**, 2533–2547.

Sausen, R., K. Gierens and U. Schumann, 1997: A diagnostic study of the global coverage by contrails part I: Present day climate. Tech. Rep. 89, DLR Institut für Physik der Atmosphäre, Oberpfaffenhofen.

Schmitt, A. and B. Brunner, 1997: Emissions from aviation and their development over time. in U. Schumann et al., editors, *Final Report on the BMBF Verbundprogram: Schadstoffe in der Luftfhart*, Report 97-04. DLR Mitteilung.

Schoeberl, M. R., C. H. Jackman and J. Rosenfield, 1998: A lagrangian estimate of aircraft effluent lifetime. *Journal of Geophysical Research*, **103**(D9), 10,817–10,825.

Schoeberl, M. R. and L. C. Sparling, 1994: Trajectory modelling. in G. Fiocco and G. Visconti, editors, *Diagnostic Tools in Atmospheric Physics*, pp. 289–305. North-Holland.

Schubert, S. D. et al., 1995: A multi-year assimilation with the GEOS-1 system: Overview and results. NASA Technical Memorandum 104606 Volume 6, NASA Goddard Space Flight Center.

Schubert, S. D., R. B. Rood and J. Pfaendtner, 1993: An assimilated dataset for earth science applications. *Bulletin of the American Meteorological Society*, **74**(12), 2331–2342.

Schumann, U., 1994: On the effect of emissions from aircraft engines on the state of the atmosphere. *Annales Geophysicae*, **12**, 365–384.

Shapiro, M. A., 1980: Turbulent mixing within tropopause folds as a mechanism for the exchange of chemical constituents between the stratosphere and teh troposphere. *Journal of the Atmospheric Sciences*, **37**, 994–1004.

Shaw, N., 1930: *Manual of Meteorology, vol III: The Physical Processes of Weather.* Cambridge University Press.

Shine, K., 1989: Sources and sinks of zonal momentum in the middle atmosphere diagnosed using the diabatic circulation. *Q. J. R. Meterol. Soc.*, **115**, 265–292.

Siegmund, P. C., P. F. J. van Velthoven and H. Kelder, 1996: Cross-tropopause transport in the extratropical northern winter hemisphere, diagnosed from high-resolution ECMWF data. *Quarterly Journal of the Royal Meteorological Society*, **122**, 1921–1941.

Sobel, A. H., R. A. Plumb and D. W. Waugh, 1997: Methods of calculating transport across the polar vortex edge. *Journal of the Atmospheric Sciences*, **54**(18), 2241–2260.

Solomon, S. et al., 1997: Heterogenous chlorine chemistry in the tropopause region. *Journal of Geophysical Research*, **102**(D17), 21,411–21,429.

Spaete, P., D. R. Johnson and T. K. Schaack, 1994: Stratospheric-tropospheric mass exchange during the presidents' day storm. *Monthly Weather Review*, **122**, 424–439.

Sparling, L. C., J. A. Kettleborough, P. H. Haynes, M. E. McIntyre, J. E. Rosenfield, M. R. Schoeberl and P. A. Newman, 1997: Diabatic cross-isentropic dispersion in the lower-stratosphere. *Journal of Geophysical Research*, **102**(D22), 25,817–25,829.

Sparling, L. C., M. R. Schoeberl, A. R. Douglass, C. J. Weaver, P. A. Newman and L. R. Lait, 1995: Trajectory modeling of emissions from lower stratospheric aircraft. *Journal of Geophysical Research*, **100**(D1), 1427–1438.

Staley, D. O., 1962: On the mechanism of mass and radioactivity transport from stratosphere to troposphere. *Journal of the Atmospheric Sciences*, **19**, 450–467.

Staley, D. O., 1982: Strontium-90 in surface air and the stratosphere: Some interpretations of the 1963-75 data. *Journal of the Atmospheric Sciences*, **39**, 1571–1590.

Stoelinga, M. T., 1996: A potential-vorticity based study of the role of diabatic heating and friction in a numerically simulated baroclinic cyclone. *Journal of the Atmospheric Sciences*, **124**, 849–74.

Stolarski, R. S., S. L. Baughcum, W. H. Brune, A. R. Douglass, D. W. Fahey, R. R. Friedl, S. C. Liu, R. A. Plumb, L. R. Poole, H. L. Wesoky, and D. R. Worsnop, 1995: *Scientific Assessment of the Atmospheric Effects of Stratospheric Aircraft.* NASA Reference Publication 1381, Washington, D.C.

Strahan, S. E., A. R. Douglass, J. E. Nielsen and K. A. Boering, 1998: The CO_2 seasonal cycle as a tracer of transport. *Journal of Geophysical Research*, **103**(D2), 13,729–13,741.

Sun, D. Z., 1993: Distribution of tropical tropospheric water vapor. *Journal of the Atmospheric Sciences*, **50**(12), 1645–60.

Swinbank, R. and A. O'Neill, 1994: A stratosphere-troposphere data assimilation system. *Monthly Weather Review*, **122**, 686–702.

Thuburn, J. and G. C. Craig, 1997: GCM tests of theories for the height of the tropopause. *Journal of the Atmospheric Sciences*, **54**, 869–882.

Thuburn, J. and G. C. Craig, 1999: Stratospheric influence on tropopause height: The radiative constraint. *submitted to Journal of the Atmospheric Sciences.*

Tie, X. X. and P. Hess, 1997: The effects of volcanic eruption on the ozone mass exchange between the stratosphere and the troposphere. *Journal of Geophysical Research*, **102**, 24,487–24,500.

Tsuda, T., Y. Murayama, H. Wiryosumarto, S. W. B. Harijono and S. Kato, 1994: Radiosonde observations of equatorial atmosphere dynamics over indonesia: 1. equatorial waves and diurnal tides. *Journal of Geophysical Research*, **99**(D5), 10,491–10,505.

van Velthoven, P. F. J. and H. Kelder, 1996: Estimates of stratosphere-troposphere exchange: Sensivity to model formulation and horizontal resolution. *Journal of Geophysical Research*, **101**, 1429–1434.

van Velthoven, P. F. J., R. Sausen, C. E. Johnson, H. Kelder, I. Köhler, A. B. Kraus, R. Ramaroson, F. Rohrer, D. Stevenson, A. Strand and W. M. F. Wauben, 1997: The passive transport of NO_x emissions from aircraft studied with a heirarchy of models. *Atmospheric Environment*, **31**(12), 1783–1799.

Volk, C. M. et al., 1996: Quantifying transport between the tropical and mid-latitude lower stratosphere. *Science*, **272**, 1763–1768.

Wang, J., J. C. Gille, P. L. Bailey, L. Pan, D. Edwards and J. R. Drummond, 1999: Retrieval of tropospheric carbon monoxide profiles from high-resolution interferom-

eter observations: A new digital gas correlation (DGC) method and applications. *Journal of the Atmospheric Sciences*, **56**, 219–232.

Wauben, W. M. F., P. F. J. van Velthoven and H. Kelder, 1997: A 3D chemistry transport model study of changes in atmospheric ozone due to aircraft NO_x emissions. *Atmospheric Environment*, **31**(12), 1819–1836.

Weaver, C. J., A. R. Douglass and D. B. Considine, 1996: A 5-year simulation of supersonic aircraft emission transport using a three-dimensional model. *Journal of Geophysical Research*, **101**(D15), 20,975–20,984.

Webster, P. J., 1983: Large-scale structure of the tropical atmosphere. in B. Hoskins and R. Pearce, editors, *Large-scale dynamical processes in the atmosphere*, pp. 235–275. Academic Press, New York.

Webster, P. J. and J. R. Holton, 1982: Cross equatorial response to middle-latitude forcing in a zonally varying basic state. *Journal of the Atmospheric Sciences*, **39**, 722–733.

Wei, M. Y., 1987: A new formulation of the exchange of mass and trace constituents between the stratosphere and the troposphere. *Journal of the Atmospheric Sciences*, **44**(20), 3079–86.

Weinheimer, A. J. et al., 1994: Meridional distributions of NO_x, NO_y and other species in the lower stratosphere and upper troposphere during AASE II. *Geophysical Research Letters*, **21**(23), 2583–2586.

Weisenstein, D. K., 1992: The chlorine budget of the present day atmosphere. *Journal of Geophysical Research*, **97**(D2), 2547–2559.

Wennberg, P. O., R. C. Cohen, R. M. Stimpfle, J. P. Koplow, J. G. Anderson, R. J. Salawitch, D. W. Fahey, E. L. Woodbridge, E. R. Keim, R. S. Gao, C. R. Webster,

R. D. May, D. W. Toohey, L. M. Avallone, M. H. Proffitt, M. Loewenstein, J. R. Podolske, K. R. Chan and S. C. Wofsy, 1994: Removal of stratospheric O_3 by radicals: In situ measurements of OH, HO_2, NO, NO_2, ClO and BrO. *Science*, **266**, 398–404.

Wirth, V., 1996: Quasi-geostrophic dynamics of an upper tropospheric PV anomaly in two idealized high resolution models and related stratosphere-troposphere exchange. *Contributions to Atmospheric Physics*, **69**(2), 333–347.

Wirth, V. and J. Egger, 1999: Diagnosing extratropical synoptic-scale stratosphere-troposphere exchange: A case study. *Quarterly Journal of the Royal Meteorological Society*, **125**.

World Meteorological Organization, 1986: *Atmospheric Ozone: 1985*. Global Ozone Research and Monitoring Project Report 16. World Meteorological Organization, Geneva.

World Meteorological Organization, 1994: *Scientific Assessment of Ozone Depletion*. WMO Report 37. World Meteorological Organization, Geneva.

Yang, H. and K. K. Tung, 1996: Cross-isentropic stratosphere-troposphere exchange of mass and water vapor. *Journal of Geophysical Research*, **101**(D5), 9413–9423.

Yulaeva, E., 1994: On the cause of the annual cycle in tropical lower- stratospheric temperatures. *Journal of the Atmospheric Sciences*, **51**(2), 169–174.

Zhang, C., 1993: On the annual cycle in highest, coldest clouds in the tropics. *Journal of Climate*, **6**, 1987–1990.

VITA

Andrew Gettelman was born in the small town of Los Angeles, California to Nancy and Alan Gettelman on January 6, 1970. After learning to play water polo, ski, and ride skate boards, he headed east and graduated from Princeton University in 1992 with a B.S.E degree in Civil Engineering and a certificate in Architecture. Though an average water polo player, he graduated Magna Cum Laude and was awarded the Calvin Dodd MacCraken Senior Thesis Award for work on modeling climate in California.

Electing (God knows why) to stay on the East Coast, Andrew worked in Washington, D.C. as a Research Associate for the Natural Resources Defense Council (NRDC) for one year. In 1993 he became the coordinator of the US Climate Action Network, working in the rough and tumble world of international environmental policy, managing the egos of Non-Governmental Organizations (NGO's) trying to save the planet.

Deciding that he really didn't understand what was going on well enough, Andrew decided to return to school to study the global atmosphere. He entered the department of Atmospheric Sciences at the University of Washington in 1994, knowing just enough about the weather to know he did not like skiing on the east coast. So he rose above it all and began research anthropogenic changes to the stratosphere.

Andrew continued to be a mediocre water polo player, but nonetheless was awarded a Ph.D. from the department in 1999 for his work on aircraft emissions and stratosphere-troposphere exchange. Along the way he also acquired a certificate in Environmental Management from the Graduate School of Business at the University of Washington, and was an inaugural member of the governing board of the University of Washington Program on the Environment.

IMAGE EVALUATION TEST TARGET (QA-3)

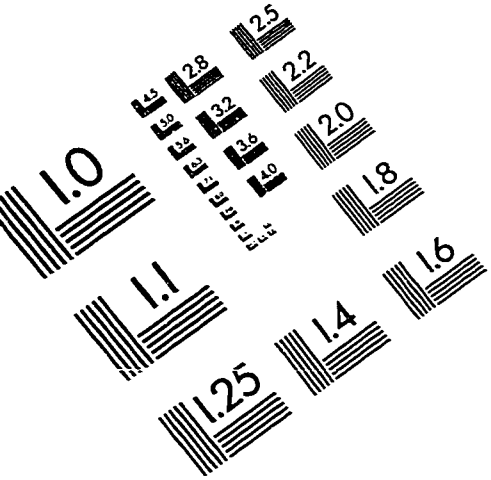

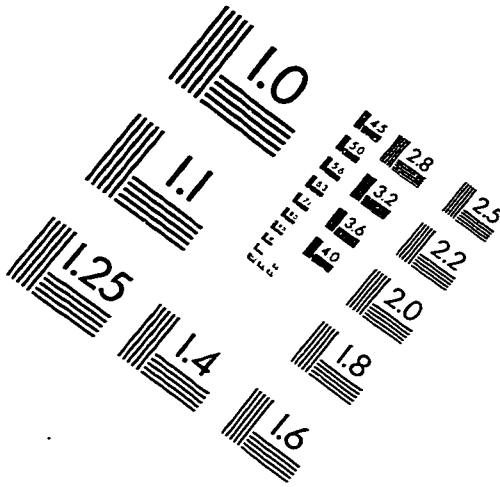

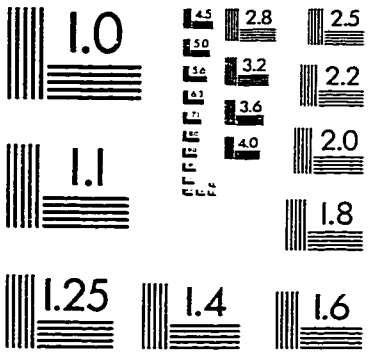

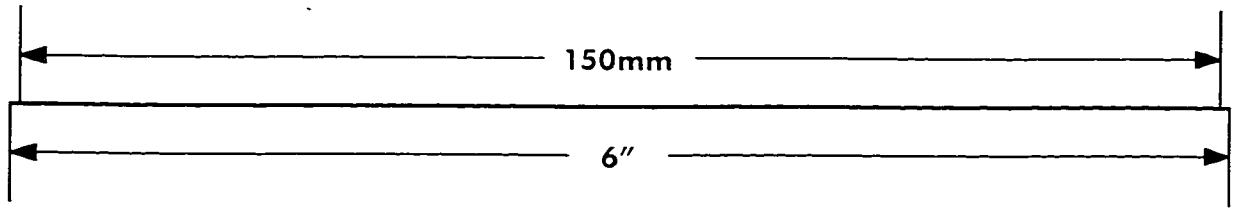

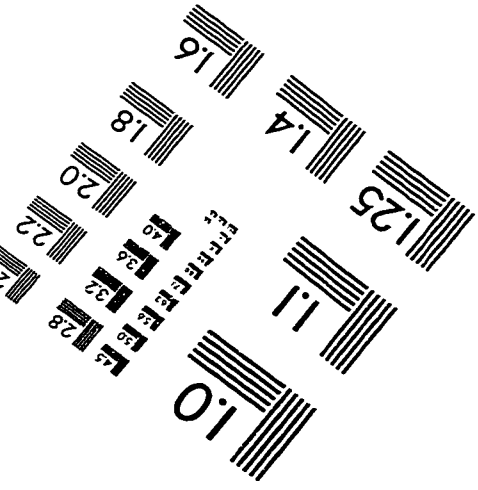

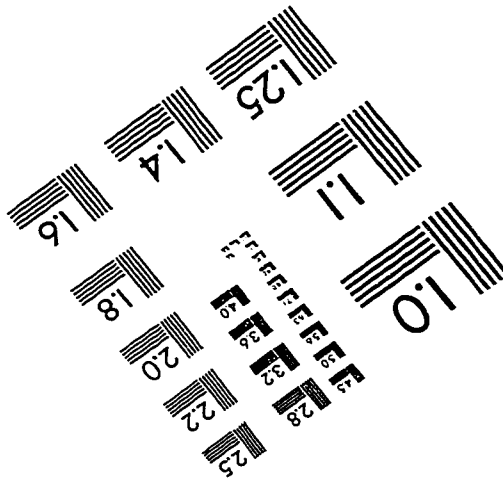

APPLIED IMAGE, Inc
1653 East Main Street
Rochester, NY 14609 USA
Phone: 716/482-0300
Fax: 716/288-5989